



HAL
open science

Drug delivery nanosystems for skeletal muscle treatment in myotonic dystrophy

Mathieu Repellin

► **To cite this version:**

Mathieu Repellin. Drug delivery nanosystems for skeletal muscle treatment in myotonic dystrophy. Bioengineering. Université de Lyon; Università degli studi (Vérone, Italie), 2022. English. NNT : 2022LYSE1147 . tel-04496909

HAL Id: tel-04496909

<https://theses.hal.science/tel-04496909>

Submitted on 9 Mar 2024

HAL is a multi-disciplinary open access archive for the deposit and dissemination of scientific research documents, whether they are published or not. The documents may come from teaching and research institutions in France or abroad, or from public or private research centers.

L'archive ouverte pluridisciplinaire **HAL**, est destinée au dépôt et à la diffusion de documents scientifiques de niveau recherche, publiés ou non, émanant des établissements d'enseignement et de recherche français ou étrangers, des laboratoires publics ou privés.



UNIVERSITÀ
di **VERONA**



N°d'ordre NNT : 2022LYSE1147

THESE de DOCTORAT DE L'UNIVERSITE DE LYON

opérée au sein de
l'Université Claude Bernard Lyon 1
en co-tutelle avec:
l'Università degli studi di Verona

Ecole Doctorale N°ED 205
Ecole Doctorale Interdisciplinaire Sciences Santé (EDISS)

Spécialité de doctorat : Ingénierie pour le vivant

Soutenue à huis clos le 18/07/2022, par :

Mathieu REPELLIN

Drug delivery nanosystems for skeletal muscle treatment in myotonic dystrophy

Devant le jury composé de :

Francisco Goycoolea, Professeur à l'Université de Leeds, Royaume-Uni,

Président

Marco Biggiogera, Professeur à l'Université de Pavia, Italie

Rapporteur

Malatesta Manuela, Professeur à l'Université de Vérone, Italie

Directrice de thèse

Stéphanie Briançon, Professeur à l'Université Lyon 1, France

Directrice de thèse

Giovanna Lollo, Maître de conférence à l'Université Lyon 1, France

Co-directrice de thèse



Mathieu REPELLIN a participé au projet INVITE de l'Université de Vérone. Le projet INVITE a reçu un financement du programme de recherche et d'innovation Horizon 2020 de l'Union européenne dans le cadre de la convention de subvention Marie Skłodowska-Curie N° 754345.

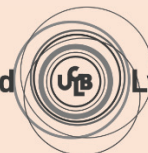


REGIONE DEL VENETO



UNIVERSITÀ
di VERONA

Université Claude Bernard



Lyon 1

UNIVERSITA' DEGLI STUDI DI VERONA

DEPARTMENT OF

Neuroscience, Biomedicine and Movement Sciences

GRADUATE SCHOOL OF

Natural Sciences and Engineering

DOCTORAL PROGRAM IN

Nanosciences and Advanced Technologies

XXXIV° Cycle

Drug delivery nanosystems for skeletal muscle treatment in myotonic dystrophy

IN *CO-TUTELLE DE THÈSE* WITH THE UNIVERSITY CLAUDE BERNARD OF LYON,
FRANCE

S.S.D. BIO/16 – Human Anatomy

UNIVERSITA' DEGLI STUDI DI VERONA:

Coordinator: Prof. Adolfo SPEGHINI

Tutor: Prof. Manuela MALATESTA

UNIVERSITY CLAUDE BERNARD LYON 1:

Tutor: Prof. Stéphanie BRIANÇON

Co-tutor: Prof. Giovanna LOLLO

Doctoral Student: Dr. Mathieu REPELLIN



invite

The project leading to this application has received funding from the European Union's Horizon 2020 research and innovation programme under the Marie Skłodowska-Curie grant agreement No 754345, under Region of Veneto Decree nr. 193 of 13/09/2016 and under Università degli Studi di Verona.

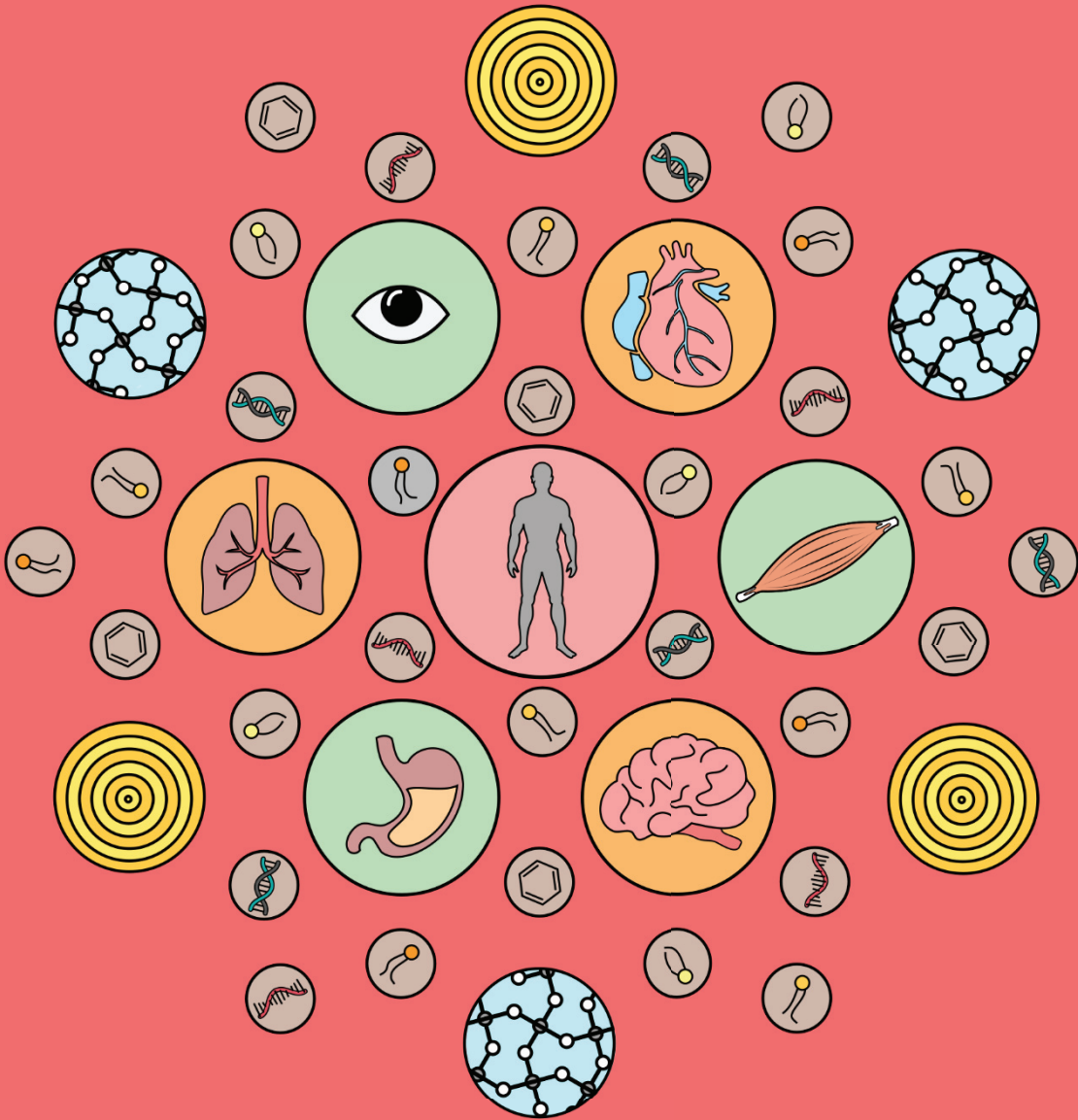


REGIONE DEL VENETO

This work is licensed under a Creative Commons Attribution-Non-Commercial
No-Derivatives 3.0 Unported License, Italy.
<http://creativecommons.org/licenses/by-nc-nd/3.0/>

*Drug delivery nanosystems for skeletal muscle treatment
in myotonic dystrophy* – Mathieu Repellin
PhD thesis

Drug delivery nanosystems for skeletal muscle treatment in myotonic dystrophy



Mathieu REPELLIN

“Life is like riding a bicycle. To keep your balance, you must keep moving.”

Albert Einstein

ACKNOWLEDGMENTS

This doctoral thesis has been carried out in co-tutelle between the “Università degli studi di Verona” in Italy and the “Université Claude Bernard Lyon 1” in France. During this amazing experience, I had the opportunity to meet and cooperate with many people to whom I would like to express all my deep gratitude. They transformed this initiatory course which is the doctorate into an enriching and formative experience but first of all in a human adventure, and for that I will always be grateful to them.

I would like to thank Mr. Marco Biggiogera and Mr. Francisco M. Goycoolea for having accepted to devote time to the evaluation of this work.

I would like to express my sincere gratitude to all my supervisors, Manuela Malatesta, Stéphanie Briançon and Giovanna Lollo. I am especially grateful to Manuela Malatesta for her supervision, advices and attention that she offered to me along this PhD thesis. I arrived with my curiosity as my main baggage, hoping that it would compensate for my lack of knowledge in biology and you offered to me a strong and solid baggage, more that I could have imagined. You did not only give me your knowledges, you also shared with me your experiences and lessons for work as for life. Many thanks for your kindness and attention that have been so pleasant and from crucial help all along my thesis. I would like to thank Stéphanie Briançon for accepting me in her research group and for her supervision during my PhD. Thank you for giving me the opportunity to work on this project. I would like to express my sincere gratitude to Giovanna Lollo, for everything she offered to me during this thesis. Your enthusiasm and kindness regarding me have been my strength all along my PhD. I still remember myself scared to do a doctorate abroad. Like a guide, you convinced me to take part in this project and fly abroad to carry out my thesis. The chance to have met you 5 years ago now, not only changed the impact of my thesis, you also transformed my entire professional and personal future. You made me grow and I will always be grateful to you.

I really would like to express my special thanks to Laurent Schaeffer for accepting me to work in collaboration in his research group. Thank you for your supervision and for your curiosity to take part in this multidisciplinary project. I am also especially grateful to Arnaud Jacquier, for his expertise and for his time that he consecrated to me. Always with a smile and encouraging words, working with you has been most enjoyable. Thanks also for all your important advices and point of view that you shared to me regarding the future. I would like also to specially thanks Julien Carras, that always has been available to help me. Many thanks for your advices and knowledges as well as for your warm kindness.

I want to express my gratitude to all researcher that helped me in the activities I undertook. Thanks to Federico Boschi for his help in confocal microscopy; to Laura Calderan and Jacqueline Sidi-boumedine for her expertises in animal experiment; to Mirco Galiè for his knowledge in cell transfection; to Massimiliano Perduca for his expertise in calorimetry analysis, to Pierre-Yves Dugas for his expertise and for all the great time passed in Cryo-TEM sessions and to Yves Chevalier for his physico-chemical expertise and his time.

I would like to express my gratitude to Cécile Martinat for her interest, kindness and accepting me to carried out some experiments in her laboratory.

Memorable will be all the people that I met along this incredible experience. I am especially grateful to all my colleagues from the University of Verona (Flavia, Enrica, Federica, Assunta, Marco, Alice, Filippo, Federico, Ilaria, Manuela, Barbara, Valeria, Giannino), they helped me and integrated me since the first day, made me feel like home. Thank you to all my colleagues from the University of Lyon (Valentina, Ilaria, Tiffanie, Valentine, Serena, Chiara, Giulia, Federica), for all the kind moments that we shared, your presence was crucial. Special thanks to Valentina that has been a cornerstone during this adventure but also in my present life. We shared wonderful times at work and outside, and I'm convinced that without you this experience would have been less pleasant and funny, thank you for everything. Special thanks also to Ilaria for her help, support, attentiveness and for her eccentricity. Working with you was a real pleasure and made time moving so fast. More than colleagues, more than friends, you will be all always part of my life.

I would like to thank all members from the department of Neurosciences, biomedicine and movement sciences of the Università di Verona. Special thanks to all members of the pharmaceutical engineering GePharm team from the LAGEPP laboratory and its director Marie-Alexandrine Bolzinger.

Many thanks to all people from secretary and technicians who ensure the good processing of a PhD thesis. Special thanks to Laura Marcazzan, Emanuela Grandis, Nadia Chapel, Delphine Arquier, Cynthia Barratier, Géraldine Agusti, Maria Perez Rodriguez and Jean-Pierre Valour.

I would like to express my sincere gratitude to all my friends, that have been always present for me and to encourage me. Many of you are present since our childhood and are as family member. Thank you for everything.

Finally, I am wholeheartedly thankful to all my family who has always believed in me, supported my decisions and encouraged me in this PhD. It is thanks to you that I can today write these words here. Special thanks to my brother, through the illness you are my greatest life lessons.

And finally, thanks to the person that is sharing my life, for everything and even more :)

You all contributed to make from this experience a wonderful and amazing human adventure that I will never forget. Although this manuscript bears my name, from my point of view this thesis bears all yours.

ABSTRACT

Myotonic dystrophy type 1 (DM1) is a genetic disorder of autosomal inheritance, characterized by progressive myopathy, myotonia and multiorgan involvement. This most common adult dystrophy is caused by an abnormal expansion of a trinucleotide repeat located on the DMPK gene. Experimental evidences support that pathogenesis of DM1 is caused by an RNA gain-of-function of the transcribed RNA from these mutant repeats, altering activities of several splicing regulators.

Currently, no cure to treat the pathological mechanism of DM1 has reached the market. Although some molecules or nucleic acid-based strategies have been proposed in a context of drug repurposing or gene therapy, important drawbacks remain related to their effective delivery. To this end, nanomedicine represents a suitable non-viral approach to provide long-term treatments with a safe and efficient biodistribution profile.

Therefore, the research project of this thesis was to set up experimental therapeutic strategies based on biocompatible nanocarriers to safely and efficiently deliver therapeutic agents in muscle cells. In this purpose, two different therapeutic strategies effective at different levels of the pathological mechanism of DM1 have been investigated. Firstly, the encapsulation of a small molecule, pentamidine, using hyaluronic acid-based nanocarriers has demonstrated an efficient internalization in murine muscle cells and murine muscle fibers while reversing pathological features in a DM1 cell model. Then, the investigations on lipid-based nanoparticles as nucleic acid carriers for enabling nucleic acid delivery has demonstrated the high efficiency of such nanosystems in murine and human muscle cells. Finally, preliminary data showed the efficient association of an antisense oligonucleotide sequence for treating the pathological mechanism of DM1, holding promises for further investigations in DM1 cell and animal models.

Overall, the present work may pave the way to novel strategies to tackle the unmet therapeutic need in DM1 to halt the disease progression or even reverse the consequences of the genetic damage.

SOMMARIO

La distrofia miotonica di tipo 1 (DM1) è una malattia genetica a trasmissione autosomica, caratterizzata da miopatia progressiva, miotonia e coinvolgimento multiorgano. Questa distrofia, la più comune dall'età adulta, è causata da un'espansione anomala di una ripetizione trinucleotidica situata sul gene DMPK. Evidenze sperimentali supportano l'ipotesi che la patogenesi di DM1 sia causata da gain-of-function dell'RNA trascritto da queste ripetizioni mutanti, alterando le attività di diversi regolatori di splicing.

Attualmente, nessuna cura per il trattamento del meccanismo patologico della DM1 è presente sul mercato. Sebbene alcune molecole o strategie basate sugli acidi nucleici siano state proposte in un contesto di riutilizzo di farmaci o terapia genica, rimangono importanti inconvenienti legati alla loro efficace somministrazione. A tal fine, la nanomedicina rappresenta un approccio non virale idoneo per fornire trattamenti a lungo termine con un profilo di biodistribuzione sicuro ed efficiente.

Quindi, il progetto di ricerca di questa tesi è consistito nell'impostare strategie terapeutiche sperimentali basate su nanocarrier biocompatibili per somministrare in modo sicuro ed efficiente agenti terapeutici alle cellule muscolari. A questo scopo sono state studiate due diverse strategie terapeutiche efficaci a diversi stadi del meccanismo patologico del DM1. In primo luogo, l'incapsulamento di una piccola molecola, la pentamidina, utilizzando nanocarrier a base di acido ialuronico ha dimostrato un'efficiente internalizzazione nelle cellule muscolari murine e nelle fibre muscolari murine e la capacità di ridurre le caratteristiche patologiche in un modello cellulare DM1. Successivamente, studi su nanoparticelle a base lipidica come vettori di acidi nucleici hanno dimostrato l'elevata efficienza di tali nanosistemi nel trasporto di diversi tipi di acidi nucleici in cellule muscolari murine e umane. Infine, dati preliminari hanno mostrato l'efficiente associazione di una sequenza oligonucleotidica antisense per il trattamento del meccanismo patologico della DM1, aprendo promettenti prospettive per ulteriori indagini su modelli cellulari e animali di DM1.

Nel complesso, il presente lavoro apre la strada a nuove strategie terapeutiche per arrestare la progressione della DM1 o addirittura bloccare gli effetti delle sue alterazioni genetiche.

SOMMAIRE

La dystrophie myotonique de type 1 (DM1) est une maladie génétique de transmission autosomique, caractérisée par une myopathie progressive, une myotonie et une atteinte de plusieurs organes. Cette dystrophie est causée par une expansion anormale d'une répétition trinuécléotidique située sur le gène DMPK. La pathogenèse de la DM1 est causée par un gain de fonction de l'ARN transcrit à partir de ces répétitions, modifiant les activités de plusieurs régulateurs d'épissage.

Actuellement, aucun remède pour traiter le mécanisme pathologique de la DM1 n'existe sur le marché. Bien que certaines molécules ou acides nucléiques aient été proposées dans un contexte de repositionnement de médicaments ou de thérapie génique, des inconvénients importants demeurent liés à leur délivrance. À cet effet, la nanomédecine représente une approche non virale appropriée pour fournir des traitements à long terme biocompatible avec une biodistribution appropriée.

Par conséquent, le projet de recherche de cette thèse a porté sur la mise en place de stratégies thérapeutiques expérimentales basées sur des nanoparticules biocompatibles pour délivrer efficacement des agents thérapeutiques dans les cellules musculaires. Dans ce but, deux stratégies thérapeutiques agissant à différents niveaux du mécanisme pathologique de la DM1 ont été étudiées. Tout d'abord, l'encapsulation d'une petite molécule, la pentamidine, à l'aide de nanoparticules à base d'acide hyaluronique a démontré une internalisation efficace dans les cellules et fibres musculaires murines tout en améliorant une caractéristique pathologique clé dans un modèle cellulaire DM1. Ensuite, des recherches sur les nanoparticules lipidiques en tant que vecteur pour permettre la délivrance d'acide nucléique ont démontré la grande efficacité de ces nanosystèmes pour délivrer différents types d'acides nucléiques dans les cellules musculaires murines et humaines. Enfin, des données préliminaires ont montré l'association efficace d'un oligonucléotide antisens pour traiter le mécanisme pathologique de la DM1, qui s'avère prometteur pour de futures investigations dans des modèles cellulaires et animaux de la DM1.

En conclusion, le présent travail ouvre la voie pour répondre au besoin thérapeutique non satisfait de la DM1, en vue d'en arrêter sa progression ou même d'inverser les conséquences de ses dommages génétiques.

TABLE OF CONTENTS

ACRONYMS	19
LIST OF FIGURES	20
LIST OF TABLES	21
INTRODUCTION	25
1. MYOTONIC DYSTROPHY TYPE 1	25
1.1. State of the art	25
1.2. Molecular pathogenic mechanism	26
1.3. Actual therapeutic strategy pipelines.....	27
1.4. Limitations of the therapeutic approaches.....	31
2. NANOMEDICINE AS NON-VIRAL DELIVERY APPROACH FOR DM1 TREATMENT	33
2.1. State of the art.....	33
2.2. Polymer and lipid-based nanoparticles.....	37
2.2.1. <i>Polymeric nanoparticles</i>	37
2.2.2. <i>Lipid-based nanoparticles</i>	41
3. AIM OF THE WORK	46
RESULTS	51
CHAPTER 1	53
Bibliographic studies	53
Electron microscopy to characterize nanoparticles in the biological environment .	55
Nanomedicine for gene delivery and drug repurposing in the treatment of muscular dystrophies.....	65
CHAPTER 2	101
Repurposing pentamidine using hyaluronic acid-based nanocarriers for skeletal muscle treatment in myotonic dystrophy	101
CHAPTER 3	141
Alcian blue staining to track the intracellular fate of hyaluronic-acid-based nanoparticles at transmission electron microscopy	143

Alcian blue staining to visualize intracellular hyaluronic-acid-based nanoparticles.151

CHAPTER 4 155

Lipid-based nanoparticles to modulate protein expression through DNA/RNA tools: a proof-of-concept for treating muscular dystrophies 155

CHAPTER 5 187

Antisense oligonucleotide delivery using lipid nanoparticles to reverse the splicing defects in DM1 187

CONCLUDING REMARKS 203

REFERENCES 213

APPENDICES 233

VALORIZATION 235

ACRONYMS

AAV: adeno-associated virus

ASO: antisense oligonucleotides

CPP: cell penetrating-peptide

CRISPR: clustered regularly interspaced short palindromic repeat

CUGBP1: CUG triplet repeat-RNA binding protein 1

dCas9: nuclease-deficient Cas9

DM1: myotonic dystrophy type 1

DMD: Duchenne muscular dystrophy

DMPK: *dystrophia myotonia protein kinase gene*

ECM: extracellular matrix

EDL: extensor digitorum longus

GFP: green fluorescent protein

gRNA: guide RNA

HA: hyaluronic acid

hnRNP H: heterogeneous nuclear ribonucleoprotein

LNP: lipid-based nanoparticles

MBNL: muscleblind-like proteins

NLC: nanostructured lipid nanocarriers

MD: muscular dystrophies

NPs: nanoparticles

PTM: pentamidine

RNase H: ribonuclease H

SLN: solid lipid nanoparticles

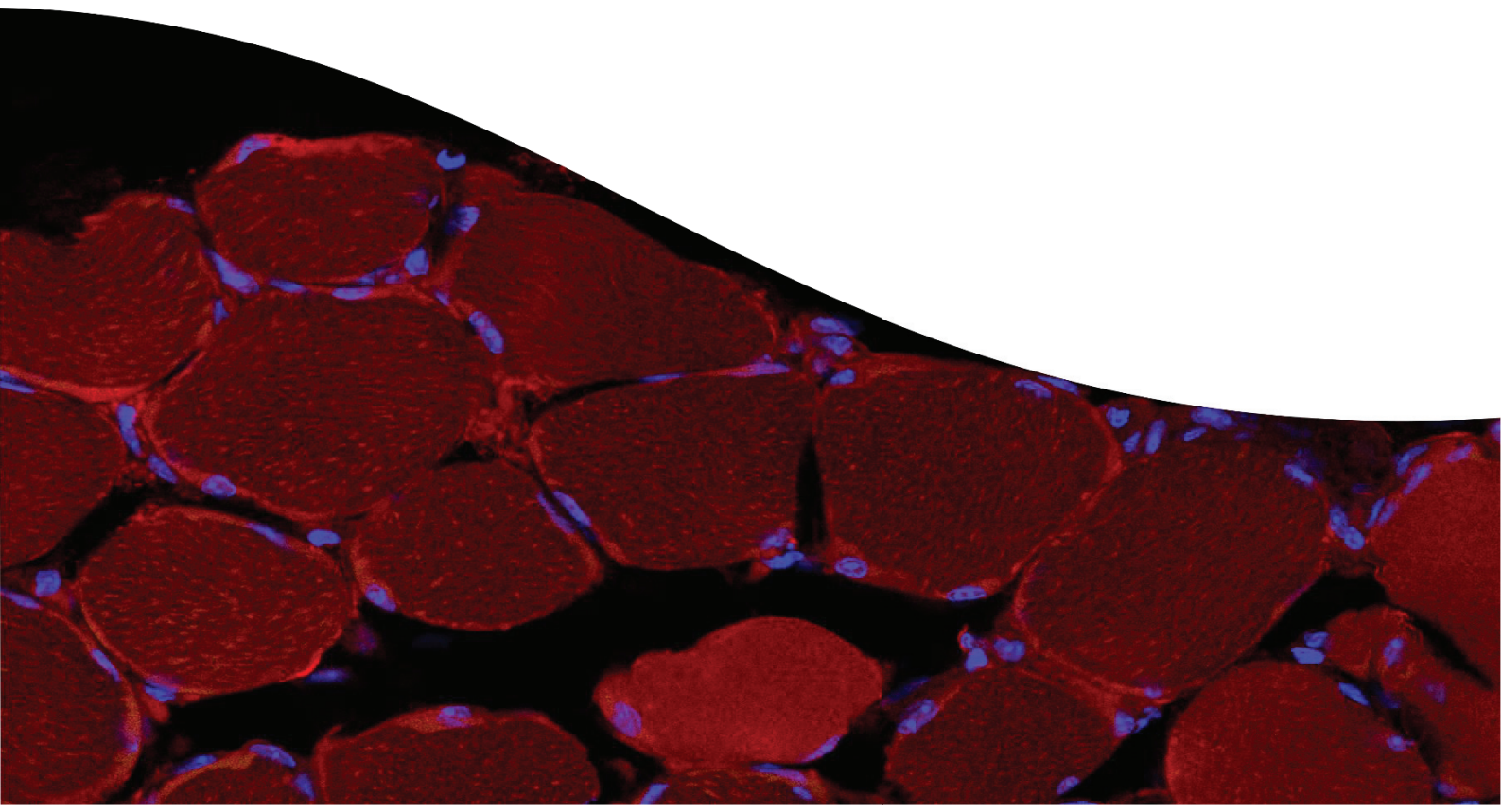
LIST OF FIGURES

Figure 1: Different steps in pathogenesis and the potential therapeutic targets in DM1.	27
Figure 2: Schematic representation of the most common classes of polymeric nanoparticles	38
Figure 3: structure of HA monomer.....	39
Figure 4: structure of PArg monomer	40
Figure 5: Schematic representation of the different structures of lipid nanoemulsion	41
Figure 6: Brief overview of the different categories of lipids and their most commonly used molecules for the development of lipid nanoparticles.	43
Figure 7: Schematic representation of the suggested structure of lipid nanoparticles nucleic acid carriers: lipid nanoparticles with nanostructured core and multilamellar lipid nanoparticles.	45
Figure 8: Physico-chemical properties and association efficiency of ASO complexed with LNP at different N/P ratio..	192
Figure 9: Intracellular distribution of ASO-LNP and release profile of ASO in C2C12 myoblasts and myotubes.....	193
Figure 10: MicroSPECT/CT (A) and fluorescent (B) in vivo imaging of C57BL/6J mice injected with ASO associated to ¹¹¹ In-LNP at a N/P ratio of 10 after 30 min, 2, 6 and 24 h.	194
Figure 11: Quantitative biodistribution of ¹¹¹ In-LNP (A) and semi-quantitative biodistribution of ASO (B) at 30 min, 2, 6 and 24 h after i.v. injection in C57B/6J mice expressed as percentage of injected dose per gram of tissue and percentage of intensity per surface area respectively (n=3 mice per group).....	196

LIST OF TABLES

Table 1: Different therapeutic drug development pipelines in pre-clinical and clinical studies for DM1.....	30
Table 2: Clinically approved nanoparticles for therapies and diagnostics (modify from Anselmo et al. ¹⁰²)	35

INTRODUCTION



1. Myotonic Dystrophy type 1

1.1. State of the art

Myotonic dystrophy type 1 (DM1) is a progressive neuromuscular genetic disorder of autosomal dominance inheritance (DM1; Steinert's disease; OMIM #160900). This most common adult form of muscular dystrophy (MD) initially reporting to affect 1 in 8,000 people worldwide, have recently demonstrated a prevalence 5 times higher of 5 in 10,000 people^{1,2}. This complex multisystemic disease is characterized with variable pathological phenotypes, onset ages and disease severities. From very early descriptions of the disease, the clinical findings have been categorized into 3 main phenotypes (mild, classic and severe)¹. Moreover, recent developments of registries and cohort studies achieved to better characterize the variability of symptoms in populations and a recent study performed by the French DM-scope registry has identified 5 overlapping subtypes in the broad clinical spectrum of DM1 (late-onset, adult, juvenile, infantile and congenital)³. These subtypes correlate with the different pathophysiology observed in this complex multisystemic disease.

The core features of DM1 are generalized skeletal muscle degeneration characterized by severe weakness and muscle wasting^{1,4,5}. Moreover, DM1-affected muscles express cardinal finding of myotonia, established by a slowing down of muscle relaxation after a normal contraction. On the other hand, this systemic disease potentially affects nearly every organ system including the cardiac, respiratory, central nervous and endocrine system, digestive track, eyesight and the reproductive organs. In mild phenotypes these biological dysfunctions are correlated to cognitive problems, hypersomnia, anxiety and depression, very disabling for patients. The involvement of the cardiac and respiratory systems in more severe phenotypes ultimately lead to important cardiac conduction defects or respiratory distress, resulting in shortened life span and arising as the most-common cause of mortality in DM1.

Although some symptoms of DM1 can be alleviated, there is currently no cure for this disease. However, the recent understanding of the molecular pathological mechanisms has allowed the investigation of diverse therapeutic approaches.

1.2. Molecular pathogenic mechanism

Over the last years, many progresses have been made in understanding the pathophysiological mechanisms involved in DM1. The gene defect responsible for this muscular dystrophy is due to an expansion of CTG trinucleotide repeats in the 3' untranslated region of the *dystrophia myotonia protein kinase* (DMPK) gene^{6,7}. This gene located on chromosome 19q13.3 codes for a myosin kinase expressed in skeletal muscle⁸. Healthy patients have between 5 and 37 CTG repeats on this gene whereas DM1 patients may express more than 2000 toxic repeats^{9,10}. Globally, the severity of the disease is correlated with this number of CTG repeats. These abnormal CTG expansions are transcribed into RNA containing CUG expansions, accumulated in the cell nuclei as ribonuclear aggregates under the form of hairpin structures and called foci^{11,12}.

Experimental evidences support that pathogenesis of DM1 is caused by an RNA gain-of-function of the mutant CUG repeats altering expression of several RNA-binding factors, including the muscleblind-like proteins (MBNLs), CUG triplet repeat-RNA binding protein 1 (CUGBP1) and heterogeneous nuclear ribonucleoprotein H (hnRNP H) proteins¹³⁻¹⁶. The alteration of these RNA-binding factors leads to the mis-regulation of DMPK RNA expression and several alternative splicing.

One of the main molecular hallmarks of DM1 is the sequestration of MBNLs proteins, in particular MBNL1, due to their high affinity for CUG expansions¹⁷. MBNLs proteins play predominant role as repressor and activator for terminal muscle differentiation^{18,19}. Therefore, the sequestration of MBNLs proteins leads to their functional loss, contributing significantly to DM1 phenotypes and responsible of characteristic features as myotonia and cataracts symptoms²⁰. On the contrary, stress responses triggered by the toxic DMPK RNA induce the stabilization of MBNL antagonists as CUGBP1 and hnRNPA1, resulting in an overexpression of these alternative splicing regulators^{15,21,22}.

Consequently, a growing number of changes in gene expression ensue from the mutant DMPK transcripts as downstream effects, resulting in a complex and variable disease. Taken together, understanding the molecular pathogenic mechanism involved in DM1 pathology provides crucial knowledge to better characterize this disease and for the development of suitable therapeutic strategies.

1.3. Actual therapeutic strategy pipelines

Nowadays, no disease-modifying therapies are available for DM1 patients, and treatments are made to only alleviate some symptoms. Over the last recent years, elucidating the mechanisms of DM1 pathogenesis have culminated in multiple strategies development pipeline for treating DM1²³. Numerous therapeutic approaches related to small molecules, oligonucleotide-based therapies, gene therapies and genome editing have been designed with the goal of specifically be effective at different levels. These therapies targeting the transcriptional, post-transcriptional or translational level have different mechanisms of action targeting from specific clinical symptoms up to root cause disease events. General concepts in therapeutic design strategy are detailed in [Figure 1](#).

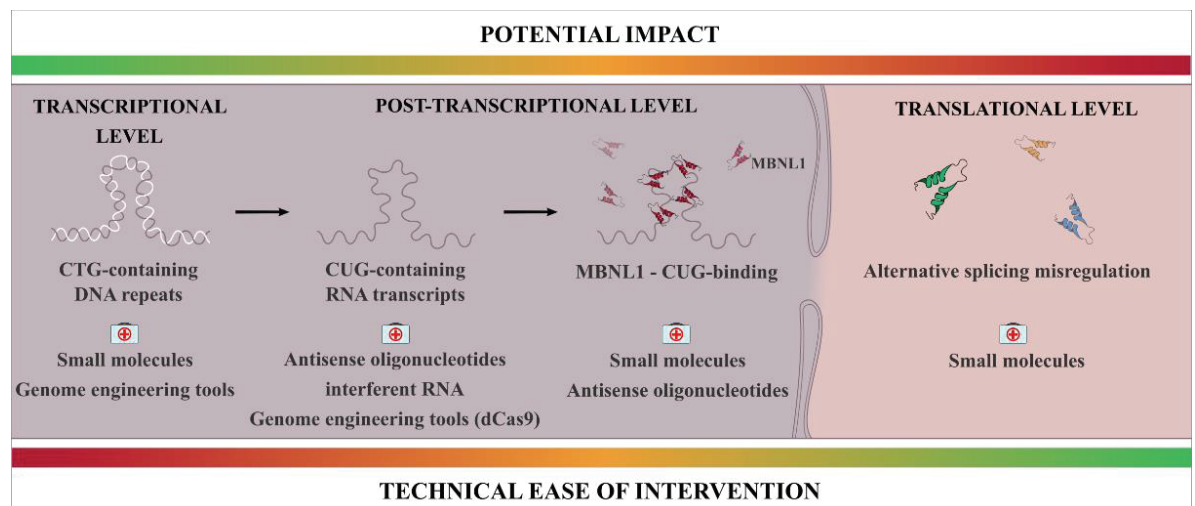


[Figure 1](#): Different steps in pathogenesis and the potential therapeutic targets in DM1.

Targeting protein expression has been the first studied approach as it is the easier way. The most investigated strategy is to inhibit interactions between MBNLs proteins and CUG repeats. In this purpose, a myriad of small molecules has been tested through drug repurposing approach or using computational rational design^{24–26}. As for example, pentamidine, erythromycin or metformin have demonstrated

their specificity and high affinity for ribonuclear foci, destabilizing the MBNL1-CUG repeats accumulation and releasing MBNL1²⁷⁻³⁰. Repurposed small molecules represent actually the most candidates in clinical trials³¹. On the other hand, oligonucleotide-based therapies focused on steric blocking antisense oligonucleotide (ASO) sequences have also demonstrated to compete with MBNL proteins for CUG-repeats binding, relieving some DM1 features³²⁻³⁴.

Correcting mutations at the RNA level is more challenging but can have a higher therapeutic impact than targeting only downstream effects. Various oligonucleotide-based strategies have been investigated for post-transcriptional knockdown of toxic RNA^{23,35,36}. The strategy that is furthest in clinical development employs ribonuclease H (RNase H)-active ASOs³⁷. Antisense oligonucleotides are specifically designed to bind to the targeted RNA by base pairing. Once bound to the complementary site, this kind of ASO induce the RNA cleavage through RNase-H enzyme degradation. This therapeutic strategy has demonstrated in DM1 muscle cells and mice models to reduce the toxic CUG-containing RNA transcripts and thereby some correlated downstream effects³⁸⁻⁴⁰. On the other hand, the clustered regularly interspaced short palindromic repeat (CRISPR) associated to DNA protein endonuclease (CRISPR/Cas system), initially design as genome engineering tool, has demonstrated an alternative approach by directly targeting the single stranded DMPK RNA. In particular, RNA-targeting nuclease-deficient Cas9 (dCas9) has been used to target and degrade DMPK CUG repeats via a designed guide RNA (gRNA)^{41,42}.

Correction strategies at the DNA level are also promising to treat the root cause of the pathologic mechanism of DM1. Theoretically, targeting the earliest stage of a disease should provide better therapeutic benefit since all associated downstream effects are reversed. However, targeting CTG-containing DNA repeats remains the most difficult and technically challenging approach^{23,35,43}. Some small molecules as pentamidine have demonstrated not only a high affinity for CUG repeats competing with MBNL1 sequestration, but also for CTG-containing DNA repeats inhibiting its transcription into CUG-containing RNA transcripts⁴⁴. On the other hand, recent technical innovations have led to the emergence of powerful genome engineering tools, as the CRISPR/Cas system, to perform sequence specific

modifications in preselected genomic locations, providing a suitable method for correcting the underlying genetic mutations in neuromuscular diseases⁴⁵. For DM1, different CRISPR/Cas9 strategies have been investigated to prevent the transcription of DMPK CTG repeats⁴⁶⁻⁴⁸:

- Promoting excision of the expanded DMPK CTG repeats via dual CRISPR/Cas9-mediated cleavage at either side of the CTG expansions⁴⁹⁻⁵².
- Inserting a premature polyadenylation signal in the 3' UTR DMPK gene, upstream of the CTG expansions, to induce premature termination of DMPK RNA synthesis⁵³.
- Inducing physically steric hindrance on the CTG expansion site using dCas9 to block the RNA polymerase II progression during the DMPK RNA synthesis⁵⁴.

With these findings in mind, multiple strategies development pipelines have been extensively evaluated as potential therapy to treat the complex pathology of DM1. However, none of these strategies are currently approved for commercialization due to some clinical limitations. A list of the different actual development pipelines in pre-clinical and clinical investigations is given in [Table 1](#).

Table 1: Different therapeutic drug development pipelines in pre-clinical and clinical studies for DM1.

Name and approach	Company	Actual stage of development	Source
Mexiletine <i>Small molecule</i>	Lupin Pharmaceuticals	Phase 3 <i>NCT04700046</i>	[55]
Metformin <i>Small molecule</i>	Tor Vergata University of Rome	Phase 3 <i>EudraCT 2013-001732-21</i>	[56]
Tideglusib <i>Small molecule</i>	AMO Pharma	Phase 3 <i>NCT03692312</i>	[57]
Erythromycin <i>Small molecule</i>	Osaka University Hospital	Phase 2 <i>JPRN-jRCT2051190069</i>	[58]
Pitolisant <i>Small molecule</i>	Harmony Biosciences	Phase 2 <i>NCT04886518</i>	[59]
ERX-963 <i>Small molecule</i>	Expansion therapeutics	Phase 1 <i>NCT03959189</i>	[60]
AOC 1001 <i>Antibody conjugated-ASO</i>	Avidity Biosciences	Phase 1 <i>NCT05027269</i>	[61]
Cugamycin <i>Small molecule</i>	The Scripps Research Institute	Pre-clinical	[62]
Pafuramidine <i>Small molecule</i>	University of Florida and Osaka	Pre-clinical	[30]
Mirtazapine <i>Small molecule</i>	Pompeu Fabra University	Pre-clinical	[63]
Chloroquine <i>Small molecule</i>	University of Valencia	Pre-clinical	[64]
ARTHEX-01 <i>microRNA</i>	Arthex Biotech	Pre-clinical	[65]
AT466 <i>AAV-ASO</i>	Audentes Therapeutics	Pre-clinical	[66]
NT0200 <i>Peptide-ASO</i>	NeuBase Therapeutics	Pre-clinical	[67]
ENZ-003 <i>RNA endonuclease</i>	Enzema Biosciences	Pre-clinical	[68]
JM642 <i>Small molecule</i>	Osaka University	Pre-clinical	[69]
CRISPR-Cas9 <i>Gene editing</i>	Genethon	Pre-clinical	[51]
PGN-EDODM1 <i>Peptide conjugated-ASO</i>	PepGen	Pre-clinical	[70]

1.4. Limitations of the therapeutic approaches

Over the last recent years, several therapeutic approaches have been investigated to target the underlying aetiology of DM1, however all faced clinical limitations. These diverse strategies offer various approaches from the treatment of downstream effects, leading to the requirement of long-term administration (since their activity will not leave a permanent mark in the genome), to the design of more challenging tools for treating the earliest phase, in a potential one-dose administration.

The development of therapeutic approaches based on small molecules via conventional medicinal chemistry have several advantages, including ease of management and manufacturing, lower costs, high-throughput screening and the opportunity of repositioning FDA-approved molecules to get to the clinic faster^{26,71}. However, this approach is mainly focused on targeting downstream effects at the splicing or protein level and not to treat the molecular pathologic cause of DM1²⁵. Although some compounds as pentamidine or furamidine have demonstrated a potential therapeutic impact at the transcriptional level of DMPK CTG repeats, these compounds exhibited a substantial toxicity, leading to clinical trial failure⁷². Taken together, long-term treatments and toxicity appear as compromising issues for their medical use through conventional administration.

RNA therapeutics such as RNAi or oligonucleotide-based therapies are very promising to inhibit MBNL1 sequestration or degrade DMPK CUG-containing transcripts. However, one important drawback of this approach relies on the effective delivery of such oligonucleotides^{73,74}. Because of their natural occurring negative charge and hydrophilic properties, naked oligonucleotides fail to diffuse across cell membranes and escape from the endocytic pathway to engage intracellularly their therapeutic role. Importantly, oligonucleotides are easily and quickly degraded in serum by nucleases, limiting drastically their pharmacokinetic profiles. Furthermore, membrane integrity of muscles from patients with DM1 is no more permeable than in healthy patients, not offering an opportunistic internalization way as in other neuromuscular diseases⁷⁵. To overcome these limitations, the main strategies investigated over the recent years has been to incorporate oligonucleotides into viral vectors⁷⁶⁻⁷⁸. However, viral vectors as

adeno-associated virus (AAV) have limited packaging capacity and induce unwanted immune system response that may cause inflammation and organ failure in severe cases. In addition, only a limited number of patients that do not harbor pre-existing antibodies against viral vectors are eligible for these therapies, representing a serious obstacle to their universal application^{79,80}.

Eliminating DMPK CTG repeats in DNA using genome editing could eliminate the pathogenesis of DM1. However, potential off-target activities are crucial shortcomings in genome engineering tools as they could lead to lethal genetic mutations that cause loss of gene function^{81,82}. Currently, researchers are in the race of creating new gene-targeting techniques with negligible off-target effects for the improvement of therapeutic gene editing or genome surgery⁸³. Another main limitation of genome engineering tools relies on their effective delivery^{84,85}. Because of the complex composition of genome editing tools, delivery vehicles are required to ensure their protection and internalization across multiple physiological barriers. The viral vectors represent the most used delivery strategies for this kind of therapeutic approach⁸⁶. However, the previously described drawbacks associated to viral vectors dampen the clinical therapeutic potential of genome engineering.

Taken together, despite the various therapeutic approaches proposed for treating DM1, several drawbacks are still mainly related to their safe and efficient delivery, disabling their clinical use and leading to find substitute delivery strategies.

2. Nanomedicine as non-viral delivery approach for DM1 treatment

An ideal therapeutic for DM1 must provide long-term effects, safe and efficient biodistribution profile in affected cells while leading to the specific elimination of the pathogenic repetitive transcripts. Currently, main interests are focused on enhancing the pharmacokinetic and biodistribution profile in muscles of the different therapeutic approaches. Despite improvements induced by viral vectors many limitations are still present and alternative delivery strategies are from crucial priority^{79,80}. In this context, the recent advances and progresses in nanomedicine have led to gain an interest for the use of this non-viral delivery approach.

2.1. State of the art

Nanotechnology has been defined as the “intentional design, characterization, production, and applications of materials, structures, devices, and systems by controlling their size and shape in the nanoscale range”⁸⁷. Because nanomaterials can be engineered to have various functions, nanotechnology represents highly useful device for medical applications. The field of nanomedicine benefit from the properties and physical characteristics of nanocarriers applied in medicine for the conception of contrast agents, diagnostic devices and drug-delivery vehicles^{88–92}. Drug-delivery vehicles represent a suitable strategy to provide safe and efficient delivery of therapeutic agents such as drug or nucleic acids. Through their encapsulation or association to nanocarriers, therapeutic agents have lower interactions with the extracellular milieu, offering a suitable protection to enzymatic or environmental degradation⁹³.

In particular, drug-delivery nanoparticles (NPs) are particularly interesting as synthetic and non-viral therapeutic delivery approach⁹⁴. Nanoparticles includes a wide range of carriers such as polymeric⁹⁵, lipid-based nanoparticles⁹⁶, mesoporous silica⁹⁷, gold⁹⁸, dendrimers⁹⁹ and so on. The first clinical approved nanomedicine was Doxil® in 1995 and led to the improvement of doxorubicin bioavailability and circulation-time, enabling its use in clinical therapeutic applications¹⁰⁰. Since then, more than 30 nanopharmaceuticals have been approved for diverse therapeutic applications as cancer, anemia and infections (see Table 2)^{101,102}. More recently, the

nanomedicine field has demonstrated its crucial importance to provide therapeutic and prophylactic approaches against emerging infection diseases, with the development of nanoparticle-based mRNA vaccines against SARS-CoV-2^{103,104}.

Momentous advances have been brought to a range of diseases through the interesting properties of non-viral nanocarriers. Several types of lipids, polymers and other components have been investigated to provide biocompatible and biodegradable properties, promising the minimum of accumulation, side-effects and toxicity^{105–107}. On the other hand, different strategies have been proposed to provide stealth nanosystems reducing the adsorption of plasma proteins on the surface and thereby the process of opsonization via the reticulo endothelial system⁹³. The strategies adopted, as the classic incorporation of PEG-components, led to the formation of a hydrating layer at the NPs surface that hinders protein adsorption, providing prolonged-circulating time in the blood system and enhanced biodistribution^{108,109}. Finally, the possibility to graft or label targeting moieties such as ligands, antibodies or peptides onto nanoparticles provide a suitable way for active targeting and enhanced the distribution in organ or cell targets^{110,111}. Taken together, nanomedicine offers several advantages to control the sustained release, improve bioavailability and clearance-time while safely enhancing the biodistribution in the target organs.

Considering the global impact of nanomedicine in the clinic, especially with their booming success in mRNA vaccines, the field of NPs drug delivery is entering a new phase, wherein nanocarriers for drug, gene and oligonucleotide delivery approaches are just beginning to scratch the surface.

Table 2: Clinically approved nanoparticles for therapies and diagnostics (modify from Anselmo et al.¹⁰²)

Name and company	Payload	Application	Approval
Liposomes			
Diprivan <i>Fresenius Kabi</i>	Propofol	Anesthetics	1989
Doxil <i>Caelyx (Janssen)</i>	Doxorubicin	Cancer	1995
DaunoXome <i>Galen</i>	Daunorubicin	Cancer	1996
Inflexal V <i>Crucell</i>	Virus antigen	Vaccine (Now discontinued)	1997
AmBisome <i>Gilead Sciences</i>	Amphotericin B	Fungal infections	1997
Myocet <i>Teva UK</i>	Doxorubicin	Cancer	2000
Visudyne <i>Bausch and Lomb</i>	Verteporfin	Macular degradation	2000
Epaxal <i>Crucell</i>	Inactivated virus	Vaccine (Now discontinued)	2003
Marqibo <i>Spectrum</i>	Vincristine	Cancer	2012
MEPACT <i>Millenium</i>	Mifamurtide	Cancer	2009
Onivyde MM-398 <i>Merrimack</i>	Irinotecan	Cancer	2015
VYXEOS CPX-351 <i>Jazz Pharmaceuticals</i>	Cytarabine/ daunorubicin	Cancer	2017
Lipid microspheres			
Definity <i>Lantheus Medical Imaging</i>	Perflutren	Imaging agent	2001
Lipid nanoparticles			
ONPATRO Patisiran <i>Alnylam Pharmaceuticals</i>	RNAi	Amyloidosis	2018
mRNA-1273 <i>Moderna</i>	mRNA	Vaccine	2020
BNT162b2 <i>Pfizer-BioNTech</i>	mRNA	Vaccine	2020

Table 3: (continued)

Name and company	Payload	Application	Approval
Phospholipid stabilized microbubble			
SonoVue <i>Bracco Imaging</i>	Hexafluoride	Imaging agent	2001
Albumin-particles			
Optison <i>GE Healthcare</i>	Perflutren	Imaging agent	1997
Abraxane <i>Celgene</i>	Paclitaxel	Cancer	2005
Iron-based particles			
CosmoFer INFeD <i>Pharmacosmos</i>	Iron	Iron-replacement	1992
DexFerrum DexIron <i>American Regent</i>	Iron	Iron-replacement	1996
Feridex I.V. <i>AMAG</i>	Iron	Imaging agent (Now discontinued)	1996
Ferrlecit <i>Sanofi</i>	Iron	Iron-replacement	1999
Venofer <i>American Regent</i>	Iron	Iron-replacement	2000
Resovist <i>Bayer Schering Pharma</i>	Iron	Imaging agent (Now discontinued)	2001
Monofer <i>Pharmacosmos</i>	Iron	Iron-replacement	2009
Feraheme Rienso <i>AMAG Takeda</i>	Iron	Iron-replacement	2009
Injectafer Ferinject <i>Vifor</i>	Iron	Iron-replacement	2013
Ferumoxtran-10 <i>AMAG</i>	Iron	Imaging agent	2013
Diafer <i>Pharmacosmos</i>	Iron	Iron-replacement	2013
Oxide nanoparticles			
NBTXR3 Hensify <i>Nanobiotix</i>	Oxide	Cancer	2019

2.2. Polymer and lipid-based nanoparticles

Over the last recent years, a wide variety of NPs have been proposed as nanocarriers for biomedical use. All these types of NPs are classified among three main classes: inorganic, polymeric and lipid-based NPs¹⁰⁶. This part focuses on the classes of polymeric and lipid-based NPs that are the most used for therapeutic agent delivery and represent the focus of the present work.

2.2.1. Polymeric nanoparticles

Polymeric NPs made from natural or synthetic polymers have received important attention due to their stability and ease of manufacturing. Their synthesis from various polymers allow for a wide variety of possible structures, surface chemistry and characteristics correlated to various properties^{95,112}. This tailor-made design enables to achieve specific drug encapsulation, controlled drug release and organ-specific localization.

Considerable researches have been made for polymeric NPs as drug-delivery systems to deliver drugs as small molecules or stabilize labile molecules (e.g., proteins, peptides, or DNA) from degradation. These properties enable to improve bioavailability, sustain release of drugs or solubilize drugs for systemic delivery leading to an enhanced therapeutic index.

Different types of interaction may be responsible for nanoparticles formation. Thus, polymeric NPs can be formulated through various techniques to enable precise control of multiples NPs features. The most used formulation processes are nanoprecipitation¹¹³, ionic gelation¹¹⁴, polymerization¹¹⁵ and emulsification (solvent displacement or diffusion)^{116,117}. More recently, the technological advances and progresses has allowed the formulation of polymeric NPs by microfluidic process to obtain outstanding reproducibility and controlled assembly^{118,119}.

By modulating the composition and the formulation process, diverse structure of polymeric NPs can be obtained^{106,120}. Nanospheres and nanocapsules are the most common forms of polymeric NPs, characterized by a solid matrix system and a vesicle surrounded by a polymeric shell respectively. Furthermore, other shapes of

polymeric NPs can be obtained such as micelles, polymersomes and dendrimers. Micelles and polymersomes are typically made of amphiphilic block copolymers exhibiting both hydrophobic and hydrophilic areas whereas dendrimers are hyperbranched polymers with complex three-dimensional architectures. These various structures lead to variable drug delivery capabilities in which therapeutics can be entrapped in the polymer matrix, encapsulated within the core or bound to the surface, ensuring its protection and delivery. The different structures of the main shapes of polymeric NPs are schematized in **Erreur ! Source du renvoi introuvable.**

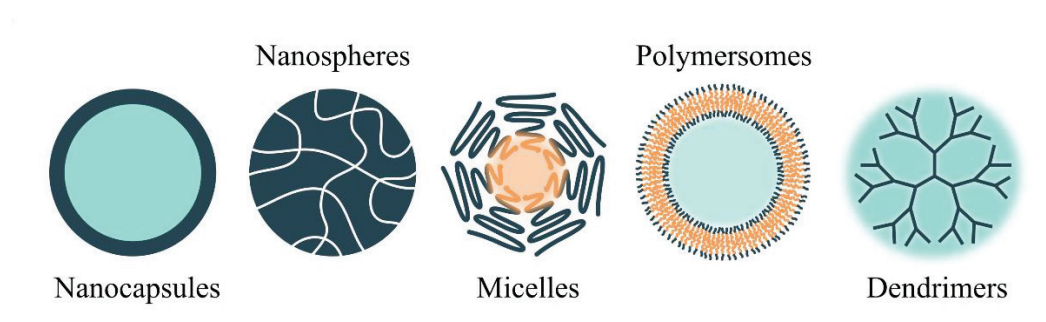


Figure 2: Schematic representation of the most common classes of polymeric nanoparticles

These conventional systems offer extensive biological advantages as they can be designed to obtain biocompatible, biodegradable, non-immunogenic and non-toxic nanosystems. The polymer of choice, as well as the products of its degradation, needs to be nontoxic to induce a minor *in vivo* inflammatory response. Contrary to synthetic polymers that are easier to produce, natural polymers from various origins (microbial, vegetal or animal) confers interesting biological benefits and biomimetic character^{95,121}. Among the most common natural polymers; chitosan¹²², gelatin¹²³, alginate¹²⁴ and hyaluronic acid (HA)¹²⁵ have been the most widely investigated for biomedical use as nanocarriers.

Interestingly, recent advances in synthesis of functionalized or stimuli-responsive polymers allowed the innovative design of surface-functionalized or activation-modulated polymeric NPs. Surface functionalization is made by various modifications such as functionalization with peptides, proteins or antibodies, obtained by absorption, covalently bounding or bio-conjugation¹²⁶. These surface modifications are mainly designed with the aim to improve the physiochemical

properties and targeting performance of the nanosystems. On the other hand, responsive-polymers are designed to achieve remote controlled release of the therapeutic agent by various stimulus-induced response (physical, chemical, biochemical or environmental)¹¹².

2.2.1.1. Hyaluronic acid

HA is a high molecular weight glycosaminoglycan formed by several identical subunits (D-glucuronic acid and N-acetyl- D-glucosamine disaccharide linked together by glycosidic bonds (see Figure 3). This natural polymer has been widely use in the pharmaceutical field thanks to its biocompatibility, biodegradability, non-toxicity, and non-immunogenicity properties¹²⁵. Moreover, HA is a component of the extracellular matrix (ECM) that play essential physiological roles, especially in organ structural stability and tissue organization.

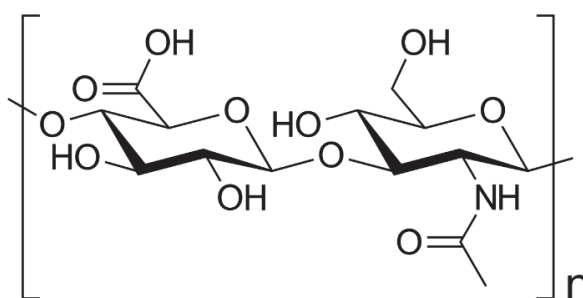


Figure 3: structure of HA monomer

One main advantage of HA as nanocarriers is that HA backbone itself can specifically recognize and interact with different cell surface proteins: among them, the most studied is CD44 receptor¹²⁷. CD44 receptors are widely-distributed type 1 transmembrane glycoprotein that binds HA and are involved in cell proliferation, adhesion, migration, hematopoiesis and lymphocyte activation. Moreover, it has been widely described that CD44 are overexpressed in cancer cells and are crucial modulator of early myogenesis^{128,129}. Thus, HA-CD44 interactions represent a potential targeting way for increasing accumulation of associated drug in CD44-expressing cells.

The strength of this natural polymer relies on his carboxylic group present in each glucuronic unit which provide a high negatively charged character enabling interactions with cationic polymers or molecules¹³⁰. Such nanosystems are

generally obtained through formation of self-assembling micelles, chemical conjugation *via* cross-linking approaches or ionic gelation^{130,131}.

2.2.1.1. Poly(L-arginine)

Poly(L-arginine) (PArg) is a peptide containing multiple arginine moieties that carry positive charge through their guanidine group (see Figure 4). This positively charged polymer belonging to the class of cell penetrating peptide (CPP). CPP are short amino acid sequences that facilitate cellular intake and uptake of molecules¹³². Most of these polymers are not cell type or tissue specific and most rely on the interactions of the positively charged amino acids at physiological pH with the negatively charged cell surface glycoproteins^{133,134}.

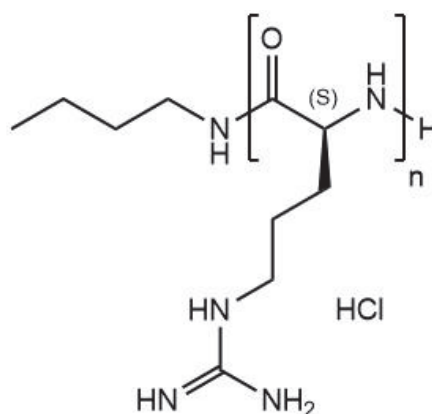


Figure 4: structure of PArg monomer

Beyond this cell penetrating properties, due to its polycationic nature, PArg is a widely used component to build polyelectrolyte multilayers. PArg has been many used as cross-linking of HA to form nanostructures through ionic gelation technic¹³⁵. Thus, different surface charged particles may be obtained by modulating the charge ratio PArg/HA. Previous work has demonstrated the ability of such HA/PArg systems to associate platinum-based drugs or PTM¹³⁶⁻¹³⁸.

Overall, polymeric NPs are suitable candidates for therapeutic agent delivery through their interesting biological advantages, range of formulation process, as well as for their targeting or controlled release abilities.

2.2.2. Lipid-based nanoparticles

Two main families of lipid-based nanoparticles have been proposed: nanoemulsions made essentially of lipids/phospholipids and liposomes/lipid-based nanoparticles only composed of phospholipids.

2.2.2.1. Lipid nanoparticles for hydrophobic drug delivery

Nanoemulsions are dispersion of two immiscible liquids stabilized using appropriate surfactants. Over the last century, nanoemulsions have received great attention in drug discovery through their capability to solubilize very hydrophobic drugs that are hardly deliverable with conventional administration method. Thereby it provides a pathway to drastically increase rate of drug dissolution and prolonged half-life, subsequently enhancing systemic bioavailability. The composition influences the structure of nanoemulsion and particularly regarding the core of the nanoparticles. Lipid nanoemulsions are classically composed of a liquid core while solid lipid nanoparticles (SLN) consist of a core of solid lipids, in which the hydrophobic drug is embedded^{139,140}. More recently, nanostructured lipid carriers (NLC) have been designed as second-generation of SLN and are characterized by a partially crystallized lipid matrix with a poorly ordered structure^{141,142}. This blend of solid and liquid lipids significantly enhances the drug loading capability and physicochemical stability while reducing the risk of uncontrolled release during storage¹⁴³. The different structures of these different lipid nanoparticles are schematized in the Figure 5.

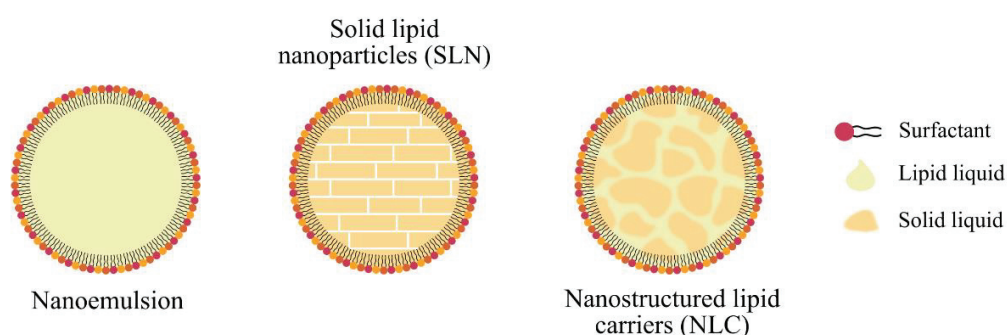


Figure 5: Schematic representation of the different structures of lipid nanoemulsion

On the other hand, lipid-based nanoparticles like liposomes are mainly composed of phospholipids. This kind of lipid nanoparticles have emerged across the

pharmaceutical industry as promising vehicles to deliver a variety of therapeutics. Among them, liposomes are the first nanomedicine that have been successfully translated to clinical application with the FDA approval of the liposomal form of Doxorubicin (Doxil®) in 1995¹⁰¹. Nowadays, a relevant number of liposomal drugs have been approved and applied to medical practice for cancer therapy, fungal diseases, analgesics or even viral vaccines^{144–146}. This well studied class of drug carriers is characterized by the presence of a self-assembled lipid bilayer enclosing an interior aqueous compartment^{147,148}. With their ability to encapsulate and deliver hydrophobic and hydrophilic drugs in the lipid bilayer and aqueous compartment respectively, liposomes provide a versatile platform for the treatment of a variety of diseases.

2.2.2.2. *Lipid nanoparticles for gene delivery*

Progress in understanding of the genetics of cellular pathogenesis has made possible therapeutic targeting of numerous genes involved in human diseases, opening the way to gene and oligonucleotide-based therapy^{149–153}. Over the last years, lipid-based nanoparticles have demonstrated their efficiency to overcome the limitations related to the cellular delivery of nucleic acids. Furthermore, contrary to viral vectors that are the most currently used vector for nucleic acids delivery, lipid-based nanoparticles have higher packaging capacity and are designed to be safe without inducing immune response⁷⁹. Recent achievements carried out on lipid nanoparticles enabling gene therapy with the approval of treatment for rare disease as Onpattro® and the development of mRNA-vaccines during Sars-Cov-2 pandemic highlights the fast-growing interest for this promising field^{103,104,154}. Lipid nanoparticles offer numerous advantages for nucleic acid delivery including modularity, ease of formulation, large payload capacity and low cytotoxicity and immunogenicity.

Owing to the modularity of the lipid composition, many lipid nanoparticles have been proposed for delivery of different types of nucleic acid^{149,155,156}. To this end, several innovative lipids have been developed and are categorized into: cationic lipid, helper lipid, ionizable lipid and gene lipid-conjugates. An overview of the different lipids commonly used is given in the Figure 6.

- *Cationic lipid*: Cationic lipids typically feature a positively permanent charged head group followed by hydrophobic tails of varying structure^{157,158}. This kind of lipids are useful to condense and deliver anionic nucleic acids through electrostatic interactions. By modulating the ratio of cationic lipids and nucleic acids (namely defined as N/P ratio in which N correspond to the number of moles of amine groups and P of phosphate groups), efficiency of the nanosystems may be modulated.
- *Helper lipid*: Helper lipids are typically included to provide particle stability and delivery efficiency^{159,160}. Through their cone-shape geometry, these lipids cause destabilization of the endosomal membrane by favoring the formation of non-bilayer hexagonal II phase, promoting cytoplasmic delivery of nucleic acids.
- *Ionizable lipid*: Ionizable lipids are neutral lipids at physiological pH that became protonated and thereby positively charged at acidic pH^{161,162}. These characteristics promote nucleic acid association, extending circulation time after administration while enhancing endosomal escape and cytoplasmic cargo release through the fusion/disruption with the endosomal membrane.
- *Lipid-conjugates*: Different types of others lipids are commonly used in combination to the ones presented above. Neutral phospholipids and cholesterol have been mainly described in the composition of lipid nanoparticles for their contributions to the structural integrity and rigidity and phase transition behavior, ensuring appropriate encapsulation of the payload and stability over time¹⁶³. PEG-lipids are another important component that plays several roles^{164,165}. Their hydrophilic-hydrophobic structure represents a steric barrier preventing binding of plasma proteins and thereby their rapid clearance by the reticuloendothelial system. Furthermore, PEG-lipids are interesting for particle size and stability properties as they confer steric repulsion between nanoparticles.

Aside from their interesting modularity through their wide possible composition, one of the main advantages of lipid nanoparticles is their ease of manufacturing. Solvent diffusion is the most used technic that consist in solubilizing lipids in

ethanol and further disperse the lipid in solution in an aqueous phase to cause the precipitation of lipid molecules, which lead to the formation of the nanoparticles¹⁶⁶. Nowadays, microfluidic technic represents the most appropriate method to obtain lipid nanoparticles through solvent diffusion¹⁶⁷. The fast and efficient mixing of the organic and aqueous phase leads to a rapid production of nanoparticles while ensuring a robust and high reproducibility. Furthermore, the physico-chemical properties can be easily modulated through the different microfluidic parameters including speed workflow and organic-aqueous phase ratio.

Lipid nanoparticles associated with nucleic acids are characterized by typical and characterizable structures¹⁶⁸⁻¹⁷⁰. Two main different types of structures are observed for these self-assembled particles, including lipid nanoparticles with nanostructured cores and multilamellar particles (Figure 7). Lipid nanoparticles with nanostructured cores exhibit an inverted hexagonal structure in which nucleic acids are both adsorbed on the surface and entrapped into aqueous compartment present in the particle core^{171,172}. On the other hand, multilamellar particles (often named as lipoplexes) are composed of concentric lamellae alternating lipid bilayers and nucleic acid monolayer condensed between them^{173,174}.

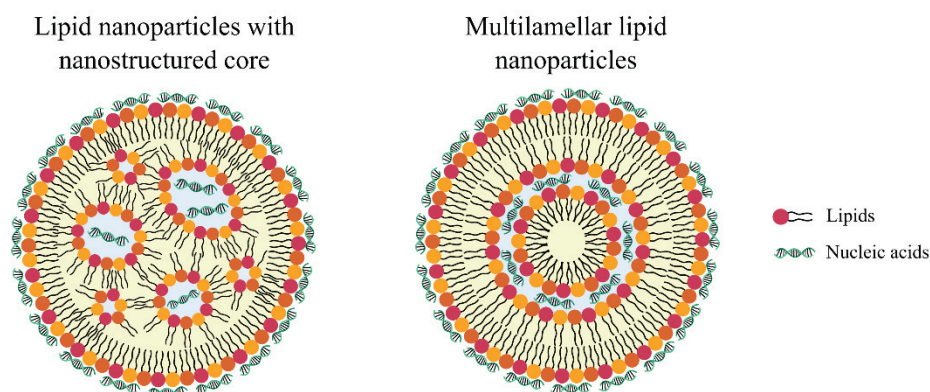


Figure 7: Schematic representation of the suggested structure of lipid nanoparticles nucleic acid carriers: lipid nanoparticles with nanostructured core and multilamellar lipid nanoparticles.

Overall, lipid-based nanoparticles represent promising and suitable type of nanoparticles to condense, deliver and intracellularly release different types of nucleic acids through their high modularity.

3. Aim of the work

The aim of this thesis is to design nanomedicine as non-viral delivery approach for the treatment of DM1. Therefore, this research project focused on two different therapeutic strategies that act at different levels of the pathological mechanism of DM1: i) inhibition of MBNL1 sequestration through the delivery of a small molecule and ii) degradation of DMPK CUG-containing transcripts via nucleic acid delivery.

The first strategy adopted was focused on the design and characterization of HA and PArg based nanoparticles (HA-PArg NPs) for the encapsulation of a small molecule, the pentamidine (PTM). Based on previous results obtained and among the scientific literature, PTM has been chosen in a context of drug repurposing to reverse the splicing defects associated in DM1. The biocompatibility, intracellular internalization and fate in C2C12 murine skeletal muscle cells and explanted murine skeletal muscle of HA-PArg NPs was studied. Finally, the therapeutic efficiency of PTM-loaded HA-PArg NPs has been tested in a DM1 cell model, established by inducing CTG expansion on the DMPK gene of C2C12 cells.

Motivated by the potential of a gene-therapy-based approach to promote targeted, efficient and long-term treatments for genetic disease, the second strategy adopted in this project was focused on the development of nucleic acid delivery using lipid-based nanoparticles. In this work the efficiency of lipid nanoparticles to deliver different types of nucleic acids such as pDNA, mRNA and siRNA was investigated in C2C12 muscle cells using green fluorescent protein (GFP) protein as reported gene, paving the way for the delivery of therapeutic sequences.

For both strategies, the following methodology has been adopted to succeed in the different objectives:

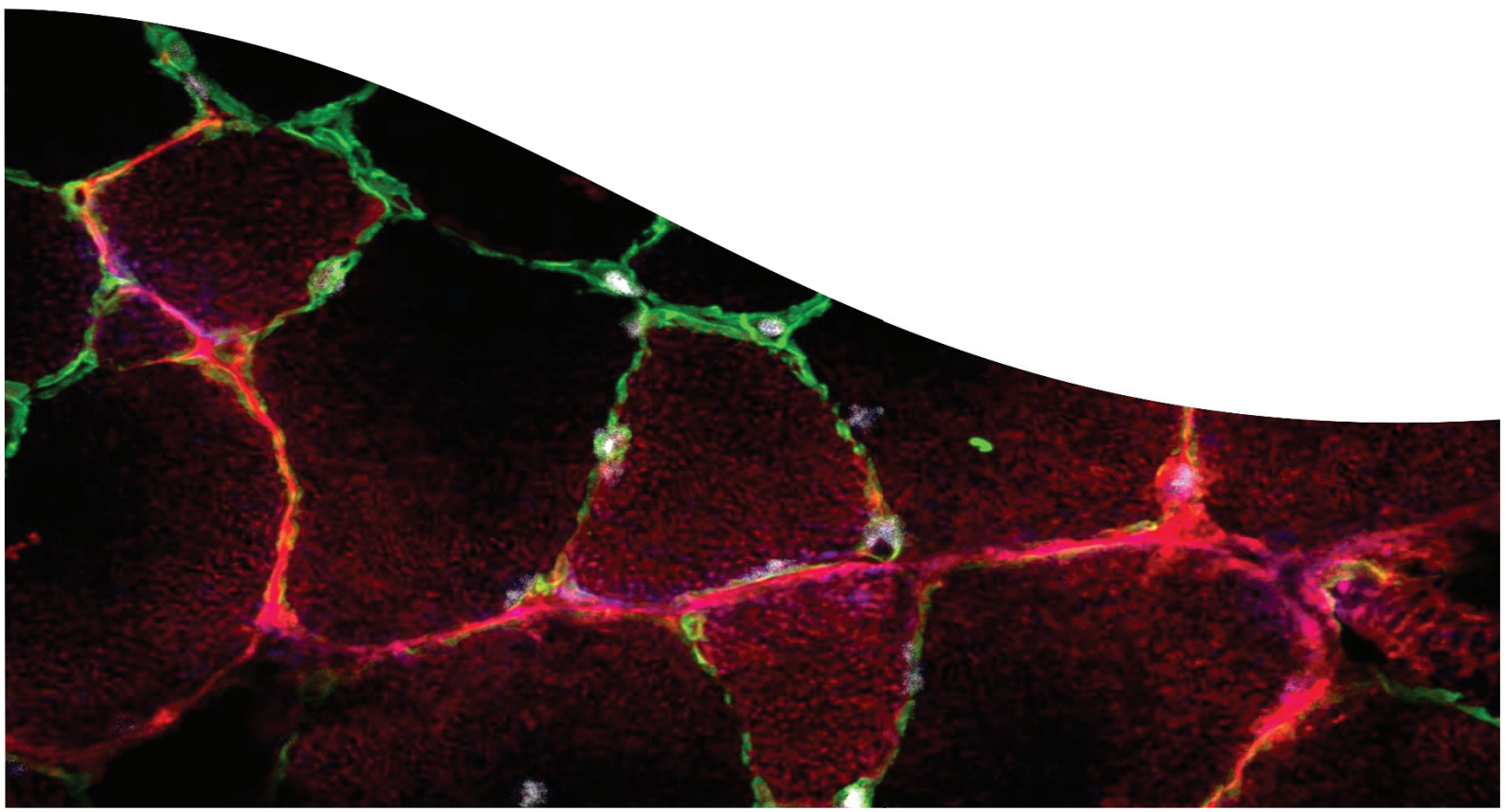
- Step 1: Based on the literature, screening of the active agent to select the most suitable nanomedicine strategy.
- Step 2: Development and optimization of the nanomedicine associated with the active agent and characterization of the nanosystems obtained in terms of physico-chemical properties, encapsulation efficiency, morphology and

stability. The objective of this step was to determine the nanocarriers that suit the most to be tested *in vitro*.

- Step 3: *In vitro* evaluation of nanomedicine in cultured skeletal muscle cell lines to assess the toxicity, internalization rate and/or mechanism, intracellular fate and therapeutic efficacy. This crucial step was required to determine the most efficient and suitable nanosystems that could be tested *in vivo*.
- Step 4: *Ex vivo* or *in vivo* testing of nanomedicine in healthy mice to assess the biodistribution of the nanosystems from the perspective of determining the most promising nanocarriers to be tested for therapeutic efficacy in mice model of DM1.

In conclusion, the different strategies and approaches adopted together with a pertinent step-by-step methodology aim to provide biocompatible delivery system able to administrate therapeutic agents to halt progression or even reverse the consequences of the genetic damage of DM1, from the perspective to tackle the unmet clinical need.

RESULTS



RESULTS

The main goal of this research project is to provide and investigate nanocarriers as efficient drug and gene delivery approach in skeletal muscle. To this end, results obtained have been divided in 5 chapters.

The first chapter contains two bibliographic studies. The first study is a brief review on the contribution of transmission and scanning electron microscopy to the characterization of nanoparticles in the biological environment, in particular to the study of their interactions with cell and tissue components. Moreover, the advantages and limits of ultrastructural techniques to evaluate the suitability of nanocarriers as drug-delivery systems were discussed. This review has been published in the journal “Microscopie”. The second study is an extensive review of the different nanosystems described in literature for MDs treatment. It focuses on nanomedicine approaches able to deliver small chemical molecules and nucleic acids to target the most common MDs. Then, the challenge related to *in vitro* and *in vivo* testing in appropriate animal models are discussed. Finally, a critical view in future developments of nanomedicine for MDs is provided. This review has been published in the journal “Pharmaceutics”.

The second chapter of this thesis is focused on the repurposing of PTM as DM1 treatment and follow on from previous work by our research groups to associate PTM to HA-based NPs¹³⁷. The resulting selected formulation gave raise to NPs of about 200 nm, negatively charged and with polydispersity index lower than 0.1. Furthermore, this nanosystem demonstrated to efficiently associate PTM with an encapsulation efficiency up to 80 % and with a loading efficiency of 15 %. This study aims to investigate HA-PArg NPs as nanocarriers for PTM delivery in murine skeletal muscle cells and organs. This work has been submitted in the journal “Nanomedicine: Nanotechnology, Biology and Medicine” and is actually under review.

The third chapter describes the innovative application of the Alcian blue staining, a long-established histochemical method for detecting glycosaminoglycans in tissue sections, applied to HA-based NPs. This original application was performed to overcome the problem of weak electron density from HA-based NPs and allows their visualization at both light and transmission electron microscope. This technique has been described in a technical note published in the “European Journal of Histochemistry”, and the detailed experimental protocol of the Alcian blue staining has been accepted for publication in the volume “Histochemistry of Single Molecules: Methods and Protocols, as of the Second Edition” that will appear in the book series “Methods in Molecular Biology” by Springer. This paper is currently in press.

The fourth chapter of this project is related to the optimization of LNP to deliver different types of nucleic acids in murine skeletal muscle cells. This high optimization process was performed in the objective to load a DM1 therapeutic nucleic acid sequence in LNP. These results are based on preliminary data by our groups for another purpose, that selected the LNP composition for mRNA delivery. In this chapter, different types and molecular weights of nucleic acid were associated to LNP and tested for modulating protein expression in order to open the range of possibilities to several gene therapy strategies for DM1. A scientific publication is actually on preparation regarding the results obtained in this chapter.

Finally, the last chapter presents the preliminary data related to the delivery of a DM1 therapeutic ASO sequence, using the previously optimized LNP system. The objective of this investigation is to provide a suitable nanosystem to be tested *in vitro* and *in vivo* in DM1 cell and animal models.

CHAPTER 1

Bibliographic studies

**Electron microscopy to characterize nanoparticles in the
biological environment**

M. Repellin, F. Carton

Microscopie (2019)

SCIENTIFIC ARTICLES

Electron microscopy to characterise nanoparticles in the biological environment

Mathieu Repellin, Flavia Carton

Department of Neurosciences, Biomedicine and Movement Sciences, Anatomy and Histology Section, University of Verona, Italy

Corresponding author: Flavia Carton, Department of Neuroscience, Biomedicine and Movement Sciences, Anatomy and Histology Section, University of Verona, Strada Le Grazie 8, 37134 Verona, Italy.
Tel. +39.045.8027561.
E-mail: flavia.carton@univr.it

Key words: Biodistribution; cellular uptake; drug delivery; nanomedicine.

SUMMARY

Nowadays the use of nanomaterials has led a growing interest in biomedical application as drug delivery systems for the treatment and the diagnosis of different pathologies. Different analytical techniques have been applied to characterise nanoparticles in the biological environment. However, in the attempt to describe in detail the interaction of NPs with the living systems and to detect the possible occurrence of cell damage or death, electron microscopies proved to be especially suitable and actually are irreplaceable techniques thanks to their image resolution at the nanoscale. In this review article, the attention will first be focused on the influence of nanoparticles features on their interaction with tissues and cells; then, the advantages and limits of transmission and scanning electron microscopy to evaluate the suitability of nanovectors as drug-delivery systems will be discussed.

Received for publication: 26 March 2019. Accepted for publication: 28 March 2019.

©Copyright M. Repellin and F. Carton, 2019

Licensee PAGEPress, Italy

microscopie 2019; 30:8188

doi:10.4081/microscopie.2019.8188

This article is distributed under the terms of the Creative Commons Attribution Noncommercial License (by-nc 4.0) which permits any noncommercial use, distribution, and reproduction in any medium, provided the original author(s) and source are credited.

Introduction

Nowadays the use of nanomaterials has led a growing interest in biomedical application as drug delivery systems for the treatment and the diagnosis of different pathologies. The delivery of therapeutic agents through nanoparticles represents an attractive option in the attempt i) to protect the therapeutics from enzymatic degradation, ii) to tune the biodistribution and targeting after systemic administration, iii) to prolong the drug circulation, and iv) to reduce the systemic toxicity of therapeutics.

According to the European Commission, “nanomaterial” means “a natural, incidental or manufactured material containing particles, in an unbound state or as an aggregate or as an agglomerate and where, for 50% or more of the particles in the number size distribution, one or more external dimensions is in the size range 1 nm - 100 nm” (http://ec.europa.eu/environment/chemicals/nanotech/faq/definition_en.htm).

Due to their small size, nanoparticles (NPs) should -at least in principle- easily enter the tissues and cells, but the biomedical impact they have on *in vitro* and *in vivo* systems are closely related to their physicochemical properties (Lin *et al.*, 2014). When nanomaterials, particularly NPs, are injected into a live organism, they come into contact with a complex physiological environment (the biological fluids, tissues, intercellular matrix and cells) (Kettiger *et al.*, 2013), the interaction with the biological components depending on the nature of the NPs such as their chemical composition, size/size distribution, shape and surface properties. To enter a cell, NPs must contact with the plasma membrane, and the mode of uptake and intracellular interaction with specific organelles is crucial to make a drug-delivery system biocompatible and effective. On the other hand, the structural and molecular features of the cells also affect the efficiency of NP uptake.

Different analytical techniques have been applied to study NPs especially as drug-delivery systems (Figure 1). However, in the attempt to describe in detail the interaction of NPs with the living systems and to detect the possible occurrence of cell damage or death, electron microscopies proved to be especially suitable and actually are irreplaceable techniques thanks to their image resolution at the nanoscale (Reifarth *et al.*, 2018).

In this review article, the attention will first be focused on the geometrical and surface properties of nanovectors that are especially important for their capability to interact with tissues and cells; then, the advantages and limits of transmission and scanning electron microscopy (TEM and SEM, respectively) to evaluate the suitability of nanovectors as drug-delivery systems will be discussed.

Influence of nanoparticle size, shape and surface properties on their interaction with the biological environment

The size strongly influences the impact NPs have on living organisms. Half-time circulation, tissue biodistribution, interactions/uptake at the cellular level, and intracellular trafficking/removal are all parameters that are affected by the particle size (Duan and Li, 2013; Kettiger *et al.*, 2013).

Regarding NP delivery in the whole organism, previous studies have demonstrated that after systemic administration small NPs (10-20 nm) are able to easily pass through the thin endothelial junction reaching different organs and tissues (Duan and Li, 2013). Small NPs are also characterized by a faster renal clearance in comparison to the bigger ones; for very large NPs (>1 μm) the clearance should also be fast, but they tend to more easily aggregate inside the blood vessel causing a mechanical retention by capillaries with a low distribution into tissue. Based on these considerations, NPs having a size between 20 and 100 nm are considered as the more suitable in terms of circulation time, biodistribution and clearance (Choi *et al.*, 2007).

At the cellular level, the NPs size has a great impact on the mechanisms of uptake and cell internalization. Normally, only lipid-soluble NPs presenting a size lower than 30 nm are able to directly cross the cellular membrane (Kettler *et al.*, 2014), whereas the uptake of bigger NPs often occurs through active, energy-dependent processes. The main mechanisms of uptake in eukaryotic cells are endocytosis (often receptor-mediated), pinocytosis and phagocytosis. In general, NPs having a size <100 nm can enter by pinocytotic pathways, whereas NPs with a size range between 120-150 nm principally enter by receptor-mediated endocytosis; NPs ranging 250 nm to 3 μm have been shown to mainly enter by phagocytosis (Foroozandeh and Aziz, 2018). The size of NPs not only influences the uptake mechanism but also affects its efficiency. Works in the literature demonstrated that the concentration of saturation as well as the uptake efficiency of NPs having a diameter around 50 nm are higher than the ones of larger NPs (Soppimath *et al.*, 2001; Mailänder and Landfester, 2009; Kumari and Yadav, 2011). It is however worth recalling that the uptake of NPs is also largely dependent on the cell type (Adjei *et al.*, 2014).

From the biological point of view, NP shape may affect the circulation time, biodistribution, targeting efficiency, cell internalization and intracellular fate (Champion and Mitragotri, 2006; Geng *et al.*, 2007; Gratton *et al.*, 2008; Muro *et al.*, 2008). Regarding the circulation life, NP shape may significantly influence the phagocytotic process by macrophagic cells: it has already been shown that NPs with one elongated axis have a longer circulation time being less

SCIENTIFIC ARTICLES

prone to be phagocytosed by macrophages (Duan and Li, 2013). Moreover, concerning the circulation profile, non-spherical shapes influence NPs *in vivo* distribution in target organs such as spleen (Devarajan *et al.*, 2010), lung (Decuzzi *et al.*, 2010) and tumour tissues (Christian *et al.*, 2009). On the other hand, *in vitro* studies demonstrated that round NPs more easily enter the cells compared to the rod-shaped ones (Wilhelm *et al.*, 2003; Limbach *et al.*, 2005).

Several studies *in vitro* and *in vivo* have also underlined the importance of the NP surface properties regarding the interaction with the anionic cell membrane, the cellular uptake and the intracellular behaviour.

Following cellular uptake, NPs interact with the intracellular milieu (cytosolic component and organelles), and their intracellular distribution and location (in the cytoplasm or the nucleus) are crucial for their functional effects. Depending on their chemical composition, NPs may target cytoplasmic organelles (such as the mitochondria, the Golgi complex or the endoplasmic reticulum) or enter the nucleus. For instance, the physicochemical characteristics of the NP surface influence the penetration through the mitochondrial

membrane (Adjei *et al.*, 2014). An intranuclear localization is required when the drug or genetic material the nanocarrier is loaded with must interact with the nuclear chromatin, but the penetration into the nucleus is strongly dependent on the dimension of the drug-loaded NPs (it is to be taken into account that molecular complexes smaller than 45 kDa are able to easily penetrate the nuclear envelope whereas the nuclear pore complexes are responsible for the transport of larger macromolecular complexes) (Adam *et al.*, 1990; Hagstrom *et al.*, 1997; Hillaireau and Couvreur, 2009).

Electron microscopy is the most adequate approach for visualizing NP-cell interactions

To visualize the uptake, intracellular distribution and degradation/release of NPs, appropriate microscopy techniques are used (Figure 1). Both light and electron microscopy may be exploited to characterize the cellular fate and performance of NPs (Costanzo *et al.*, 2017).

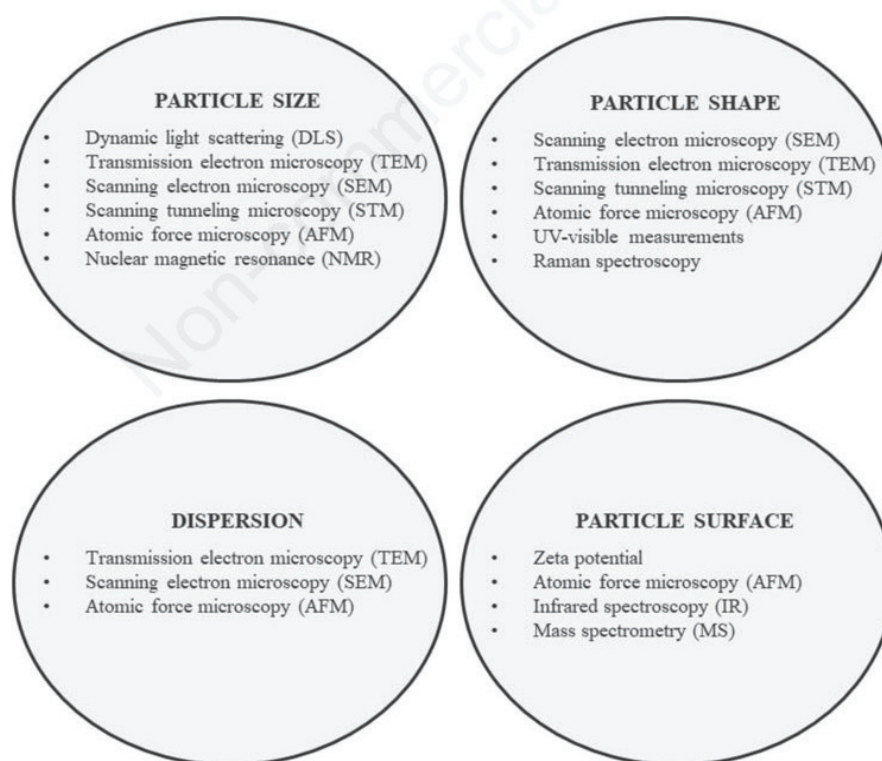


Figure 1. Techniques commonly used for the characterization of nanomaterials.

Conventional and confocal fluorescence microscopy allow to locate properly labelled nanoconstructs at the surface or inside the cells (Costanzo *et al.*, 2016), and super-resolution microscopy promises to be adequate for tracking them at the subcellular level (Jin *et al.*, 2018; Shang *et al.*, 2018); however, TEM and SEM, thanks to their much higher resolution, are the techniques of choice to investigate nanostructured materials inside the cells at the nanoscale.

SEM, as a surface imaging technique, is a powerful and popular approach to acquire information on the size, shape and surface morphology of nanomaterials (Lin *et al.*, 2014), as well as to elucidate the interaction of NPs with the plasma membrane: as a consequence of its great depth of focus, SEM provides detailed three-dimensional topographic images of the cell surface, thus being particularly appropriate to get insight into the mechanisms of NP internalization. Besides the morphological evidence, SEM may also allow to collect information on the chemical composition through the analysis of the element-specific X-ray emission (Hall *et al.*, 2007; Wang and Lee, 2008): this would especially be useful to discriminate the simultaneous presence at the cell surface of NPs with different metal components.

Analyzing the cell surface by SEM usually needs to dehydrate the biological samples and make the surface conductive, by coating with a thin metallic layer: as a negative aspect of this procedure, alteration of the plasmalemmal structures (such as microvilli or caveolae) or shrinkage of the NPs may occur (Boots *et al.*, 2004). It is however worth recalling that the possibility exists to operate at low voltage with environmental SEM (ESEM): thanks to a partial vacuum, high humidity level and a lower energetic beam, this instrument allows obtaining reasonably good images of still partially hydrated biological samples in the absence of conductive coating (Perez-Arantegui and Mulvey, 2005). Nonetheless, this method engenders a lower resolution imaging (Oatley *et al.*, 1966). Another drawback of SEM for NP investigation is that image pixels are collected one by one by scanning the sample surface, which leads to a long exposure time to the electron beam that may cause degradation of beam-sensitive NPs (Klang *et al.*, 2013).

TEM is the most exploited tool for characterizing nanomaterials as it provides images at higher spatial resolution than SEM, from the micrometer level up to the sub-nanometric or atomic level.

First, TEM can be used to characterize newly synthesized nanomaterials: observing dispersed NPs on formvar-coated grids it is possible to acquire information on the size, size distribution and shape of the nanoconstructs as well as on the interparticle interaction (aggregation or dispersion). When coupled with the appropriate analytical techniques through the electron interaction with the sample, TEM can

also supply data on the chemical composition of nanomaterials (Kettiger *et al.*, 2013).

In thin sections of resin-embedded samples the internal NP morphology may be investigated (Kola-Mustapha, 2019), while freeze-fracture techniques are suitable to elucidate the inner organization, crystallinity and granularity of NPs (in fact, the sample is vitrified by rapid freezing and then fractured, thus adequately preserving the native state) (Kuntsche *et al.*, 2011). This latter technique is also appropriate to observe the physico-chemical modifications of the nanovectors upon drug incorporation.

However, the most significant application of TEM in the field of nanobiology is for investigating the behavior of NPs while interacting with cells. By SEM, the NP interaction with the plasma membrane can be observed, but the cellular uptake and the intracellular dynamics of the nanoconstructs may be more accurately described using TEM on thin sections, by taking static snapshots of the events occurring within a tissue or a cell at different times upon NP administration (Figure 2).

These investigations at the cellular level are crucial, once a new synthesized nanomaterial is characterized physico-chemically, in order to understand its effects and possible toxicity (Klang *et al.*, 2013).

Indeed, TEM provides images *in situ* of the biological mechanisms responsible for the internalization and eventual interaction of NPs with specific organelles.

The chemical nature of the nanosystems is responsible for their uptake as single particles or multi-particulate aggregates; furthermore, in the literature detailed ultrastructural reports were published demonstrating how NPs of different composition enter the cells, either associated with intracellular vesicles following the endocytic or phagocytic process or occurring free in the cytosol (Park *et al.*, 2006; Grant and Donaldson, 2009; Martens *et al.*, 2014; Venkatachalam *et al.*, 2015; Costanzo *et al.*, 2016; Wong *et al.*, 2017; Guglielmi *et al.*, 2019). When endocytosed, NPs generally follow the lysosomal pathway, while when free in the cytosol, they may interact with (and eventually penetrate) organelles such as the mitochondria or the nucleus. In the former case, NP degradation by the lysosomal enzymes is likely to occur, although ultrastructural evidence has sometimes been provided for the mechanism of endosomal escape (Hillaireau and Couvreur, 2009; Martens *et al.*, 2014; Wong *et al.*, 2017; Foroozandeh and Aziz, 2018; Guglielmi *et al.*, 2019), by which a membrane-bounded NP may exit the organelle to be released in the cytosol. On the other hand, cytosolic NP may re-enter the endo-lysosomal pathway through autophagic processes (Costanzo *et al.*, 2016).

Thus, depending on their chemical and physical properties NPs may interact with intracellular organelles and

SCIENTIFIC ARTICLES

undergo rupture and degradation by completely different and often peculiar ways that obviously affect the intracellular release (and the action) of the loaded drugs (Malatesta,

2016). In addition, it is worth reminding that the same nanoconstruct may differently behave (as for the uptake and degradation) in cells of different origin.

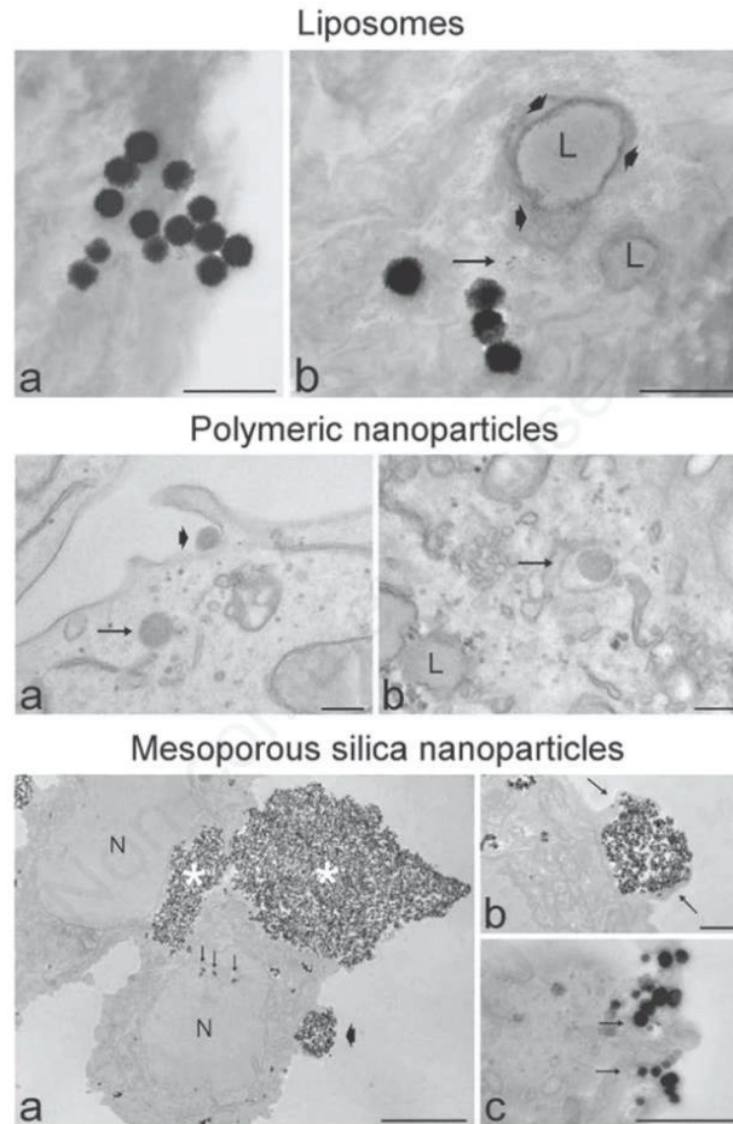


Figure 2. Interactions between different NPs and cultured cells analysed at TEM. Liposomes: a) Several liposomes enter the cell apparently without endocytotic process and occur free in the cytoplasm; note their loose filamentous periphery. b) Electron dense fine granular material (arrow) occur in the cytosol in close proximity to liposomes and lipid droplets (L); scale bars: 500 nm. Polymeric nanoparticles: a) Two NPs occurs at the cell periphery: one adhering to the cell surface (arrowhead), the other freely distributed in the cytosol (arrow). b) A NP is enclosed in an endosome (arrow). Scale bars: 200 nm. Mesoporous silica nanoparticles: a) Large aggregates of NPs occur at the cell surface (asterisks); small clusters of NPs are visible inside the cytoplasm, even inside nuclear invaginations (arrows); the arrowhead indicates the detail showed in b. b) A NP cluster is internalised *via* phagocytosis by the extrusion of pseudopodia (arrows). c) Small clusters of NPs enter the cells by endocytosis (arrows). Scale bars: a) 5 μ m; b,c) 500 nm. Adapted from Costanzo *et al.*, *Eur J Histochem* 2016;60:2640.

Concluding remarks

Nanoconstructs for biomedical applications are synthesized starting from biocompatible compounds and tested to confirm their low cytotoxicity. This is obviously correct but the ever growing experimental evidence demonstrates that to validate a nanovector of whatever nature as an efficient drug-delivery system it is necessary to exhaustively know how it behaves once inside the target cell.

To track NP presence, dynamic relocation and ultimate disposal, imaging techniques are needed: among them, electron microscopies are undoubtedly the most appropriate and versatile tools.

They surely have important drawbacks: the procedures for sample preparation are often complicated and time-consuming, the application of histochemical methods to chemically characterize the specimens are much trickier than in light microscopy, and the need to operate in the vacuum makes the artefactual dehydration and coating/embedding mandatory. However, despite these limits, SEM and especially TEM will remain unreplacable for nanomedical research also in the years to come.

Acknowledgments

M.R. is a PhD student in receipt of a fellowship from the INVITE project of the University of Verona, (PhD Programme in Nanoscience and Advanced Technologies). This project has received funding from the European Union's Horizon 2020 Research and Innovation Programme under the Marie Skłodowska-Curie grant agreement No. 754345.

References

- Adam SA, Marr RS, Gerace L. Nuclear protein import in permeabilized mammalian cells requires soluble cytoplasmic factors. *J Cell Biol* 1990;111:807-16.
- Adjei IM, Sharma B, Labhasetwar V. Nanoparticles: cellular uptake and cytotoxicity. *Adv Exp Med Biol* 2014;811:73-91.
- Bootz A, Vogel V, Schubert D, Kreuter J. Comparison of scanning EM, dynamic light scattering and analytical ultracentrifugation for the sizing of poly(butyl cyanoacrylate) nanoparticles. *Eur J Pharm Biopharm* 2004;57:369-75.
- Champion JA, Mitragotri S. Role of target geometry in phagocytosis. *Proc Natl Acad Sci USA* 2006;103:4930-4.
- Choi HS, Liu W, Misra P, Tanaka E, Zimmer JP, Ipe BI, et al. Renal clearance of quantum dots. *Nat Biotechnol* 2007;25:1165-70.
- Christian DA, Cai S, Garbuzenko OB, Harada T, Minko T, Discher DE. Flexible filaments for in vivo imaging and delivery: persistent circulation of filomicelles opens the dosage window for sustained tumor shrinkage. *Mol Pharm* 2009;6:1343-52.
- Costanzo M, Carton F, Marengo A, Berlier G, Stella B, Arpicco S, et al. Fluorescence and electron microscopy to visualize the intracellular fate of nanoparticles for drug delivery. *Eur J Histochem* 2016;60:2640.
- Costanzo M, Carton F, Malatesta M. Microscopy techniques in nanomedical research. *Microscopie* 2017;27:66-71.
- Decuzzi P, Godin B, Tanaka T, Lee SY, Chiappini C, Liu X, et al. Size and shape effects in the biodistribution of intravascularly injected particles. *J Control Release* 2010;14:320-7.
- Devarajan PV, Jindal AB, Patil RR, Mulla F, Gaikwad RV, Samad A. Particle shape: a new design parameter for passive targeting in splenotropic drug delivery. *J Pharm Sci* 2010;99:2576-81.
- Duan X, Li Y. Physicochemical characteristics of nanoparticles affect circulation, biodistribution, cellular internalization, and trafficking. *Small* 2013;9:1521-32.
- Foroozandeh P, Aziz AA. Insight into cellular uptake and intracellular trafficking of nanoparticles. *Nanoscale Res Lett* 2018;13:339.
- Geng Y, Dalhaimer P, Cai S, Tsai R, Tewari M, Minko T, et al. Shape effects of filaments versus spherical particles in flow and drug delivery. *Nat Nanotechnol* 2007;2:249-55.
- Grant BD, Donaldson JG. Pathways and mechanisms of endocytic recycling. *Nat Rev Mol Cell Biol* 2009;10:597-608.
- Gratton SE, Ropp PA, Pohlhaus PD, Luft JC, Madden VJ, Napier ME et al. The effect of particle design on cellular internalization pathways. *Proc Natl Acad Sci USA* 2008;105:11613-8.
- Guglielmi V, Carton F, Vattemi G, Arpicco S, Stella B, Berlier G, et al. Uptake and intracellular distribution of different types of nanoparticles in primary human myoblasts and myotubes. *Int J Pharm* 2019;560:347-56.
- Hagstrom JE, Ludtke JJ, Bassik MC, Sebesteyén MG, Adam SA, Wolff JA. Nuclear import of DNA in digitonin-permeabilized cells. *J Cell Sci* 1997;110:2323-31.
- Hall JB, Dobrovolskaia MA, Patri AK, McNeil SE. Characterization of nanoparticles for therapeutics. *Nanomedicine* 2007;2:789-803.
- Hillaireau H, Couvreur P. Nanocarriers' entry into the cell: relevance to drug delivery. *Cell Mol Life Sci* 2009;66:2873-96.
- Jin D, Xi P, Wang B, Zhang L, Enderlein J, van Oijen AM. Nanoparticles for super-resolution microscopy and sim-

SCIENTIFIC ARTICLES

- gle-molecule tracking. *Nat Methods* 2018;15:415-23.
- Kettiger H1, Schipanski A, Wick P, Huwyler J. Engineered nanomaterial uptake and tissue distribution: from cell to organism. *Int J Nanomedicine* 2013;8:3255-69.
- Kettler K, Veltman K, van de Meent D, van Wezel A, Hendriks AJ. Cellular uptake of nanoparticles as determined by particle properties, experimental conditions, and cell type. *Environ Toxicol Chem* 2014;33:481-92.
- Klang V, Valenta C, Matsko NB. Electron microscopy of pharmaceutical systems. *Micron* 2013;44:45-74.
- Kola-Mustapha AT. Microscopy of nanomaterial for drug delivery. In: Shyam SM, Shivendu R, Nandita D, Raghendra M, Sabu T. *Characterization and biology of nanomaterials for drug delivery: nanoscience and nanotechnology in drug delivery*. Amsterdam: Elsevier; 2019. pp. 265-80.
- Kumari A, Yadav SK. Cellular interactions of therapeutically delivered nanoparticles. *Expert Opin Drug Deliv* 2011;8:141-51.
- Kuntsche J, Horst JC, Bunjes H. Cryogenic transmission electron microscopy (cryo-TEM) for studying the morphology of colloidal drug delivery systems. *Int J Pharm* 2011;417:120-37.
- Limbach LK, Li Y, Grass RN, Brunner TJ, Hintermann MA, Muller M, et al. Oxide nanoparticle uptake in human lung fibroblasts: effects of particle size, agglomeration, and diffusion at low concentrations. *Environ Sci Technol* 2005;39:9370-6.
- Lin PC, Lin S, Wang PC, Sridhar R. Techniques for physicochemical characterization of nanomaterials. *Biotechnol Adv* 2014;32:711-26.
- Mailänder V, Landfester K. Interaction of nanoparticles with cells. *Biomacromolecules* 2009;10:2379-400.
- Malatesta M. Transmission electron microscopy for nanomedicine: novel applications for long-established techniques. *Eur J Histochem* 2016;60:2751.
- Martens TF, Remaut K, Demeester J, De Smedt S, Braeckmans K. Intracellular delivery of nanomaterials: how to catch endosomal escape in the act. *Nano Today* 2014;9:344-64.
- Muro S, Garnacho C, Champion JA, Leferovich J, Gajewski C, Schuchman EH, et al. Control of endothelial targeting and intracellular delivery of therapeutic enzymes by modulating the size and shape of ICAM-1-targeted carriers. *Mol Ther* 2008;16:1450-8.
- Oatley CW, Nixon WC, Pease RFW. Scanning EM. In: Marton L, Editor. *Advances in electronics and electron physics*. Amsterdam: Elsevier; 1966. pp. 181-247.
- Park M, Salgado JM, Ostroff L, Helton TD, Robinson CG, Harris KM, et al. Plasticity-induced growth of dendritic spines by exocytic trafficking from recycling endosomes. *Neuron* 2006;52:817-30.
- Perez-Arategui J, Mulvey T. Electron microscopy. In: Worsfold P, Townshend A, Poole C, Editors. *Encyclopedia of analytical science*. Amsterdam: Elsevier; 2005. pp 114-24.
- Reifarth M, Hoepfner S, Schubert US. Uptake and intracellular fate of engineered nanoparticles in mammalian cells: capabilities and limitations of transmission electron microscopy-polymer-based nanoparticles. *Adv Mater* 2018;30.
- Shang L, Gao P, Wang H, Popescu R, Gerthsen D, Nienhaus GU. Protein-based fluorescent nanoparticles for super-resolution STED imaging of live cells. *Chem Sci* 2017;8:2396-400.
- Soppimath KS, Aminabhavi TM, Kulkarni AR, Rudzinski WE. Biodegradable polymeric nanoparticles as drug delivery devices. *J Control Release* 2001;70:1-20.
- Venkatachalam K, Wong CO, Zhu MX. The role of TRPMLs in endolysosomal trafficking and function. *Cell Calcium* 2015;58:48-56.
- Wang ZL, Lee JL. Electron microscopy techniques for imaging and analysis of nanoparticles. In: Rajiv K, Mittal KL, Editors. *Developments in surface contamination and cleaning*. Amsterdam: Elsevier; 2008. pp. 396-408.
- Wilhelm C, Billotey C, Roger J, Pons JN, Bacri JC, Gazeau F. Intracellular uptake of anionic superparamagnetic nanoparticles as a function of their surface coating. *Biomaterials* 2003;24:1001-11.
- Wong CO, Gregory S, Hu H, Chao Y, Sepúlveda VE, He Y, et al. Lysosomal degradation is required for sustained phagocytosis of bacteria by macrophages. *Cell Host Microbe* 2017;21:719-30.

**Nanomedicine for gene delivery and drug repurposing in
the treatment of muscular dystrophies**

*I. Andreana, M. Repellin, F. Carton, D. Kryza, S. Briançon, B. Chazaud, R.
Mounier, S. Arpicco, M. Malatesta, B. Stella, G. Lollo*

Pharmaceutics (2021)



Review

Nanomedicine for Gene Delivery and Drug Repurposing in the Treatment of Muscular Dystrophies

Ilaria Andreana ^{1,2,†}, Mathieu Repellin ^{1,3,†}, Flavia Carton ^{3,4,†}, David Kryza ^{1,5}, Stéphanie Briançon ¹ ,
Bénédicte Chazaud ⁶ , Rémi Mounier ⁶, Silvia Arpicco ², Manuela Malatesta ³ , Barbara Stella ^{2,*}
and Giovanna Lollo ^{1,*}

- ¹ Laboratoire d'Automatique, de Génie des Procédés et de Génie Pharmaceutique, Université Claude Bernard Lyon 1, CNRS UMR 5007, 43 bd 11 Novembre 1918, 69622 Villeurbanne, France; ilaria.andreana@unito.it (I.A.); mathieu.repellin@univ-lyon1.fr (M.R.); david.kryza@univ-lyon1.fr (D.K.); stephanie.briancon@univ-lyon1.fr (S.B.)
- ² Department of Drug Science and Technology, University of Turin, Via P. Giuria 9, 10125 Torino, Italy; silvia.arpicco@unito.it
- ³ Department of Neurosciences, Biomedicine and Movement Sciences, Anatomy and Histology Section, University of Verona, Strada Le Grazie 8, 37134 Verona, Italy; flavia.carton@uniupo.it (F.C.); manuela.malatesta@univr.it (M.M.)
- ⁴ Department of Health Sciences, University of Eastern Piedmont, Via Solaroli 17, 28100 Novara, Italy
- ⁵ Hospices Civils de Lyon, 69437 Lyon, France
- ⁶ Institut NeuroMyoGène, University of Lyon, INSERM U1217, CNRS UMR 5310, 8 Avenue Rockefeller, 69008 Lyon, France; benedicte.chazaud@inserm.fr (B.C.); remi.mounier@inserm.fr (R.M.)
- * Correspondence: barbara.stella@unito.it (B.S.); giovanna.lollo@univ-lyon1.fr (G.L.); Tel.: +39-011-670-66-60 (B.S.); +33-0-4-72-44-85-84 (G.L.)
- † These authors contributed equally to this work.



Citation: Andreana, I.; Repellin, M.; Carton, F.; Kryza, D.; Briançon, S.; Chazaud, B.; Mounier, R.; Arpicco, S.; Malatesta, M.; Stella, B.; et al. Nanomedicine for Gene Delivery and Drug Repurposing in the Treatment of Muscular Dystrophies. *Pharmaceutics* **2021**, *13*, 278. <https://doi.org/10.3390/pharmaceutics13020278>

Academic Editor: Avi Domb

Received: 29 December 2020

Accepted: 14 February 2021

Published: 19 February 2021

Publisher's Note: MDPI stays neutral with regard to jurisdictional claims in published maps and institutional affiliations.



Copyright: © 2021 by the authors. Licensee MDPI, Basel, Switzerland. This article is an open access article distributed under the terms and conditions of the Creative Commons Attribution (CC BY) license (<https://creativecommons.org/licenses/by/4.0/>).

Abstract: Muscular Dystrophies (MDs) are a group of rare inherited genetic muscular pathologies encompassing a variety of clinical phenotypes, gene mutations and mechanisms of disease. MDs undergo progressive skeletal muscle degeneration causing severe health problems that lead to poor life quality, disability and premature death. There are no available therapies to counteract the causes of these diseases and conventional treatments are administered only to mitigate symptoms. Recent understanding on the pathogenetic mechanisms allowed the development of novel therapeutic strategies based on gene therapy, genome editing CRISPR/Cas9 and drug repurposing approaches. Despite the therapeutic potential of these treatments, once the actives are administered, their instability, susceptibility to degradation and toxicity limit their applications. In this frame, the design of delivery strategies based on nanomedicines holds great promise for MD treatments. This review focuses on nanomedicine approaches able to encapsulate therapeutic agents such as small chemical molecules and oligonucleotides to target the most common MDs such as Duchenne Muscular Dystrophy and the Myotonic Dystrophies. The challenge related to in vitro and in vivo testing of nanosystems in appropriate animal models is also addressed. Finally, the most promising nanomedicine-based strategies are highlighted and a critical view in future developments of nanomedicine for neuromuscular diseases is provided.

Keywords: nanoparticles; Duchenne Muscular Dystrophy; myotonic dystrophy; antisense oligonucleotides; small molecules; CRISPR/Cas9

1. Introduction

Muscular dystrophies (MDs) are a group of chronic inherited genetic diseases, with a worldwide estimated prevalence of 19.8–25.1 per 100,000 persons [1,2]. These multi-organ diseases mainly affect muscles, especially skeletal muscles, which undergo a progressive degeneration causing severe health problems that lead to poor life quality, loss of independence, disability and premature death [3,4]. Among the various types of MDs described

so far, the most common are the Duchenne Muscular Dystrophy (DMD) and Myotonic Dystrophies (DMs) [2,3,5].

Currently, no therapies are available to counteract the pathogenic causes of these diseases, and conventional treatments based on immunosuppressants such as corticosteroids or anti-inflammatory treatments are aimed to only mitigate symptoms [6–10]. Although corticosteroids are considered as the “gold standard” to preserve muscle strength in MDs, especially in DMD, their long-term administration is associated with serious adverse effects such as leg oedema, glaucoma, depression, hypertension, hyperglycaemia, osteoporosis, osteonecrosis and fractures [11–13]. Medical devices such as pacemaker, respiratory assistance or wheelchairs, rehabilitative therapy and as a last resort surgery are also widely used in the management of MDs patients [14–16]. Altogether, these approaches represent the current restricted therapies and methods approved to reduce pain and improve the quality of life. Recently, a variety of possible therapeutic strategies have been proposed such as repurposing US Food and Drug Administration (FDA)-approved molecules for the treatment of other diseases or developing novel gene therapy for exon-skipping strategy or genome editing [17–22]. However, due to their rapid clearance or associated adverse effects, further refinements are required to enter clinics.

Over the last several years, drug delivery nanosystems, referred to as nanomedicine, have been extensively explored for the development of more effective and safer treatments with main applications in cancers [23–26], central nervous system-related disorders [27–29] and immune diseases [30–32]. More recently, nanomedicine has also been investigated for the treatment of viral infections [33] such as the lately approved Moderna’s and Pfizer’s Covid-19 nanoparticle-based vaccines [34–37]. In cancer therapy, nanomedicine holds potential to improve current treatments by reducing side effects of chemotherapeutic agents. Moreover, combination approaches and immunomodulation strategies have been successfully developed to boost their performances [38–40]. Nevertheless, only 15 nanoparticle-based cancer therapies have received clinical approval and entered the market, such as the recent liposomal Onivyde[®] and Vyxeos[®] formulations [41,42].

Currently, novel nanomedicines are optimized for the treatment of skeletal muscle pathologies like MDs. However, multiple biological and pharmaceutical barriers challenge nanomedicine delivery to skeletal muscles. Biological barriers are embodied by the complex architecture of the skeletal muscle, which encompasses the skeletal muscle parenchyma itself, connective tissue, blood vessels and nerves. One of the main hurdles for delivery to skeletal muscles lies in the presence of the dense extracellular matrix (ECM), which accounts for 1 to 10% of the muscle mass [43–45]. Mostly made of fibrous-forming proteins (collagens, glycoproteins, proteoglycans and glycosaminoglycans) it hampers nanoparticles (NPs) penetration by retaining them in the ECM via electrostatic and mechanical interactions [46,47].

Pharmaceutical barriers encompass formulation and associated aspects related to scaling up of nanomedicine products. Recently, formulation techniques based on scalable processes have been developed to allow transposition of nanomedicine to industrial settings [48–50].

In addition to these barriers, an important requirement is that NPs have to be biocompatible to prevent additional muscle degeneration of severely injured skeletal muscles. For instance, sarcolemma membrane of DMD patients is severely affected and therefore more susceptible to damage by any treatment [51].

The present review aims at highlighting the major advances in the nanomedicine-based strategies for treating MDs. We reviewed the most recent approaches to treat MDs focused on oligonucleotides or antisense oligonucleotides, and small molecules and how nanocarriers have been designed to deliver them to muscle cells. In addition, the genome editing CRISPR/Cas9 system is also described. Finally, future perspectives for nanomedicine optimisation are presented.

2. Muscular Dystrophies Characterised by Gene Alteration

Most common MDs are represented by the two well-known DMD and DMs [1,3,4]. These two types of dystrophies are caused by diverse gene mutations and lead to different molecular pathogenesis, as illustrated in Figure 1.

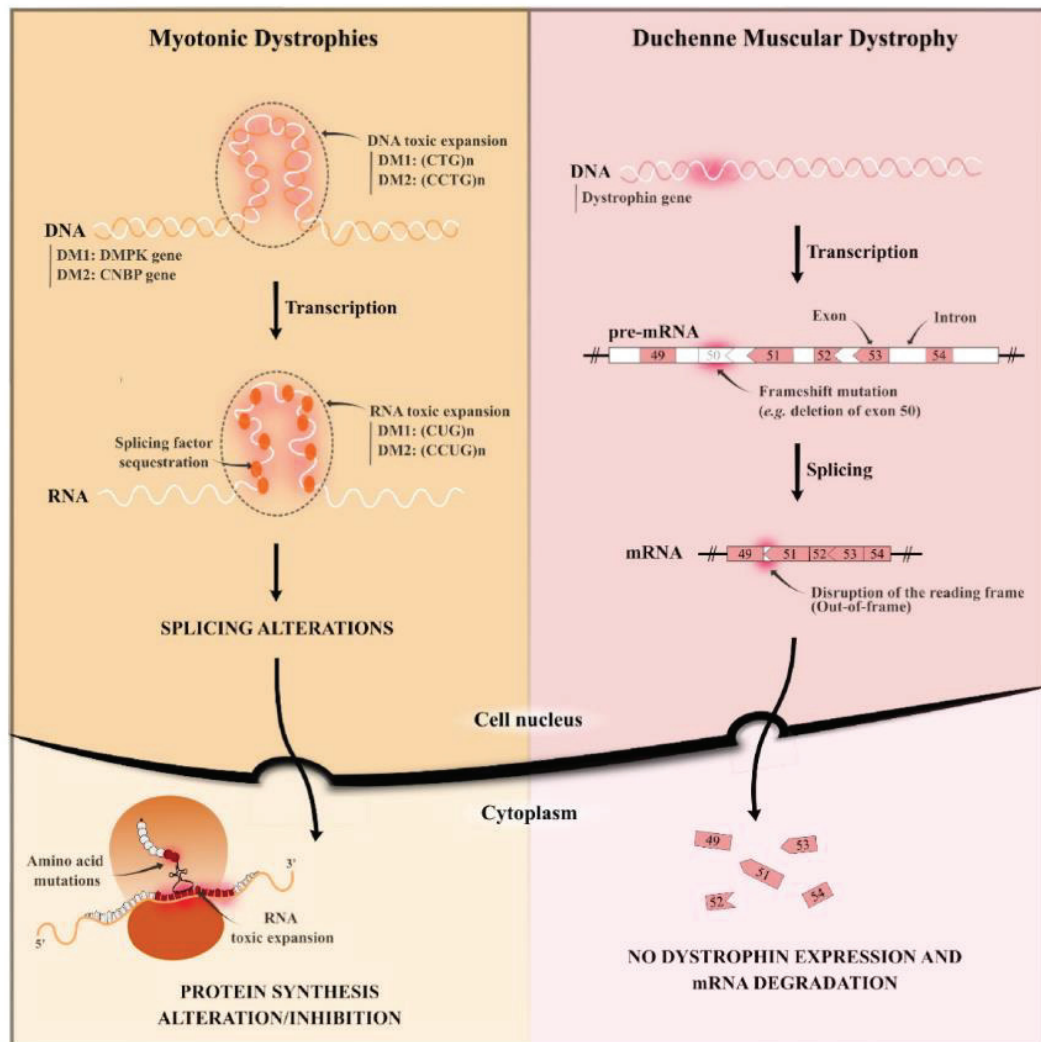


Figure 1. Schematic representation of the pathogenesis of both Myotonic Dystrophies and Duchenne Muscular Dystrophy. (DM1: Myotonic Dystrophy type 1; DM2: Myotonic Dystrophy type 2.)

2.1. Duchenne Muscular Dystrophy

DMD is the most common form of MD characterised by progressive muscle degeneration and weakness, firstly affecting proximal muscles. This X-linked recessive rare disorder appears essentially in males with a worldwide prevalence of one in 5000 boys in early childhood and the clinical signs are not revealed at birth [52]. In most cases, the diagnosis is established around four years old, when the first symptoms start to appear. The disease progression is fast and the patients completely lose their motor functions around 10 years old. DMD patients develop also important cardiac and respiratory complications that generally manifest around 10 years old and are prevalent in most patients by 20 years old [53].

DMD is caused by mutations in the dystrophin gene (DMD gene) located on chromosome Xp21.2 that codes for the dystrophin protein through its 79 exons [54]. Dystrophin protein is essential for muscle homeostasis: it is localised on the plasma membrane of cardiac and skeletal muscles (sarcolemma), connecting the cytoskeleton to the ECM through the dystroglycan complex (DGC) and stabilising the muscle fibre during contraction. Lack of dystrophin induces severe muscle weakness, inflammation and wasting, described as cardinal signs of DMD. Diverse mutations on DMD gene have been reported worldwide [55]. Over the years, DMD gene has been characterised, identifying which mutations lead to a severe DMD phenotype [56,57]. Of DMD cases, 60–70% are caused by large deletions of one or more exons. Point mutations affect 15–30% of DMD patients, and there are smaller changes that do not involve an entire exon. Among them, nonsense mutations cause a premature stop in the gene which results in reduced dystrophin production or no production at all. Duplications affect only 10% of DMD patients and can occur throughout all 79 exons of the dystrophin gene. Understanding the nature of mutations improves the identification of therapeutic approaches able to rescue genetic mutations [58,59].

2.2. Myotonic Dystrophies (Type 1 and 2)

Myotonic dystrophies (DMs) are genetic disorders of autosomal dominance inheritance and represent the second most common form of MDs in adulthood [60,61]. These multisystemic diseases cause progressive dysfunctions of multiple organs and tissues (e.g., muscle tissues, skin, endocrine system, ocular system, central nervous system) among which skeletal muscle is the most severely affected tissue [5]. Muscle damages are characterised by progressive myopathy, muscle weakness, and progressive myotonia which is defined as a slow-down of muscle relaxation after a normal contraction. Most serious features concern the cardiopulmonary system and can lead to premature death, amounting to 70% of deaths [62].

Two distinct forms of DM caused by similar mutations are identified: i) DM1, also named Steinert disease (OMIM 160900), which is the most common and severe form; and ii) DM2, termed proximal myotonic myopathy (OMIM 602668). These DMs are caused by pathological expansions of small DNA sequences regarding two different genes [63]. DM1 is due to a (CTG) n expansion in the 3' UTR region of the DMPK gene, while DM2 is caused by a (CCTG) n expansion in the first intron of the ZNF9/CNBP gene. Mutant (CTG) n and (CCTG) n expansions are highly unstable, leading to different repeat sizes constantly generated and increasing when transmitted from one generation to the next [64]. These mutant DNA expansions are transcribed into (CUG) n and (CCUG) n mutant RNA expansions for DM1 and DM2, respectively, aggregated in the nucleus in specific hairpin structures that are called nuclear foci [65].

The most accepted pathogenic hypothesis for DMs is an RNA-gain-of-function due to mutant RNA expansions that alter RNA-binding splicing regulators [66]. As illustrated in Figure 1, the main molecular hallmark of DMs is the sequestration of Muscleblind protein (MBNL), resulting in a local reduction of these protein levels [67]. It is responsible for several symptoms depending on the DM type and repeat size range, such as myotonia, muscle weakness, cardiac arrhythmia, diabetes, cataracts, male hypogonadism, cognitive disorders and hypersomnia [68]. Other splicing factors are mis-regulated in DMs, such as the up-regulation of CUGBP1 [63] and hnRNP H protein [69,70]. Understanding the molecular pathogenic mechanism helped the development and identification of diverse therapeutic approaches such as the reduction of toxic RNA levels [71,72], the prevention of the MBNL protein sequestration, or the inhibition of the signalling pathway that leads to CUGBP1 up-regulation [73–75].

3. Targets and How to Reach Them: DNA and RNA

MDs are genetic disorders caused by localised mutations of DNA. Such DNA mutations result in a lack of dystrophin protein in DMD and an alteration of the protein production in DMs (Figure 1) [57,76]. No curative therapies are available to treat the

pathogenic causes, and the identification of new therapeutic approaches to target genetic mutations is urgently needed [10]. The most recent strategies to counteract MDs concern gene therapy and repurposing of drugs, as summarised in Table 1. In order to reach the target and achieve therapeutic effect, active agents must attain skeletal muscle tissue. A representation of their localisation is reported in Figure 2.

Table 1. Therapeutic strategies for the treatment of MDs (DMD, Duchenne Muscular Dystrophy; DM, Myotonic Dystrophy; ASO, antisense oligonucleotide; CRISPR, clustered regularly interspaced short palindromic repeats).

Approach	Active Agent	Target	Pathology	Limitations	Development Phase	Reference
Antisense oligonucleotides	Etelprisen	mRNA	DMD	Rapid degradation by exonuclease Low cellular uptake Activation of immune system Inflammatory effects	FDA approved (Clin. Trial NCT02255552)	[77]
	Drisapersen				Phase III (Clin. Trial NCT01254019)	[78,79]
	cEt ASO	CUG/CCUG ^{exp}	DM		Preclinical studies	[80,81]
CRISPR/Cas9	Not approved	DNA	DMD	Higher accumulation in proliferating cells than in fully differentiated cells Rapid degradation	Preclinical studies	[82–85]
	Not approved	CTG ^{exp} DNA	DM	Uncompleted repair of protein expression Low transfection efficiency	Preclinical studies	[86]
Small molecules	Aminoglycoside antibiotics	Non-sense mutations on mRNA	DMD	Ototoxicity Nephrotoxicity	Preclinical studies	[87–89]
	Ataluren	Non-sense mutations on mRNA	DMD	High dosage required	EMA approved (Clin. Trial NCT01826487)	[90,91]
	Pentamidine	CUG ^{exp} RNA	DM	Nephrotoxicity Off-label use	Preclinical studies	[18,92]
	Furamidine and erythromicin	CTG ^{exp} DNA	DM	Off-label use	Preclinical studies	[93–95]
	ISOX and vorinostat	MBNL1-splicing factors	DM1	Off-label use	Preclinical studies	[96]

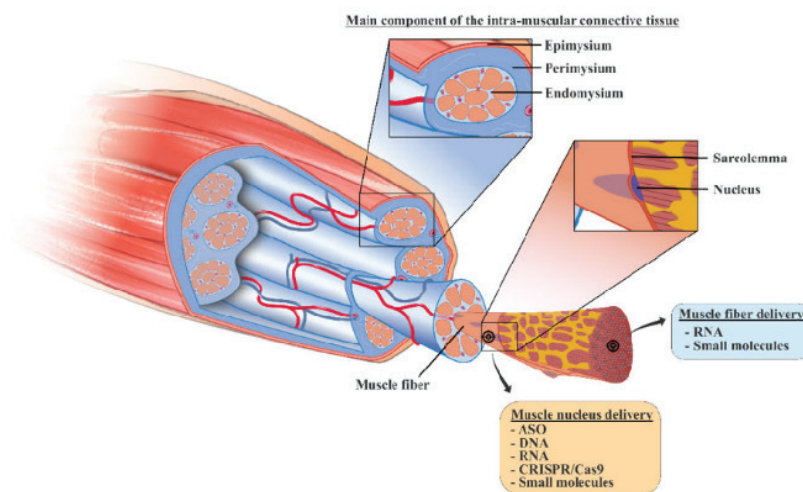


Figure 2. Organization of the skeletal muscle tissue and the target-tissue related to the class of experimental molecules (ASO, antisense oligonucleotide; CRISPR, clustered regularly interspaced short palindromic repeats).

3.1. Gene Therapy and Genome Editing for MDs

Gene therapy aims at targeting gene mutations. Genetic strategy and genome editing offer the advantage of a durable and possibly curative approach. They aimed at improving patient's quality of life by i) reducing the administration frequency, thus increasing their compliance to the treatment [97,98], and ii) providing a personalised therapy for the correction of genetic mutations [99].

Application of gene therapy in muscle pathologies is performed by exon-skipping [58] and CRISPR/Cas9 system [59]. Exon-skipping is based on the use of small pieces of modified oligonucleotides, termed antisense oligonucleotides (ASOs), which recognise and bind specific sequences of mRNA [58,100]. ASOs exert their activity in the nucleus by: (i) blocking protein maturation and splicing alteration of pre-mRNA, (ii) degrading targeted RNA by RNase H-enzyme and reducing mRNA level [101]. Despite their promising features, drawbacks related to ASO's instability, limited distribution to all diseased tissues, rapid body clearance and difficulties of cellular internalisation have been described [102]. To overcome these issues, chemical modifications on ASO chemical structure have been studied. Several ASO drugs were modified using the phosphorothioate backbone modification where one of the non-bridging oxygen atoms of the phosphodiester linkage was replaced with sulphur. This modification increased the half-life of ASOs [103] and reduced their degradation by exonucleases [104]. However, ASO-based therapies present potential toxicities such as the off-target RNA hybridisation and the possibility to alter protein expression [105]. In addition, they can be recognised by the immune system, inducing proinflammatory effects [106].

In DMD patients affected by an out-of-frame mutation of DMD gene, ASO therapy can restore the reading frame of mRNA leading to the expression of a partially functional dystrophin protein [107]. Eteplirsen was approved in 2016 by the FDA as the first antisense therapy for DMD. Eteplirsen is a 30-nucleotide phosphorodiamidate morpholino (PMO) ASO that resulted in an increased dystrophin production in all patients treated by weekly intravenous (I.V.) infusion for at least 24 weeks [77]. Drisapersen, a 2'-O-methylphosphorothioate ASO, is another exon-skipping therapy for DMD in clinical development. Phase 3 study (DMD114044; NCT01254019) evaluated the efficacy of drisapersen after subcutaneous (S.C.) injection. The six-minute walk distance (6MWD) was the primary endpoint considered, and no differences were reported between placebo and treated patients. Data analysis considering secondary endpoints such as the North Star Ambulatory Assessment (NSAA), 4-stair climb ascent velocity and 10-metre walk/run velocity, showed lack of statistical significance due to the greater data variability and subgroup heterogeneity. However, statistically significant results were obtained in the young patients treated in the early stage of the pathology [78]. Further studies were focused on the preclinical optimisation of drisapersen, testing its efficacy on young and older DMD mouse model, *mdx*. This mouse model is characterised by an induced nonsense point mutation in the dystrophin gene, which leads to a loss of functional protein expression [108]. Preclinical investigation showed a comparable efficiency of exon-skipping mechanism in young and older mice, but functional and physical improvement was only reported for treated young mice, meaning that the stage of pathology is relevant for treatment efficacy. In vivo studies highlighted that an early intervention with drisapersen led to functional benefits despite the low level of dystrophin restoration. In addition, the application of drisapersen was also limited by the reported side effects at the injection site and mostly proteinuria, which increased α 1-microglobulin levels [79]. Although ASO therapy and exon-skipping reached important outcomes, their applicability is limited to patients affected by out-of-frame mutation and requires continuous administrations throughout the lifetime of the patients [109,110].

ASO therapy is also reported for the treatment of DM where it targets and neutralises toxic CUG/CCUG^{exp} RNAs which sequester splicing factors [111]. Although there is no approved ASO therapy for DM1, in vitro and in vivo results are promising [112–114]. It has been reported that ASOs containing 2'-4'-constrained ethyl (cEt) modifications can be employed to target DMPK genes and substantially reduce CUG^{exp} RNA nuclear

foci in patient-derived DM1 myoblasts [80]. Klein et al. developed an arginine rich Pip6a cell-penetrating peptide-conjugated PMO ASO to overcome the poor distribution of ASOs in skeletal muscle. Pipa6-conjugated ASO directed against CUG^{exp} allowed an effective concentration of ASOs in muscle fibres recovering MBNL1-dependent splicing defects [81].

In contrast to ASO therapy, genome editing induces a permanent correction of gene mutation [115]. Initially, engineered zinc finger nucleases (ZFNs) and transcription activator-like effector (TALENs) have been used to permanently remove splicing sequences in DMD gene and to restore dystrophin expression [116,117]. Recently, Clustered Regularly Interspaced Short Palindromic Repeats (CRISPR) in association with specific DNA endonuclease protein called Cas9, targeting DNA sequencing, has been investigated to restore the genetic mutation [118–120]. Cas9 nuclease requires a single guide RNA (sgRNA) to form a complex with DNA by recognition with a defined 20 bp DNA sequence, known as protospacer. The protospacer sequence is immediately followed by a short sequence called protospacer-adjacent motif (PAM), needed by Cas9 for DNA cleavage and for genome editing to start [121].

Promising results of CRISPR/Cas9 in MD treatment were reported. Dystrophin recovery by CRISPR/Cas9 system was observed in a new DMD mouse model characterised by a lacking exon 44 of the dystrophin gene, one of the hotspot regions for DMD gene mutation. In this study, Cas9 and sgRNA, the main gene editing components, were encoded by adeno-associated viruses serotype 9 (AAVs). The ratio between AAVs encoding for Cas9 and for sgRNA had an important effect on gene correction. Higher level of sgRNA ensured higher Cas9 activity, which increased dystrophin restoration due to long-lasting presence of sgRNA that allows continuous editing in myofibers. Combination of optimized sgRNA and AAV vectors for delivery increased long-term correction of dystrophin mutation in mice [82]. AAV9 have been already associated to CRISPR/Cas9 system for dystrophin recovery in a deltaE50-MD canine model of DMD, which leads to loss of exon 50. An sgRNA was optimised to target a region adjacent to the exon 51 splice acceptor site, and it resulted in high frequency of reframing events. Dystrophin protein expression was restored to 60% by intramuscular (I.M.) injection of AAV9-Cas9 and AAVs-sgRNA-51 [83]. Besides, CRISPR/Cas9 ability to target repeated DNA sequences also provides a possible strategy in DM therapy [122]. Dastidar et al. evaluated CRISPR/Cas9 activity, delivered through viral vector to excise CTG repeats in DM1 patient-derived cells, leading to the normalisation of DMPK gene expression and the degradation of toxic RNAs. The study demonstrated the potential application of CRISPR/Cas9 excision in trinucleotides repeat expansion up to 1200 repeats [88].

Genome editing by CRISPR/Cas9 strategy requires an efficient delivery system. AAV are used most often and have a low cargo capacity as compared with other viral vectors, requiring a high AAV dose to deliver sgRNA for gene reprogramming in vivo [21], increasing the risk of immunogenicity [123]. Traditional genome editing based on CRISPR/Cas9 technologies introduces double-stranded (ds) DNA breaks at a target locus as the first step to gene correction. However, the potential applications of Cas9 nucleases are limited in part by their reliance on DNA breaks, which could cause deletions, insertions or chromosomal rearrangements. Due to recent advances, CRISPR/Cas9-associated base editing (BE) approaches have emerged. These strategies do not require a dsDNA backbone but mediate the direct conversion of base pairs, advancing the treatment of genetic disorders associated with single nucleotide mutations [124,125]. Cytosine and adenine base-editors are the most used tools to exert mutation transition (Cytosine (C) > Thymine (T) and Adenine (A) > Guanine (G)), guided by a new CRISPR/Cas9 system which targets the non-edited DNA strand [126]. Ryu et al. demonstrated the application of BE in DMD treatment, using a dual trans-splicing AAV to deliver adenine base editors (ABE). ABE treatments achieve a precise A-to-G base mutation, restoring dystrophin expression in 17% of myofibers, following I.M. into tibialis anterior in *mdx* mice [127]. Moreover, due to increased interest in BE, non-viral vectors are under investigation to replace viral constructs as delivery systems [21]. Jiang et al. demonstrated a successful delivery of ABE using lipid nanoparticles in Tyrosinemia

I mice, correcting the gene mutation and showing the promise of the BE approach [128]. Despite the far-reaching capabilities of the BE strategy, a major limitation of this technique has been the ability to generate precise edits beyond the allowed transition mutations. Anzalone et al. described a new genome editing strategy called prime editing. This search-and-replace technology directly writes new genetic information into targeted DNA using a catalytically impaired Cas fused to an engineered reverse transcriptase enzyme, and a prime editing guide RNA (pegRNA) able to recognise and bind the target site [129]. This technology with its simplicity and precision holds great promise for the correction of point mutation in human genetic disorders.

3.2. Drug Repurposing

Another current approach in MD treatment is drug repurposing, a strategy for identifying new applications for approved or investigational drugs that are outside the scope of the original medical indication. Drug repurposing has promising expectations regarding efficacy, safety, cost and translation to the clinical setting. This is because repurposed drugs have been already studied in preclinical models and humans for safety assessments. Moreover, in many cases the formulation aspects are already developed [130].

In order to select the right candidate in a repurposing strategy, a systematic approach that combines computational techniques and experimental studies is required. Computational approaches are based on data-analysis (gene expression, chemical structure, genotype or proteomic data, or electronic health records (EHRs)), to validate the repurposing hypothesis. Experimental approaches are also required to identify target interactions and efficacy in appropriate models [131]. Table 1 lists the most common drugs used for repurposing strategies in DMD and DM.

About 10% of DMD patients present a nonsense mutation, which induces a premature stop codon in dystrophin mRNA leading to non-functional protein [132–134]. Some compounds are able to bind the stop codon, forcing the translational machinery to incorporate amino acids into the assembling protein, overcoming the stop signal and obtaining a functional protein [87]. Restoration of dystrophin protein was studied using gentamicin, an aminoglycoside antibiotic made of a mixture of major and minor aminoglycoside components [88]. Barton-Davis et al. demonstrated the possibility of treating DMD nonsense mutation using gentamicin. The drug was administered by S.C. injection to *mdx* mice at different dosages to identify the optimal dose to restore the full-length dystrophin [87,89]. To determine the efficacy on the suppression of premature stop codon in *mdx* mice, evaluation of dystrophin protection against contraction-induced damage was examined. The number of damaged fibres was reduced in treated *mdx* mice, as compared with wild type mice. Prolonged use of gentamicin implicates nephrotoxicity, limiting the long-term administration required for genetic diseases [135]. To address toxicity issues, new aminoglycosides and non-aminoglycosides were explored. Friesen et al. demonstrated the efficacy and greater read through-safety window than other compounds, of a minor gentamicin component called gentamicin X2, which shows a lower toxicity than gentamicin [136]. From the evaluation of neuromast toxicity (cytotoxic concentration, CC50), as a substitute for ototoxicity, CC50 of gentamicin X2 was significantly reduced compared to gentamicin. Minor component X2 has great potential for clinical utility in treating genetic diseases caused by nonsense mutations. Among non-aminoglycoside compounds, ataluren is a novel, orally administered, synthetic molecule that suppresses nonsense mutation in a way similar to aminoglycosides and increases dystrophin production [90]. Data from a phase III trial did not show improvement in 6MWD of treated patients, but less physical deterioration was demonstrated for patients receiving ataluren than for those receiving placebo. Results reported in this trial confirmed the clinical benefit of ataluren in terms of preservation of muscle function in DMD patients [91]. Further studies should evaluate the long-term benefits the drug.

In DM, the toxic foci made of CUG/CCUG^{exp} RNA aggregates are able to sequester MBNL1 splicing factor, thus altering the protein expression [61]. As an example, pentamidine, furamidine and erythromycin can inhibit the sequestration of splicing factors such as MBNL1 by CUG^{exp} RNA sequence. Docking analyses are useful to predict the binding conformation of small molecules to appropriate binding sites. They have been reported for rational screens of molecules that might selectively bind CUG structures and consequently improve biological activity in DM1 models [137].

Recently, pentamidine, a diamine compound that FDA approved for the treatment of trypanosomiasis and leishmaniasis infections [138], has been proposed for MD treatment and its efficacy was evaluated *in vitro* and *in vivo*. Pentamidine treatment reduced CUG^{exp} RNA level and rescued mis-splicing events in HeLa DM1 transfected cells, which expressed 960 interrupted CUG repeats. The number of nuclear foci was reduced by 21% [139]. The efficacy of pentamidine treatment was evaluated on DM1 mouse model HSA^{LR} (human skeletal actin long repeat length) that expresses ~250 CUG repeats into the final exon of human skeletal actin [18]. Pentamidine was administered by intraperitoneal (I.P.) injection and the correction of chloride-1 and Serca1 mRNA mis-splicing was assayed. The treatment partially reversed mis-splicing events. *In vivo* studies highlighted a narrow dosage window for pentamidine which cannot be used over 30 mg/kg twice a day. To overcome dosage toxicity, chemical modifications were performed to enhance the specificity to CUG^{exp} RNA and to reduce the dosage. Based on the chemical backbone of pentamidine, other drugs showing chemical similarities were selected. Furamidine is a diamine compound that rescues the mis-splicing events *in vitro* and *in vivo* models [92]. In HSA^{LR} mice, furamidine increased MNBL1 functional expression by inhibiting transcription of CTG^{exp} DNA and by disrupting the MNBL-CUG^{exp} complex [93]. Compared to pentamidine, furamidine presented the lowest number of off-target gene expression changes [94]. In combination with erythromycin, furamidine enhanced the effects on MNBL-CUG^{exp} complex disruption, reducing nuclear foci presence in patient-derived DM1 cells, without specific toxic effects [95]. Considering the reduction of MBNL1 in DM1 affected cells, small molecules improve the pathological condition by overexpression of splicing factors. For example, ISOX and vorinostat were tested in normal and DM1 fibroblasts, increasing MBNL1 expression and revealing positive effects on DM1 models [96].

Globally, repurposing of small molecules for the treatment of DM requires extensive investigation concerning their off-label use and the need of novel approaches to define their therapeutic potential for a different disease.

4. New Treatments based on Nanocarriers as Alternative Strategies to Facilitate Skeletal Muscle Targeting

Over the last years, the application of nanomedicine as a promising innovative approach to treat different pathologies such as MDs has been investigated. The architectural and structural complexities of skeletal muscles challenge nanomedicine delivery, especially due to the important presence of ECM [45,140]. To restrict interactions with ECM, administration of NPs by I.V. appears as a potential strategy for targeting skeletal muscle. The dense blood capillary network of skeletal muscles increases NPs access to muscle fibres [141,142]. However, once in the blood circulation, NPs can be rapidly cleared through the mononuclear phagocyte system via opsonisation or complexation with plasma proteins [143–146]. Physical and chemical instability [147,148], immunogenicity [149,150] or premature degradation [151] are other limiting factors that might interfere with NPs delivery.

In addition, long-term administration is required to cure chronic disorders such as MDs, which makes biocompatibility and biodegradability of the nanosystems important requirements [152]. NPs should persist long enough to reverse muscle damages without involving any additional muscle degeneration, before undergoing gradual degradation [51,153]. Therefore, their design has to be optimised to associate or encapsulate active compounds and to deliver them to skeletal muscles. As illustrated in Figure 3, various NPs structures have been described [154]. RNA- and DNA-based nanocarriers are obtained via electrostatic and hydrophobic-hydrophobic interactions with polymers or

lipids [155–157]. In the case of delivery of the small molecules, their chemical properties, such as their molecular size, structure and n-octanol-water partition coefficient have an impact on the selection criteria for nanocarrier strategy [158,159]. Interestingly, synthetic nanocarriers interacting by electrostatic and hydrophobic-hydrophobic interactions have been demonstrated to deliver complex CRISPR/Cas9 systems under various forms such as DNA, mRNA or ribonucleoproteins [160–162].

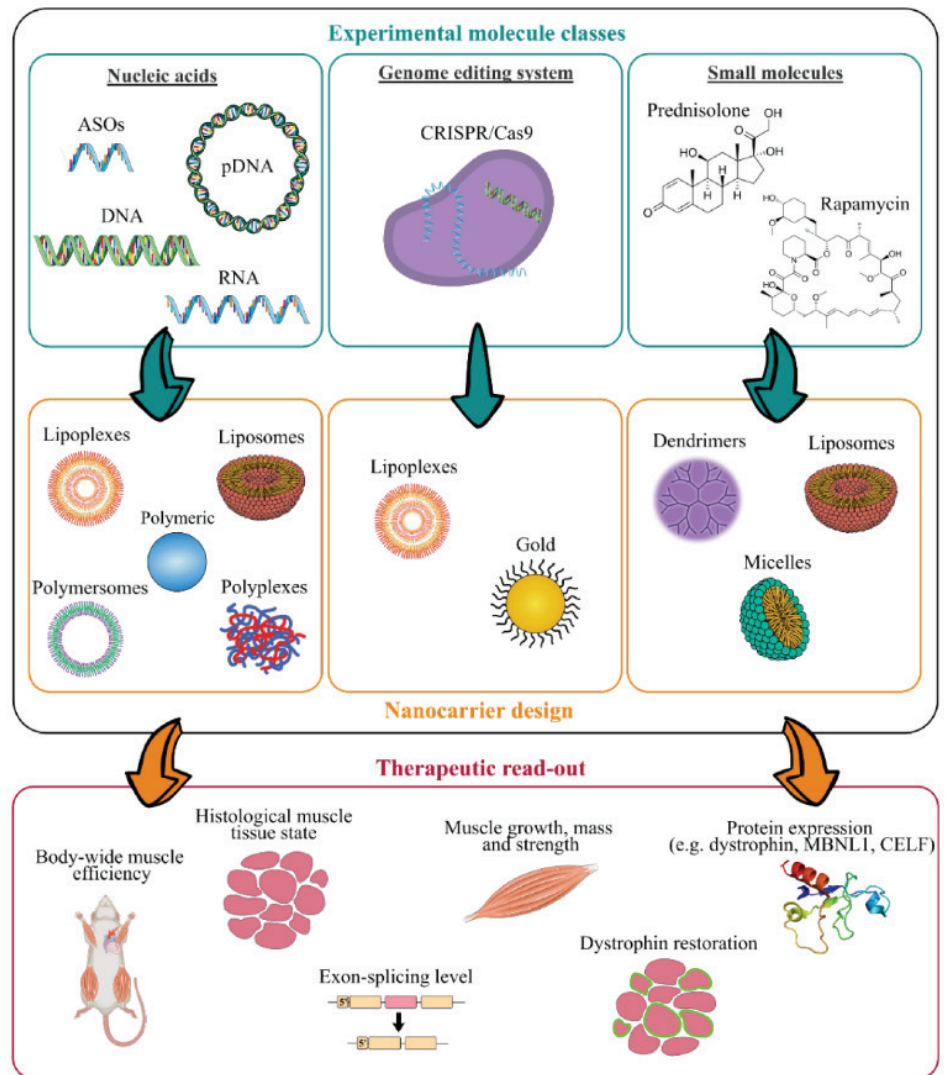


Figure 3. Work flow for the design of innovative nanomedicine and therapeutic readout. (ASOs, antisense oligonucleotides; CRISPR, clustered regularly interspaced short palindromic repeats).

As illustrated in Figure 3, many experimental molecules and macromolecules have been selected as candidates for MD therapies, and a wide range of nanocarriers has allowed their delivery to skeletal muscles, promoting in most of the cases their therapeutic potential.

The present section aims at highlighting nanosystems used for DMD and DM applications that reached preclinical studies. An overview of the various described nanosystems is reported in Table 2.

Table 2. Recapitulative table of the diverse described nanosystems tested in vivo for treating MDs (PEI, polyethylenimine; PEG, polyethylene glycol; PLGA, poly(lactic-co-glycolic acid); PMMA, poly(methyl methacrylate); NIPAM, N-isopropylacrylamide; PEA, poly(ethylene adipate); PLys, poly(L-lysine); PPE-EA, poly(2-aminoethyl propylene phosphate); PAMAM-OH, hydroxyl-terminated poly(amidoamine); DMPC, L- α -dimyristoylphosphatidylcholine; (C12(EO)23), polyoxyethylene(23) lauryl ether; NPs, nanoparticles; ASO, antisense oligonucleotide; PMO, phosphorodiamidate morpholino oligomer; GA, glatiramer acetate; CRISPR, clustered regularly interspaced short palindromic repeats; I.M., intramuscular injection; I.V., intravenous injection; I.P., intraperitoneal).

Class of Nanocarriers	Nanocarrier Composition	Muscle Pathology	Loaded Molecules	Therapeutic Target	Mouse Model	Advantages and Limitations	Admin. Route	Ref.
Polymeric	PEI-PEG	DMD	2'-OMe ASO	Dystrophin pre-mRNA	mdx	(+) high dystrophin-positive fibers increased (+) long term residual efficacy over 6 weeks (-) low general transfection efficiency	I.M.	[163]
	PEI-PEG/PLGA	DMD	2'-OMe ASO	Dystrophin pre-mRNA	mdx	(-) no improvement compared to PEI-PEG-ASO	I.M.	[164]
	PEI-Pluronic®	DMD	PMO ASO	Dystrophin pre-mRNA	mdx	(+) dystrophin-positive fibers increased up to 4-fold after I.M. (+) dystrophin-positive fibers increased up to 3-fold in all skeletal muscles after I.V. (+) dystrophin-positive fibers increased up to 5-fold in heart after I.V. (+) low muscle tissue, liver and kidney toxicity (-) mild general transfection efficiency	I.M./I.V.	[165]
		DMD	2'-OMe ASO	Dystrophin pre-mRNA	mdx	(+) dystrophin-positive fibers increased up to 10-fold	I.M.	[166]
	PEG-polycaprolactone PEG-(polylactic acid)	DMD	PMO ASO	Dystrophin pre-mRNA	mdx	(+) dystrophin-positive fibers increased up to 3-fold (+) low muscle tissue toxicity (-) mild general transfection efficiency	I.M.	[167]
	PMMA	DMD	2'-OMe ASO	Dystrophin pre-mRNA	mdx	(+) dystrophin-positive fibers increased up to 7-fold (-) slow biodegradability	I.P.	[168]
	PMMA/NIPAM	DMD	2'-OMe ASO	Dystrophin pre-mRNA	mdx	(+) dystrophin-positive fibers increased up to 4-fold (+) body-wide dystrophin restoration after I.V. (+) exon-skipping level enhanced up to 20-fold (+) long term residual efficacy over 90 days	I.P./I.V.	[169, 170]
		DMD	2'-OMe ASO	Dystrophin pre-mRNA	mdx	(+) dystrophin-positive fibers increased up to 3–10-fold	I.M.	[171]
	PEA	DMD	PMO ASO	Dystrophin pre-mRNA	mdx	(+) dystrophin-positive fibers increased up to 3-fold after I.M. (+) body-wide dystrophin-positive fibers increased up to 3-fold after I.V.	I.M./I.V.	[171]
		Muscle atrophy/ DMD	pDNA	Cell nucleus	mdx	(+) transfection efficiency enhanced up to 6-fold	I.M.	[172]
PLys-PEG	Muscle atrophy	pDNA	Cell nucleus	Balb/c	(+) transfection efficiency enhanced up to 10-fold	I.V.	[173]	

Table 2. Cont.

Class of Nanocarriers	Nanocarrier Composition	Muscle Pathology	Loaded Molecules	Therapeutic Target	Mouse Model	Advantages and Limitations	Admin. Route	Ref.
	PPE-EA	Muscle atrophy	pDNA	Cell nucleus	Balb/c	(+) transfection efficiency enhanced up to 13-fold (+) long term residual efficacy over 14 days	I.M.	[174]
	Atelocollagen	Muscle atrophy/ DMD	siRNA	Cytoplasm	mdx	(+) higher mass muscle increase	I.M./I.V.	[175]
	PAMAM-OH	Muscle atrophy	Angiotensin (1-7)	Cytoplasm	Balb/c	(+) higher anti-atrophic effects	I.P.	[176]
Lipidic	PEG-bubble liposomes	DMD	PMO ASO	Dystrophin pre-mRNA	mdx	(+) dystrophin-positive fibers increased up to 1.5-fold (+) exon-skipping level enhanced up to 5-fold	I.M.	[177]
		DM1	PMO ASO	Cln1 pre-mRNA	HSA ^{LR}	(+) increased expression of Cln1 protein up to 1.4-fold	I.M.	[178]
	Nanolipodendrosomes	DMD	MyoD and GA	Cytoplasm	SW-1	(+) slight mass muscle increase	I.M.	[179]
	Nanoliposomes	DMD	Glucocorticoide	Cell nucleus	mdx	(+) lower inflammatory induced response (+) lower bone catabolic effects	I.V.	[180]
	Hybrid liposomes DMPC and (C ₁₂ (EO) ₂₃)	DMD	Gentamicin	Ribosomes	mdx	(+) dystrophin-positive fibers increased up to 4-fold (+) lower ototoxicity and nephrotoxicity	I.P.	[181]
	Perfluorocarbon	DMD	Rapamycin	mTORC1 complex	mdx	(+) high muscle strength increase (+) high cardiac contractile performance increase	I.V.	[182]
	Lipid NPs	DMD	CRISPR/Cas9	Dystrophin DNA sequence	ΔEx44	(+) dystrophin expression restored up to 5%	I.M.	[183]
Inorganic	Gold	DMD	CRISPR/Cas9	Dystrophin DNA sequence	mdx	(+) HDR in the dystrophin gene enhanced up to 18-fold	I.M.	[184]

4.1. Antisense Oligonucleotides

ASO-based therapy is a powerful tool for inducing post-transcriptional modifications and thereby regulating target genes. There are several classes of ASOs for therapeutic purposes which differ from their phosphate backbone and ribose sugar group modifications [185]. Most ASOs used for DMD and DM are 2'-O-methyl (2'-O-Me), phosphorothioate (PS) ASO and PMO oligomer modified ASOs. Depending on their chemistry, different strategies can be obtained to modulate gene expression.

The phosphodiester and phosphorothioate internucleotide linkages confer a highly negative charge to PS or 2'-O-Me ASOs. Hence, the most common approach to incorporate such ASOs into NPs remains to form stable complexes with cationic polymers or lipids. Polyplexes have been currently used for this purpose [186]. Poly(ethylene imine) (PEI) was one of the first cationic polymers explored for gene therapy because of its efficient binding association to nucleic acids and good transfection efficiency [187]. Nonetheless, the high positive surface potential results in significant toxicity, especially for in vivo skeletal muscle delivery, due to interactions with many biological components. To reduce the surface potential, poly(ethylene glycol) (PEG) has been added to the formulation [188,189]. Lutz's group developed PEI-PEG NPs obtained by the complexation of 2'-O-Me ASOs with a cationic copolymer of PEI and PEG, to restore dystrophin expression in *mdx* mice [163,190,191]. PEI was conjugated to nonionic linear PEG to provide NPs with a steric shield, greatly

improving their biocompatibility. PEI-PEG-ASOs were shown to locally improve the levels of dystrophin expression up to 20% of normal dystrophin expression in WT animals after I.M. injection without eliciting toxicity. However, cationic PEI-PEG showed poor muscle distribution, evidenced by large untransfected areas in muscles, due to the nanoparticle entrapment into the ECM by non-specific binding [163].

In line with Lutz's group, Sirsi et al. proposed a strategy to shield the positive charges of PEI-PEG-ASO polyplexes by encapsulating them into PLGA nanospheres [164]. In vitro release studies in physiological medium showed a low PEI-PEG-ASO release from PLGA nanospheres. Such slow release was correlated to the Mw of PLGA; high PLGA Mw (72 kDa) impaired complex release, while lower PLGA Mw (17 kDa) reached 66.5% release over 26 days. This different release span could be ascribed to the kinetic rate of hydrolysis of PLGA. However, in vivo studies in *mdx* mouse following I.M. injection of free or PLGA (17 kDa) encapsulated PEI-PEG-ASOs showed that dystrophin expression was not improved, probably related to an incomplete ASO release of PEI-PEG-ASOs from PLGA. Despite this lack of dystrophin expression, polyplexes encapsulation through PLGA nanospheres appears to be an efficient sustained delivery strategy of interest for treating chronic diseases.

Wang et al. designed PEI conjugated with Pluronic® polycarbamates (PCM) to deliver 2'-O-Me ASOs in *mdx* mice [166]. After I.M. administration, PEI-PCM NPs showed a local increased number of dystrophin-positive fibres up to three-eight fold, superior to ASO alone or unmodified ASO-PEI NPs. The addition of the carbamate hydrophobic groups contributed to ASO complexation to the NPs and enhanced transfection efficiency. 2'-O-Me ASOs were also complexed using poly(ester-amine) (PEA), a constructed polymer obtained from PEI conjugated with Pluronic®. This polyplex demonstrated an efficacy similar to that of PCM with a number of dystrophin-positive fibres up to 3–10 fold higher than ASO alone [171].

Cationic polymethylmethacrylate (PMMA) NPs are other promising systems intended for nucleic acids delivery [192]. Rimessi et al. proved that cationic PMMA (named T1 NPs) complexed with 2'-O-Me PS ASOs, administered by I.P. injection, restored dystrophin expression in body-wide striated muscles of *mdx* mice [168]. Dystrophin appeared expressed at moderate levels on the membrane of myofibers of the diaphragm, gastrocnemius and quadriceps and was restored at lower levels on the membrane of cardiomyocytes, showing the wide muscle distribution of T1 NPs. However, PMMA NPs are slowly degradable and might form small aggregates at high concentration in blood circulation, limiting their clinical use [192]. Based on these results, Ferlini et al. designed PMMA/N-isopropylacrylamide+ (NIPAM) NPs (ZM2 NPs) to improve the potential of PMMA-based NPs [169]. PMMA core was shielded with NIPAM cationic copolymer and used to bind and convey 2'-O-Me PS ASOs to *mdx* mice following I.P. administration. ZM2-ASOs NPs induced efficient and widespread dystrophin restoration at low dose of ASOs in both striated and smooth muscles, with a dystrophin expression up to 40% of muscle fibres and an exon-skipping level up to 20% after seven days. Moreover, these nanocarriers showed long-term residual efficacy over 90 days, demonstrating their potential as gene delivery systems for ASO delivery [170].

Other non-ribose modified ASOs less frequently used for MDs applications are PMO. These ASO modifications are aimed at increasing their nuclease resistance and mRNA binding efficacy, but provide poor cellular uptake and rapid blood clearance related to the uncharged nature conferred by the morpholino rings [193,194]. In contrast to negatively charged ASOs, the use of cationic entities as a delivery vehicle is not suitable with this well-established ASO delivery strategy. For efficient delivery of these neutral oligonucleotide analogues, lipophilic interactions through PMO and hydrophobic carriers are privileged [195]. Kim et al. showed, as proof of concept, the potential of non-ionic PEG-polycaprolactone and PEG-(polylactic acid) polymersomes for the I.M. administration of PMO for DMD application into *mdx* mice [167]. The polymersomes successfully enhanced dystrophin expression in the entire muscle length increasing three-fold the number of

dystrophin-positive fibres as compared with free-PMO. Furthermore, these degradable carriers were biocompatible upon injection in the muscle, showing long-circulating properties with an improvement of dystrophin expression over three weeks after a single injection.

Wang et al. proved previously described PCM NPs for PMO delivery in *mdx* mice to be a strategy for DMD therapy [165]. Hydrophobic region of the carbamate groups enabled the formation of ASO-PCM carriers. These NPs dramatically improved dystrophin expression in muscles after I.M. injections with up to 57% of dystrophin-positive fibres, four-fold superior to ASO alone. After I.V. administration, up to 15% of myofibers were dystrophin-positive, resulting in a transfection efficiency 3-fold superior to ASO alone. In heart muscle, PCMs demonstrated an improvement of dystrophin-positive cardiomyocytes up to 5-fold superior, nevertheless leading to only 5% of dystrophin-positive cells. Hydrophobic PCM NPs showed high toxicity, whereas more hydrophilic PCM NPs were found ineffective to deliver PMO, emphasising the importance of a polymer's hydrophobic and hydrophilic balance to improve charge-neutral PMO delivery.

Amphiphilic PEA NPs previously described for 2'-OME ASO complexation, also proved to be efficient in delivering PMOs for DMD application in *mdx* mice [171]. PEA-PMOs induced three-fold more dystrophin positive myofibers than PMOs alone after both I.M. and I.V. injection, with the widespread presence of dystrophin-positive fibres in diaphragm, biceps and heart after systemic delivery.

Other works demonstrated that bubble liposomes combined with ultrasound exposure are an effective tool to enhance the delivery of PMOs in both HSA^{LR} and *mdx* mice for DM and DMD applications, respectively. The interesting transfection efficiency properties of these liposomes containing ultrasound imaging gas rely on their ability to cavitate under ultrasound exposure. This combination produces transient pores in cell membranes, enabling the direct entry of the therapeutic compounds into the cytoplasm without involvement of the endosomal pathway [196,197]. Koebis et al., demonstrated that bubble liposomes-PMO I.M. delivered in HSA^{LR} mice locally improved the alternative splicing of the chloride channel 1 (*Clcn1*) gene, downregulating the high *Clcn1* protein level in DM muscles and thereby enhancing one of the multiple DM features [178]. To our knowledge, this is the only study on ASO delivery using nanomedicine for DM applications that has been tested in vivo. Negishi et al. showed the potency of identical bubble liposomes to deliver PMO for DMD application [177]. This combination of bubble liposomes and PMOs, followed by ultrasound exposure, locally restored dystrophin expression in *mdx* mice muscles with an exon 23-skipping improvement to less than two times and a number of dystrophin positive fibres ~five-fold superior as compared with PMO alone. Thus, the co-administration of bubble liposomes combined with ultrasound exposure may provide an effective non-invasive method for PMO therapy.

Overall, to effectively deliver ASOs in skeletal muscle, nanomedicine is a fundamental tool to ensure protection from degradation while improving both tissue and intracellular uptake. The equilibrium of the degree of hydrophobicity, Mw and charge potential is the key to ensure an optimum compromise between stable complex formation, efficiency and tissue compatibility. With regard to all studies presented above, nanomedicine has achieved encouraging improvement of ASO's efficiency with special attention to skeletal muscles. Furthermore, systemic administration has showed promising results on the body-wide carrier distribution into skeletal, smooth and also cardiac muscles.

4.2. Oligonucleotides

RNA and DNA-based therapeutics are efficient and versatile strategies to regulate gene expression, making this class of drugs attractive for a variety of applications. Similar to negatively charged ASOs, strategies for oligonucleotides delivery are mainly based on electrostatic interactions [198–201].

Kinouchi et al. used atelocollagen (ATCOL) to condense a siRNA downregulating myostatin, a negative regulator of skeletal muscle growth [175]. ATCOL is a highly purified collagen chosen for its biocompatibility with skeletal muscle, as collagen occurs naturally

as one of its principal components [43]. Moreover, it has been reported that ATCOL displays low in vivo immunogenicity and toxicity [202,203]. ATCOL-siRNA NPs markedly decreased the protein levels of myostatin and thereby increased muscle mass within two weeks after a single I.M. injection in *mdx* mice. The authors also demonstrated the potential of systemic ATCOL-siRNA delivery to repress myostatin expression, inducing muscle hypertrophy in normal mice.

Poly(2-aminoethyl propylene phosphate) (PPE-EA) polymer has also demonstrated good potential for pDNA delivery to the muscle tissue in healthy Balb/c mice [204]. The high PPE-EA molecular weight ensures suitable hydrolytic stability of the PPE-EA/pDNA complexes. Furthermore, the cleavage of the PPE-EA phosphoester bond in physiological conditions gives this polymer interesting biodegradability properties. In vivo gene transfer efficiency was evaluated using LacZ, coding for β -galactosidase, as a model gene. After I.M. injection, PPE-EA/pDNA demonstrated a significantly higher and delayed β -galactosidase expression in muscles, up to 17-fold superior to DNA alone, highlighting the great potential of PPE-EA polymer as muscle gene delivery [174].

Itaka et al. designed PEG-poly(L-lysine) (PEG-PLys)/pDNA NPs-mediated gene delivery systems for skeletal muscle in order to find novel strategies to inhibit tumour growth through the extensive capillary network wrapped around the muscle fibres [173]. The authors designed PEG-PLys to reconcile DNA binding affinity within cationic PLys core, and tolerance under physiologic conditions through the electrically neutral shell of PEG [205]. The transgene expression efficacy in the skeletal muscle of healthy Balb/c mice was evaluated using pDNA encoding luciferase and GFP, as a model gene. After injection into the blood stream of murine muscle limbs, PEG-PLys/pDNA induced a luciferase expression up to 10-fold higher than pDNA alone in the injected muscle over 25 days. Moreover, PEG-PLys/pDNA promoted an increased number of fluorescent-positive muscle fibres compared to pDNA alone, a better time-dependent profile of transgene expression without any overt signs of toxicity. Thus, PEG-PLys NPs provide prolonged transgene expression in skeletal muscle, which is promising for the field of muscle pathologies.

Hyperbranched poly(ester amine)s (demonstrated an efficient PEAs) obtained from chemical modifications of PEI also demonstrated interesting properties as pDNA delivery carriers in C2C12 murine muscle cells and *mdx* mice [172]. The authors cross-linked low-molecular-weight PEI polymers to raise a dispersed positive charge density into the core and enhanced gene transfection efficiency while reducing PEI associated cytotoxicity. These biodegradable NPs effectively condensed a pDNA coding for GFP and showed a low in vitro cytotoxicity on muscle cells. PEAs/pDNA complexes in vitro transfection with up to 87% of fluorescent-positive C2C12 muscle cells, suggesting a transfection efficiency 2–3-fold higher than that of cells transfected with PEI/pDNA. Finally, these nanosystems also proved to have good potential for muscle gene delivery, showing a substantial increase in fluorescent-positive muscle fibres after I.M. administration.

In a way similar to ASOs, the main strategies adopted to deliver oligonucleotides into skeletal muscle rely on the use of materials ensuring electrostatic and hydrophobic interactions. Finding a compromise between hydrophobic and charge degree is crucial in gene delivery to ensure carriers stability and great transfection efficiency while sustaining high tissue integrity. Although these studies have been presented as promising proof-of-concept for skeletal muscle delivery, further investigations using oligonucleotides designed for treating MDs could warrant the use of such nanocarriers to critically cure affected muscles.

4.3. Small Molecules

Drug repurposing is an effective strategy to reuse existing licensed drugs for novel medical indication while reducing development time, costs and minimising risk of failure [112,206]. In addition, nanomedicine has been used to enhance therapeutic potential of drugs with restricted pharmacological profile and encompass toxicity limitations and poor availability [207–210].

One of the first small molecules encapsulated for MD applications was gentamicin, to enhance its poor delivery profile to the muscle tissue and to decrease its toxicity [120,181]. In order to overcome these drawbacks, Yukihiro et al. encapsulated gentamicin into liposomes made of phosphatidylcholine or phosphocholine and PEG. Efficient accumulation of these nanosystems in the cytoplasm and cytoplasmic membranes of myofibers after I.P. injection was observed. Gentamicin-loaded liposomes increased the percentage of dystrophin positive myofibers up to 7.7% compared to 2.4% for gentamicin alone and were able to suppress the drug related ototoxicity and nephrotoxicity. However, despite the positive features of liposomes, which led to an enhanced pharmacological profile of gentamicin, this small molecule is candidate for only nonsense DMD mutations, thus restricting its clinical potential only to a narrow population of DMD patients [211].

Regulating downregulated myogenic recovery factors such as Myogenic differentiation 1 (MyoD) appears to be a good strategy to restore muscle differentiation and regeneration [212]. For this purpose, Afzal et al. designed nanolipodendrosomes loaded with synthesised MyoD and glatiramer acetate (GA), a synthetic drug that increases the level of anti-inflammatory cytokines [179]. The results demonstrated that these loaded nanosystems significantly improved muscle mass of lower-limbs in healthy SW-1 mice after I.M. injection, while no improvement was observed in the other muscles. Authors suggested that further research would warrant the use of nanolipodendrosomes loaded with these two candidate drugs to ameliorate muscle regeneration.

Bibee et al. developed lipid NPs of perfluorocarbon (PFC) to deliver rapamycin [182], an immunosuppressant and anti-inflammatory agent that proved to restore defective autophagy mechanism in *mdx* mice, associated with many side effects [213]. The main advantage of PFC NPs is their exceedingly good stability in blood, as they were originally developed as a blood substitute [214,215]. After systemic injection, nanocarriers were able to rescue a correct autophagy flux in *mdx* mice, thus improving both skeletal muscle strength and cardiac contractile performance. On the other hand, no equivalent improvement was achieved with conventional oral rapamycin administration delivered at a concentration even 10-fold superior, corresponding to the pharmacological doses. Furthermore, these muscle performance improvements were observed in young or adult wild-type mice as well as in aged mice, demonstrating the broad efficiency of this therapy. Clinically, potential deleterious consequences of rapamycin could be mitigated by the lower required dose administration of rapamycin once loaded into PFC NPs.

Lowering the severe side effects associated with chronic glucocorticosteroid administration has been investigated by Turjeman et al., encapsulating methylprednisolone hemisuccinate (MPS) into PEGylated nanoliposomes (NSSL) [180]. These smaller liposomes (80 nm) benefit from the inflamed tissues' unique vascular abnormality, achieving muscle passive targeting and accumulation into the inflamed tissue [216,217]. NSSL/MPS were mostly internalised into the diaphragm of young *mdx* mice after I.V. injection, due to the multiple tissue damages occurring in this organ at this stage, resulting in NPs leakage from capillaries. A significant decrease of TGF- β 1 protein level was observed in serum, as a result of protective effects against inflammation. NSSL/MPS significantly ameliorated osteoporosis in elderly *mdx* mice, whereas MPS alone further increased bone catabolic effects, increasing DMD phenotype. Finally, differences in NSSL/MPS treatment doses showed diverse muscle benefits: lower doses demonstrating advantages in terms of muscle strength, whereas higher doses showing benefits in terms of mobility.

Márquez-Miranda et al. developed hydroxyl-terminated poly(amidoamine) (PAMAM-OH) dendrimer as a carrier for angiotensin (1–7), an anti-atrophic bioactive heptapeptide highly beneficial in the treatment of skeletal muscle pathologies [176]. PAMAM-OH dendrimers were used to increase angiotensin (1–7) short half-life, hydrolytic stability and poor systemic distribution. To observe the anti-atrophic effect of angiotensin (1–7), the authors unilaterally immobilised lower hind limbs of normal mice for 14 days. Loaded nanosystems demonstrated the ability to restore muscle strength and recover fibres diameter of immobilised limbs to levels similar to non-immobilised limbs after I.P. administration,

whereas angiotensin (1–7) alone did not induce any recovery. Moreover, bone micro-architectural structure in elderly *mdx* mice was less damaged over 58 weeks of NSSL-MPS administration compared to mice treated with MPS. Altogether, these findings highlight the potency of PAMAM-OH/angiotensin (1–7) nanocarriers as an efficient general treatment of dystrophies for mitigating muscle atrophy.

Many therapeutic approaches have been explored through the screening of small molecules to reverse pathological consequences of MDs. Despite several advantages including lower costs, ease of therapy management and faster development process, small molecules are intended only to target downstream effects at the splicing or protein level and not to correct mutations at the DNA or RNA levels. In the studies presented above, nanomedicine has allowed for an increase in the therapeutic impact of experimental small molecules or well-known effective molecules, while significantly decreasing potential deleterious side effects.

4.4. CRISPR/Cas9 System

CRISPR/Cas9 system is a recent and powerful genome editing tool of great interest to treat genetic disorders such as DMD and DM [100,218]. The delivery of Cas9/sgRNA ribonucleoprotein complexes via non-viral delivery systems has been investigated to boost its clinical applications [219,220]. Challenges rely principally on the large size of Cas9 protein and the difficulty to prevent ribonucleoprotein complexes from degrading during the entire formulation and delivery process [183]. Lee et al. used gold NPs (GNP) to develop innovative carriers for the delivery of the entire CRISPR/Cas9 system (named CRISPR-Gold) to restore dystrophin expression by inducing in vivo homologous directed repair (HDR) in *mdx* mice [184]. Authors selected GNP as they can be easily coated with a densely packed layer of DNA and can be internalised by a variety of cell types [221,222]. To obtain complex CRISPR-Gold, the authors coated GNP with a thiol-terminated DNA to efficiently hybridize thiol-terminated donor DNA and trigger its rapid release once into the cytoplasm by disulfide-bond cleavage. Cas9 protein/sgRNA was then adsorbed onto the NPs, then finally covered with PAsp(DET) endosomal disruptive polymer. CRISPR-Gold demonstrated the ability to efficiently deliver in vitro and in vivo both the protein and the nucleic acid of the CRISPR/Cas9 system, through their affinity with the GNP coating of packed layer DNA. Injected simultaneously with cardiotoxin to induce further muscle damage, CRISPR-Gold revealed in *mdx* mice an HDR efficiency up to 18 times higher than CRISPR/Cas9 system itself with 5.4% restoration of the dystrophin gene. Moreover, cryosections of CRISPR-Gold-injected muscles showed a robust dystrophin expression nearly similar to that of wild-type mice muscle and reduced levels of muscle fibrosis, a sign of better tissue health. CRISPR-Gold delivered under clinically relevant conditions (without cardiotoxin) were shown to enhance animal strength and agility in *mdx* mice with HDR efficiency of 1% in the dystrophin gene and minimal off-target genomic damage. Finally, this work evidenced the absence of a broad immune response that could be potentially induced by the Cas9 bacterial protein, suggesting the possible safety of multiple injections of CRISPR-Gold. In conclusion, the authors designed NPs able to bind all CRISPR/Cas9 components but also to intracellularly deliver them through endosomal disruptive and disulphide reduction mechanisms. Complex and innovative CRISPR-Gold has the potential to regenerate wild-type dystrophin to a fully functional level, appearing as a promising treatment for genetic diseases such as DMD.

Recently, Wei et al. efficiently delivered Cas9/sgRNA ribonucleoprotein complexes to muscle, brain, liver and lungs using lipid NPs [183]. By adjusting the molecular components and ratios of lipids, the authors achieved tissue-specific gene editing in liver and lungs of healthy mice C57BL/6J after systemic injection. More interestingly, these nanosystems were evaluated in Δ Ex44 DMD mice and were proven to restore dystrophin expression up to ~5% after I.M. administration.

To our knowledge, NPs here presented are the only CRISPR/Cas9 delivery systems using non-viral NPs that have been described for MD applications. Although CRISPR/Cas9

is currently one of the most efficient tools for genome editing, non-viral delivery strategies are needed to improve precise gene correction.

5. Limitations In In Vitro and In Vivo Testing of Novel Treatments

The evaluation of nanomedicine behaviour in appropriate in vitro and in vivo models able to mimic physiology and phenotypes of MDs is an important requirement for their clinical translation. For preliminary studies and screening of different drugs, in vitro and ex vivo models based on immortalised or mutant human and animal cells, muscle preservation systems or tissue engineered constructs have been set-up as alternatives to rare patient cells. In addition, different animal models have been also set up to provide accurate in vivo MD models. An overview of the common used in vitro, ex vivo or in vivo models for testing novel MD treatments is provided in Figure 4.

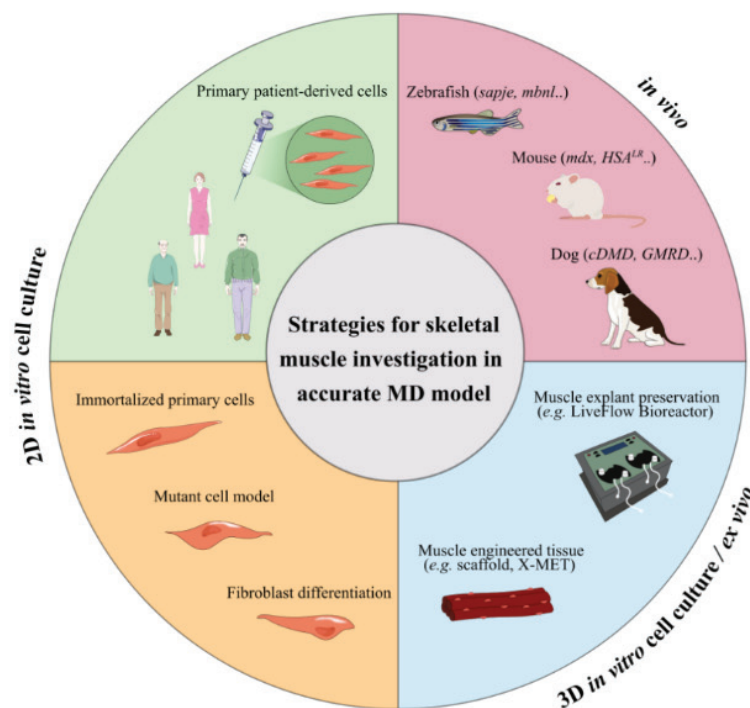


Figure 4. Strategies and accurate models to explore MD treatments. Broad in vitro, ex vivo and in vivo MD models to promote the translation of nanomedicine-based therapies (MD, muscular dystrophies; X-MET, ex vivo-vascularized muscle engineered tissue).

In vitro studies provide a unique preliminary resource to clarify the potential risk of NPs administration [223]. Primary cells are the most representative cell model for studying the molecular hallmarks of these pathologies as they are directly isolated from the patient's tissue [224]. However, their use is limited by the poor availability of muscle tissue due to the small samples collected by biopsy and the limited proliferative capacity of the satellite cells isolated from the explanted tissue [225–229]. To overcome these limitations, different strategies have been proposed. Genetic mutation characteristics of the pathology can be exogenously introduced into immortalised cell lines such as HeLa, C2C12 myoblasts or induced pluripotent stem cells (iPS). Even if these experimental models do not reproduce the entire genomic context, these transfected cells express the main features of the pathogenic mechanism, providing a cell-based model for studying the splicing defects of MDs [18,86,230]. Another approach consists in the immortalisation of primary muscle cells by reducing their replicative senescence with the use of telomere shortening, inhibiting the dominant p16 pathway [223,231–233]. Skin fibroblasts from patient skin biopsies can

also differentiate into multinucleated myotubes by inducing the myogenic regulator factor MyoD [223,224,234,235]. However, these 2D monolayer cultures inaccurately representing in vitro tissue cells and cellular response to therapeutic treatments might be erroneous due to the unnatural microenvironment [236,237]. In this context, 3D culture systems have gained increasing interest as they are able to provide accurate models of organs or tissue physiology and associated disorders. However, they are not exempt from limitations, such as lack of nutrients and oxygen distribution, and accumulation of wastes into the core of 3D culture [236,238,239]. Diverse biomimetic engineered muscle constructs, such as scaffold or organoid cell culture, have demonstrated structural and functional characteristics similar to native muscle, mimicking the tissue complexity [240–242]. These skeletal muscle organoids offer an attractive alternative to preliminary in vivo studies for disease modelling and in vitro drug screening.

Ex-vivo models have also reproduced accurate natural environment models for broad applications, overcoming 3D cell culture challenges related to heterogeneous oxygen, nutrient and metabolic waste distribution [237,243–245]. One possible approach for muscle investigations is culturing skeletal muscle explants as intact muscle fibres (myofibers) or intact muscles, preserving cell/tissue architecture and its relationship with the surrounding anatomical structures [246]. Moreover, fluid dynamic systems may improve the organ preservation, overcoming the loss of vasculature function by mimicking the physiological flow for nutrient supply and catabolite withdrawal, thus supporting the metabolic activity of the explanted tissues [243,247]. Recently, Carton et al. demonstrated the great benefit in terms of structural preservation obtained by maintaining explanted soleus murine muscle in a bioreactor under dynamic conditions [248]. The progressive structural deterioration of the muscle tissue was markedly slowed, prolonging its preservation up to two days. This innovative system allows experimental testing on the living organism with positive ethical impact, overcoming animal injuries related to therapeutic trial. Bioengineered three-dimensional vascularised skeletal muscle tissue (named X-MET) has also been developed by Carosio et al., using heterogeneous primary cell populations such as myoblasts, fibroblasts and endothelial cells [249]. This vascularised ex-vivo system closely mimicking the cellular complexity of the muscle tissue showed biomechanical properties and activity similar to adult skeletal muscles. Furthermore, X-MET transplanted into damaged muscle has demonstrated interesting properties to restore muscle functionality.

To further investigate therapeutic efficacy, in vivo testing remains the most representative means of study for understanding the complex cellular and tissue mechanisms' interactions [250,251]. Over the last years, various animal models of MDs have contributed to clarifying the molecular phenotypes involved in these pathologies and investigating drug screening [252–254]. Several DMD animal models have been developed by reproducing the deficient dystrophin expression. As previously reported, the *mdx* mouse (BL10-*mdx*) is the most commonly used DMD animal model and is characterised by the presence of a stop codon located in exon 23 that leads to loss of full-length dystrophin whereas smaller isoforms are still expressed [89,255]. Recently, D2-*mdx* mouse models issued from a different genetic background (DBA2/J) have demonstrated a more pronounced phenotype closer to patients [256]. Furthermore, Desguerre et al. described a model of chronic mechanical muscle injury to trigger muscle fibrosis at the same time of dystrophin-deficiency expression in *mdx* hindlimb muscle [257]. DMD canine model (cDMD, GRMD) also carries dystrophin deficit and expresses clinical phenotypes more severely than *mdx* mouse, better aligning with the progressive course of DMD and thereby better translating to humans [252,258,259]. Two zebrafish dystrophin mutants, *sapje* and *sapje-like* (*sapc/100*), carry a mutation in the dystrophin gene, which results in a premature stop codon, thus mimicking muscle dysfunction with a severe phenotype [260,261]. Other less common DMD animal models include *Caenorhabditis elegans*, *Drosophila melanogaster*, feline, rat and pig models [252].

Regarding DM, animal models have been developed by reproducing CUG expansion, MBNL-deficient or CELF-overexpressing phenotypes. Two main mouse models are com-

monly used for the study of DM1 and DM2: DMSXL mice, carrying ~ 1000–1800 CTG repeats with multisystemic transgene expression, and HSA^{LR} mice that express human skeletal actin (HSA) transcripts containing ~ 250 trinucleotide repeats within the 3' DMPK UTR with skeletal muscle transgene expression [262,263]. These murine models reproduce the DM1 and DM2 pathogenesis similarly to the human phenotype [264–268]. Two zebrafish models of MBNL loss of function, typical of DM1, have been generated to study the pathological aspects that characterise skeletal and heart muscles in DM [269,270]. Other transgenic animals, such as *Caenorhabditis elegans* and *Drosophila melanogaster* have also been engineered to mimic some characteristics of DM phenotypes [252,262].

Although no animal model is able to completely recapitulate the aspects of the multisystemic phenotypes typical of MDs, their use is required to provide critical in-depth assessment of proof-of-principle concept studies and preclinical experiments. The actual growing interest and knowledge for development of in vitro and ex vivo alternatives to reduce clinical animal experimentation could warrant novel and better methods for assisting in assessment of MDs therapy.

6. Future Perspectives

The recent understanding of the pathogenic mechanisms of MDs highlights the urgent need of new and more effective treatments [20,100]. Nanomedicine demonstrated to enhance the therapeutic potential of gene therapy and drug repurposing approaches. As an example, pentamidine-loaded nanomedicines were used to explore the activity of the drug, not only as an anti-leishmaniasis agent but also as an anticancer agent to reduce drug associated toxicity, such as its severe nephrotoxicity [271,272]. Ongoing investigations are aimed at demonstrating the efficacy of this novel formulation to treat DM1 (study in progress).

New therapeutic approaches needed a continuous administration throughout patient's life, making the biocompatibility and biodegradability of delivery systems a crucial feature to preserve skeletal muscle from additional alterations. As presented in this review, the main advantages of nanosystems rely on their physico-chemical properties, namely composition, size and surface potential that can be modulated to avoid nanocarrier toxicity, and to load specific actives and deliver them in a target site.

To disclose the potential of nanomedicine application to MDs treatment, the gap between in vitro and in vivo testing has to be filled. In addition, to understand the fate of nanosystems once administered to MDs mice, biodistribution studies need to be addressed. To date, only a few investigations reported NPs biodistribution into skeletal muscles through different administration routes as I.V., I.P. and I.M. (tibialis anterior and gastrocnemius muscles) [173,273,274]. After systemic administration, NPs spread into tissues through blood systemic circulation, then, extravasate into the ECM before reaching muscle fibres. It has been suggested that the dense blood capillary network wrapping skeletal myofibers could be favourable to NPs accumulation and distribution following I.V. injection [196]. Hydrodynamic injection is also known to facilitate gene delivery by transient enhancement of the plasma membrane's permeability [142,275,276]. However, the applied pressure due to the hindrance of the blood flow might cause oedema and inflammation, restricting the translation of this technique to clinic [277].

Overcoming the ECM barrier remains another important goal to improve NPs distribution in skeletal muscle fibres. Surface engineered nanosystems have been designed to actively promote the interaction between nanosystems and cells [278]. The high specificity of antibodies for their corresponding antigen provides a selective and potent approach for therapeutic NPs targeting [279]. As an example, the murine monoclonal antibody (3E10), capable of binding the surface of muscle cells, has been reported to improve active targeting [280,281]. However, no scientific studies on antibody-functionalised NPs have been conducted for skeletal muscle targeting so far. More commonly used, short peptides sequences (e.g., ASSLNIA or SKTFNTHPQSTP) have proved promising as NPs functionalization for specific tissue-targeting [282–284]. Several examples of peptides

targeting muscle cells have been reported [285–287] and association to nanosystems may lead to improved selectivity of NPs for skeletal muscle. Polymeric nanosystems have been functionalised with active targeting agents that preferentially bind active molecules or receptors expressed on the surface of muscle cells. Active targeting-dependent uptake has been demonstrated using PLGA nanocarriers functionalised with a muscle-homing peptide M12 [288]. Biodistribution studies revealed a preferential accumulation of targeted NPs in skeletal muscle cells in *mdx* mice, compared to untargeted nanocarriers, increasing the accumulation of polymeric NPs and enhancing therapeutic efficacy [274].

As presented in this review, nanomedicine holds promise for the development of efficient and safe MD treatments. With the rise in biologic products development, there is an increasing interest for effective biocompatible delivery systems that can be better suited for biologics leading to more effective therapeutic strategies. Further development of nanomedicine in this area is expected to result from complementary expertise in different research fields. Indeed, a multi-disciplinary study in drug discovery, nanomedicine, biotechnology, biology and medicine is key to providing valid and reliable strategies that can offer unprecedented opportunities to MD patients.

Author Contributions: I.A., M.R. and F.C. wrote the first draft of the review. G.L., B.S., S.A., M.M., S.B. and D.K. reviewed the manuscript and contributed to the critical analysis and the future perspectives of the work. R.M. and B.C. helped with the description of the disease. G.L., B.S., S.A. and M.M. conceptualised the work. All authors have read and agreed to the published version of the manuscript.

Funding: I.A. has a fellowship from the Italian Ministry of University and Research. M.R. has a fellowship from the INVITE project of the University of Verona (PhD Programme in Nanoscience and Advanced Technologies). INVITE is an initiative funded by European Union’s Horizon 2020 Research and Innovation Programme under the Marie Skłodowska-Curie grant agreement No. 754345.

Institutional Review Board Statement: Not applicable.

Informed Consent Statement: Not applicable.

Data Availability Statement: Not applicable.

Acknowledgments: Euronanomed III (Joint Translational Call 2017, Project RESOLVE), the Italian Ministry of University and Research–University of Turin “Fondi Ricerca Locale (ex-60%)”. Figures have been designed using Inkscape v.0.92.2 software. Some scientific illustrations were used from Servier Medical Art templates, which are licensed under a Creative Commons Attribution 3.0 Unported License; <https://smart.servier.com>.

Conflicts of Interest: The authors declare no conflict of interest.

References

- Shieh, P.B. Muscular dystrophies and other genetic myopathies. *Neurol. Clin.* **2013**, *31*, 1009–1029. [[CrossRef](#)] [[PubMed](#)]
- Theadom, A.; Rodrigues, M.; Roxburgh, R.; Balalla, S.; Higgins, C.; Bhattacharjee, R.; Jones, K.; Krishnamurthi, R.; Feigin, V. Prevalence of muscular dystrophies: A systematic literature review. *Neuroepidemiology* **2014**, *43*, 259–268. [[CrossRef](#)] [[PubMed](#)]
- Mercuri, E.; Bönnemann, C.G.; Muntoni, F. Muscular dystrophies. *Lancet Lond. Engl.* **2019**, *394*, 2025–2038. [[CrossRef](#)]
- Carter, J.C.; Sheehan, D.W.; Prochoroff, A.; Birnkrant, D.J. Muscular Dystrophies. *Clin. Chest Med.* **2018**, *39*, 377–389. [[CrossRef](#)]
- Johnson, N.E. Myotonic Dystrophies. *Continuum* **2019**, *25*, 1682–1695. [[CrossRef](#)] [[PubMed](#)]
- Meola, G. Clinical aspects, molecular pathomechanisms and management of myotonic dystrophies. *Acta Myol.* **2013**, *32*, 154–165.
- Messina, S.; Vita, G.L. Clinical management of Duchenne muscular dystrophy: The state of the art. *Neurol. Sci.* **2018**, *39*, 1837–1845. [[CrossRef](#)] [[PubMed](#)]
- Nio, Y.; Tanaka, M.; Hirozane, Y.; Muraki, Y.; Okawara, M.; Hazama, M.; Matsuo, T. Phosphodiesterase 4 inhibitor and phosphodiesterase 5 inhibitor combination therapy has antifibrotic and anti-inflammatory effects in *mdx* mice with Duchenne muscular dystrophy. *FASEB J.* **2017**, *31*, 5307–5320. [[CrossRef](#)] [[PubMed](#)]
- Zanotti, S.; Bragato, C.; Zucchella, A.; Maggi, L.; Mantegazza, R.; Morandi, L.; Mora, M. Anti-fibrotic effect of pirfenidone in muscle derived-fibroblasts from Duchenne muscular dystrophy patients. *Life Sci.* **2016**, *145*, 127–136. [[CrossRef](#)]
- McDonald, C.M.; Henricson, E.K.; Abresch, R.T.; Duong, T.; Joyce, N.C.; Hu, F.; Clemens, P.R.; Hoffman, E.P.; Cnaan, A.; Gordish-Dressman, H.; et al. Long-term effects of glucocorticoids on function, quality of life, and survival in patients with Duchenne Muscular Dystrophy: A prospective cohort study. *Lancet* **2018**, *391*, 451–461. [[CrossRef](#)]

11. Kao, K.-T.; Joseph, S.; Capaldi, N.; Brown, S.; Di Marco, M.; Dunne, J.; Horrocks, I.; Shepherd, S.; Ahmed, S.F.; Wong, S.C. Skeletal disproportion in glucocorticoid-treated boys with Duchenne muscular dystrophy. *Eur. J. Pediatr.* **2019**, *178*, 633–640. [[CrossRef](#)] [[PubMed](#)]
12. Mayo, A.L.; Craven, B.C.; McAdam, L.C.; Biggar, W.D. Bone health in boys with Duchenne muscular dystrophy on long-term daily deflazacort therapy. *Neuromuscul. Disord.* **2012**, *22*, 1040–1045. [[CrossRef](#)]
13. Ward, L.M.; Weber, D.R. Growth, pubertal development, and skeletal health in boys with Duchenne muscular dystrophy. *Curr. Opin. Endocrinol. Diabetes Obes.* **2019**, *26*, 39–48. [[CrossRef](#)]
14. Birnkrant, D.J.; Bushby, K.; Bann, C.M.; Apkon, S.D.; Blackwell, A.; Brumbaugh, D.; Case, L.E.; Clemens, P.R.; Hadjiyannakis, S.; Pandya, S.; et al. Diagnosis and management of Duchenne muscular dystrophy, part 1: Diagnosis, and neuromuscular, rehabilitation, endocrine, and gastrointestinal and nutritional management. *Lancet Neurol.* **2018**, *17*, 251–267. [[CrossRef](#)]
15. Fayssoil, A.; Lazarus, A.; Wahbi, K.; Ognà, A.; Nardi, O.; Lofaso, F.; Clair, B.; Orlikowski, D.; Annane, D. Cardiac implantable electronic devices in tracheotomized muscular dystrophy patients: Safety and risks. *Int. J. Cardiol.* **2016**, *222*, 975–977. [[CrossRef](#)] [[PubMed](#)]
16. Bach, J.R.; Saporito, L.R.; Shah, H.R.; Sinquee, D. Decanulation of patients with severe respiratory muscle insufficiency: Efficacy of mechanical insufflation-exsufflation. *J. Rehabil. Med.* **2014**, *46*, 1037–1041. [[CrossRef](#)]
17. Warf, M.B.; Nakamori, M.; Matthys, C.M.; Thornton, C.A.; Berglund, J.A. Pentamidine reverses the splicing defects associated with myotonic dystrophy. *Proc. Natl. Acad. Sci. USA* **2009**, *106*, 18551–18556. [[CrossRef](#)]
18. Konieczny, P.; Selma-Soriano, E.; Rapisarda, A.S.; Fernandez-Costa, J.M.; Perez-Alonso, M.; Artero, R. Myotonic dystrophy: Candidate small molecule therapeutics. *Drug Discov. Today* **2017**, *22*, 1740–1748. [[CrossRef](#)] [[PubMed](#)]
19. Lee, J.E.; Bennett, C.F.; Cooper, T.A. RNase H-mediated degradation of toxic RNA in myotonic dystrophy type 1. *Proc. Natl. Acad. Sci. USA* **2012**, *109*, 4221–4226. [[CrossRef](#)]
20. Verhaart, I.E.C.; Aartsma-Rus, A. Therapeutic developments for Duchenne muscular dystrophy. *Nat. Rev. Neurol.* **2019**, *15*, 373–386. [[CrossRef](#)]
21. Zhang, Y.; Li, H.; Min, Y.L.; Sanchez-Ortiz, E.; Huang, J.; Mireault, A.A.; Shelton, J.M.; Kim, J.; Mammen, P.P.A.; Bassel-Duby, R.; et al. Enhanced CRISPR-Cas9 correction of Duchenne muscular dystrophy in mice by a self-complementary AAV delivery system. *Sci. Adv.* **2020**, *6*, eaay6812. [[CrossRef](#)]
22. Lo Scudato, M.; Poulard, K.; Sourd, C.; Tomé, S.; Klein, A.F.; Corre, G.; Huguet, A.; Furling, D.; Gourdon, G.; Buj-Bello, A. Genome editing of expanded CTG repeats within the human DMPK gene reduces nuclear RNA foci in the muscle of DM1 mice. *Mol. Ther.* **2019**, *27*, 1372–1388. [[CrossRef](#)]
23. Pedrini, I.; Gazzano, E.; Chegaev, K.; Rolando, B.; Marengo, A.; Kopecka, J.; Fruttero, R.; Ghigo, D.; Arpicco, S.; Riganti, C. Liposomal nitrooxy-doxorubicin: One step over caelyx in drug-resistant human cancer cells. *Mol. Pharm.* **2014**, *11*, 3068–3079. [[CrossRef](#)] [[PubMed](#)]
24. Autio, K.A.; Dreicer, R.; Anderson, J.; Garcia, J.A.; Alva, A.; Hart, L.L.; Milowsky, M.I.; Posadas, E.M.; Ryan, C.J.; Graf, R.P.; et al. Safety and efficacy of BIND-014, a docetaxel nanoparticle targeting prostate-specific membrane antigen for patients with metastatic castration-resistant prostate cancer: A phase 2 clinical trial. *JAMA Oncol.* **2018**, *4*, 1344–1351. [[CrossRef](#)]
25. Van der Meel, R.; Sulheim, E.; Shi, Y.; Kiessling, F.; Mulder, W.J.M.; Lammers, T. Smart cancer nanomedicine. *Nat. Nanotechnol.* **2019**, *14*, 1007–1017. [[CrossRef](#)]
26. Wang-Gillam, A.; Hubner, R.A.; Siveke, J.T.; Von Hoff, D.D.; Belanger, B.; de Jong, F.A.; Mirakhor, B.; Chen, L.-T. NAPOLI-1 phase 3 study of liposomal irinotecan in metastatic pancreatic cancer: Final overall survival analysis and characteristics of long-term survivors. *Eur. J. Cancer* **2019**, *108*, 78–87. [[CrossRef](#)] [[PubMed](#)]
27. Hanif, S.; Muhammad, P.; Chesworth, R.; Rehman, F.U.; Qian, R.; Zheng, M.; Shi, B. Nanomedicine-Based Immunotherapy for Central Nervous System Disorders. *Acta Pharmacol. Sin.* **2020**, *41*, 936–953. [[CrossRef](#)] [[PubMed](#)]
28. You, L.; Wang, J.; Liu, T.; Zhang, Y.; Han, X.; Wang, T.; Guo, S.; Dong, T.; Xu, J.; Anderson, G.J.; et al. Targeted brain delivery of rabies virus glycoprotein 29-modified deferoxamine-loaded nanoparticles reverses functional deficits in Parkinsonian mice. *ACS Nano* **2018**, *12*, 4123–4139. [[CrossRef](#)]
29. Dos Santos Tramontin, N.; da Silva, S.; Arruda, R.; Ugioni, K.S.; Canteiro, P.B.; de Bem Silveira, G.; Mendes, C.; Silveira, P.C.L.; Muller, A.P. Gold nanoparticles treatment reverses brain damage in Alzheimer’s disease model. *Mol. Neurobiol.* **2020**, *57*, 926–936. [[CrossRef](#)] [[PubMed](#)]
30. Pearson, R.M.; Podojil, J.R.; Shea, L.D.; King, N.J.C.; Miller, S.D.; Getts, D.R. Overcoming challenges in treating autoimmunity: Development of tolerogenic immune-modifying nanoparticles. *Nanomedicine* **2019**, *18*, 282–291. [[CrossRef](#)]
31. Zhao, G.; Liu, A.; Zhang, Y.; Zuo, Z.-Q.; Cao, Z.-T.; Zhang, H.-B.; Xu, C.-F.; Wang, J. Nanoparticle-delivered siRNA targeting Bruton’s tyrosine kinase for rheumatoid arthritis therapy. *Biomater. Sci.* **2019**, *7*, 4698–4707. [[CrossRef](#)] [[PubMed](#)]
32. Horwitz, D.A.; Bickerton, S.; Koss, M.; Fahmy, T.M.; La Cava, A. Suppression of murine Lupus by CD4+ and CD8+ treg cells induced by T cell-targeted nanoparticles loaded with interleukin-2 and transforming growth factor β . *Arthritis Rheumatol.* **2019**, *71*, 632–640. [[CrossRef](#)]
33. Fries, C.N.; Curvino, E.J.; Chen, J.-L.; Permar, S.R.; Fouda, G.G.; Collier, J.H. Advances in nanomaterial vaccine strategies to address infectious diseases impacting global health. *Nat. Nanotechnol.* **2020**, 1–14. [[CrossRef](#)] [[PubMed](#)]
34. Nanomedicine and the COVID-19 vaccines. *Nat. Nanotechnol.* **2020**, 1. [[CrossRef](#)]

35. Sahin, U.; Muik, A.; Derhovanesian, E.; Vogler, I.; Kranz, L.M.; Vormehr, M.; Baum, A.; Pascal, K.; Quandt, J.; Maurus, D.; et al. COVID-19 vaccine BNT162b1 elicits human antibody and TH1 T cell responses. *Nature* **2020**, *586*, 594–599. [[CrossRef](#)] [[PubMed](#)]
36. Baden, L.R.; El Sahly, H.M.; Essink, B.; Kotloff, K.; Frey, S.; Novak, R.; Diemert, D.; Spector, S.A.; Rouphael, N.; Creech, C.B.; et al. Efficacy and safety of the mRNA-1273 SARS-CoV-2 vaccine. *N. Engl. J. Med.* **2020**, *384*, 403–416. [[CrossRef](#)] [[PubMed](#)]
37. Chung, Y.H.; Beiss, V.; Fiering, S.N.; Steinmetz, N.F. COVID-19 vaccine frontrunners and their nanotechnology design. *ACS Nano* **2020**, *14*, 12522–12537. [[CrossRef](#)]
38. Kranz, L.M.; Diken, M.; Haas, H.; Kreiter, S.; Loquai, C.; Reuter, K.C.; Meng, M.; Fritz, D.; Vascotto, F.; Hefesha, H.; et al. Systemic RNA delivery to dendritic cells exploits antiviral defence for cancer immunotherapy. *Nature* **2016**, *534*, 396–401. [[CrossRef](#)] [[PubMed](#)]
39. Xin, X.; Kumar, V.; Lin, F.; Kumar, V.; Bhattarai, R.; Bhatt, V.R.; Tan, C.; Mahato, R.I. Redox-responsive nanoplatfor for codelivery of miR-519c and gemcitabine for pancreatic cancer therapy. *Sci. Adv.* **2020**, eabd6764. [[CrossRef](#)] [[PubMed](#)]
40. Sasso, M.S.; Lollo, G.; Pitorre, M.; Solito, S.; Pinton, L.; Valpione, S.; Bastiat, G.; Mandruzzato, S.; Bronte, V.; Marigo, I.; et al. Low dose gemcitabine-loaded lipid nanocapsules target monocytic myeloid-derived suppressor cells and potentiate cancer immunotherapy. *Biomaterials* **2016**, *96*, 47–62. [[CrossRef](#)] [[PubMed](#)]
41. Lancet, J.E.; Uy, G.L.; Cortes, J.E.; Newell, L.F.; Lin, T.L.; Ritchie, E.K.; Stuart, R.K.; Strickland, S.A.; Hogge, D.; Solomon, S.R.; et al. CPX-351 (cytarabine and daunorubicin) liposome for injection versus conventional cytarabine plus daunorubicin in older patients with newly diagnosed secondary acute myeloid leukemia. *J. Clin. Oncol.* **2018**, *36*, 2684–2692. [[CrossRef](#)]
42. Salvioni, L.; Rizzuto, M.A.; Bertolini, J.A.; Pandolfi, L.; Colombo, M.; Prosperi, D. Thirty years of cancer nanomedicine: Success, frustration, and hope. *Cancers* **2019**, *11*, 1855. [[CrossRef](#)]
43. Gillies, A.R.; Lieber, R.L. Structure and function of the skeletal muscle extracellular matrix. *Muscle Nerve* **2011**, *44*, 318–331. [[CrossRef](#)]
44. Yhee, J.Y.; Yoon, H.Y.; Kim, H.; Jeon, S.; Hergert, P.; Im, J.; Panyam, J.; Kim, K.; Nho, R.S. The effects of collagen-rich extracellular matrix on the intracellular delivery of glycol chitosan nanoparticles in human lung fibroblasts. *Int. J. Nanomed.* **2017**, *12*, 6089–6105. [[CrossRef](#)] [[PubMed](#)]
45. Sleboda, D.A.; Stover, K.K.; Roberts, T.J. Diversity of extracellular matrix morphology in vertebrate skeletal muscle. *J. Morphol.* **2020**, *281*, 160–169. [[CrossRef](#)] [[PubMed](#)]
46. Engin, A.B.; Nikitovic, D.; Neagu, M.; Henrich-Noack, P.; Docea, A.O.; Shtilman, M.I.; Golokhvast, K.; Tsatsakis, A.M. Mechanistic understanding of nanoparticles' interactions with extracellular matrix: The cell and immune system. *Part. Fibre Toxicol.* **2017**, *14*, 22. [[CrossRef](#)] [[PubMed](#)]
47. Stylianopoulos, T.; Poh, M.Z.; Insin, N.; Bawendi, M.G.; Fukumura, D.; Munn, L.L.; Jain, R.K. Diffusion of particles in the extracellular matrix: The effect of repulsive electrostatic interactions. *Biophys. J.* **2010**, *99*, 1342–1349. [[CrossRef](#)] [[PubMed](#)]
48. Zhigaltsev, I.V.; Belliveau, N.; Hafez, I.; Leung, A.K.K.; Huft, J.; Hansen, C.; Cullis, P.R. Bottom-up design and synthesis of limit size lipid nanoparticle systems with aqueous and triglyceride cores using millisecond microfluidic mixing. *Langmuir* **2012**, *28*, 3633–3640. [[CrossRef](#)]
49. Evers, M.J.W.; Kulkarni, J.A.; van der Meel, R.; Cullis, P.R.; Vader, P.; Schifflers, R.M. State-of-the-art design and rapid-mixing production techniques of lipid nanoparticles for nucleic acid delivery. *Small Methods* **2018**, *2*, 1700375. [[CrossRef](#)]
50. Feng, J.; Markwalter, C.E.; Tian, C.; Armstrong, M.; Prud'homme, R.K. Translational formulation of nanoparticle therapeutics from laboratory discovery to clinical scale. *J. Transl. Med.* **2019**, *17*, 200. [[CrossRef](#)] [[PubMed](#)]
51. Ebner, D.C.; Bialek, P.; El-Kattan, A.F.; Ambler, C.M.; Tu, M. Strategies for skeletal muscle targeting in drug discovery. *Curr. Pharm. Des.* **2015**, *21*, 1327–1336. [[CrossRef](#)] [[PubMed](#)]
52. Mah, J.K.; Korngut, L.; Fiest, K.M.; Dykeman, J.; Day, L.J.; Pringsheim, T.; Jette, N. A Systematic review and meta-analysis on the epidemiology of the muscular dystrophies. *Can. J. Neurol. Sci.* **2015**, *43*, 163–177. [[CrossRef](#)]
53. Nascimento Osorio, A.; Medina Cantillo, J.; Camacho Salas, A.; Madruga Garrido, M.; Vilchez Padilla, J.J. Consensus on the diagnosis, treatment and follow-up of patients with Duchenne muscular dystrophy. *Neurologia* **2019**, *34*, 469–481. [[CrossRef](#)]
54. Koenig, M.; Hoffman, E.P.; Bertelson, C.J.; Monaco, A.P.; Feener, C.; Kunkel, L.M. Complete cloning of the Duchenne muscular dystrophy (DMD) cDNA and preliminary genomic organization of the DMD gene in normal and affected individuals. *Cell* **1987**, *50*, 509–517. [[CrossRef](#)]
55. Zhu, J.F.; Liu, H.H.; Zhou, T.; Tian, L. Novel mutation in exon 56 of the dystrophin gene in a child with Duchenne muscular dystrophy. *Int. J. Mol. Med.* **2013**, *32*, 1166–1170. [[CrossRef](#)] [[PubMed](#)]
56. Muntoni, F.; Torelli, S.; Ferlini, A. Dystrophin and mutations: One gene, several proteins, multiple phenotypes. *Lancet Neurol.* **2003**, *2*, 731–740. [[CrossRef](#)]
57. Koenig, M.; Beggs, A.H.; Moyer, M.; Scherpf, S.; Heindrich, K.; Bettecken, T.; Meng, G.; Müller, C.R.; Lindlöf, M.; Kaariainen, H.; et al. The molecular basis for Duchenne versus Becker muscular dystrophy: Correlation of severity with type of deletion. *Am. J. Hum. Genet.* **1989**, *45*, 498–506. [[PubMed](#)]
58. Miyatake, S.; Mizobe, Y.; Takizawa, H.; Hara, Y.; Yokota, T.; Takeda, S.; Aoki, Y. Exon skipping therapy using phosphorodiamidate morpholino oligomers in the *mdx52* mouse model of Duchenne muscular dystrophy. *Methods Mol. Biol.* **2018**, *1687*, 123–141. [[CrossRef](#)]
59. Zhu, P.; Wu, F.; Mosenson, J.; Zhang, H.; He, T.-C.; Wu, W.-S. CRISPR/Cas9-mediated genome editing corrects dystrophin mutation in skeletal muscle stem cells in a mouse model of muscle dystrophy. *Mol. Ther. Nucleic Acids* **2017**, *7*, 31–41. [[CrossRef](#)]

60. Bird, T.D. Myotonic Dystrophy Type 1. In *GeneReviews*[®]; Adam, M.P., Ardinger, H.H., Pagon, R.A., Wallace, S.E., Bean, L.J., Stephens, K., Amemiya, A., Eds.; University of Washington: Seattle, WA, USA, 1993–2020.
61. Thornton, C.A. Myotonic dystrophy. *Neurol. Clin.* **2014**, *32*, 705–719. [[CrossRef](#)] [[PubMed](#)]
62. Turner, C.; Hilton-Jones, D. The myotonic dystrophies: Diagnosis and management. *J. Neurol. Neurosurg. Psychiatry* **2010**, *81*, 358–367. [[CrossRef](#)]
63. Lee, J.E.; Cooper, T.A. Pathogenic mechanisms of myotonic dystrophy. *Biochem. Soc. Trans.* **2009**, *37*, 1281–1286. [[CrossRef](#)]
64. De Temmerman, N.; Sermon, K.; Seneca, S.; De Rycke, M.; Hilven, P.; Lissens, W.; Van Steirteghem, A.; Liebaers, I. Intergenerational instability of the expanded CTG repeat in the DMPK gene: Studies in human gametes and preimplantation embryos. *Am. J. Hum. Genet.* **2004**, *75*, 325–329. [[CrossRef](#)]
65. Malatesta, M.; Cardani, R.; Pellicciari, C.; Meola, G. RNA transcription and maturation in skeletal muscle cells are similarly impaired in myotonic dystrophy and sarcopenia: The ultrastructural evidence. *Front. Aging Neurosci.* **2014**, *6*, 196. [[CrossRef](#)]
66. Nakamori, M.; Sobczak, K.; Puwanant, A.; Welle, S.; Eichinger, K.; Pandya, S.; Dekdebrun, J.; Heatwole, C.R.; McDermott, M.P.; Chen, T.; et al. Splicing biomarkers of disease severity in myotonic dystrophy. *Ann. Neurol.* **2013**, *74*, 862–872. [[CrossRef](#)] [[PubMed](#)]
67. Miller, J.W.; Urbinati, C.R.; Teng-Umuay, P.; Stenberg, M.G.; Byrne, B.J.; Thornton, C.A.; Swanson, M.S. Recruitment of human muscleblind proteins to (CUG)_n expansions associated with myotonic dystrophy. *EMBO J.* **2000**, *19*, 4439–4448. [[CrossRef](#)] [[PubMed](#)]
68. Meola, G.; Cardani, R. Myotonic dystrophies: An update on clinical aspects, genetic, pathology, and molecular pathomechanisms. *Biochim. Biophys. Acta* **2015**, *1852*, 594–606. [[CrossRef](#)] [[PubMed](#)]
69. Paul, S.; Dansithong, W.; Kim, D.; Rossi, J.; Webster, N.J.; Comai, L.; Reddy, S. Interaction of muscleblind, CUG-BP1 and hnRNP H proteins in DM1-associated aberrant IR splicing. *EMBO J.* **2006**, *25*, 4271–4283. [[CrossRef](#)]
70. Perdoni, F.; Malatesta, M.; Cardani, R.; Giagnacovo, M.; Mancinelli, E.; Meola, G.; Pellicciari, C. RNA/MBNL1-containing foci in myoblast nuclei from patients affected by myotonic dystrophy type 2: An immunocytochemical study. *Eur. J. Histochem.* **2009**, *53*, e18. [[CrossRef](#)]
71. Mulders, S.A.M.; van den Broek, W.J.A.A.; Wheeler, T.M.; Croes, H.J.E.; van Kuik-Romeijn, P.; de Kimpe, S.J.; Furling, D.; Platenburg, G.J.; Gourdon, G.; Thornton, C.A.; et al. Triplet-repeat oligonucleotide-mediated reversal of RNA toxicity in myotonic dystrophy. *Proc. Natl. Acad. Sci. USA* **2009**, *106*, 13915–13920. [[CrossRef](#)]
72. Sardone, V.; Zhou, H.; Muntoni, F.; Ferlini, A.; Falzarano, M.S. Antisense oligonucleotide-based therapy for neuromuscular disease. *Molecules* **2017**, *22*, 563. [[CrossRef](#)] [[PubMed](#)]
73. Kanadia, R.N.; Shin, J.; Yuan, Y.; Beattie, S.G.; Wheeler, T.M.; Thornton, C.A.; Swanson, M.S. Reversal of RNA missplicing and myotonia after muscleblind overexpression in a mouse poly(CUG) model for myotonic dystrophy. *Proc. Natl. Acad. Sci. USA* **2006**, *103*, 11748–11753. [[CrossRef](#)]
74. Arambula, J.F.; Ramisetty, S.R.; Baranger, A.M.; Zimmerman, S.C. A simple ligand that selectively targets CUG trinucleotide repeats and inhibits MBNL protein binding. *Proc. Natl. Acad. Sci. USA* **2009**, *106*, 16068–16073. [[CrossRef](#)]
75. Childs-Disney, J.L.; Hoskins, J.; Rzuczek, S.G.; Thornton, C.A.; Disney, M.D. Rationally designed small molecules targeting the RNA that causes myotonic dystrophy type 1 are potently bioactive. *ACS Chem. Biol.* **2012**, *7*, 856–862. [[CrossRef](#)]
76. Udd, B.; Krahe, R. The myotonic dystrophies: Molecular, clinical, and therapeutic challenges. *Lancet Neurol.* **2012**, *11*, 891–905. [[CrossRef](#)]
77. Mendell, J.R.; Rodino-Klapac, L.R.; Sahenk, Z.; Roush, K.; Bird, L.; Lowes, L.P.; Alfano, L.; Gomez, A.M.; Lewis, S.; Kota, J.; et al. Eteplirsen for the treatment of Duchenne muscular dystrophy. *Ann. Neurol.* **2013**, *74*, 637–647. [[CrossRef](#)]
78. Goemans, N.; Mercuri, E.; Belousova, E.; Komaki, H.; Dubrovsky, A.; McDonald, C.M.; Kraus, J.E.; Loubakos, A.; Lin, Z.; Champion, G.; et al. A randomized placebo-controlled phase 3 trial of an antisense oligonucleotide, drisapersen, in Duchenne muscular dystrophy. *Neuromuscul. Disord.* **2018**, *28*, 4–15. [[CrossRef](#)]
79. Goemans, N.M.; Tulinius, M.; van den Akker, J.T.; Burm, B.E.; Ekhardt, P.F.; Heuvelmans, N.; Holling, T.; Janson, A.A.; Platenburg, G.J.; Sipkens, J.A.; et al. Systemic administration of PRO051 in Duchenne’s muscular dystrophy. *N. Engl. J. Med.* **2011**, *365*, 1513–1522. [[CrossRef](#)]
80. Pandey, S.K.; Wheeler, T.M.; Justice, S.L.; Kim, A.; Younis, H.S.; Gattis, D.; Jauvin, D.; Puymirat, J.; Swayze, E.E.; Freier, S.M.; et al. Identification and characterization of modified antisense oligonucleotides targeting DMPK in mice and nonhuman primates for the treatment of myotonic dystrophy type 1s. *J. Pharmacol. Exp. Ther.* **2015**, *355*, 329–340. [[CrossRef](#)] [[PubMed](#)]
81. Klein, A.F.; Varela, M.A.; Arandel, L.; Holland, A.; Naouar, N.; Arzumanov, A.; Seoane, D.; Revillod, L.; Bassez, G.; Ferry, A.; et al. Peptide-conjugated oligonucleotides evoke long-lasting myotonic dystrophy correction in patient-derived cells and mice. *J. Clin. Invest.* **2019**, *129*, 4739–4744. [[CrossRef](#)]
82. Min, Y.L.; Li, H.; Rodriguez-Caycedo, C.; Mireault, A.A.; Huang, J.; Shelton, J.M.; McAnally, J.R.; Amoasii, L.; Mammen, P.P.A.; Bassel-Duby, R.; et al. CRISPR-Cas9 corrects Duchenne muscular dystrophy exon 44 deletion mutations in mice and human cells. *Sci. Adv.* **2019**, *5*, eaav4324. [[CrossRef](#)]
83. Amoasii, L.; Hildyard, J.C.W.; Li, H.; Sanchez-Ortiz, E.; Mireault, A.; Caballero, D.; Harron, R.; Stathopoulou, T.-R.; Massey, C.; Shelton, J.M.; et al. Gene editing restores dystrophin expression in a canine model of Duchenne muscular dystrophy. *Science* **2018**, *362*, 86–91. [[CrossRef](#)] [[PubMed](#)]
84. Hotta, A. Genome editing gene therapy for Duchenne muscular dystrophy. *J. Neuromuscul. Dis.* **2015**, *2*, 343–355. [[CrossRef](#)]

85. Amoasii, L.; Long, C.; Li, H.; Mireault, A.A.; Shelton, J.M.; Sanchez-Ortiz, E.; Mcanally, J.R.; Bhattacharyya, S.; Schmidt, F.; Grimm, D.; et al. Single-cut genome editing restores dystrophin expression in a new mouse model of muscular dystrophy. *Sci. Transl. Med.* **2017**, *29*, eaan8081. [[CrossRef](#)]
86. Dastidar, S.; Ardui, S.; Singh, K.; Majumdar, D.; Nair, N.; Fu, Y.; Reyon, D.; Samara, E.; Gerli, M.F.M.; Klein, A.F.; et al. Efficient CRISPR/Cas9-mediated editing of trinucleotide repeat expansion in myotonic dystrophy patient-derived iPSC and myogenic cells. *Nucleic Acids Res.* **2018**, *46*, 8275–8298. [[CrossRef](#)]
87. Wagner, K.R.; Hamed, S.; Hadley, D.W.; Gropman, A.L.; Burstein, A.H.; Escolar, D.M.; Hoffman, E.P.; Fischbeck, K.H. Gentamicin treatment of Duchenne and Becker muscular dystrophy due to nonsense mutations. *Ann. Neurol.* **2001**, *49*, 706–711. [[CrossRef](#)]
88. Barton-Davis, E.R.; Cordier, L.; Shoturma, D.I.; Leland, S.E.; Sweeney, H.L. Aminoglycoside antibiotics restore dystrophin function to skeletal muscles of *mdx* mice. *J. Clin. Investig.* **1999**, *104*, 375–381. [[CrossRef](#)] [[PubMed](#)]
89. Vitiello, L.; Tibaudou, L.; Pegoraro, E.; Bello, L.; Canton, M. Teaching an old molecule new tricks: Drug repositioning for Duchenne muscular dystrophy. *Int. J. Mol. Sci.* **2019**, *20*, 6053. [[CrossRef](#)] [[PubMed](#)]
90. Welch, E.M.; Barton, E.R.; Zhuo, J.; Tomizawa, Y.; Friesen, W.J.; Trifillis, P.; Paushkin, S.; Patel, M.; Trotta, C.R.; Hwang, S.; et al. PTC124 targets genetic disorders caused by nonsense mutations. *Nature* **2007**, *447*, 87–91. [[CrossRef](#)] [[PubMed](#)]
91. McDonald, C.M.; Campbell, C.; Torricelli, R.E.; Finkel, R.S.; Flanigan, K.M.; Goemans, N.; Heydemann, P.; Kaminska, A.; Kirschner, J.; Muntoni, F.; et al. Ataluren in patients with nonsense mutation Duchenne muscular dystrophy (ACT DMD): A multicentre, randomised, double-blind, placebo-controlled, phase 3 trial. *Lancet* **2017**, *390*, 1489–1498. [[CrossRef](#)]
92. Siboni, R.B.; Bodner, M.J.; Khalifa, M.M.; Docter, A.G.; Choi, J.Y.; Nakamori, M.; Haley, M.M.; Berglund, J.A. Biological efficacy and toxicity of diamidines in myotonic dystrophy type 1 models. *J. Med. Chem.* **2015**, *58*, 5770–5780. [[CrossRef](#)]
93. Jenquin, J.R.; Coonrod, L.A.; Silverglate, Q.A.; Pellitier, N.A.; Hale, M.A.; Xia, G.; Nakamori, M.; Berglund, J.A. Furamide rescues myotonic dystrophy type I associated mis-splicing through multiple mechanisms. *ACS Chem. Biol.* **2018**, *13*, 2708–2718. [[CrossRef](#)]
94. Reddy, K.; Jenquin, J.R.; Cleary, J.D.; Berglund, J.A. Mitigating RNA toxicity in myotonic dystrophy using small molecules. *Int. J. Mol. Sci.* **2019**, *20*, 4017. [[CrossRef](#)] [[PubMed](#)]
95. Jenquin, J.R.; Yang, H.; Huigens III, R.W.; Nakamori, M.; Berglund, J.A. Combination treatment of erythromycin and furamide provides additive and synergistic rescue of mis-splicing in myotonic dystrophy type 1 models. *ACS Pharmacol. Transl. Sci.* **2019**, *2*, 247–263. [[CrossRef](#)] [[PubMed](#)]
96. Zhang, F.; Bodycombe, N.E.; Haskell, K.M.; Sun, Y.L.; Wang, E.T.; Morris, C.A.; Jones, L.H.; Wood, L.D.; Pletcher, M.T. A flow cytometry-based screen identifies MBNL1 modulators that rescue splicing defects in myotonic dystrophy type I. *Hum. Mol. Genet.* **2017**, *26*, 3056–3068. [[CrossRef](#)]
97. Naldini, L. Gene therapy returns to centre stage. *Nature* **2015**, *526*, 351–360. [[CrossRef](#)]
98. Fischer, A.; Hacein-Bey-Abina, S.; Cavazzana-Calvo, M. 20 years of gene therapy for SCID. *Nat. Immunol.* **2010**, *11*, 457–460. [[CrossRef](#)] [[PubMed](#)]
99. Dunbar, C.E.; High, K.A.; Joung, J.K.; Kohn, D.B.; Ozawa, K.; Sadelain, M. Gene therapy comes of age. *Science* **2018**, *359*, eaan4672. [[CrossRef](#)] [[PubMed](#)]
100. Smith, R.A.; Miller, T.M.; Yamanaka, K.; Monia, B.P.; Condon, T.P.; Hung, G.; Lobsiger, C.S.; Ward, C.M.; McAlonis-Downes, M.; Wei, H.; et al. Antisense oligonucleotide therapy for neurodegenerative disease. *J. Clin. Investig.* **2006**, *116*, 2290–2296. [[CrossRef](#)]
101. Liang, X.H.; Sun, H.; Nichols, J.G.; Croke, S.T. RNase H1-dependent antisense oligonucleotides are robustly active in directing RNA cleavage in both the cytoplasm and the nucleus. *Mol. Ther.* **2017**, *25*, 2075–2092. [[CrossRef](#)]
102. Geary, R.S.; Norris, D.; Yu, R.; Bennett, C.F. Pharmacokinetics, biodistribution and cell uptake of antisense oligonucleotides. *Adv. Drug Deliv. Rev.* **2015**, *87*, 46–51. [[CrossRef](#)]
103. Liang, X.-H.; Shen, W.; Sun, H.; Kinberger, G.A.; Prakash, T.P.; Nichols, J.G.; Croke, S.T. Hsp90 protein interacts with phosphorothioate oligonucleotides containing hydrophobic 2'-modifications and enhances antisense activity. *Nucleic Acids Res.* **2016**, *44*, 3892–3907. [[CrossRef](#)]
104. He, X.-Y.; Wang, J.; Lu, D.-D.; Wang, S.-Q. Synthesis and antisense properties of 2'- β -F-arabinouridine modified oligonucleotides with 4'-C-OME substituent. *Molecules* **2018**, *23*, 2374. [[CrossRef](#)]
105. Hagedorn, P.H.; Pontoppidan, M.; Bisgaard, T.S.; Berrera, M.; Dieckmann, A.; Ebeling, M.; Møller, M.R.; Hudlebusch, H.; Jensen, M.L.; Hansen, H.F.; et al. Identifying and avoiding off-target effects of RNase H-dependent antisense oligonucleotides in mice. *Nucleic Acids Res.* **2018**, *46*, 5366–5380. [[CrossRef](#)]
106. Bosgra, S.; Sipkens, J.; De Kimpe, S.; Den Besten, C.; Datson, N.; Van Deutekom, J. The pharmacokinetics of 2'-O-methyl phosphorothioate antisense oligonucleotides: Experiences from developing exon skipping therapies for Duchenne muscular dystrophy. *Nucleic Acid Ther.* **2019**, *29*, 305–322. [[CrossRef](#)] [[PubMed](#)]
107. Hara, Y.; Mizobe, Y.; Miyatake, S.; Takizawa, H.; Nagata, T.; Yokota, T.; Takeda, S.I.; Aoki, Y. Exon skipping using antisense oligonucleotides for laminin-alpha2-deficient muscular dystrophy. *Methods Mol. Biol.* **2018**, *1828*, 553–564. [[CrossRef](#)] [[PubMed](#)]
108. Sicinski, P.; Geng, Y.; Ryder-Cook, A.S.; Barnard, E.A.; Darlison, M.G.; Barnard, P.J. The molecular basis of muscular dystrophy in the *mdx* mouse: A point mutation. *Science* **1989**, *244*, 1578–1580. [[CrossRef](#)]
109. Kinali, M.; Arechavala-Gomeza, V.; Feng, L.; Cirak, S.; Hunt, D.; Adkin, C.; Guglieri, M.; Ashton, E.; Abbs, S.; Nihoyannopoulos, P.; et al. Local restoration of dystrophin expression with the morpholino oligomer AVI-4658 in Duchenne muscular dystrophy: A single-blind, placebo-controlled, dose-escalation, proof-of-concept study. *Lancet Neurol.* **2009**, *8*, 918–928. [[CrossRef](#)]

110. Watanabe, N.; Nagata, T.; Satou, Y.; Masuda, S.; Saito, T.; Kitagawa, H.; Komaki, H.; Takagaki, K.; Takeda, S. NS-065/NCNP-01: An antisense oligonucleotide for potential treatment of exon 53 skipping in Duchenne muscular dystrophy. *Mol. Ther. Nucleic Acids* **2018**, *13*, 442–449. [[CrossRef](#)]
111. Gao, Z.; Cooper, T.A. Antisense oligonucleotides: Rising stars in eliminating RNA toxicity in myotonic dystrophy. *Hum. Gene Ther.* **2013**, *24*, 499–507. [[CrossRef](#)] [[PubMed](#)]
112. Huguët, A.; Medja, F.; Nicole, A.; Vignaud, A.; Guiraud-Dogan, C.; Ferry, A.; Decostre, V.; Hogrel, J.Y.; Metzger, F.; Hoeflich, A.; et al. Molecular, physiological, and motor performance defects in DMSXL mice carrying >1,000 CTG repeats from the human DM1 locus. *PLoS Genet.* **2012**, *8*, e1003043. [[CrossRef](#)] [[PubMed](#)]
113. Wheeler, T.M.; Leger, A.J.; Pandey, S.K.; MacLeod, A.R.; Nakamori, M.; Cheng, S.H.; Wentworth, B.M.; Bennett, C.F.; Thornton, C.A. Targeting nuclear RNA for in vivo correction of myotonic dystrophy. *Nature* **2012**, *488*, 111–115. [[CrossRef](#)]
114. Jauvin, D.; Chrétien, J.; Pandey, S.K.; Martineau, L.; Revillod, L.; Bassez, G.; Lachon, A.; McLeod, A.R.; Gourdon, G.; Wheeler, T.M.; et al. Targeting DMPK with antisense oligonucleotide improves muscle strength in myotonic dystrophy type 1 mice. *Mol. Ther. Nucleic Acids* **2017**, *7*, 465–474. [[CrossRef](#)]
115. Ousterout, D.G.; Kabadi, A.M.; Thakore, P.I.; Majoros, W.H.; Reddy, T.E.; Gersbach, C.A. Multiplex CRISPR/Cas9-based genome editing for correction of dystrophin mutations that cause Duchenne muscular dystrophy. *Nat. Commun.* **2015**, *6*, 6244. [[CrossRef](#)]
116. Ousterout, D.G.; Kabadi, A.M.; Thakore, P.I.; Perez-Pinera, P.; Brown, M.T.; Majoros, W.H.; Reddy, T.E.; Gersbach, C.A. Correction of dystrophin expression in cells from Duchenne Muscular Dystrophy patients through genomic excision of exon 51 by Zinc Finger Nucleases. *Mol. Ther.* **2015**, *23*, 523–532. [[CrossRef](#)] [[PubMed](#)]
117. Ousterout, D.G.; Perez-Pinera, P.; Thakore, P.I.; Kabadi, A.M.; Brown, M.T.; Qin, X.; Fedrigo, O.; Mouly, V.; Tremblay, J.P.; Gersbach, C.A. Reading frame correction by targeted genome editing restores dystrophin expression in cells from Duchenne Muscular Dystrophy patients. *Mol. Ther.* **2013**, *21*, 1718–1726. [[CrossRef](#)]
118. Doudna, J.A.; Charpentier, E. Genome editing. The new frontier of genome engineering with CRISPR-Cas9. *Science* **2014**, *346*, 1258096. [[CrossRef](#)]
119. Nance, M.E.; Hakim, C.H.; Yang, N.N.; Duan, D. Nanotherapy for Duchenne muscular dystrophy. *Wiley Interdiscip. Rev. Nanomed. Nanobiotechnol.* **2018**, *10*, e1472. [[CrossRef](#)] [[PubMed](#)]
120. Amitai, G.; Sorek, R. CRISPR-Cas adaptation: Insights into the mechanism of action. *Nat. Rev. Microbiol.* **2016**, *14*, 67–76. [[CrossRef](#)]
121. Kleinstiver, B.P.; Prew, M.S.; Tsai, S.Q.; Topkar, V.V.; Nguyen, N.T.; Zheng, Z.; Gonzales, A.P.W.; Li, Z.; Peterson, R.T.; Yeh, J.-R.J.; et al. Engineered CRISPR-Cas9 nucleases with altered PAM specificities. *Nature* **2015**, *523*, 481–485. [[CrossRef](#)] [[PubMed](#)]
122. Wang, Y.; Hao, L.; Wang, H.; Santostefano, K.; Thapa, A.; Cleary, J.; Li, H.; Guo, X.; Terada, N.; Ashizawa, T.; et al. Therapeutic genome editing for myotonic dystrophy type 1 using CRISPR/Cas9. *Mol. Ther.* **2018**, *26*, 2617–2630. [[CrossRef](#)]
123. Naso, M.F.; Tomkowicz, B.; Perry, W.L.; Strohl, W.R. Adeno-associated virus (AAV) as a vector for gene therapy. *BioDrugs* **2017**, *31*, 317–334. [[CrossRef](#)] [[PubMed](#)]
124. Komor, A.C.; Kim, Y.B.; Packer, M.S.; Zuris, J.A.; Liu, D.R. Programmable editing of a target base in genomic DNA without double-stranded DNA cleavage. *Nature* **2016**, *533*, 420–424. [[CrossRef](#)] [[PubMed](#)]
125. Gaudelli, N.M.; Komor, A.C.; Rees, H.A.; Packer, M.S.; Badran, A.H.; Bryson, D.I.; Liu, D.R. Programmable base editing of A•T to G•C in genomic DNA without DNA cleavage. *Nature* **2017**, *551*, 464–471. [[CrossRef](#)]
126. Abudayyeh, O.O.; Gootenberg, J.S.; Franklin, B.; Koob, J.; Kellner, M.J.; Ladha, A.; Joung, J.; Kirchgatterer, P.; Cox, D.B.T.; Zhang, F. A Cytosine deaminase for programmable single-base RNA editing. *Science* **2019**, *365*, 382–386. [[CrossRef](#)] [[PubMed](#)]
127. Ryu, S.-M.; Koo, T.; Kim, K.; Lim, K.; Baek, G.; Kim, S.-T.; Kim, H.S.; Kim, D.-E.; Lee, H.; Chung, E.; et al. Adenine base editing in mouse embryos and an adult mouse model of Duchenne Muscular Dystrophy. *Nat Biotechnol* **2018**, *36*, 536–539. [[CrossRef](#)]
128. Jiang, T.; Henderson, J.M.; Coote, K.; Cheng, Y.; Valley, H.C.; Zhang, X.-O.; Wang, Q.; Rhym, L.H.; Cao, Y.; Newby, G.A.; et al. Chemical modifications of adenine base editor mRNA and guide RNA expand its application scope. *Nat Commun* **2020**, *11*, 1979. [[CrossRef](#)]
129. Anzalone, A.V.; Randolph, P.B.; Davis, J.R.; Sousa, A.A.; Koblan, L.W.; Levy, J.M.; Chen, P.J.; Wilson, C.; Newby, G.A.; Raguram, A.; et al. Search-and-replace genome editing without double-strand breaks or donor DNA. *Nature* **2019**, *576*, 149–157. [[CrossRef](#)]
130. Pushpakom, S.; Iorio, F.; Eyers, P.A.; Escott, K.J.; Hopper, S.; Wells, A.; Doig, A.; Williams, T.; Latimer, J.; McNamee, C.; et al. Drug repurposing: Progress, challenges and recommendations. *Nat. Rev. Drug Discov.* **2019**, *18*, 41–58. [[CrossRef](#)]
131. Knapp, S. New opportunities for kinase drug repurposing and target discovery. *Br. J. Cancer* **2018**, *118*, 936–937. [[CrossRef](#)]
132. Wittenstein, A.; Caspi, M.; David, Y.; Shorer, Y.; Nadar-Ponniah, P.T.; Rosin-Arbesfeld, R. Serum starvation enhances nonsense mutation readthrough. *J. Mol. Med.* **2019**, *97*, 1695–1710. [[CrossRef](#)] [[PubMed](#)]
133. Chowdhury, H.M.; Siddiqui, M.A.; Kanneganti, S.; Sharmin, N.; Chowdhury, M.W.; Nasim, M.T. Aminoglycoside-mediated promotion of translation readthrough occurs through a non-stochastic mechanism that competes with translation termination. *Hum. Mol. Genet.* **2018**, *27*, 373–384. [[CrossRef](#)]
134. Shimizu-Motohashi, Y.; Komaki, H.; Motohashi, N.; Takeda, S.; Yokota, T.; Aoki, Y. Restoring dystrophin expression in Duchenne muscular dystrophy: Current status of therapeutic approaches. *J. Pers. Med.* **2019**, *9*, 1. [[CrossRef](#)]
135. Hayward, R.S.; Harding, J.; Molloy, R.; Land, L.; Longcroft-Neal, K.; Moore, D.; Ross, J.D.C. Adverse effects of a single dose of gentamicin in adults: A systematic review. *Br. J. Clin. Pharmacol.* **2018**, *84*, 223–238. [[CrossRef](#)] [[PubMed](#)]

136. Friesen, W.J.; Johnson, B.; Sierra, J.; Zhuo, J.; Vazirani, P.; Xue, X.; Tomizawa, Y.; Baiazitov, R.; Morrill, C.; Ren, H.; et al. The minor gentamicin complex component, X2, is a potent premature stop codon readthrough molecule with therapeutic potential. *PLoS ONE* **2018**, *13*, e0206158. [[CrossRef](#)]
137. Gonzalez, A.L.; Konieczny, P.; Llamusi, B.; Delgado-Pinar, E.; Borrell, J.I.; Teixidó, J.; García-España, E.; Pérez-Alonso, M.; Estrada-Tejedor, R.; Artero, R. In silico discovery of substituted pyrido[2,3-d] pyrimidines and pentamidine-like compounds with biological activity in myotonic dystrophy models. *PLoS ONE* **2017**, *12*, e0178931. [[CrossRef](#)]
138. Díaz, M.V.; Miranda, M.R.; Campos-Estrada, C.; Reigada, C.; Maya, J.D.; Pereira, C.A.; López-Muñoz, R. Pentamidine exerts in vitro and in vivo anti *Trypanosoma cruzi* activity and inhibits the polyamine transport in *Trypanosoma cruzi*. *Acta Trop.* **2014**, *134*, 1–9. [[CrossRef](#)] [[PubMed](#)]
139. Coonrod, L.A.; Nakamori, M.; Wang, W.; Carrell, S.; Cameron, L.; Bodner, M.J.; Siboni, R.B.; Docter, A.G.; Haley, M.M.; Charles, A.; et al. Reducing levels of toxic RNA with small molecules. *ACS Chem. Biol.* **2013**, *8*, 2528–2537. [[CrossRef](#)] [[PubMed](#)]
140. Theocharis, A.D.; Skandalis, S.S.; Gialeli, C.; Karamanos, N.K. Extracellular matrix structure. *Adv. Drug Deliv. Rev.* **2016**, *97*, 4–27. [[CrossRef](#)]
141. Zhang, G.; Budker, V.; Williams, P.; Subbotin, V.; Wolff, J.A. Efficient expression of naked DNA delivered intraarterially to limb muscles of nonhuman primates. *Hum. Gene Ther.* **2001**, *12*, 427–438. [[CrossRef](#)]
142. Hagstrom, J.E.; Hegge, J.; Zhang, G.; Noble, M.; Budker, V.; Lewis, D.L.; Herweijer, H.; Wolff, J.A. A facile nonviral method for delivering genes and siRNAs to skeletal muscle of mammalian limbs. *Mol. Ther.* **2004**, *10*, 386–398. [[CrossRef](#)] [[PubMed](#)]
143. Gref, R.; Minamitake, Y.; Peracchia, M.T.; Trubetskoy, V.; Torchilin, V.; Langer, R. Biodegradable long-circulating polymeric nanospheres. *Science* **1994**, *263*, 1600–1603. [[CrossRef](#)] [[PubMed](#)]
144. Longmire, M.; Choyke, P.L.; Kobayashi, H. Clearance properties of nano-sized particles and molecules as imaging agents: Considerations and caveats. *Nanomedicine* **2008**, *3*, 703–717. [[CrossRef](#)] [[PubMed](#)]
145. Gustafson, H.H.; Holt-Casper, D.; Grainger, D.W.; Ghandehari, H. Nanoparticle uptake: The phagocyte problem. *Nano Today* **2015**, *10*, 487–510. [[CrossRef](#)] [[PubMed](#)]
146. Blanco, E.; Shen, H.; Ferrari, M. Principles of nanoparticle design for overcoming biological barriers to drug delivery. *Nat. Biotechnol.* **2015**, *33*, 941–951. [[CrossRef](#)] [[PubMed](#)]
147. Nguyen, V.H.; Lee, B.-J. Protein corona: A new approach for nanomedicine design. *Int. J. Nanomed.* **2017**, *12*, 3137–3151. [[CrossRef](#)]
148. Tenzer, S.; Docter, D.; Kuharev, J.; Musyanovych, A.; Fetz, V.; Hecht, R.; Schlenk, F.; Fischer, D.; Kiouptsi, K.; Reinhardt, C.; et al. Rapid formation of plasma protein corona critically affects nanoparticle pathophysiology. *Nat. Nanotechnol.* **2013**, *8*, 772–781. [[CrossRef](#)]
149. Stano, A.; Nembrini, C.; Swartz, M.A.; Hubbell, J.A.; Simeoni, E. Nanoparticle size influences the magnitude and quality of mucosal immune responses after intranasal immunization. *Vaccine* **2012**, *30*, 7541–7546. [[CrossRef](#)] [[PubMed](#)]
150. Hoshyar, N.; Gray, S.; Han, H.; Bao, G. The effect of nanoparticle size on in vivo pharmacokinetics and cellular interaction. *Nanomedicine* **2016**, *11*, 673–692. [[CrossRef](#)] [[PubMed](#)]
151. Vlasova, I.I.; Kapralov, A.A.; Michael, Z.P.; Burkert, S.C.; Shurin, M.R.; Star, A.; Shvedova, A.A.; Kagan, V.E. Enzymatic oxidative biodegradation of nanoparticles: Mechanisms, significance and applications. *Toxicol. Appl. Pharmacol.* **2016**, *299*, 58–69. [[CrossRef](#)] [[PubMed](#)]
152. Tidball, J.G.; Welc, S.S.; Wehling-Henricks, M. Immunobiology of inherited muscular dystrophies. *Compr. Physiol.* **2018**, *8*, 1313–1356. [[CrossRef](#)]
153. Smoak, M.M.; Mikos, A.G. Advances in biomaterials for skeletal muscle engineering and obstacles still to overcome. *Mater. Today Bio* **2020**, *7*, 100069. [[CrossRef](#)] [[PubMed](#)]
154. Evers, M.M.; Toonen, L.J.A.; van Roon-Mom, W.M.C. Antisense oligonucleotides in therapy for neurodegenerative disorders. *Adv. Drug Deliv. Rev.* **2015**, *87*, 90–103. [[CrossRef](#)]
155. Kauffman, K.J.; Webber, M.J.; Anderson, D.G. Materials for non-viral intracellular delivery of messenger RNA therapeutics. *J. Control. Release* **2016**, *240*, 227–234. [[CrossRef](#)]
156. Parlea, L.; Puri, A.; Kasprzak, W.; Bindewald, E.; Zakrevsky, P.; Satterwhite, E.; Joseph, K.; Afonin, K.A.; Shapiro, B.A. Cellular delivery of RNA nanoparticles. *ACS Comb. Sci.* **2016**, *18*, 527–547. [[CrossRef](#)] [[PubMed](#)]
157. Wahane, A.; Waghmode, A.; Kapphahn, A.; Dhuri, K.; Gupta, A.; Bahal, R. Role of lipid-based and polymer-based non-viral vectors in nucleic acid delivery for next-generation gene therapy. *Molecules* **2020**, *25*, 2866. [[CrossRef](#)] [[PubMed](#)]
158. Mastria, E.M.; Cai, L.Y.; Kan, M.J.; Li, X.; Schaal, J.L.; Fiering, S.; Gunn, M.D.; Dewhirst, M.W.; Nair, S.K.; Chilkoti, A. Nanoparticle formulation improves doxorubicin efficacy by enhancing host antitumor immunity. *J. Control. Release* **2018**, *269*, 364–373. [[CrossRef](#)] [[PubMed](#)]
159. Yu, A.-M.; Choi, Y.H.; Tu, M.-J. RNA drugs and RNA targets for small molecules: Principles, progress, and challenges. *Pharmacol. Rev.* **2020**, *72*, 862–898. [[CrossRef](#)]
160. Givens, B.E.; Naguib, Y.W.; Geary, S.M.; Devor, E.J.; Salem, A.K. Nanoparticle based delivery of CRISPR/Cas9 genome editing therapeutics. *AAPS J.* **2018**, *20*, 108. [[CrossRef](#)]
161. Liu, C.; Zhang, L.; Liu, H.; Cheng, K. Delivery strategies of the CRISPR-Cas9 gene-editing system for therapeutic applications. *J. Control. Release* **2017**, *266*, 17–26. [[CrossRef](#)]
162. Min, Y.-L.; Bassel-Duby, R.; Olson, E.N. CRISPR correction of Duchenne muscular dystrophy. *Annu. Rev. Med.* **2019**, *27*, 239–255. [[CrossRef](#)] [[PubMed](#)]

163. Williams, J.H.; Schray, R.C.; Sirsi, S.R.; Lutz, G.J. Nanopolymers improve delivery of exon skipping oligonucleotides and concomitant dystrophin expression in skeletal muscle of *mdx* mice. *BMC Biotechnol.* **2008**, *8*, 35. [[CrossRef](#)] [[PubMed](#)]
164. Sirsi, S.R.; Schray, R.C.; Wheatley, M.A.; Lutz, G.J. Formulation of poly(lactide-co-glycolic acid) nanospheres for encapsulation and sustained release of poly(ethylene imine)-poly(ethylene glycol) copolymers complexed to oligonucleotides. *J. Nanobiotechnol.* **2009**, *7*, 1. [[CrossRef](#)] [[PubMed](#)]
165. Wang, M.; Wu, B.; Lu, P.; Cloer, C.; Tucker, J.D.; Lu, Q. Polyethylenimine-modified Pluronics (PCMs) improve morpholino oligomer delivery in cell culture and dystrophic *mdx* mice. *Mol. Ther.* **2013**, *21*, 210–216. [[CrossRef](#)]
166. Wang, M.; Wu, B.; Lu, P.; Tucker, J.D.; Milazi, S.; Shah, S.N.; Lu, Q.L. Pluronic-PEI copolymers enhance exon-skipping of 2'-O-methyl phosphorothioate oligonucleotide in cell culture and dystrophic *mdx* mice. *Gene Ther.* **2014**, *21*, 52–59. [[CrossRef](#)] [[PubMed](#)]
167. Kim, Y.; Tewari, M.; Pajeroski, J.D.; Cai, S.; Sen, S.; Williams, J.; Sirsi, S.; Lutz, G.; Discher, D.E. Polymersome delivery of siRNA and antisense oligonucleotides. *J. Control. Release* **2009**, *134*, 132–140. [[CrossRef](#)]
168. Rimessi, P.; Sabatelli, P.; Fabris, M.; Braghetta, P.; Bassi, E.; Spitali, P.; Vattemi, G.; Tomelleri, G.; Mari, L.; Perrone, D.; et al. Cationic PMMA nanoparticles bind and deliver antisense oligoribonucleotides allowing restoration of dystrophin expression in the *mdx* mouse. *Mol. Ther.* **2009**, *17*, 820–827. [[CrossRef](#)] [[PubMed](#)]
169. Ferlini, A.; Sabatelli, P.; Fabris, M.; Bassi, E.; Falzarano, S.; Vattemi, G.; Perrone, D.; Gualandi, F.; Maraldi, N.M.; Merlini, L.; et al. Dystrophin restoration in skeletal, heart and skin arrector pili smooth muscle of *mdx* mice by ZM2 NP-AON complexes. *Gene Ther.* **2010**, *17*, 432–438. [[CrossRef](#)]
170. Bassi, E.; Falzarano, S.; Fabris, M.; Gualandi, F.; Merlini, L.; Vattemi, G.; Perrone, D.; Marchesi, E.; Sabatelli, P.; Spamacci, K.; et al. Persistent dystrophin protein restoration 90 days after a course of intraperitoneally administered naked 2'OMePS AON and ZM2 NP-AON complexes in *mdx* Mice. *J. Biomed. Biotechnol.* **2012**, *2012*, 1–8. [[CrossRef](#)]
171. Wang, M.; Wu, B.; Tucker, J.D.; Bollinger, L.E.; Lu, P.; Lu, Q. Poly(ester amine) composed of polyethylenimine and Pluronic enhance delivery of antisense oligonucleotides in vitro and in dystrophic *mdx* mice. *Mol. Ther. Nucleic Acids* **2016**, *5*, e341. [[CrossRef](#)]
172. Wang, M.; Tucker, J.D.; Lu, P.; Wu, B.; Cloer, C.; Lu, Q. Tris[2-(acryloyloxy)ethyl]isocyanurate cross-linked low-molecular-weight polyethylenimine as gene delivery carriers in cell culture and dystrophic *mdx* mice. *Bioconjug. Chem.* **2012**, *23*, 837–845. [[CrossRef](#)] [[PubMed](#)]
173. Itaka, K.; Osada, K.; Morii, K.; Kim, P.; Yun, S.-H.; Kataoka, K. Polyplex nanomicelle promotes hydrodynamic gene introduction to skeletal muscle. *J. Control. Release* **2010**, *143*, 112–119. [[CrossRef](#)]
174. Wang, J.; Zhang, P.-C.; Mao, H.-Q.; Leong, K.W. Enhanced gene expression in mouse muscle by sustained release of plasmid DNA using PPE-EA as a carrier. *Gene Ther.* **2002**, *9*, 1254–1261. [[CrossRef](#)]
175. Kinouchi, N.; Ohsawa, Y.; Ishimaru, N.; Ohuchi, H.; Sunada, Y.; Hayashi, Y.; Tanimoto, Y.; Moriyama, K.; Noji, S. Atelocollagen-mediated local and systemic applications of myostatin-targeting siRNA increase skeletal muscle mass. *Gene Ther.* **2008**, *15*, 1126–1130. [[CrossRef](#)]
176. Márquez-Miranda, V.; Abrigo, J.; Rivera, J.C.; Araya-Duran, I.; Aravena, J.; Simon, F.; Pacheco, N.; Gonzalez-Nilo, F.D.; Cabello-Verrugio, C. The complex of PAMAM-OH dendrimer with angiotensin (1-7) prevented the disuse-induced skeletal muscle atrophy in mice. *Int. J. Nanomed.* **2017**, *12*, 1985–1999. [[CrossRef](#)]
177. Negishi, Y.; Ishii, Y.; Shiono, H.; Akiyama, S.; Sekine, S.; Kojima, T.; Mayama, S.; Kikuchi, T.; Hamano, N.; Endo-Takahashi, Y.; et al. Bubble liposomes and ultrasound exposure improve localized morpholino oligomer delivery into the skeletal muscles of dystrophic *mdx* mice. *Mol. Pharm.* **2014**, *11*, 1053–1061. [[CrossRef](#)] [[PubMed](#)]
178. Koebis, M.; Kiyatake, T.; Yamaura, H.; Nagano, K.; Higashihara, M.; Sonoo, M.; Hayashi, Y.; Negishi, Y.; Endo-Takahashi, Y.; Yanagihara, D.; et al. Ultrasound-enhanced delivery of morpholino with bubble liposomes ameliorates the myotonia of myotonic dystrophy model mice. *Sci. Rep.* **2013**, *3*, 2242. [[CrossRef](#)] [[PubMed](#)]
179. Afzal, E.; Zakeri, S.; Keyhanvar, P.; Bagheri, M.; Mahjoubi, P.; Asadian, M.; Omoomi, N.; Dehqanian, M.; Ghalandarlaki, N.; Darvishmohammadi, T.; et al. Nanolipodendrosome-loaded glatiramer acetate and myogenic differentiation 1 as augmentation therapeutic strategy approaches in muscular dystrophy. *Int. J. Nanomed.* **2013**, *8*, 2943–2960. [[CrossRef](#)]
180. Turjeman, K.; Yanay, N.; Elbaz, M.; Bavli, Y.; Gross, M.; Rabie, M.; Barenholz, Y.; Nevo, Y. Liposomal steroid nano-drug is superior to steroids as-is in *mdx* mouse model of Duchenne muscular dystrophy. *Nanomedicine* **2019**, *16*, 34–44. [[CrossRef](#)] [[PubMed](#)]
181. Yukihiro, M.; Ito, K.; Tanoue, O.; Goto, K.; Matsushita, T.; Matsumoto, Y.; Masuda, M.; Kimura, S.; Ueoka, R. Effective drug delivery system for Duchenne muscular dystrophy using hybrid liposomes including gentamicin along with reduced toxicity. *Biol. Pharm. Bull.* **2011**, *34*, 712–716. [[CrossRef](#)] [[PubMed](#)]
182. Bibee, K.P.; Cheng, Y.; Ching, J.K.; Marsh, J.N.; Li, A.J.; Keeling, R.M.; Connolly, A.M.; Golumbek, P.T.; Myerson, J.W.; Hu, G.; et al. Rapamycin nanoparticles target defective autophagy in muscular dystrophy to enhance both strength and cardiac function. *FASEB J.* **2014**, *28*, 2047–2061. [[CrossRef](#)] [[PubMed](#)]
183. Wei, T.; Cheng, Q.; Min, Y.-L.; Olson, E.N.; Siegwart, D.J. Systemic nanoparticle delivery of CRISPR-Cas9 ribonucleoproteins for effective tissue specific genome editing. *Nat. Commun.* **2020**, *11*, 3232. [[CrossRef](#)]
184. Lee, K.; Conboy, M.; Park, H.M.; Jiang, F.; Kim, H.J.; Dewitt, M.A.; Mackley, V.A.; Chang, K.; Rao, A.; Skinner, C.; et al. Nanoparticle delivery of Cas9 ribonucleoprotein and donor DNA in vivo induces homology-directed DNA repair. *Nat. Biomed. Eng.* **2017**, *1*, 889–901. [[CrossRef](#)]

185. Järver, P.; O'Donovan, L.; Gait, M.J. A chemical view of oligonucleotides for exon skipping and related drug applications. *Nucleic Acid Ther.* **2014**, *24*, 37–47. [[CrossRef](#)] [[PubMed](#)]
186. Zhang, P.; Wagner, E. History of polymeric gene delivery systems. *Top. Curr. Chem.* **2017**, *375*, 26. [[CrossRef](#)] [[PubMed](#)]
187. Boussif, O.; Lezoualc'h, F.; Zanta, M.A.; Mergny, M.D.; Scherman, D.; Demeneix, B.; Behr, J.P. A versatile vector for gene and oligonucleotide transfer into cells in culture and *in vivo*: Polyethylenimine. *Proc. Natl. Acad. Sci. USA* **1995**, *92*, 7297–7301. [[CrossRef](#)]
188. Lu, Q.L.; Mann, C.J.; Lou, F.; Bou-Gharios, G.; Morris, G.E.; Xue, S.; Fletcher, S.; Partridge, T.A.; Wilton, S.D. Functional amounts of dystrophin produced by skipping the mutated exon in the *mdx* dystrophic mouse. *Nat. Med.* **2003**, *9*, 1009–1014. [[CrossRef](#)] [[PubMed](#)]
189. Lu, Q.L.; Bou-Gharios, G.; Partridge, T.A. Non-viral gene delivery in skeletal muscle: A protein factory. *Gene Ther.* **2003**, *10*, 131–142. [[CrossRef](#)] [[PubMed](#)]
190. Williams, J.H.; Sirsi, S.R.; Latta, D.R.; Lutz, G.J. Induction of dystrophin expression by exon skipping in *mdx* mice following intramuscular injection of antisense oligonucleotides complexed with PEG–PEI copolymers. *Mol. Ther.* **2006**, *14*, 88–96. [[CrossRef](#)]
191. Lutz, G.J.; Sirsi, S.R.; Williams, J.H. PEG–PEI copolymers for oligonucleotide delivery to Cells and tissues. *Methods Mol. Biol.* **2008**, *433*, 141–158. [[CrossRef](#)] [[PubMed](#)]
192. Castaldello, A.; Brocca-Cofano, E.; Voltan, R.; Triulzi, C.; Altavilla, G.; Laus, M.; Spamacci, K.; Ballestri, M.; Tondelli, L.; Fortini, C.; et al. DNA prime and protein boost immunization with innovative polymeric cationic core-shell nanoparticles elicits broad immune responses and strongly enhance cellular responses of HIV-1 tat DNA vaccination. *Vaccine* **2006**, *24*, 5655–5669. [[CrossRef](#)]
193. Summerton, J.; Weller, D. Morpholino antisense oligomers: Design, preparation, and properties. *Antisense Nucleic Acid Drug Dev.* **1997**, *7*, 187–195. [[CrossRef](#)] [[PubMed](#)]
194. Miller, C.M.; Harris, E.N. Antisense oligonucleotides: Treatment strategies and cellular internalization. *RNA Dis.* **2016**, *3*, e1393. [[CrossRef](#)]
195. Järver, P.; Zaghoul, E.M.; Arzumanov, A.A.; Saleh, A.F.; McClorey, G.; Hammond, S.M.; Hällbrink, M.; Langel, Ü.; Smith, C.I.E.; Wood, M.J.A.; et al. Peptide nanoparticle delivery of charge-neutral splice-switching morpholino oligonucleotides. *Nucleic Acid Ther.* **2015**, *25*, 65–77. [[CrossRef](#)] [[PubMed](#)]
196. Suzuki, R.; Takizawa, T.; Negishi, Y.; Hagsiwa, K.; Tanaka, K.; Sawamura, K.; Utoguchi, N.; Nishioka, T.; Maruyama, K. Gene delivery by combination of novel liposomal bubbles with perfluoropropane and ultrasound. *J. Control. Release* **2007**, *117*, 130–136. [[CrossRef](#)]
197. Negishi, Y.; Endo, Y.; Fukuyama, T.; Suzuki, R.; Takizawa, T.; Omata, D.; Maruyama, K.; Aramaki, Y. Delivery of siRNA into the cytoplasm by liposomal bubbles and ultrasound. *J. Control. Release* **2008**, *132*, 124–130. [[CrossRef](#)] [[PubMed](#)]
198. Tros de Ilarduya, C.; Sun, Y.; Düzgüneş, N. Gene delivery by lipoplexes and polyplexes. *Eur. J. Pharm. Sci.* **2010**, *40*, 159–170. [[CrossRef](#)]
199. Kulkarni, J.A.; Cullis, P.R.; van der Meel, R. Lipid nanoparticles enabling gene therapies: From concepts to clinical utility. *Nucleic Acid Ther.* **2018**, *28*, 146–157. [[CrossRef](#)]
200. Li, D.; Sharili, A.S.; Connelly, J.; Gautrot, J.E. Highly stable RNA capture by dense cationic polymer brushes for the design of cyto-compatible, serum-stable siRNA delivery vectors. *Biomacromolecules* **2018**, *19*, 606–615. [[CrossRef](#)]
201. Kulkarni, J.A.; Myhre, J.L.; Chen, S.; Tam, Y.Y.C.; Danescu, A.; Richman, J.M.; Cullis, P.R. Design of lipid nanoparticles for in vitro and in vivo delivery of plasmid DNA. *Nanomedicine* **2017**, *13*, 1377–1387. [[CrossRef](#)]
202. Sano, A.; Maeda, M.; Nagahara, S.; Ochiya, T.; Honma, K.; Itoh, H.; Miyata, T.; Fujioka, K. Atelocollagen for protein and gene delivery. *Adv. Drug Deliv. Rev.* **2003**, *55*, 1651–1677. [[CrossRef](#)] [[PubMed](#)]
203. Ochiya, T.; Nagahara, S.; Sano, A.; Itoh, H.; Terada, M. Biomaterials for gene delivery: Atelocollagen-mediated controlled release of molecular medicines. *Curr. Gene Ther.* **2001**, *1*, 31–52. [[CrossRef](#)]
204. Wang, J.; Mao, H.-Q.; Leong, K.W. A novel biodegradable gene carrier based on polyphosphoester. *J. Am. Chem. Soc.* **2001**, *123*, 9480–9481. [[CrossRef](#)]
205. Itaka, K.; Yamauchi, K.; Harada, A.; Nakamura, K.; Kawaguchi, H.; Kataoka, K. Polyion complex micelles from plasmid DNA and poly(ethylene glycol)-poly(L-lysine) block copolymer as serum-tolerable polyplex system: Physicochemical properties of micelles relevant to gene transfection efficiency. *Biomaterials* **2003**, *24*, 4495–4506. [[CrossRef](#)]
206. Parvathaneni, V.; Kulkarni, N.S.; Muth, A.; Gupta, V. Drug repurposing: A promising tool to accelerate the drug discovery process. *Drug Discov. Today* **2019**, *24*, 2076–2085. [[CrossRef](#)] [[PubMed](#)]
207. He, H.; Markoutsas, E.; Li, J.; Xu, P. Repurposing disulfiram for cancer therapy via targeted nanotechnology through enhanced tumor mass penetration and disassembly. *Acta Biomater.* **2018**, *68*, 113–124. [[CrossRef](#)] [[PubMed](#)]
208. Amini, M.A.; Abbasi, A.Z.; Cai, P.; Lip, H.; Gordijo, C.R.; Li, J.; Chen, B.; Zhang, L.; Rauth, A.M.; Wu, X.Y. Combining tumor microenvironment modulating nanoparticles with doxorubicin to enhance chemotherapeutic efficacy and boost antitumor immunity. *J. Natl. Cancer Inst.* **2019**, *111*, 399–408. [[CrossRef](#)] [[PubMed](#)]
209. Lim, S.; Park, J.; Shim, M.K.; Um, W.; Yoon, H.Y.; Ryu, J.H.; Lim, D.-K.; Kim, K. Recent advances and challenges of repurposing nanoparticle-based drug delivery systems to enhance cancer immunotherapy. *Theranostics* **2019**, *9*, 7906–7923. [[CrossRef](#)] [[PubMed](#)]

210. Gregoriou, Y.; Gregoriou, G.; Yilmaz, V.; Kapnisis, K.; Prokopi, M.; Anayiotos, A.; Strati, K.; Dietis, N.; Constantinou, A.I.; Andreou, C. Resveratrol loaded polymeric micelles for theranostic targeting of breast cancer cells. *Nanotheranostics* **2021**, *5*, 113–124. [[CrossRef](#)]
211. Dunant, P.; Walter, M.C.; Karpati, G.; Lochmüller, H. Gentamicin fails to increase dystrophin expression in dystrophin-deficient muscle. *Muscle Nerve* **2003**, *27*, 624–627. [[CrossRef](#)] [[PubMed](#)]
212. Zammit, P.S. Function of the myogenic regulatory factors Myf5, MyoD, Myogenin and MRF4 in skeletal muscle, satellite cells and regenerative myogenesis. *Semin. Cell Dev. Biol.* **2017**, *72*, 19–32. [[CrossRef](#)] [[PubMed](#)]
213. Sehgal, S.N. Sirolimus: Its discovery, biological properties, and mechanism of action. *Transplant. Proc.* **2003**, *35*, 7S–14S. [[CrossRef](#)]
214. Flaim, S.F. Pharmacokinetics and side effects of perfluorocarbon-based blood substitutes. *Artif. Cells. Blood Substit. Immobil. Biotechnol.* **1994**, *22*, 1043–1054. [[CrossRef](#)]
215. Spahn, D.R. Blood substitutes. Artificial oxygen carriers: Perfluorocarbon emulsions. *Crit. Care* **1999**, *3*, R93–R97. [[CrossRef](#)] [[PubMed](#)]
216. Watanabe, A.; Tanaka, H.; Sakurai, Y.; Tange, K.; Nakai, Y.; Ohkawara, T.; Takeda, H.; Harashima, H.; Akita, H. Effect of particle size on their accumulation in an inflammatory lesion in a dextran sulfate sodium (DSS)-induced colitis model. *Int. J. Pharm.* **2016**, *509*, 118–122. [[CrossRef](#)]
217. Chen, K.-H.; Lundy, D.J.; Toh, E.K.-W.; Chen, C.-H.; Shih, C.; Chen, P.; Chang, H.-C.; Lai, J.J.; Stayton, P.S.; Hoffman, A.S.; et al. Nanoparticle distribution during systemic inflammation is size-dependent and organ-specific. *Nanoscale* **2015**, *7*, 15863–15872. [[CrossRef](#)]
218. Jinek, M.; Chylinski, K.; Fonfara, I.; Hauer, M.; Doudna, J.A.; Charpentier, E. A programmable dual-RNA-guided DNA endonuclease in adaptive bacterial immunity. *Science* **2012**, *337*, 816–821. [[CrossRef](#)]
219. Luther, D.C.; Lee, Y.W.; Nagaraj, H.; Scaletti, F.; Rotello, V.M. Delivery approaches for CRISPR/Cas9 therapeutics *in vivo*: Advances and challenges. *Expert Opin. Drug Deliv.* **2018**, *15*, 905–913. [[CrossRef](#)] [[PubMed](#)]
220. Lino, C.A.; Harper, J.C.; Carney, J.P.; Timlin, J.A. Delivering CRISPR: A review of the challenges and approaches. *Drug Deliv.* **2018**, *25*, 1234–1257. [[CrossRef](#)]
221. Ding, Y.; Jiang, Z.; Saha, K.; Kim, C.S.; Kim, S.T.; Landis, R.F.; Rotello, V.M. Gold nanoparticles for nucleic acid delivery. *Mol. Ther.* **2014**, *22*, 1075–1083. [[CrossRef](#)] [[PubMed](#)]
222. Chithrani, B.D.; Ghazani, A.A.; Chan, W.C.W. Determining the size and shape dependence of gold nanoparticle uptake into mammalian cells. *Nano Lett.* **2006**, *6*, 662–668. [[CrossRef](#)]
223. Arandel, L.; Polay Espinoza, M.; Matloka, M.; Bazinet, A.; De Dea Diniz, D.; Naouar, N.; Rau, F.; Jollet, A.; Edom-Vovard, F.; Mamchaoui, K.; et al. Immortalized human myotonic dystrophy muscle cell lines to assess therapeutic compounds. *Dis. Model. Mech.* **2017**, *10*, 487–497. [[CrossRef](#)]
224. Matloka, M.; Klein, A.F.; Rau, F.; Furling, D. Cells of matter—*in vitro* models for myotonic dystrophy. *Front. Neurol.* **2018**, *9*, 361. [[CrossRef](#)] [[PubMed](#)]
225. Bigot, A.; Klein, A.F.; Gasnier, E.; Jacquemin, V.; Ravassard, P.; Butler-Browne, G.; Mouly, V.; Furling, D. Large CTG repeats trigger P16-dependent premature senescence in myotonic dystrophy type 1 muscle precursor cells. *Am. J. Pathol.* **2009**, *174*, 1435–1442. [[CrossRef](#)]
226. Hayflick, L. The limited *in vitro* lifetime of human diploid cell strains. *Exp. Cell Res.* **1965**, *37*, 614–636. [[CrossRef](#)]
227. Renault, V.; Piron-Hamelin, G.; Forestier, C.; DiDonna, S.; Decary, S.; Hentati, F.; Saillant, G.; Butler-Browne, G.S.; Mouly, V. Skeletal muscle regeneration and the mitotic clock. *Exp. Gerontol.* **2000**, *35*, 711–719. [[CrossRef](#)]
228. Renna, L.V.; Cardani, R.; Botta, A.; Rossi, G.; Fossati, B.; Costa, E.; Meola, G. Premature senescence in primary muscle cultures of myotonic dystrophy type 2 is not associated with P16 induction. *Eur. J. Histochem.* **2014**, *58*, 2444. [[CrossRef](#)] [[PubMed](#)]
229. Thornell, L.-E.; Lindstöm, M.; Renault, V.; Klein, A.; Mouly, V.; Ansved, T.; Butler-Browne, G.; Furling, D. Satellite cell dysfunction contributes to the progressive muscle atrophy in myotonic dystrophy type 1. *Neuropathol. Appl. Neurobiol.* **2009**, *35*, 603–613. [[CrossRef](#)]
230. Liang, R.; Dong, W.; Shen, X.; Peng, X.; Aceves, A.G.; Liu, Y. Modeling myotonic dystrophy 1 in C2C12 myoblast cells. *J. Vis. Exp.* **2016**, *113*, 54078. [[CrossRef](#)]
231. Mamchaoui, K.; Trollet, C.; Bigot, A.; Negroni, E.; Chaouch, S.; Wolff, A.; Kandalla, P.K.; Marie, S.; Di Santo, J.; St Guily, J.L.; et al. Immortalized pathological human myoblasts: Towards a universal tool for the study of neuromuscular disorders. *Skelet. Muscle* **2011**, *1*, 34. [[CrossRef](#)] [[PubMed](#)]
232. O'Connor, M.S.; Carlson, M.E.; Conboy, I.M. Differentiation rather than aging of muscle stem cells abolishes their telomerase activity. *Biotechnol. Prog.* **2009**, *25*, 1130–1137. [[CrossRef](#)] [[PubMed](#)]
233. Massenet, J.; Gitiaux, C.; Magnan, M.; Cuvellier, S.; Hubas, A.; Nusbaum, P.; Dilworth, F.J.; Desguerre, I.; Chazaud, B. Derivation and characterization of immortalized human muscle satellite cell clones from muscular dystrophy patients and healthy individuals. *Cells* **2020**, *9*, 1780. [[CrossRef](#)]
234. Chaouch, S.; Mouly, V.; Goyenvallé, A.; Vulin, A.; Mamchaoui, K.; Negroni, E.; Di Santo, J.; Butler-Browne, G.; Torrente, Y.; Garcia, L.; et al. Immortalized skin fibroblasts expressing conditional MyoD as a renewable and reliable source of converted human muscle cells to assess therapeutic strategies for muscular dystrophies: Validation of an exon-skipping approach to restore dystrophin in Duchenne muscular dystrophy Cells. *Hum. Gene Ther.* **2009**, *20*, 784–790. [[CrossRef](#)] [[PubMed](#)]

235. Cooper, S.T.; Kizana, E.; Yates, J.D.; Lo, H.P.; Yang, N.; Wu, Z.H.; Alexander, I.E.; North, K.N. Dystrophinopathy carrier determination and detection of protein deficiencies in muscular dystrophy using lentiviral MyoD-forced myogenesis. *Neuromuscul. Disord.* **2007**, *17*, 276–284. [[CrossRef](#)]
236. Edmondson, R.; Broglie, J.J.; Adcock, A.F.; Yang, L. Three-dimensional cell culture systems and their applications in drug discovery and cell-based biosensors. *Assay Drug Dev. Technol.* **2014**, *12*, 207–218. [[CrossRef](#)] [[PubMed](#)]
237. Duval, K.; Grover, H.; Han, L.-H.; Mou, Y.; Pegoraro, A.F.; Fredberg, J.; Chen, Z. Modeling physiological events in 2D vs. 3D cell culture. *Physiology* **2017**, *32*, 266–277. [[CrossRef](#)]
238. Knight, E.; Przyborski, S. Advances in 3D cell culture technologies enabling tissue-like structures to be created *in vitro*. *J. Anat.* **2015**, *227*, 746–756. [[CrossRef](#)]
239. Jeffries, G.D.M.; Xu, S.; Lobovkina, T.; Kirejev, V.; Tusseau, F.; Gyllenstein, C.; Singh, A.K.; Karila, P.; Moll, L.; Orwar, O. 3D micro-organisation printing of mammalian cells to generate biological tissues. *Sci. Rep.* **2020**, *10*, 19529. [[CrossRef](#)]
240. Liu, Y.; Wu, B.; Gong, L.; An, C.; Lin, J.; Li, Q.; Jiang, D.; Jin, K.; Mechakra, A.; Bumpetch, V.; et al. Dissecting cell diversity and connectivity in skeletal muscle for myogenesis. *Cell Death Dis.* **2019**, *10*, 427. [[CrossRef](#)]
241. Juhas, M.; Engelmayer, G.C.; Fontanella, A.N.; Palmer, G.M.; Bursac, N. Biomimetic Engineered muscle with capacity for vascular integration and functional maturation *in vivo*. *Proc. Natl. Acad. Sci. USA* **2014**, *111*, 5508–5513. [[CrossRef](#)] [[PubMed](#)]
242. Borselli, C.; Cezar, C.A.; Shvartsman, D.; Vandeburgh, H.H.; Mooney, D.J. The role of multifunctional delivery scaffold in the ability of cultured myoblasts to promote muscle regeneration. *Biomaterials* **2011**, *32*, 8905–8914. [[CrossRef](#)]
243. McLean, I.C.; Schwerdtfeger, L.A.; Tobet, S.A.; Henry, C.S. Powering ex vivo tissue models in microfluidic systems. *Lab. Chip* **2018**, *18*, 1399–1410. [[CrossRef](#)]
244. Gowing, G.; Svendsen, S.; Svendsen, C.N. Ex vivo gene therapy for the treatment of neurological disorders. *Prog. Brain Res.* **2017**, *230*, 99–132. [[CrossRef](#)] [[PubMed](#)]
245. Mobini, S.; Song, Y.H.; McCrary, M.W.; Schmidt, C.E. Advances in ex vivo models and lab-on-a-chip devices for neural tissue engineering. *Biomaterials* **2019**, *198*, 146–166. [[CrossRef](#)] [[PubMed](#)]
246. Smith, L.R.; Meyer, G.A. Skeletal muscle explants: *Ex-vivo* models to study cellular behavior in a complex tissue environment. *Connect. Tissue Res.* **2020**, *61*, 248–261. [[CrossRef](#)] [[PubMed](#)]
247. Kim, D.; Wu, X.; Young, A.T.; Haynes, C.L. Microfluidics-based in vivo mimetic systems for the study of cellular biology. *Acc. Chem. Res.* **2014**, *47*, 1165–1173. [[CrossRef](#)] [[PubMed](#)]
248. Carton, F.; Calderan, L.; Malatesta, M. Incubation under fluid dynamic conditions markedly improves the structural preservation in vitro of explanted skeletal muscles. *Eur. J. Histochem.* **2017**, *61*, 2862. [[CrossRef](#)]
249. Carosio, S.; Barberi, L.; Rizzuto, E.; Nicoletti, C.; Del Prete, Z.; Musarò, A. Generation of *ex vivo*-vascularized muscle engineered tissue (X-MET). *Sci. Rep.* **2013**, *3*, 1420. [[CrossRef](#)] [[PubMed](#)]
250. Fischer, H.C.; Chan, W.C. Nanotoxicity: The growing need for in vivo study. *Curr. Opin. Biotechnol.* **2007**, *18*, 565–571. [[CrossRef](#)]
251. Bostrom, M.; O’Keefe, R. What experimental approaches (eg, *in vivo*, *in vitro*, tissue retrieval) are effective in investigating the biologic effects of particles? *J. Am. Acad. Orthop. Surg.* **2008**, *16*, S63–S67. [[CrossRef](#)]
252. McGreevy, J.W.; Hakim, C.H.; McIntosh, M.A.; Duan, D. Animal models of Duchenne muscular dystrophy: From basic mechanisms to gene therapy. *Dis. Model. Mech.* **2015**, *8*, 195–213. [[CrossRef](#)]
253. Wells, D.J. Tracking progress: An update on animal models for Duchenne muscular dystrophy. *Dis. Model. Mech.* **2018**, *11*, dmm035774. [[CrossRef](#)]
254. Collins, C.A.; Morgan, J.E. Duchenne’s muscular dystrophy: Animal models used to investigate pathogenesis and develop therapeutic strategies. *Int. J. Exp. Pathol.* **2003**, *84*, 165–172. [[CrossRef](#)]
255. Bulfield, G.; Siller, W.G.; Wight, P.A.; Moore, K.J. X Chromosome-linked muscular dystrophy (*mdx*) in the mouse. *Proc. Natl. Acad. Sci. USA* **1984**, *81*, 1189–1192. [[CrossRef](#)]
256. van Putten, M.; Putker, K.; Overzier, M.; Adamzek, W.A.; Pasteuning-Vuhman, S.; Plomp, J.J.; Aartsma-Rus, A. Natural disease history of the D2-*mdx* mouse model for Duchenne muscular dystrophy. *FASEB J.* **2019**, *33*, 8110–8124. [[CrossRef](#)]
257. Desguerre, I.; Arnold, L.; Vignaud, A.; Cuvellier, S.; Yacoub-Youssef, H.; Gherardi, R.K.; Chelly, J.; Chretien, F.; Mounier, R.; Ferry, A.; et al. A new model of experimental fibrosis in hindlimb skeletal muscle of adult *mdx* mouse mimicking muscular dystrophy. *Muscle Nerve* **2012**, *45*, 803–814. [[CrossRef](#)] [[PubMed](#)]
258. Ng, R.; Banks, G.B.; Hall, J.K.; Muir, L.A.; Ramos, J.N.; Wicki, J.; Odom, G.L.; Konieczny, P.; Seto, J.; Chamberlain, J.R.; et al. Animal models of muscular dystrophy. *Prog. Mol. Biol. Transl. Sci.* **2012**, *105*, 83–111. [[CrossRef](#)] [[PubMed](#)]
259. Komegay, J.N. The golden retriever model of Duchenne muscular dystrophy. *Skelet. Muscle* **2017**, *7*, 9. [[CrossRef](#)]
260. Kawahara, G.; Karpf, J.A.; Myers, J.A.; Alexander, M.S.; Guyon, J.R.; Kunkel, L.M. Drug screening in a zebrafish model of Duchenne muscular dystrophy. *Proc. Natl. Acad. Sci. USA* **2011**, *108*, 5331–5336. [[CrossRef](#)] [[PubMed](#)]
261. Widrick, J.J.; Kawahara, G.; Alexander, M.S.; Beggs, A.H.; Kunkel, L.M. Discovery of novel therapeutics for muscular dystrophies using zebrafish phenotypic screens. *J. Neuromuscul. Dis.* **2019**, *6*, 271–287. [[CrossRef](#)]
262. Sicot, G.; Gomes-Pereira, M. RNA toxicity in human disease and animal models: From the uncovering of a new mechanism to the development of promising therapies. *Biochim. Biophys. Acta* **2013**, *1832*, 1390–1409. [[CrossRef](#)] [[PubMed](#)]
263. Gomes-Pereira, M.; Cooper, T.A.; Gourdon, G. Myotonic dystrophy mouse models: Towards rational therapy development. *Trends Mol. Med.* **2011**, *17*, 506–517. [[CrossRef](#)] [[PubMed](#)]

264. Guiraud-Dogan, C.; Huguet, A.; Gomes-Pereira, M.; Brisson, E.; Bassez, G.; Junien, C.; Gourdon, G. DM1 CTG expansions affect insulin receptor isoforms expression in various tissues of transgenic mice. *Biochim. Biophys. Acta* **2007**, *1772*, 1183–1191. [[CrossRef](#)]
265. Lin, X.; Miller, J.W.; Mankodi, A.; Kanadia, R.N.; Yuan, Y.; Moxley, R.T.; Swanson, M.S.; Thornton, C.A. Failure of MBNL1-dependent post-natal splicing transitions in myotonic dystrophy. *Hum. Mol. Genet.* **2006**, *15*, 2087–2097. [[CrossRef](#)] [[PubMed](#)]
266. Mankodi, A.; Logigian, E.; Callahan, L.; McClain, C.; White, R.; Henderson, D.; Krym, M.; Thornton, C.A. Myotonic dystrophy in transgenic mice expressing an expanded CUG repeat. *Science* **2000**, *289*, 1769–1773. [[CrossRef](#)]
267. Mankodi, A.; Takahashi, M.P.; Jiang, H.; Beck, C.L.; Bowers, W.J.; Moxley, R.T.; Cannon, S.C.; Thornton, C.A. Expanded CUG repeats trigger aberrant splicing of CIC-1 chloride channel pre-mRNA and hyperexcitability of skeletal muscle in myotonic dystrophy. *Mol. Cell* **2002**, *10*, 35–44. [[CrossRef](#)]
268. Seznec, H.; Agbulut, O.; Sergeant, N.; Savouret, C.; Ghestem, A.; Tabet, N.; Willer, J.C.; Ourth, L.; Duros, C.; Brisson, E.; et al. Mice transgenic for the human myotonic dystrophy region with expanded CTG repeats display muscular and brain abnormalities. *Hum. Mol. Genet.* **2001**, *10*, 2717–2726. [[CrossRef](#)]
269. Hinman, M.N.; Richardson, J.I.; Sockol, R.A.; Aronson, E.D.; Stednitz, S.J.; Murray, K.N.; Berglund, J.A.; Guillemain, K. Zebrafish mbnl mutants model physical and molecular phenotypes of myotonic dystrophy. *bioRxiv* **2020**, 665380. [[CrossRef](#)]
270. Machuca-Tzili, L.E.; Buxton, S.; Thorpe, A.; Timson, C.M.; Wigmore, P.; Luther, P.K.; Brook, J.D. Zebrafish deficient for Muscleblind-like 2 exhibit features of myotonic dystrophy. *Dis. Model. Mech.* **2011**, *4*, 381–392. [[CrossRef](#)]
271. Carton, F.; Chevalier, Y.; Nicoletti, L.; Tarnowska, M.; Stella, B.; Arpicco, S.; Malatesta, M.; Jordheim, L.P.; Briançon, S.; Lollo, G. Rationally designed hyaluronic acid-based nano-complexes for pentamidine delivery. *Int. J. Pharm.* **2019**, *568*, 118526. [[CrossRef](#)] [[PubMed](#)]
272. Stella, B.; Andreana, I.; Zonari, D.; Arpicco, S. Pentamidine-loaded lipid and polymer nanocarriers as tunable anticancer drug delivery systems. *J. Pharm. Sci.* **2020**, *109*, 1297–1302. [[CrossRef](#)]
273. Falzarano, M.S.; Bassi, E.; Passarelli, C.; Braghetta, P.; Ferlini, A. Biodistribution studies of polymeric nanoparticles for drug delivery in mice. *Hum Gene Ther.* **2014**, *25*, 927–928. [[CrossRef](#)]
274. Huang, D.; Yue, F.; Qiu, J.; Deng, M.; Kuang, S. Polymeric nanoparticles functionalized with muscle-homing peptides for targeted delivery of phosphatase and tensin homolog inhibitor to skeletal muscle. *Acta Biomater.* **2020**, *118*, 196–206. [[CrossRef](#)] [[PubMed](#)]
275. Herweijer, H.; Wolff, J.A. Gene therapy progress and prospects: Hydrodynamic gene delivery. *Gene Ther.* **2007**, *14*, 99–107. [[CrossRef](#)]
276. Kumbhari, V.; Li, L.; Piontek, K.; Ishida, M.; Fu, R.; Khalil, B.; Garrett, C.M.; Liapi, E.; Kalloo, A.N.; Selaru, F.M. Successful liver-directed gene delivery by ERCP-guided hydrodynamic injection (with Videos). *Gastrointest. Endosc.* **2018**, *88*, 755–763. [[CrossRef](#)] [[PubMed](#)]
277. Le Guen, Y.T.; Le Gall, T.; Midoux, P.; Guégan, P.; Braun, S.; Montier, T. Gene transfer to skeletal muscle using hydrodynamic limb vein injection: Current applications, hurdles and possible optimizations. *J. Gene Med.* **2020**, *22*, e3150. [[CrossRef](#)] [[PubMed](#)]
278. Ashfaq, U.A.; Riaz, M.; Yasmeen, E.; Yousaf, M. Recent advances in nanoparticle-based targeted drug-delivery systems against cancer and role of tumor microenvironment. *Crit. Rev. Ther. Drug Carrier Syst.* **2017**, *34*, 317–353. [[CrossRef](#)]
279. Pietersz, G.A.; Wang, X.; Yap, M.L.; Lim, B.; Peter, K. Therapeutic targeting in nanomedicine: The future lies in recombinant antibodies. *Nanomedicine* **2017**, *12*, 1873–1889. [[CrossRef](#)] [[PubMed](#)]
280. Arahata, K.; Ishiura, S.; Ishiguro, T.; Tsukahara, T.; Suhara, Y.; Eguchi, C.; Ishihara, T.; Nonaka, I.; Ozawa, E.; Sugita, H. Immunostaining of skeletal and cardiac muscle surface membrane with antibody against Duchenne muscular dystrophy peptide. *Nature* **1988**, *333*, 861–863. [[CrossRef](#)]
281. Zhang, R.; Kim, A.S.; Fox, J.M.; Nair, S.; Basore, K.; Klimstra, W.B.; Rimkunas, R.; Fong, R.H.; Lin, H.; Poddar, S.; et al. Mxra8 is a receptor for multiple arthritogenic alphaviruses. *Nature* **2018**, *557*, 570–574. [[CrossRef](#)] [[PubMed](#)]
282. Poon, W.; Zhang, X.; Bekah, D.; Teodoro, J.G.; Nadeau, J.L. Targeting B16 tumors in vivo with peptide-conjugated gold nanoparticles. *Nanotechnology* **2015**, *26*, 285101. [[CrossRef](#)] [[PubMed](#)]
283. Yu-Wai-Man, C.; Tagalakakis, A.D.; Manunta, M.D.; Hart, S.L.; Khaw, P.T. Receptor-targeted liposome-peptide-siRNA nanoparticles represent an efficient delivery system for MRTF silencing in conjunctival fibrosis. *Sci. Rep.* **2016**, *6*, 21881. [[CrossRef](#)] [[PubMed](#)]
284. Tajau, R.; Rohani, R.; Abdul Hamid, S.S.; Adam, Z.; Mohd Janib, S.N.; Salleh, M.Z. Surface functionalisation of poly-APO-b-polyol ester cross-linked copolymers as core-shell nanoparticles for targeted breast cancer therapy. *Sci. Rep.* **2020**, *10*, 21704. [[CrossRef](#)] [[PubMed](#)]
285. Yu, C.-Y.; Yuan, Z.; Cao, Z.; Wang, B.; Qiao, C.; Li, J.; Xiao, X. A muscle-targeting peptide displayed on AAV2 improves muscle tropism on systemic delivery. *Gene Ther.* **2009**, *16*, 953–962. [[CrossRef](#)]
286. Seow, Y.; Yin, H.; Wood, M.J.A. Identification of a novel muscle targeting peptide in *mdx* mice. *Peptides* **2010**, *31*, 1873–1877. [[CrossRef](#)]
287. Tsoumpira, M.K.; Fukumoto, S.; Matsumoto, T.; Takeda, S.; Wood, M.J.A.; Aoki, Y. Peptide-conjugate antisense based splice-correction for Duchenne muscular dystrophy and other neuromuscular diseases. *EBioMedicine* **2019**, *45*, 630–645. [[CrossRef](#)]
288. Gao, X.; Zhao, J.; Han, G.; Zhang, Y.; Dong, X.; Cao, L.; Wang, Q.; Moulton, H.M.; Yin, H. Effective dystrophin restoration by a novel muscle-homing peptide-morpholino conjugate in dystrophin-deficient *mdx* mice. *Mol. Ther.* **2014**, *22*, 1333–1341. [[CrossRef](#)]

CHAPTER 2

Repurposing pentamidine using hyaluronic acid-based nanocarriers for skeletal muscle treatment in myotonic dystrophy

M. Repellin, F. Carton, F. Boschi, M. Galiè, M. Perduca, L. Calderan, A. Jacquier, J. Carras, L. Schaeffer, S. Briançon, G. Lollo, M. Malatesta

Submitted (2022)

Nanomedicine: Nanotechnology, Biology, and Medicine
Repurposing pentamidine using hyaluronic acid-based nanocarriers for skeletal muscle treatment in myotonic dystrophy
 --Manuscript Draft--

Manuscript Number:	
Article Type:	Original Article
Keywords:	nanoparticles; biomaterials; C2C12 cells; muscular dystrophies; DM1 cell model
Corresponding Author:	Manuela Malatesta University of Verona Verona, ITALY
First Author:	Mathieu REPELLIN
Order of Authors:	Mathieu REPELLIN Flavia Carton Federico Boschi Mirco Galìè Massimiliano Perduca Laura Calderan Arnaud Jacquier Julien Carras Laurent Schaeffer Stéphanie Briançon Giovanna Lollo Manuela Malatesta
Abstract:	In a context of drug repurposing, pentamidine (PTM), an FDA-approved antiparasitic drug, has been proposed to reverse the splicing defects associated in myotonic dystrophy type 1 (DM1). However, clinical use of PTM is hindered by substantial toxicity, leading to find alternative delivery strategies. In this work we proposed hyaluronic acid-based nanoparticles as a novel encapsulation strategy to efficiently deliver PTM to skeletal muscle cells. In vitro studies on C2C12 myoblasts and myotubes showed an efficient nanoparticles internalization with minimal toxicity. More interestingly, our findings evidenced for the first time the endosomal escape of hyaluronic acid-based nanocarriers. Ex vivo studies showed an efficient nanoparticles internalization within skeletal muscle fibers. Finally, the therapeutic efficacy of PTM-loaded nanosystems to reduce the number of nuclear foci has been demonstrated in a novel DM1 in vitro model. So far, current data demonstrated the potency of hyaluronic acid-based nanosystems as efficient nanocarrier for delivering PTM into skeletal muscle and mitigate DM1 pathology.

Repurposing pentamidine using hyaluronic acid-based nanocarriers for skeletal muscle treatment in myotonic dystrophy

Mathieu Repellin^{1,2*}, Flavia Carton^{1,&.*}, Federico Boschi³, Mirco Galì¹, Massimiliano Perduca⁴, Laura Calderan¹, Arnaud Jacquier^{5,6}, Julien Carras^{5,6}, Laurent Schaeffer^{5,6}, Stéphanie Briançon², Giovanna Lollo², Manuela Malatesta¹

Affiliations

¹Department of Neurosciences, Biomedicine and Movement Sciences, Anatomy and Histology Section, University of Verona, Strada Le Grazie 8, 37134 Verona, Italy

²University of Lyon, Université Claude Bernard Lyon 1, CNRS, LAGEPP UMR 5007, 43 bd 11 Novembre 1918, 69622 Villeurbanne, France

³Department of Computer Science, University of Verona, strada Le Grazie 15, 37134 Verona, Italy

⁴Department of Biotechnology, Biocrystallography and Nanostructure Laboratory, University of Verona, Strada Le Grazie 15, 37134 Verona, Italy

⁵Institut NeuroMyogène, University of Lyon1, CNRS UMR 5310, INSERM U1217, 8 avenue Rockefeller, 69008 Lyon, France

⁶Centre de Biotechnologie Cellulaire, CBC Biotec, CHU de Lyon – Hospices civils de Lyon groupement Est, Bron, France

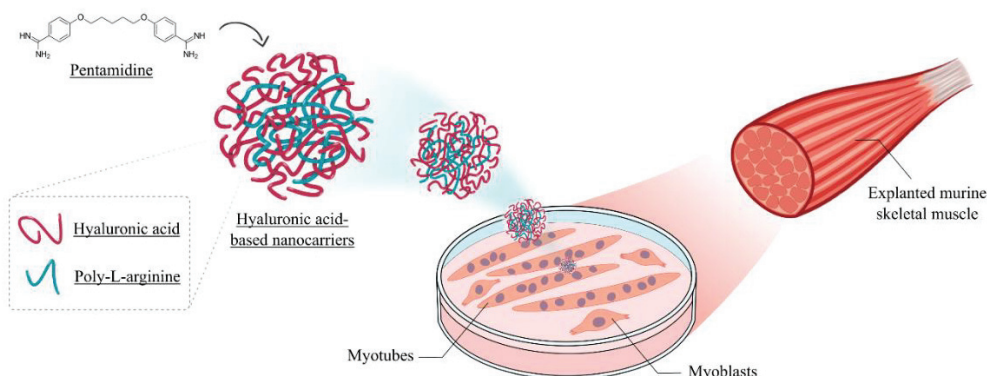
***These authors contributed equally to this work.**

[&]Flavia Carton's present address: University of Eastern Piedmont, Department of Health Sciences, Via Solaroli 17, 28100 Novara, Italy

Corresponding Authors: Manuela Malatesta, Department of Neurosciences, Biomedicine and Movement Sciences, Anatomy and Histology Section, University of Verona, Strada Le Grazie 8, 37134 Verona, Italy. Tel. +30.045.8027569. E-mail: manuela.malatesta@univr.it

Word count: Abstract 156 words, main text (text + figure legends) 6460 words, 8 main figures, 3 supplementary figures, 55 references.

Graphical abstract



Highlights:

- Hyaluronic acid-based nanoparticles were efficiently internalized into muscle cells both *in vitro* and *ex vivo*
- CD44 receptors play a key role in the uptake of hyaluronic acid-based nanoparticles
- Novel established DM1 cell model accurately represents the DM1 pathological phenotype
- Pentamidine loaded into nanoparticles highly decreased the number of DM1 nuclear foci
- Pentamidine loaded hyaluronic acid-based nanoparticles offers an innovative strategy for DM1 treatment

Abstract

In a context of drug repurposing, pentamidine (PTM), an FDA-approved antiparasitic drug, has been proposed to reverse the splicing defects associated in myotonic dystrophy type 1 (DM1). However, clinical use of PTM is hindered by substantial toxicity, leading to find alternative delivery strategies. In this work we proposed hyaluronic acid-based nanoparticles as a novel encapsulation strategy to efficiently deliver PTM to skeletal muscle cells. *In vitro* studies on C2C12 myoblasts and myotubes showed an efficient nanoparticles internalization with minimal toxicity. More interestingly, our findings evidenced for the first time the endosomal escape of hyaluronic acid-based nanocarriers. *Ex vivo* studies showed an efficient nanoparticles internalization within skeletal muscle fibers. Finally, the therapeutic efficacy of PTM-loaded nanosystems to reduce the number of nuclear foci has been demonstrated in a novel DM1 *in vitro* model. So far, current data demonstrated the potency of hyaluronic acid-based nanosystems as efficient nanocarrier for delivering PTM into skeletal muscle and mitigate DM1 pathology.

Keywords: nanoparticles, biomaterials, C2C12 cells, muscular dystrophies, DM1 cell model

1. Introduction

Myotonic dystrophies (DM) are dominantly-inherited genetic disorders characterized by progressive myopathy, myotonia and multiorgan involvement, leading to possibly premature death¹. Two distinct forms of DM have been identified, among which Myotonic Dystrophy type 1 (DM1) is the most common and severe form (OMIM:160900), with an estimated prevalence of 1/8000². The most accredited molecular pathological mechanism relies on the abnormal CTG expansion located in the 3' untranslated region of the DMPK (dystrophia myotonia protein kinase) gene^{3,4}. This mutant (CTG)_n DNA is transcribed into (CUG)_n RNA, forming hairpin structures accumulating as nuclear foci. It is well documented that these nuclear foci are associated with a strong mis-regulation of splicing factors⁵⁻⁷. This deregulation is triggered by two leading biological events: on one hand the sequestration and loss-of-function of Muscleblind-like (MBNL) proteins, in particular Muscleblind-like 1 (MBNL1); on the other hand an up-regulation of CUG RNA-binding protein Elav-Like Family Member 1

(CELF1)^{8–10}. The resulting effects on RNA alterations and protein metabolism lead to the multiple features of this complex multisystemic disease.

No therapeutic treatment is presently available for treating DM1 and conventional approaches are applied to mitigate symptoms; however, various therapeutic strategies are currently under development¹¹. In particular, one current approach to faster and safer drug development phase is drug repurposing, aiming to identify new therapeutic purposes of existing drugs¹² as in the case of pentamidine (PTM). PTM, an FDA-approved antiparasitic drug currently used to treat patients with *Trypanosomiasis*, *Leishmaniasis* and *Pneumocystis* infections, has been proposed as potential anticancer agent and more recently as experimental DM1 treatment^{13–15}. PTM demonstrated to significantly reduce the formation of nuclear foci in experimental models, eluding MBNL1 sequestration and, consequently, reversing some splicing defects.¹⁴ However, PTM manifested a narrow window of efficacy due to substantial toxicity at the potentially effective doses^{14,16}. In this context, the recent advent of nanotechnology led to the development of novel therapeutic approaches with a higher safety profile. Nanomedicine enhances therapeutic potential of drugs with restricted pharmacological profile while overcoming their poor availability^{17,18}. The use of nanocarriers improve the internalization of associated drug while decreasing the effective doses required to exert the therapeutic activity and side-effects associated.

We recently designed hyaluronic acid-based nanoparticles (HA-PArg NPs) as carriers to successfully associate PTM¹⁹. Hyaluronic acid (HA) and poly(L-arginine) (PArg) have been selected as biocompatibles and biodegradables materials for developing HA-PArg NPs. Moreover, HA is an essential component of the extracellular and pericellular matrixes that plays a significant role in regulating muscle cell behavior during repair and regeneration via interaction with CD44 receptors²⁰. CD44 receptors are widely-distributed type 1 transmembrane glycoprotein that binds HA and are involved in cell proliferation, adhesion, migration, hematopoiesis and lymphocyte activation. Although different isoforms of CD44 have been identified and are overexpressed by cancer cells and macrophages, CD44 have been investigated on myoblasts and myotubes as crucial modulator of early myogenesis. Therefore, interactions between HA and CD44 receptors represents an effective strategy for increasing accumulation of associated drug at the pathological site. Complementary, PArg was used to crosslink HA and form

nanoparticles, while maximizing the amount of associated PTM. Moreover, this cationic poly(aminoacid) belonging to the cell-penetrating peptide polymers is able to improve intracellular delivery of therapeutic agents²¹.

In the present work, we focused on the potential of HA-PArg NPs as safe and efficient nanocarriers for PTM delivery to skeletal muscle. To this aim, *i*) HA-PArg NPs biocompatibility, cellular uptake, intracellular distribution and fate have been investigated on cycling (myoblasts) and terminally differentiated non-cycling (myotubes) C2C12 cells, a spontaneously immortalized mouse myoblast cell line commonly used to mimic skeletal muscle *in vitro* ; *ii*) HA-PArg NPs biodistribution and targeting efficiency have been evaluated in explanted murine soleus muscle maintained *in vitro* under fluid dynamic conditions; *iii*) the therapeutic efficacy of PTM loaded HA-PArg NPs has been tested in C2C12 cell line transfected with human (CTG)_n DNA, as a DM1 cell model.

2. Materials and Methods

2.1. Materials

Sodium hyaluronate (weight-average molar mass, $M_w=3.9\times 10^4$ g·mol⁻¹) was purchased from Lifecore Biomedical (Minnesota, USA). Poly(L-arginine) ($M_w=5.9\times 10^3$ g·mol⁻¹) was provided by Polypeptide Therapeutic Solutions (Valencia, Spain). Fluoresceinamine, PTM and anti-rat CD44 monoclonal antibody (clone IM7, all isoforms) was obtained from Sigma-Aldrich (Saint-Quentin-Fallavier, France). Cyanine5 amine was purchased from Lumiprobe (Maryland, USA). Bafilomycin A1 was provided by MedChemExpress (NJ, USA). Alcian Blue 8GX, Mannitol, MTT reagent and PKH26 Red Fluorescent Cell Linker was obtained from Sigma-Aldrich (Milan, Italy). Anti-rabbit EEA1 (clone C45B10, #3288) and anti-mouse Rab7 antibody (clone E9O7E, #95746) was provided by Cell Signaling technology inc (Danvers, Massachusetts, USA).

2.2. HA-PArg NPs preparation and physico-chemical characterization

2.2.1. Blank, fluorescent and PTM-loaded NPs preparation

HA-PArg NPs were prepared by polyelectrolyte complexation¹⁹. Briefly, to obtain blank nanoparticles, 0.5 mL of sodium hyaluronate solution prepared at 7 mg·mL⁻¹ were added to 0.5 mL of PArg solution at 0.53 mg·mL⁻¹ and left, under magnetic stirring for 30 min. Fluorescent HA-PArg NPs used for imaging study were prepared replacing 20 % w/w of

sodium hyaluronate by fluoresceinamine-hyaluronate (HA-FITC) or cyanine5 (HA-cy5). HA-FITC and HA-cy5 were synthesized based on method described by Gómez-Gaete et al²² and Fudala et al²³. PTM-loaded NPs were obtained by the same process, adding 0.5 mL of PTM to 1.5 mg.mL⁻¹ of PArg solution before mixing with HA. Also freeze-dried NPs were prepared according to the protocol previously established¹⁹.

2.2.2. Physico-chemical characterization of nanoparticles

NPs size distribution and surface electrical charge were measured using Malvern Zetasizer® Nano ZS (Malvern Instruments S.A, Worcestershire, UK). Hydrodynamic diameter and polydispersity index (PDI) were measured by Dynamic Light Scattering (DLS) using the cumulants method. Analyses were carried out at 25 °C with an angle of detection of 173°. Zeta potential (ζ) was determined by electrophoresis technique. All samples were diluted to 0.4 mg.mL⁻¹ in KCl 1 mM and analyses were performed in triplicate.

Colloidal stability was investigated by differential scanning calorimetry (DSC) analysis using a Nano DSC (TA Instruments, New Castle, DE). For this purpose, freeze-dried HA-PArg NPs and PTM-loaded NPs were resuspended at the concentration of 20 mg.mL⁻¹ in Dulbecco's modified Eagle medium (DMEM) supplemented with 5 % (v/v) fetal bovine serum (FBS), 1 % (w/v) Glutamine, 0.5 % (v/v) Amphotericin B, 100 units/mL of Penicillin-Streptomycin (Gibco, MA, USA). Dialyzed PTM-loaded NPs purified from the non-encapsulated PTM were obtained by overnight dialysis (14,000 Da MW cut off membranes, Sigma-Aldrich, Milan, Italy) against water. Then, suspensions were supplemented with 5 % of mannitol before being freeze-dried as described above and resuspended in the same cell culture medium. All samples were degassed beforehand under vacuum and ultrasonic conditions for 10 min. 700 μ L of each sample were loaded in the sample cell, while the same volume of reference medium was loaded in the reference one and DSC analysis were carried out on a temperature range of 18 to 90 °C at a rate of 2 °C.min⁻¹; cell pressure was maintained at a constant value of 3 Atm along the whole experiment.

Data were collected by the Nano DSCRun 4.7.1 software and analyzed by the NanoAnalyze 3.11.0 software (TA Instruments, New Castle, DE).

2.3. HA-PArg NPs administration to healthy myoblasts and myotubes

2.3.1. Cell culture

C2C12 myoblasts (an immortalized murine muscle cell line purchased from ATCC® CRL-1772) were cultured under humidified atmosphere with 5 % CO₂ at 37 °C, in 75 cm² plastic flasks using Dulbecco's modified Eagle medium, supplemented with 10 % (v/v) fetal bovine serum (FBS), 1 % (w/v) Glutamine, 0.5 % (v/v) Amphotericin B, 100 units/mL of Penicillin-Streptomycin (Gibco). For myoblasts, cells were trypsinized (0.25% trypsin with 0.05 % EDTA in PBS) when sub-confluent, seeded at the required concentrations (see below) and incubated for 24 h before NPs treatment. To induce differentiation into myotubes, myoblasts were trypsinized, seeded at the appropriate concentration and grown at 80 % confluence; then, the growth medium was shifted to a differentiation medium with 1 % FBS for 6 days. Therefore, myotubes were treated with NPs after 6 days of differentiation. All experiments were performed in cells below passage 10. During NPs or PTM treatment, FBS was reduced to 5 % (v/v) to limit any possible NPs aggregation^{24,25}.

2.3.2. Cytotoxicity assays

The cytotoxicity of HA-PArg NPs, PTM-loaded NPs and PTM on myoblasts and myotubes was evaluated by MTT assay. MTT assay is an indicator of cell metabolism and the reduction in absorbance value is related to a loss of oxidoreductase enzyme activity due to the toxicity of the treatment²⁶. Cells were seeded in flat-bottom 96-well plates (2×10^3 cells/well); four wells for each condition were seeded. Myoblasts and myotubes were treated with different PTM concentrations (1 to 120 μM) either as PTM solubilized in the medium (stock solution prepared in milli-Q water) or loaded into the PTM-loaded NPs; in parallel, some cell samples were exposed to the equivalent corresponding HA-PArg NPs (4 to 428 $\mu\text{g}\cdot\text{mL}^{-1}$). Untreated cell samples were used as control. Cells were treated for 2 h, then some samples were evaluated for cell cytotoxicity, while others were given fresh medium and further grown until 24 or 48 h. This procedure allowed to avoid cytotoxic effects due to the non-internalized NPs in the medium. At each incubation time, the medium was replaced by 100 μL of MTT solution (0.5 $\text{mg}\cdot\text{mL}^{-1}$ in medium) and incubated for 3 h at 37 °C in a cell incubator. Then, MTT solution was removed and formazan crystals were dissolved in 100 μL of DMSO. The absorbance was

measured at 570 nm using a ChroMate 4300 ELISA microplate reader (Awareness Technology Inc, Palm City, FL, USA). Statistical significance ($p < 0.05$) was determined using one-way ANOVA followed by Kruskal-Wallis test.

2.3.3. Uptake, intracellular distribution and fate of NPs

The uptake, intracellular distribution and fate of HA-PArg NPs in both myoblasts and myotubes were investigated by confocal fluorescence microscopy (CFM) and transmission electron microscopy (TEM). Cells were seeded onto glass coverslips (12 mm in diameter) in 24-multiwell plate (6×10^3 cells/well). Both myoblasts and myotubes were treated with either HA-PArg-FITC NPs or HA-PArg NPs for CFM and TEM, respectively. Cells were incubated with NPs for 2, 24 and 48 h and then processed for microscopy analyses.

For CFM, cells were fixed with 4 % (v/v) paraformaldehyde in PBS, pH 7.4 for 30 min at room temperature. Cell cytoplasm was stained with 0.4 % Trypan blue (Gibco, Monza, Italy) in water for 30 s, while cell nuclei were counterstained with Hoechst 33342 (1:1000 in PBS) for 5 min; then samples were mounted in a mixture of PBS/glycerol (1:1). Imaging was performed by a Leica TCS SP5 AOBS system (Leica microsystem Italia) using a 40X objective with for fluorescence excitation, a diode laser at 405 nm for Hoechst 33342, an Ar laser at 488 nm for FITC and a He/Ne laser at 543 nm for Trypan blue.

For TEM, cells were fixed with 2.5 % (v/v) glutaraldehyde and 2 % (v/v) paraformaldehyde in 0.1 M phosphate buffered, pH 7.4, for 2 h at 4 °C, post-fixed with 1.5% potassium ferrocyanide and 1% osmium tetroxide for 1 h, dehydrated with acetone and embedded in Epon resin. In order to preserve the spatial relationships between cells and NPs, both myoblasts and myotubes were processed for TEM as monolayers²⁷. Ultrathin sections were observed in a Philips Morgagni transmission electron microscope (FEI Company Italia Srl, Milan, Italy) operating at 80 kV and equipped with a Megaview II camera for digital image acquisition.

All images were processed using Paint Shop Pro software (JASC Software Inc., MN, USA).

2.3.4. Endocytic internalization pathway

Endocytic uptake pathway of HA-PArg NPs was investigated by immunofluorescence analyses. Cells were plated as described for CFM conditions, then treated for 5 min with HA-PArg NPs fluorescently labelled using HA-cy5 in order to obtain a potent fluorescence signal and fixed as for CFM analysis. Cells were stained for early and late endosomes and CD44 receptors using EEA1, Rab7 and CD44 primary antibody, respectively (1:100). Cell samples were washed and incubated with complementary Alexa-fluor 488-conjugated secondary antibody (1:1000) and DAPI (stock at 20 mM diluted 1:2000) for 1 h at room temperature. Imaging was performed by a Zeiss LSM800 confocal laser scanning microscope (Carl Zeiss AG, Oberkochen, Germany) using a 63X objective (Plan-Apochromat 63x/1.40 oil DIC M27) with for fluorescence excitation, a diode laser at 405 nm for DAPI, a diode laser at 488 nm for Alexa fluor 488 and a diode laser at 640nm for HA-cy5.

2.3.5. Endosomal escape

In order to investigate the effect of the acidic endosomal environment on the physico-chemical properties of HA-PArg NPs, freeze-dried HA-PArg NPs were resuspended in 1 mM HEPES buffer adjusted at different pH values, from 3 to 7.4 with hydrochloric acid. NPs size and surface charge were measured using a Malvern Zetasizer® Nano ZS as previously described. Then, NPs intracellular uptake was studied in presence of bafilomycin A1, a specific potent inhibitor of vacuolar-type H⁺-ATPases responsible of endosomal acidification²⁸. Myoblasts were seeded as for the intracellular distribution study and were pre-incubated with 1 μ M bafilomycin A1 for 1 h. For CFM, myoblasts were incubated with PKH26 Red Fluorescent Cell Linker to stain the plasma membrane and then treated with HA-PArg-FITC NPs and 1 μ M of bafilomycin A1 for 30 min; this procedure allows the identification of endosomes containing NPs thanks to the overlapping of the two fluorophores^{29,30}. For TEM, myoblasts were treated with HA-PArg NPs and 1 μ M of bafilomycin A1 for 2 and 24 h. Cells were fixed and processed as previously described for CFM and TEM. In addition, some samples were submitted to the critical-electrolyte-concentration Alcian Blue method to unequivocally detect at TEM the HA-PArg NPs internalized in the cells.³¹ Briefly, cells were fixed with 3 % (v/v) glutaraldehyde in PBS pH 7 for 30 min at room temperature, stained with 1 % (w/v)

Alcian blue 8GX in 3 % (v/v) acetic acid for 2 h at room temperature, post-fixed with 1 % osmium tetroxide for 1 h at room temperature, dehydrated and embedded in resin.

2.4. Biodistribution and targeting efficacy of HA-PArg NPs in skeletal muscle

For the biodistribution and targeting studies, soleus muscles were isolated and excised from healthy 3-month-old male Balb/c mice sacrificed with an overdose of CO₂ and then proceeding with cervical dislocation in the frame of a research project approved by the Italian Ministry of Health (protocol code: ZA/14/18). Fluorescent HA-PArg-FITC NPs not diluted (5 µL at 3770 µg.mL⁻¹) were administered to the muscles, positioned in a horizontal plane immediately after the explantation, by inserting horizontally a Hamilton microsyringe into the distal extremity, as shown in figure 7A. Muscles were then maintained under fluid dynamic conditions in a LiveFlow bioreactor (IV-Tech, Massarosa, LU, Italy) kept in an incubator at 37 °C in a CO₂ humidified atmosphere for 3, 6 and 24 h. The culture medium was composed of medium 199 (Gibco) supplemented with 25 mM NaHCO₃, 5.5 mM glucose, 2.54 mM CaCl₂ (Merk, Kenilworth, NJ, USA), 0.6 nM insulin (Sigma-Aldrich, St. Louis, MO, USA), 0.1 % BSA (Gibco), 200 uU/mL penicillin-streptomycin (Gibco) and 0.5% Amphotericin B (Gibco). After incubation, the muscles were cryofixed in isopentane, embedded in OCT and 5 µm-thick sections were collected in a cryostat. Cryosections were hydrated in PBS, stained with Trypan Blue (1:10 in PBS) for 20 s and Hoechst 33342 (1:2000 in PBS) for 5 min, and mounted in a mixture of PBS/glycerol (1:1). Samples were observed with an Olympus BX51 microscope (Olympus Italia Srl, Milan, Italy), equipped with a 100 W mercury lamp (Olympus Italia Srl).

2.5. Efficacy assays of PTM-loaded NPs in cells transfected with human (CTG)_n expansion

2.5.1. Cell transfection

C2C12 cells were transfected with *tet* inducible bidirectional plasmids expressing GFP in one direction and in the other a human DMPK genomic segment, containing exons 11-15 with either 0 (pBItetDMPKSGFP, Addgene #96903, used as control) or 960 (pBItetDT960GFP, Addgene #80419), interrupted CTG repeats located in exon 15. This system was generated by Lee et al³² and allows the *tet* inducible concomitant expression of GFP and CTG repeats from the same promoter so that CTG expressing clones might

be identified by green fluorescence after doxycycline administration. Cells were grown in Dulbecco's modified Eagle medium, supplemented with 10 % (v/v) FBS and 1 % (w/v) Glutamine. C2C12 were first transfected with 1 μg of pTet-On Advanced Vector (Clontech, Mountain View, CA, USA), carrying the inducible mammalian expression system and a neomycin resistance marker, using TransfexTM reagent (ATCC#CRL-1772, Sesto San Giovanni, MI, Italy), according to manufacturer's instructions. Forty-eight h later, transfected cells were selected with 400 $\mu\text{g}\cdot\text{mL}^{-1}$ G418 (Clontech). Then stable clones were co-transfected with 1 μg of pTK-Hyg Vector (Clontech), carrying an hygromycin resistance marker, and 1 μg of either pBItetDMPKSGFP or pBItetDT960GFP, expressing GFP and modeling a wide range of CTG repeats expression level. Two-days later, transfected cells were selected with 200 $\mu\text{g}\cdot\text{mL}^{-1}$ hygromycin B (Clontech). Transfected cells were maintained in medium with both 200 $\mu\text{g}\cdot\text{mL}^{-1}$ G418 and hygromycin B and gene transcription was activated by adding 1 $\mu\text{g}\cdot\text{mL}^{-1}$ of doxycycline (Clontech) for 48 h.

2.5.2. Efficacy assays

PTM-loaded NPs efficacy was tested on established C2C12 (CTG)₉₆₀ transfected cell line. Cells were seeded onto glass coverslips (12 mm in diameter) in 24-multiwell plate (5 x 10³ cells/well) and incubated for 48 h to allow gene transcription. C2C12 (CTG)₉₆₀ were treated for 24 and 48 h with 10 or 30 μM of PTM either as PTM solubilized in medium (stock solution prepared in milli-Q water) or loaded into the PTM-loaded NPs. Untreated cells were used as cell control. At each incubation time point, cells were fixed with 4 % (v/v) paraformaldehyde in PBS for 15 min at 4 °C and then post-fixed in ethanol for 30 min at -20°C. Slides were first incubated with primary anti-MBNL1 antibody 3A4 (Santa-Cruz Biotechnology, Dallas, USA) at a dilution 1:20 in PBS containing 0.1 % BSA and 0.05 % Tween20, overnight at 4 °C. Afterward, slides were incubated with secondary Cy3-labeled goat anti-mouse IgG antibody (Jackson Laboratories, PA, USA) diluted 1:100 in PBS for 1 h at room temperature, stained for DNA with Hoechst (33342) at a dilution 1:10000 for 3 min and mounted in PBS/glycerol (1:1). Samples were observed with the Olympus BX51 microscope as specified above. For each sample, the number of nuclear foci by nucleus were manually counted for 500 GFP positive cells, testifying the effective cell transfection. Statistical significance was determined using two-tailed Student t tests.

3. Results

3.1. NPs preparation, characterization and stability

HA-PArg NPs were obtained by polyelectrolyte complexation of negatively charged HA and positively charged PArg using the ionic gelation technique^{19,33}. NPs showed a mean diameter around 200 nm and a polydispersity index lower than 0.1, indicating that the particles obtained were homogeneous and monodispersed. The surface potential of the NPs was negative (about -35 mV) due to the carboxylic groups of HA exposed on the surface. Moreover, these nanocarriers were able to associate PTM in a high amount (80 %). The presence of HA-FITC and HA-cy5 did not affect the physico-chemical properties of the system, fluorescently labelled NPs showed similar size and zeta potential values.

Colloidal stability of HA-PArg NPs and PTM-loaded NPs in cell culture medium was assessed using DSC analysis to determine their behavior in complex biological environment (supplementary figure 1). DSC thermographs of HA-PArg NPs showed no thermal change of the systems until 50 °C if compared with the reference medium, followed by two slightly endothermic inflections probably associated with a structural rearrangement inside the nanosystems. DSC curves of PTM demonstrated an important exothermic peak at 33 °C whereas once loaded into NPs this important exothermic change was shifted at 37 °C. To elucidate if the thermic change observed for PTM-loaded NPs was due to the amount of PTM not encapsulated or due to a destabilization of the nanosystems, PTM-loaded NPs were dialyzed overnight to remove excess of PTM. DSC thermograph of dialyzed PTM-loaded NPs demonstrated no exothermic peak but only the slight inflections after 50 °C correlated to the nanosystems. The absence of exothermic peak after dialysis can explain that this peak was related to the non-encapsulated PTM present in solution or poorly associate with the external NPs surface.

3.2. HA-PArg NPs administration to healthy myoblasts and myotubes

3.2.1. Cytotoxicity

Results of myoblasts and myotubes viability studies are reported in figure 1. In myoblasts at all time points (2h, 24h and 48h), HA-PArg NPs presented an overall higher biocompatibility compared to PTM-loaded NPs, while no significant difference was observed between PTM-loaded NPs and PTM solution. At the highest concentration

tested, 120 μM of PTM, both drug alone or drug-loaded NPs strongly reduced cell viability. Myoblasts treated with HA-PArg NPs and PTM-loaded NPs showed a cell viability above 75 % until 48 h at a concentration of 107 and 36 $\mu\text{g}\cdot\text{mL}^{-1}$ respectively. In myotubes, cytotoxicity of PTM-loaded NPs was significantly higher compared to PTM at all time points studies. HA-PArg NPs and PTM-loaded NPs were cytocompatibles (viability above 75 %) with myotubes treated for 48 h at a concentration of 107 $\mu\text{g}\cdot\mu\text{L}^{-1}$.

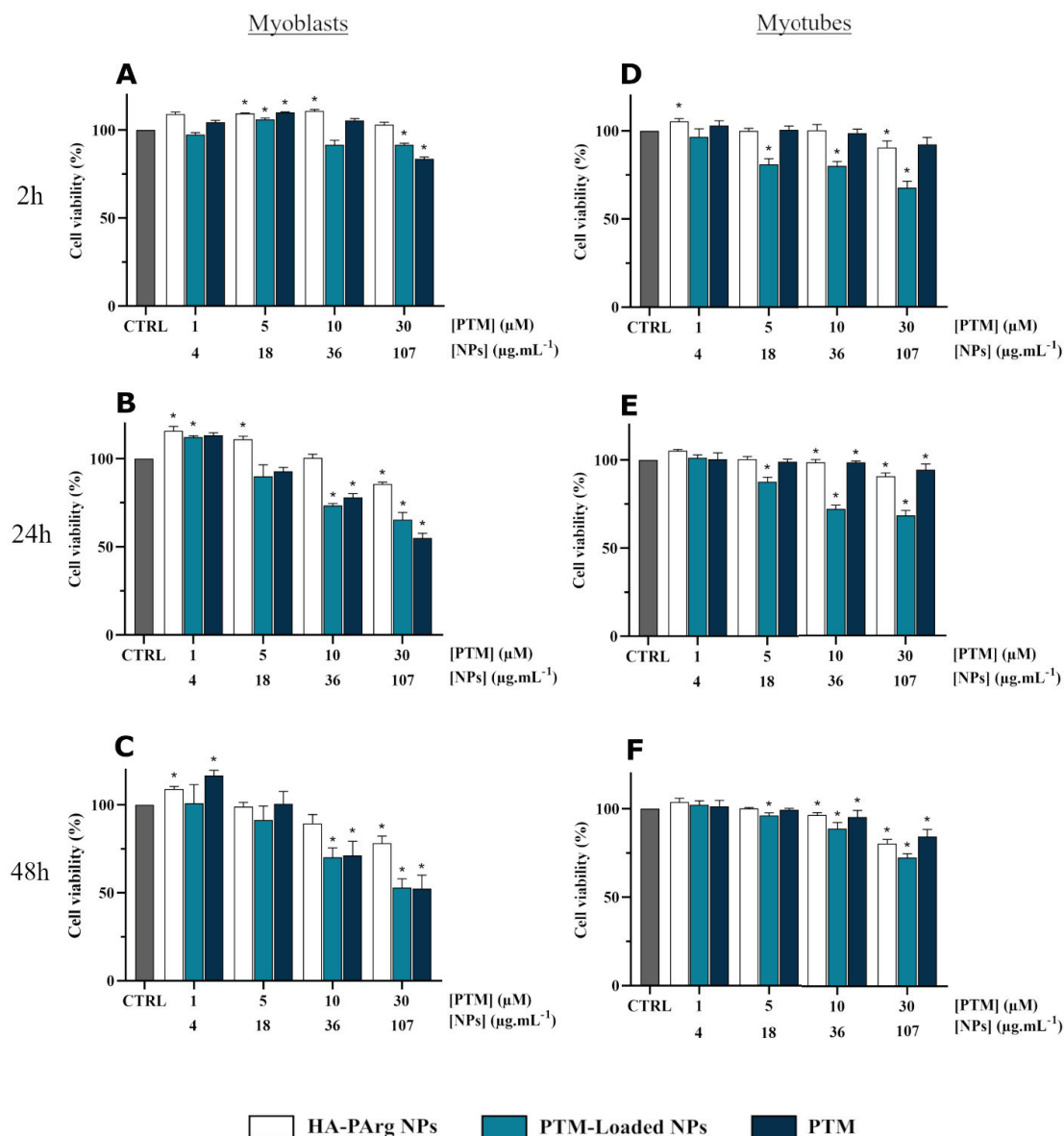


Fig. 1. Cytotoxicity values measured by MTT assay in C2C12 myoblasts (A-C) and myotubes (D-F) treated with HA-PArg NPs, PTM-Loaded NPs and PTM after 2 h (A, D), 24 h (B, E) and 48 h (C, F) treatments. Box-plots show the mean value \pm SE values of triplicates. * $p < 0.05$ as compared to the control.

3.2.2. Uptake, intracellular distribution and fate

Internalization and intracellular fate of HA-PArg NPs were investigated at CFM and TEM analysis. CFM observations showed that HA-PArg NPs occurred in myoblasts after 2 h incubation, they were preferentially distributed in the peripheral cytoplasmic region and appeared as single small fluorescing spots (figure 2A). After 24 and 48 h, the amount of internalized HA-PArg NPs accumulated in the perinuclear region, the NPs appearing as large fluorescing clusters (figure 2B). In myotubes, the uptake and intracellular distribution of HA-PArg NPs showed the same pattern as in myoblasts; however, the amount of internalized NPs was smaller in comparison to myoblasts and never appeared as large clusters (figure 2C, D).

TEM observations confirmed the presence of HA-PArg NPs after a 2 h incubation: they were found to adhere to the cell surface and to be internalized *via* endocytosis (figure 3A). However, only a few NPs were observed inside endosomes (figure 3B), while many NPs were found to escape endosomes (figure 3C). Most NPs occurred free in the cytosol (figure 3D), although some NPs were partially surrounded by a dual membrane indicating autophagic processes (figure 3E). After 24 h, many HA-PArg NPs accumulated in the cytosol in the perinuclear region (figure 3F) and often showed a larger size in comparison to NPs observed after 2 h incubation. In some myoblasts, HA-PArg NPs accumulated in huge amounts and some of them were found to bud from the cell surface (figure 4A). After 48 h, myoblasts showed the same features as after 24 h (not shown). In myotubes, HA-PArg NPs underwent endocytosis and endosomal escape similarly to myoblasts; NPs were found to distribute along the myofibrils bundles (figure 4B) and no large clusters were ever observed.

HA-PArg NPs were never found inside cell nuclei. Moreover, no cell organelle damage or alteration was observed in both myoblasts and myotubes.

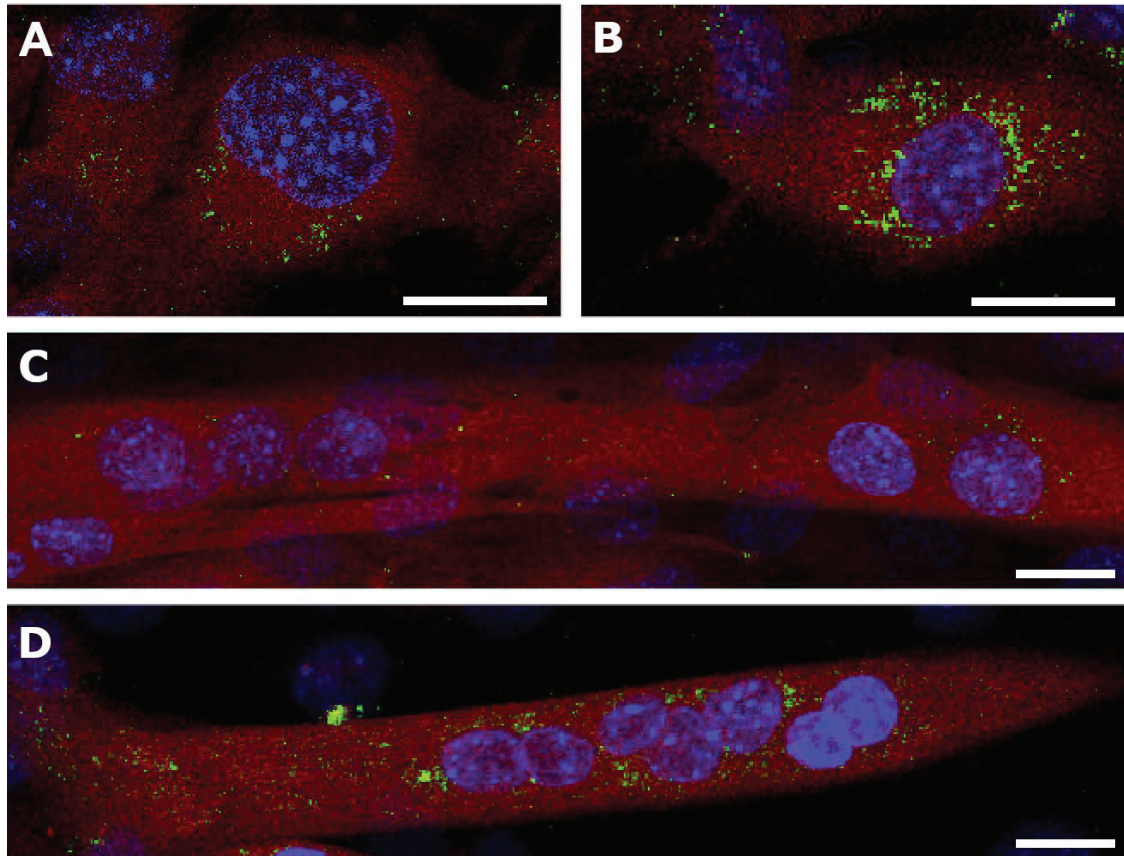


Fig. 2. CFM analysis of myoblasts (A,B) and myotubes (C,D) treated with HA-PArg-FITC NPs for 2 h (A,C) and 24 h (B,D). Cell cytoplasm were stained for Trypan blue and cell nuclei were counterstained for Hoechst 33342. Note the lower internalization in myotubes. Bars, 20 μm.

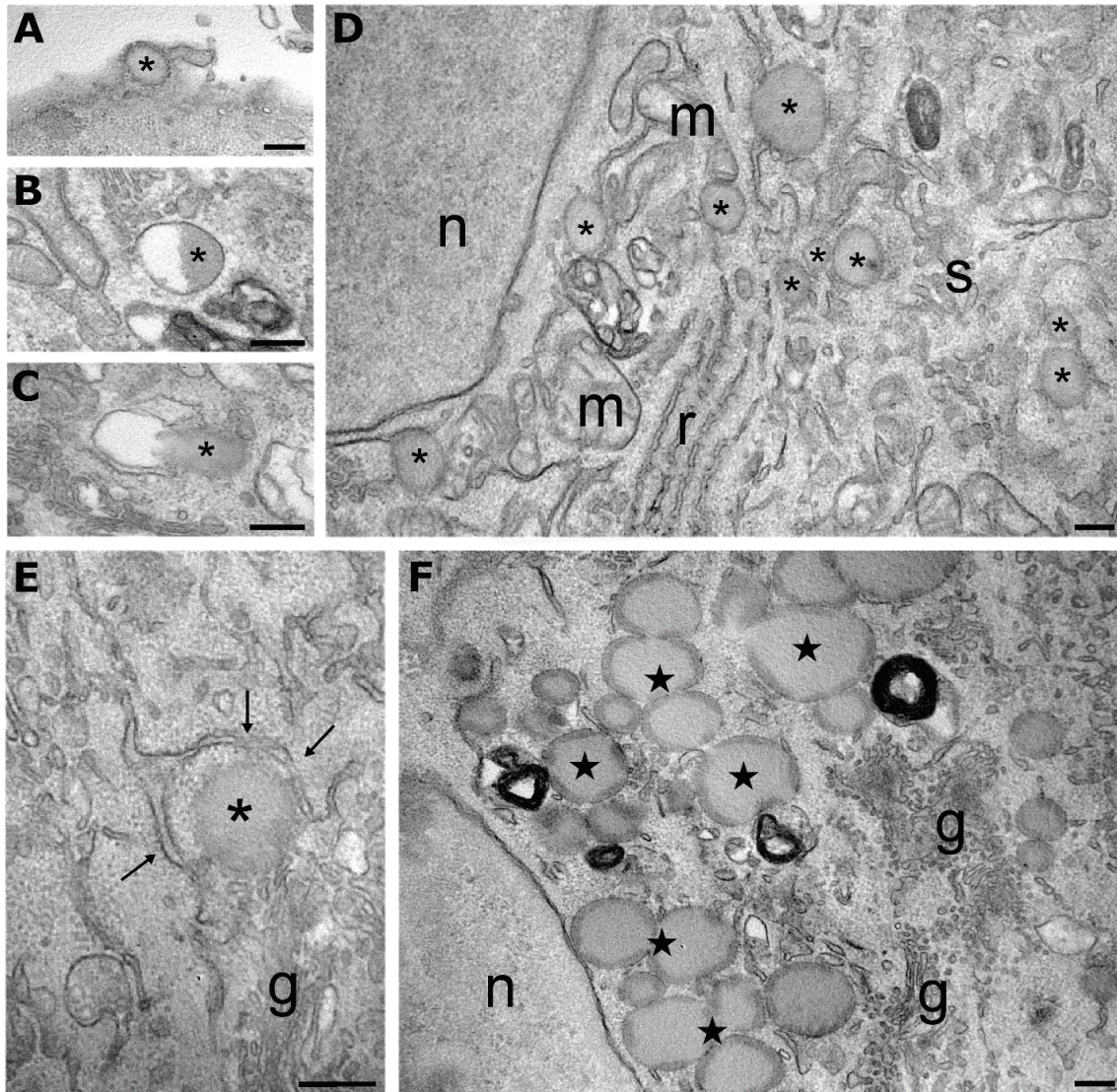


Fig. 3. Transmission electron micrographs of C2C12 myoblasts treated with HA-PArg NPs. (A-E) After 2 h, NPs (asterisks) were found to adhere to the cell surface, entering via endocytic process (A), occur inside endosomes (B) and escape from endosomes (C), thus accumulating free in the cytosol (D). (E) A free NP (asterisk) is partially enclosed by autophagic dual membranes (thin arrows). (F) After 24 h, clusters of large HA-Parg NPs (stars) accumulated in the cytoplasm; however, the cellular components were well preserved. n, nucleus; g, Golgi complex; m, mitochondria; r, rough endoplasmic reticulum; s, smooth endoplasmic reticulum. Bars, 200 nm.

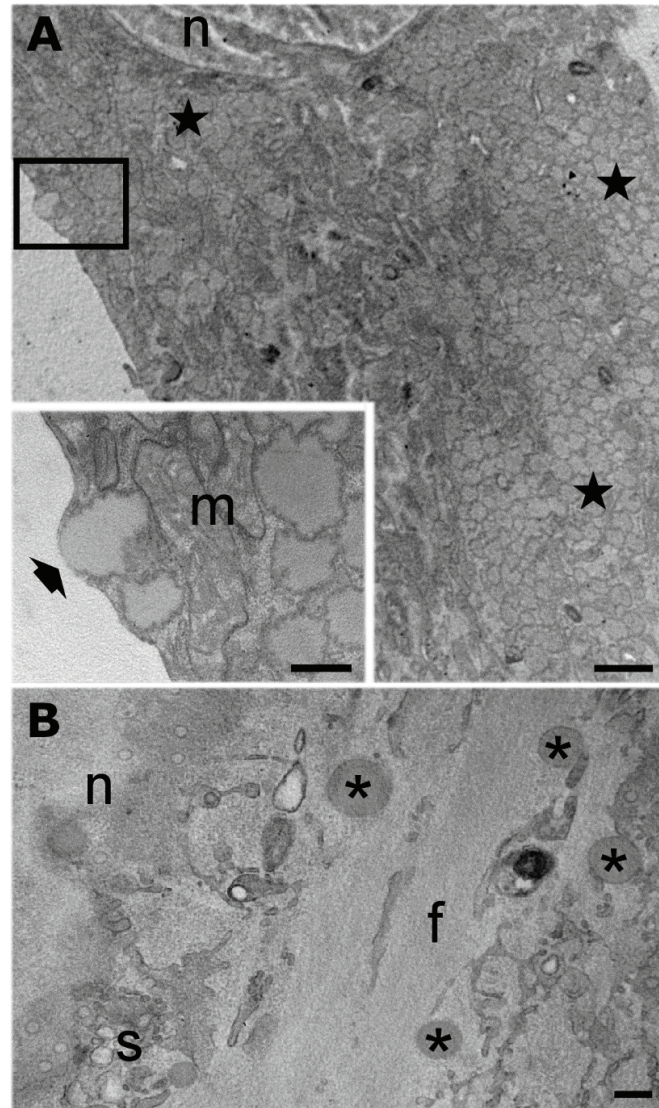


Fig. 4. Transmission electron micrographs of C2C12 myoblasts and myotubes treated with HA-PArg NPs. (A) A myoblast containing large clusters HA-PArg NPs (stars). The inset is a high magnification of the framed area showing a HA-PArg NP budding from the cell surface (arrowhead). (B) A myotube show many HA-PArg NPs (asterisks) occurring free in the cytosol, especially along the myofibrils bundles (f). n, nucleus; m, mitochondria; s, smooth endoplasmic reticulum. Bars, 1 μm (A); 200 nm (B and inset).

3.2.3. Endocytic uptake pathway

To further elucidate the NPs endocytic pathway, we investigate the intracellular distribution of HA-PArg-cy5 NPs into diverse vesicles (figure 5). CFM optical sections showed a quite immediate internalization of HA-PArg NPs, with an intracellular distribution of NPs in early and late endosomes after only 5 min incubation time. More interestingly, HA-PArg NPs were highly localized inside CD44-labelled vesicles demonstrating the importance of CD44 receptors in the NPs uptake.

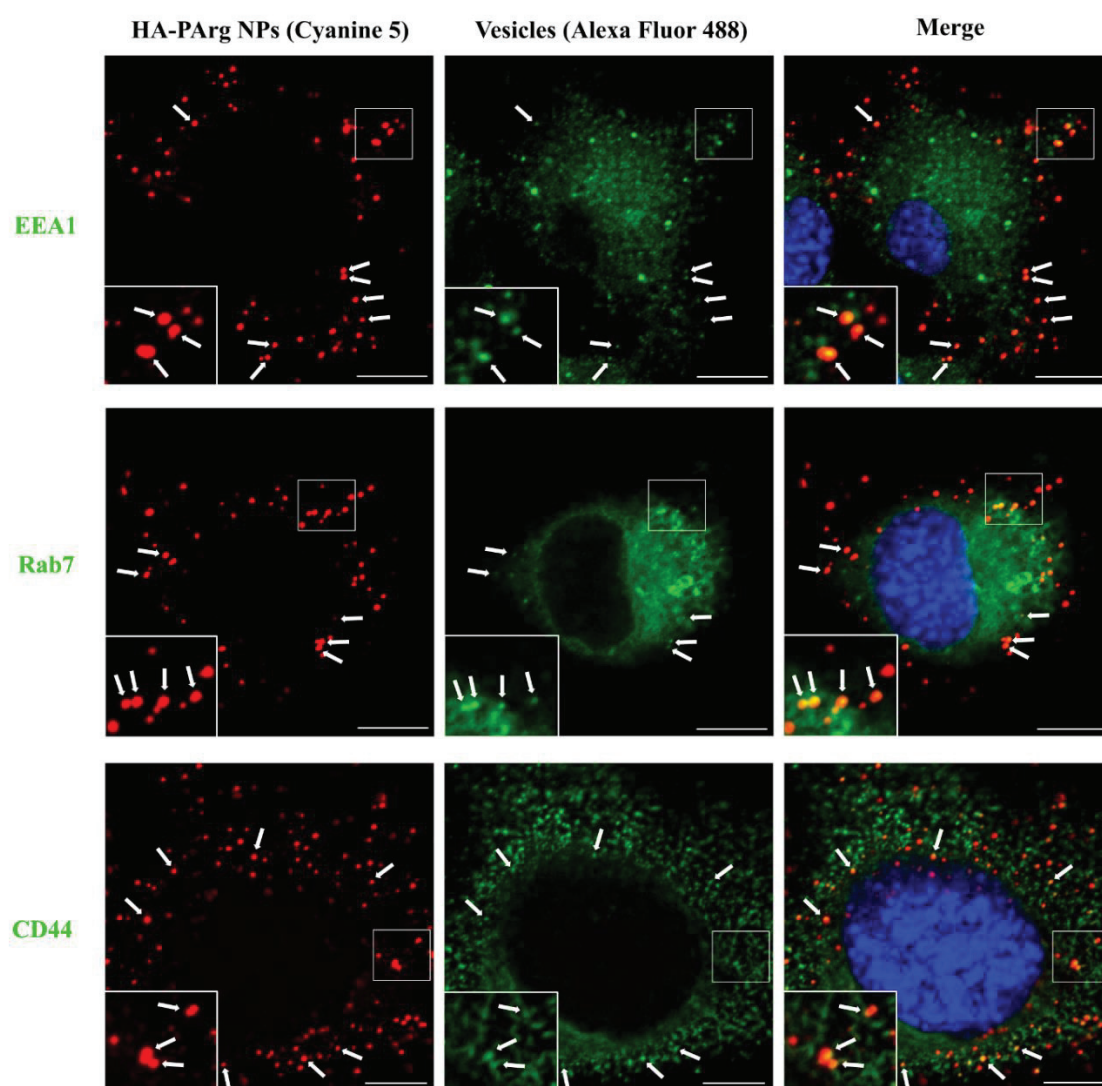


Fig. 5. CFM analysis of the intracellular localization of HA-PArg-cy5 NPs into diverse vesicles in C2C12 myoblasts. After 5 min incubation, HA-PArg NPs (red fluorescent signal) were co-localizing with early/late endosomes and CD44 vesicles (green fluorescent signal). Bars, 10 μ m.

3.2.4. Endosomal acidification inhibition

Acidic environment demonstrated to influence the surface charge of NPs without affecting their size and distribution (supplementary figure 2). Zeta potential analysis showed a surface charge of HA-PArg NPs around -40 mV at physiological pH and decreased over -10 mV at pH = 3.

At CFM, myoblasts untreated with bafilomycin A1 showed a fluorescent HA-PArg-FITC NPs distribution both inside endosomes (yellow signal due to the overlapping of the green NPs and the red endosomes signals) and free into the cytosol (green signal) (figure 6A), whereas in myoblasts treated with bafilomycin A1 the yellow signal was prevalent, demonstrating that NPs were localized mainly inside endosomes (figure 6B).

TEM observations demonstrated the presence of many NPs inside endosomes after 2 h, while NPs escaping endosomes or occurring free in the cytosol were quite rare (figure 6C). After 24 h, large vacuoles (secondary lysosomes) containing heterogeneous materials accumulated in the cytoplasm; among this material, many roundish structures reminiscent of small NPs were observed (figure 6D). Alcian blue staining specific for HA was found in most of these roundish structures, demonstrating that they were HA-PArg NPs remnants; some spread HA staining was also observed inside the secondary lysosomes.

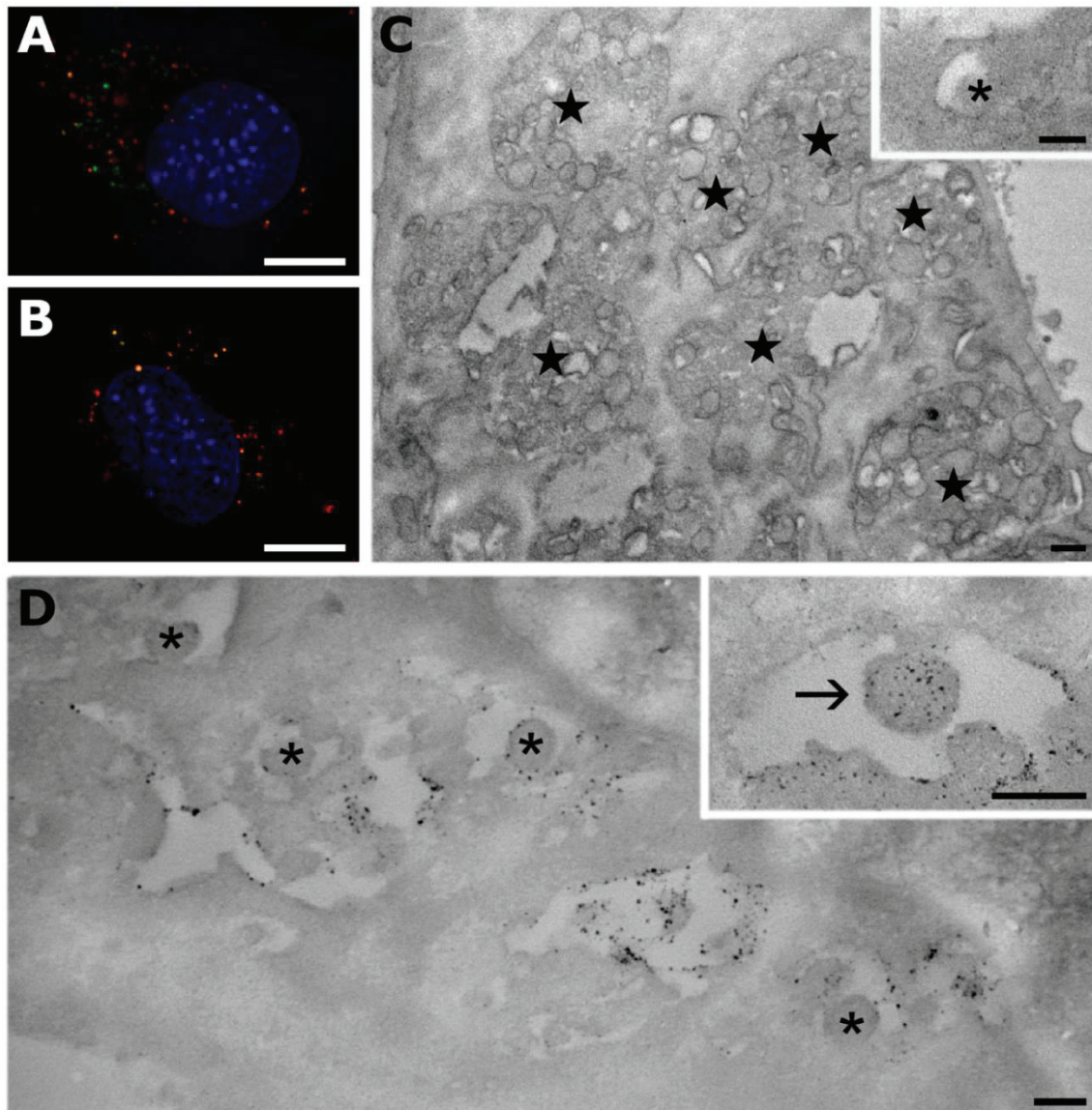


Fig. 6. CFM and TEM analysis of C2C12 myoblasts treated with HA-PArg NPs and bafilomycin A1. (A) CFM optical sections of myoblasts treated with HA-PArg-FITC NPs (B) and co-treated with bafilomycin A1. Note the higher number of green spots (free NPs) in A. Bars, 10 μm . (C, D) Transmission electron micrographs of myoblasts co-treated with HA-PArg NPs and bafilomycin A1. (C) A NPs (asterisks) inside an endosome (inset). Numerous secondary lysosomes containing NP remnants (stars) accumulate in the cytoplasm. (D) Alcian Blue staining reveals NP remnants still containing HA inside a secondary lysosome (arrow); other NP remnants are weakly or not labelled (asterisks). HA signal is also scattered inside the lysosomes. Bars, 200 nm.

3.3. Biodistribution and targeting efficacy of HA-PArg NPs in skeletal muscle

Biodistribution and targeting efficacy of HA-PArg NPs were evaluated in explanted murine skeletal muscles maintained *in vitro* in a fluid dynamic system able to considerably improve organ preservation³⁴. Conventional fluorescence microscopy demonstrated the presence of HA-PArg-FITC NPs into murine soleus muscles at both short and long incubation time. After 3 h of incubation, HA-PArg-FITC NPs were found exclusively inside muscle sections collected at the middle of the muscle, corresponding to the area where they were injected (figure 7A). Despite their huge entrapment into the connective tissue, NPs were found slightly internalized inside myofibers already after this short incubation time (figure 7B). After 24 h, NPs were found internalized in higher amount inside myofibers, while the level of NPs entrapped in the connective tissue drastically decreased due to phagocytic activity of macrophages (figure 7C). Moreover, NPs were found to be homogeneously distributed along the entire soleus muscle, even in muscle sections collected at the extremity of the belly.

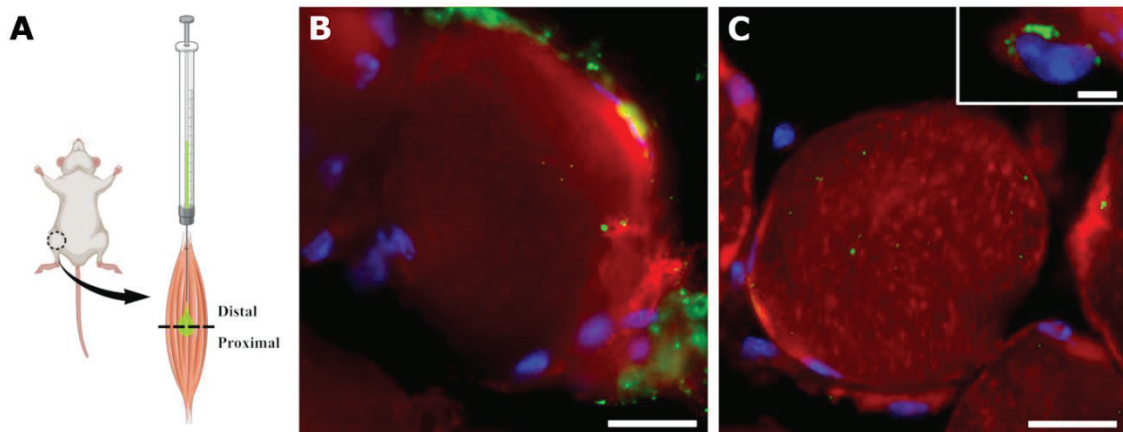


Fig. 7. HA-PArg NPs biodistribution into skeletal muscle. (A) Representative schema of fluorescent HA-PArg-FITC NPs administration method into murine soleus muscle. (B, C) Conventional fluorescent cross sections images of murine soleus muscle treated with HA-PArg-FITC NPs and maintained under fluid dynamic conditions for 3 h (B) and 24 h (C). Note the phagocyte that internalized some HA-PArg-FITC NPs occurring in the extracellular matrix (C, inset). Bars, 25 μm ; 5 μm (inset)

3.4. Efficacy assays of PTM-loaded NPs in cells transfected with human (CTG)_n expansion

To establish a stable cell line modeling DM1 pathology, C2C12 were transfected with plasmid containing either 0 or 960 CUG repeats and demonstrated a high but incomplete transfection efficiency rate, resulting in a cell population composed of transfected cell clones (expressing GFP) or untransfected ones. Transfected C2C12 cells containing 960 CUG repeats accumulated MBNL1 in nuclear foci, whereas cells containing 0 CUG repeats (data not shown) or untransfected cells showed a diffuse nuclear MBNL1 distribution (figure 8A). Detailed results of the quantitative evaluation of nuclear foci are reported in figure 8B, C. In summary, both PTM concentrations tested induced a significant reduction in the number of nuclear foci, with some differences depending on the administration method (as PTM-loaded NPs or PTM as-in) and the incubation time (24 or 48 h). After 24 h, untreated C2C12 (CUG)₉₆₀ showed up to 6 nuclear foci per cell nucleus while the majority of cells contained 1-2 foci per cell. C2C12 (CUG)₉₆₀ treated with PTM-Loaded NPs showed up to 4 foci per nucleus while a large number of cells did not contain foci. No statistically significant difference was observed for cells treated with 10 or 30 μ M PTM-Loaded NPs. As for C2C12 (CUG)₉₆₀ treated with PTM as-in, no statistical difference in number of foci was found with PTM-loaded NPs for the concentration of 10 μ M (although the tendency to the reduction of foci was more evident in cells treated with NPs); conversely, the reduction was significantly stronger in cells treated with PTM-loaded NPs 30 μ M. Statistical comparisons of PTM-loaded NPs 10 μ M vs PTM-loaded NPs 30 μ M or PTM as-in 10 μ M vs PTM as-in 10 μ M did not give significant difference (figure supplementary 3).

After 48 h, results were generally similar to those found after 24 h. However, PTM-loaded NPs induced a stronger reduction in number of foci in comparison to PTM as-in at both the drug concentrations tested and statistical comparisons of PTM-loaded NPs 10 μ M vs PTM-loaded NPs 30 μ M revealed a significantly stronger reduction of foci in cells treated with the higher drug concentration.

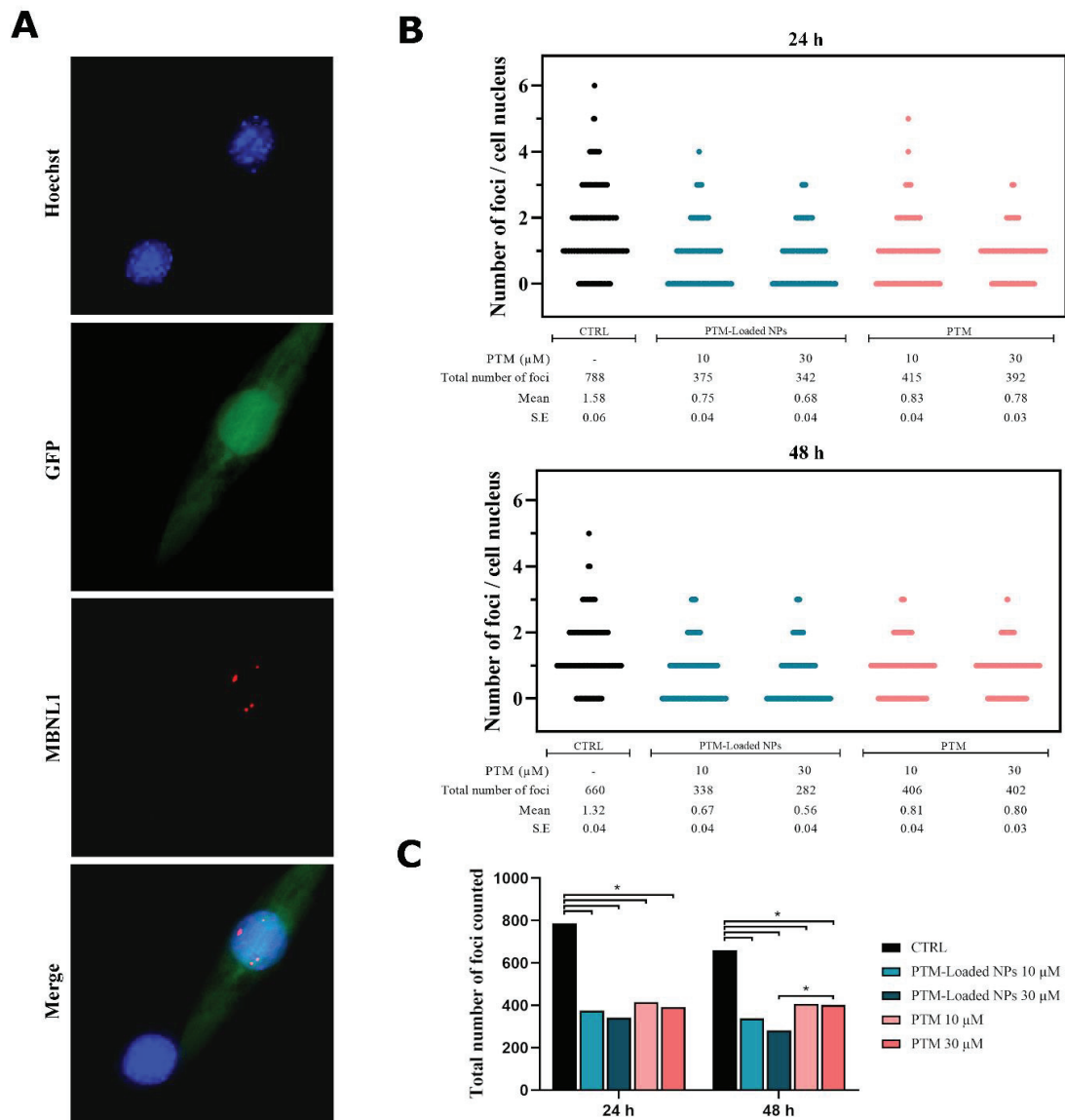


Fig. 8. PTM-Loaded NPs efficacy on C2C12 (CUG)₉₆₀ transfected cells. (A) Conventional fluorescence images of C2C12 myoblasts, the untransfected one does not express GFP, while the myoblast transfected with 960 interrupted CTG repeats plasmid expresses GFP and nuclear foci. (B) Dot-plots of the nuclear foci distribution and (C) box-plots of the total number of foci in C2C12 (CUG)₉₆₀ myoblasts untreated, treated with PTM-loaded NPs or PTM for 24 h and 48 h (n = 500).

4. Discussion

The aim of the present work was to repurpose PTM using HA-PArg NPs to treat skeletal muscle cells affected by DM1. HA-PArg NPs were studied for their safety and intracellular fate in cultured myoblast and myotubes, for their biodistribution in the whole muscle and, finally, for their efficacy in PTM delivery to a DM1 *in vitro* model.

In order to identify the most suitable conditions to treat muscle cells, HA-PArg NPs were tested for their toxicity in myoblasts and myotubes at increasing concentrations. MTT assays revealed that HA-PArg NPs are well tolerated by myoblasts and myotubes up to 48 h, while PTM-loaded NPs were tolerated on myoblasts only until the concentration of 36 $\mu\text{g}\cdot\text{mL}^{-1}$. Globally, HA-PArg NPs and PTM-loaded NPs showed a higher toxicity on myoblasts than on myotubes, especially for the highest concentrations. This discrepancy is likely related to the different cytokinetic and metabolic features of the two cell types³⁰: myoblasts are actively cycling cells which undergo mitosis about every 20 h, thus implying a high metabolic rate³⁵, whereas, due to their terminal differentiation, myotubes are non-cycling cells³⁶ and most of their metabolic activity is devoted to the preservation of the contractile apparatus^{37,38}.

The determination of safe HA-PArg NPs concentration was crucial to allow the investigation of their internalization extent and pathway, together with their intracellular fate. Accordingly, the microscopical analysis (at CFM and TEM) revealed that HA-PArg NPs enter rapidly both myoblasts and myotubes by endocytosis. CFM analysis demonstrated that CD44 receptors play a key role in the internalization of HA-PArg NPs, suggesting CD44-mediated endocytosis as one possible preferentially endocytic route in the uptake of HA-PArg NPs^{39,40}. Moreover, the lower amount of HA-binding CD44 receptors on the surface of differentiated cells may explain the less efficient internalization of HA-PArg NPs into myotubes^{20,41,42}.

In addition, once in the cytoplasm, HA-PArg NPs rapidly escape endosomes as demonstrated by the lack of overlapping between NPs and endosomes fluorescence as well as by the frequent ultrastructural observation of NPs protruding from endosomes. Although some free NPs re-enter the lytic pathway by autophagic activity, the large majority escape digestion (as demonstrated by the scarce residual bodies) and occur free in the cytosol for long time, frequently showing an increase in size, maybe due to

hydration or fusion processes (as suggested by TEM observations). It can be therefore inferred that the ability to escape the lysosomal pathway is the primary cause for the intracellular accumulation of large amounts of free HA-PArg NPs, which undergo extrusion in overloaded cells. Interestingly, even in cells containing a great quantity of NPs, no evident sign of organelle damage was observed at TEM, supporting the notion of the biocompatibility of these nanocarriers¹⁹. It is worth noting that HA-PArg NPs have never been found inside cell nuclei, even in the cycling myoblasts, avoiding the unpredictable long-term risks of interactions between nanomaterials and nucleic acids or nuclear factors. Therefore, although in a comparative *in vitro* study muscle cells proved to be much more sensitive to NPs than other cell types⁴³, our results demonstrate that HA-PArg NPs may be safely administered to muscle cells.

Understanding the diverse steps of the intracellular fate of a nanocarrier is of paramount importance in order to plan a therapeutic strategy; in this view, the ability of HA-PArg NPs to escape endosomes was thoroughly studied. To date, a scientific explanation for the endosomal escape process has been provided only for cationic nanocarriers based on the “proton sponge effect”⁴⁴, but this is not applicable to the anionic HA-PArg NPs. Our findings demonstrated that the inhibition of vacuolar-type H⁺-ATPases responsible for endosomal acidification lead to a drastic decrease in NPs endosomal escape and cytosolic NPs accumulation, while many secondary lysosomes containing heterogeneous material appeared in the cytoplasm. The Alcian blue staining³¹ was crucial to identify therein HA-PArg NPs remnants and the HA released due to the enzymatic degradation. These data provide unequivocal evidence that the intravacuolar acidification arising from the gradual maturation of endosomes plays a key role in the escape of this nanocarrier. Thereby, we hypothesized that buffering effect is responsible for HA protonation, decreasing HA and PArg interactions within HA-PArg NPs. This effect promotes the fusion of the cationic PArg with the organelle membrane, causing the rupture of the endosomal barriers and leading to the escape of HA-PArg NPs into the cytosol. In fact, arginine rich peptides considered as cell-penetrating peptides has demonstrated to enhance intracellular delivery of arginine-coated polymeric NPs^{45–47}. So far, this work is one of the first to evidence buffering effect on negative polymeric NPs.

Interestingly, HA-PArg NPs proved to efficiently enter not only cultured muscle cells, but also myofibers in the whole skeletal muscle. This is an essential feature in view of a

therapeutic application since skeletal muscles are complex organs made of elongated contractile cells (myofibers) and quiescent resident stem cells (satellite cells) join together by vascularized connective sheaths. HA-PArg NPs proved to be successfully internalized by myofibers in the whole muscle. Fluorescent HA-PArg-FITC NPs were injected into explanted skeletal muscle maintained *in vitro* under fluid dynamic conditions mimicking the physiological environment, thus ensuring controlled experimental conditions and excellent functional and structural preservation³⁴. The microscopy analysis of HA-PArg NPs distribution revealed that these nanocarriers spread within the whole muscle in a few hours, rapidly enter the myofibers and are efficiently removed from the connective tissue by macrophages (as a further evidence of the optimal preservation of the explanted organ). HA-PArg NPs can be therefore envisaged as nanocarriers suitable for i.m. administration.

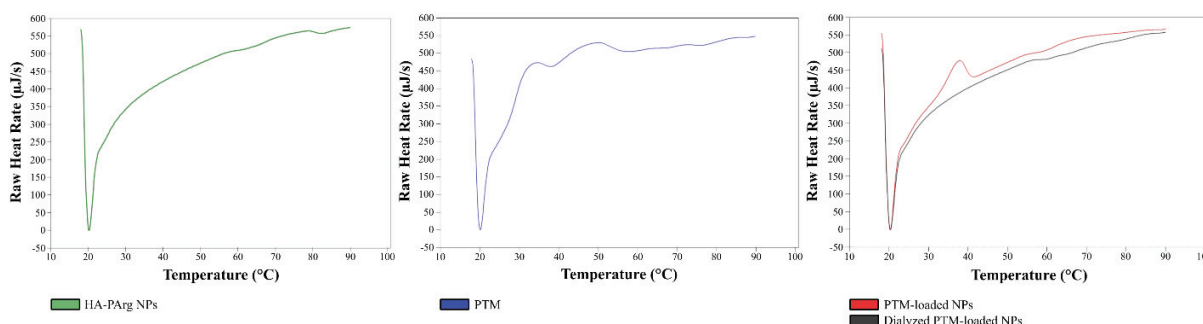
The therapeutic efficacy of PTM-loaded NPs was evaluated in C2C12 myoblasts transfected with human (CTG)_n DNA, in order to obtain an *in vitro* model expressing DM1 pathological phenotype. Transfected C2C12 myoblasts have been already used to study DM1 pathogenic mechanisms^{48,49} as well as to test experimental therapeutic approaches⁵⁰. Transfected C2C12 myoblasts were treated for 24 and 48 h with either 10 or 30 μ M PTM, administered as PTM-loaded NPs or as-in, then the number of nuclear foci was assessed in 500 cells per sample. Nuclear RNA foci as well as Muscleblind-like protein 1 sequestration are molecular pathology hallmarks of DM1⁵¹, and the number of foci has been widely used as a parameter to monitor the effects of therapeutic drugs^{14,32,52–55}. Both PTM concentrations induced a significant reduction in the number of foci with respect to control after both 24 h and 48 h. Interestingly, in cells treated with 10 μ M PTM, PTM-loaded NPs and PTM as-in induced a similar effect after 24h, but after 48 h the reduction was significantly higher in cells incubated with NPs; in cells treated with 30 μ M PTM, the PTM-loaded NPs proved to be more efficient in reducing the number of foci at both 24 and 48 h. It is likely that the therapeutic advantage of PTM-loaded NPs relies on their high uptake into myoblasts and sustained release of PTM in the cytosol after escaping the lytic pathway. Moreover, by comparing the efficacy of the two PTM concentrations in reducing the number of nuclear foci, it is evident that, after 48 h, NPs are more efficient when loaded with 30 μ M PTM, whereas no difference occur in samples

treated with PTM as-in. This could be related again to the ability of internalized NPs to protect the drug from enzymatic degradation and progressively release it into the cell.

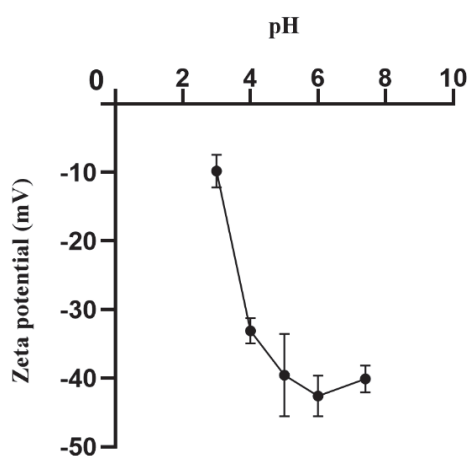
5. Conclusions

Our results demonstrate that the HA-PArg NPs are stable and biocompatible system that can be used for both cycling myoblasts and non-cycling myotubes: they enter the intracellular environment by endocytosis, undergo endosomal escape and accumulate in the cytosol without inducing microscopically detectable cytological alterations. Although the differentiation stage affects the uptake efficiency, nanocarriers are well internalized also by myofibers when injected into the whole skeletal muscle and, as a further advantage, the NPs entrapped in the connective tissue are physiologically removed by macrophages thus reducing the risk of inflammatory events. Moreover, when loaded with PTM, HA-PArg NPs are able to significantly reduce the number of nuclear foci in a DM1 cell model. All these features make these nanocarriers potential candidates for delivering therapeutic agents *in vivo* for treating muscle cells in DM1. The results obtained herein using an established muscle cell line provide the experimental background for further studies to test these nanocarriers in DM1 animal models, to evaluate their efficacy in a living organism and define the most appropriate administration dose and route. Exploring the potential of nanotechnology to cure non-renewing cells affected by genetic diseases as DM1 represents a new challenge but, using appropriate experimental models and taking into account the multiple physicochemical interactions between nanocarriers and biological environment, this research field may offer novel responses to the needs of patients presently destined to disability and premature death.

Supporting Informations



Supplementary figure 1: DSC thermographs of HA-PArg NPs, PTM and PTM-loaded NPs.



Supplementary figure 2: Zeta potential evolution of HA-PArg NPs in 1 mM HEPES buffer adjusted to different pH values (mean \pm SE, $n = 2$)

<i>t tests</i>	24 h	48 h
CTRL vs Loaded-NPs 10 μ M	$p < 0.001$	$p < 0.001$
CTRL vs Loaded-NPs 30 μ M	$p < 0.001$	$p < 0.001$
CTRL vs PTM 10 μ M	$p < 0.001$	$p < 0.001$
CTRL vs PTM 30 μ M	$p < 0.001$	$p < 0.001$
Loaded-NPs 10 μ M vs PTM 10 μ M	$p = 0.147$	$p = 0.005$
Loaded-NPs 30 μ M vs PTM 30 μ M	$p = 0.035$	$p < 0.001$
PTM-Loaded NPs 10 μ M vs PTM-Loaded NPs 30 μ M	$p = 0.212$	$p = 0.022$
PTM 10 μ M vs PTM 30 μ M	$p = 0.356$	$p = 0.858$

Supplementary figure 3: Results of statistical comparisons (t-test) of the number of foci in C2C12 (CUG)₉₆₀ myoblasts untreated, treated with PTM-loaded NPs or PTM.

Acknowledgments

MR is a PhD student in receipt of a fellowship from the INVITE project of the University of Verona, (PhD Programme in Nanoscience and Advanced Technologies). This project has received funding from the European Union's Horizon 2020 Research and Innovation Programme under the Marie Skłodowska-Curie grant agreement No. 754345.

Confocal microscopy observations were performed at the Centro Piattaforme Tecnologiche of the University of Verona and at the Lymic – Platim of the University of Lyon.

References

- (1) Thornton, C. A. Myotonic Dystrophy. *Neurol Clin* **2014**, *32* (3), 705–719, viii. <https://doi.org/10.1016/j.ncl.2014.04.011>.
- (2) Meola, G. Clinical Aspects, Molecular Pathomechanisms and Management of Myotonic Dystrophies. *Clinical aspects* 12.
- (3) Brook, J. D.; McCurrach, M. E.; Harley, H. G.; Buckler, A. J.; Church, D.; Aburatani, H.; Hunter, K.; Stanton, V. P.; Thirion, J. P.; Hudson, T. Molecular Basis of Myotonic Dystrophy: Expansion of a Trinucleotide (CTG) Repeat at the 3' End of a Transcript Encoding a Protein Kinase Family Member. *Cell* **1992**, *68* (4), 799–808. [https://doi.org/10.1016/0092-8674\(92\)90154-5](https://doi.org/10.1016/0092-8674(92)90154-5).
- (4) Lee, J. E.; Cooper, T. A. Pathogenic Mechanisms of Myotonic Dystrophy. *Biochem Soc Trans* **2009**, *37* (0 6). <https://doi.org/10.1042/BST0371281>.
- (5) Philips, A. V.; Timchenko, L. T.; Cooper, T. A. Disruption of Splicing Regulated by a CUG-Binding Protein in Myotonic Dystrophy. *Science* **1998**, *280* (5364), 737–741. <https://doi.org/10.1126/science.280.5364.737>.
- (6) Nakamori, M.; Sobczak, K.; Puwanant, A.; Welle, S.; Eichinger, K.; Pandya, S.; Dekdebrun, J.; Heatwole, C. R.; McDermott, M. P.; Chen, T.; Cline, M.; Tawil, R.; Osborne, R. J.; Wheeler, T. M.; Swanson, M.; Moxley, R. T.; Thornton, C. A. Splicing Biomarkers of Disease Severity in Myotonic Dystrophy. *Ann Neurol* **2013**, *74* (6), 862–872. <https://doi.org/10.1002/ana.23992>.

- (7) Michel, L.; Huguet-Lachon, A.; Gourdon, G. Sense and Antisense DMPK RNA Foci Accumulate in DM1 Tissues during Development. *PLoS One* **2015**, *10* (9). <https://doi.org/10.1371/journal.pone.0137620>.
- (8) Miller, J. W.; Urbinati, C. R.; Teng-Umnuay, P.; Stenberg, M. G.; Byrne, B. J.; Thornton, C. A.; Swanson, M. S. Recruitment of Human Muscleblind Proteins to (CUG)(n) Expansions Associated with Myotonic Dystrophy. *EMBO J.* **2000**, *19* (17), 4439–4448. <https://doi.org/10.1093/emboj/19.17.4439>.
- (9) Ishiura, S.; Kino, Y.; Nezu, Y.; Onishi, H.; Ohno, E.; Sasagawa, N. Regulation of Splicing by MBNL and CELF Family of RNA-Binding Protein. *Acta Myol* **2005**, *24* (2), 74–77.
- (10) Nezu, Y.; Kino, Y.; Sasagawa, N.; Nishino, I.; Ishiura, S. Expression of MBNL and CELF mRNA Transcripts in Muscles with Myotonic Dystrophy. *Neuromuscul. Disord.* **2007**, *17* (4), 306–312. <https://doi.org/10.1016/j.nmd.2007.01.002>.
- (11) Andreana, I.; Repellin, M.; Carton, F.; Kryza, D.; Briançon, S.; Chazaud, B.; Mounier, R.; Arpicco, S.; Malatesta, M.; Stella, B.; Lollo, G. Nanomedicine for Gene Delivery and Drug Repurposing in the Treatment of Muscular Dystrophies. *Pharmaceutics* **2021**, *13* (2), 278. <https://doi.org/10.3390/pharmaceutics13020278>.
- (12) Pushpakom, S.; Iorio, F.; Eyers, P. A.; Escott, K. J.; Hopper, S.; Wells, A.; Doig, A.; Guilliams, T.; Latimer, J.; McNamee, C.; Norris, A.; Sanseau, P.; Cavalla, D.; Pirmohamed, M. Drug Repurposing: Progress, Challenges and Recommendations. *Nature Reviews Drug Discovery* **2019**, *18* (1), 41–58. <https://doi.org/10.1038/nrd.2018.168>.
- (13) Bray, P. G.; Barrett, M. P.; Ward, S. A.; de Koning, H. P. Pentamidine Uptake and Resistance in Pathogenic Protozoa: Past, Present and Future. *Trends in Parasitology* **2003**, *19* (5), 232–239. [https://doi.org/10.1016/S1471-4922\(03\)00069-2](https://doi.org/10.1016/S1471-4922(03)00069-2).
- (14) Warf, M. B.; Nakamori, M.; Matthys, C. M.; Thornton, C. A.; Berglund, J. A. Pentamidine Reverses the Splicing Defects Associated with Myotonic Dystrophy. *Proc Natl Acad Sci U S A* **2009**, *106* (44), 18551–18556. <https://doi.org/10.1073/pnas.0903234106>.

- (15) Coonrod, L. A.; Nakamori, M.; Wang, W.; Carrell, S.; Hilton, C. L.; Bodner, M. J.; Siboni, R. B.; Docter, A. G.; Haley, M. M.; Thornton, C. A.; Berglund, J. A. Reducing Levels of Toxic RNA with Small Molecules. *ACS Chem. Biol.* **2013**, *8* (11), 2528–2537. <https://doi.org/10.1021/cb400431f>.
- (16) Johnson, N. E. Myotonic Muscular Dystrophies: *CONTINUUM: Lifelong Learning in Neurology* **2019**, *25* (6), 1682–1695. <https://doi.org/10.1212/CON.0000000000000793>.
- (17) McClements, D. J. Encapsulation, Protection, and Delivery of Bioactive Proteins and Peptides Using Nanoparticle and Microparticle Systems: A Review. *Adv Colloid Interface Sci* **2018**, *253*, 1–22. <https://doi.org/10.1016/j.cis.2018.02.002>.
- (18) Su, H.; Wang, Y.; Gu, Y.; Bowman, L.; Zhao, J.; Ding, M. Potential Applications and Human Biosafety of Nanomaterials Used in Nanomedicine. *J Appl Toxicol* **2018**, *38* (1), 3–24. <https://doi.org/10.1002/jat.3476>.
- (19) Carton, F.; Chevalier, Y.; Nicoletti, L.; Tarnowska, M.; Stella, B.; Arpicco, S.; Malatesta, M.; Jordheim, L. P.; Briançon, S.; Lollo, G. Rationally Designed Hyaluronic Acid-Based Nano-Complexes for Pentamidine Delivery. *Int J Pharm* **2019**, *568*, 118526. <https://doi.org/10.1016/j.ijpharm.2019.118526>.
- (20) Mylona, E.; Jones, K. A.; Mills, S. T.; Pavlath, G. K. CD44 Regulates Myoblast Migration and Differentiation. *J Cell Physiol* **2006**, *209* (2), 314–321. <https://doi.org/10.1002/jcp.20724>.
- (21) Lollo, G.; Gonzalez-Paredes, A.; Garcia-Fuentes, M.; Calvo, P.; Torres, D.; Alonso, M. J. Polyarginine Nanocapsules as a Potential Oral Peptide Delivery Carrier. *J Pharm Sci* **2017**, *106* (2), 611–618. <https://doi.org/10.1016/j.xphs.2016.09.029>.
- (22) Gómez-Gaete, C.; Tsapis, N.; Silva, L.; Bourgaux, C.; Besnard, M.; Bochot, A.; Fattal, E. Supramolecular Organization and Release Properties of Phospholipid-Hyaluronan Microparticles Encapsulating Dexamethasone. *European Journal of Pharmaceutics and Biopharmaceutics* **2008**, *70* (1), 116–126. <https://doi.org/10.1016/j.ejpb.2008.04.013>.

- (23) Fudala, R.; Mummert, M. E.; Gryczynski, Z.; Rich, R.; Borejdo, J.; Gryczynski, I. Lifetime-Based Sensing of the Hyaluronidase Using Fluorescein Labeled Hyaluronic Acid. *J Photochem Photobiol B* **2012**, *106*, 69–73. <https://doi.org/10.1016/j.jphotobiol.2011.10.005>.
- (24) Nguyen, V. H.; Lee, B.-J. Protein Corona: A New Approach for Nanomedicine Design. *Int J Nanomedicine* **2017**, *12*, 3137–3151. <https://doi.org/10.2147/IJN.S129300>.
- (25) Francia, V.; Yang, K.; Deville, S.; Reker-Smit, C.; Nelissen, I.; Salvati, A. Corona Composition Can Affect the Mechanisms Cells Use to Internalize Nanoparticles. *ACS Nano* **2019**, *13* (10), 11107–11121. <https://doi.org/10.1021/acsnano.9b03824>.
- (26) Stockert, J. C.; Horobin, R. W.; Colombo, L. L.; Blázquez-Castro, A. Tetrazolium Salts and Formazan Products in Cell Biology: Viability Assessment, Fluorescence Imaging, and Labeling Perspectives. *Acta Histochem* **2018**, *120* (3), 159–167. <https://doi.org/10.1016/j.acthis.2018.02.005>.
- (27) Costanzo, M.; Malatesta, M. Embedding Cell Monolayers to Investigate Nanoparticle-Plasmalemma Interactions at Transmission Electron Microscopy. *Eur J Histochem* **2019**, *63* (1). <https://doi.org/10.4081/ejh.2019.3026>.
- (28) Panyam, J.; Zhou, W.-Z.; Prabha, S.; Sahoo, S. K.; Labhasetwar, V. Rapid Endo-Lysosomal Escape of Poly(DL-Lactide-Co-Glycolide) Nanoparticles: Implications for Drug and Gene Delivery. *FASEB J* **2002**, *16* (10), 1217–1226. <https://doi.org/10.1096/fj.02-0088com>.
- (29) Malatesta, M.; Giagnacovo, M.; Costanzo, M.; Conti, B.; Genta, I.; Dorati, R.; Galimberti, V.; Biggiogera, M.; Zancanaro, C. Diaminobenzidine Photoconversion Is a Suitable Tool for Tracking the Intracellular Location of Fluorescently Labelled Nanoparticles at Transmission Electron Microscopy. *Eur J Histochem* **2012**, *56* (2), e20. <https://doi.org/10.4081/ejh.2012.20>.
- (30) Costanzo, M.; Vurro, F.; Cisterna, B.; Boschi, F.; Marengo, A.; Montanari, E.; Meo, C. D.; Matricardi, P.; Berlier, G.; Stella, B.; Arpicco, S.; Malatesta, M. Uptake and Intracellular Fate of Biocompatible Nanocarriers in Cycling and Noncycling Cells. *Nanomedicine (Lond)* **2019**, *14* (3), 301–316. <https://doi.org/10.2217/nmm-2018-0148>.

- (31) Carton, F.; Repellin, M.; Lollo, G.; Malatesta, M. Alcian Blue Staining to Track the Intracellular Fate of Hyaluronic-Acid-Based Nanoparticles at Transmission Electron Microscopy. *Eur J Histochem* **2019**, *63* (4). <https://doi.org/10.4081/ejh.2019.3086>.
- (32) Lee, J. E.; Bennett, C. F.; Cooper, T. A. RNase H-Mediated Degradation of Toxic RNA in Myotonic Dystrophy Type 1. *Proc Natl Acad Sci U S A* **2012**, *109* (11), 4221–4226. <https://doi.org/10.1073/pnas.1117019109>.
- (33) Matha, K.; Lollo, G.; Taurino, G.; Respaud, R.; Marigo, I.; Shariati, M.; Bussolati, O.; Vermeulen, A.; Remaut, K.; Benoit, J.-P. Bioinspired Hyaluronic Acid and Polyarginine Nanoparticles for DACHPt Delivery. *Eur J Pharm Biopharm* **2020**, *150*, 1–13. <https://doi.org/10.1016/j.ejpb.2020.02.008>.
- (34) Carton, F.; Calderan, L.; Malatesta, M. Incubation under Fluid Dynamic Conditions Markedly Improves the Structural Preservation in Vitro of Explanted Skeletal Muscles. *Eur J Histochem* **2017**, *61* (4), 2862. <https://doi.org/10.4081/ejh.2017.2862>.
- (35) Malatesta, M.; Grecchi, S.; Chiesa, E.; Cisterna, B.; Costanzo, M.; Zancanaro, C. Internalized Chitosan Nanoparticles Persist for Long Time in Cultured Cells. *Eur J Histochem* **2015**, *59* (1), 2492. <https://doi.org/10.4081/ejh.2015.2492>.
- (36) Strohman, R. C.; Paterson, B.; Fluck, R.; Przybyla, A. Cell Fusion and Terminal Differentiation of Myogenic Cells in Culture. *J Anim Sci* **1974**, *38* (5), 1103–1110. <https://doi.org/10.2527/jas1974.3851103x>.
- (37) Kislinger, T.; Gramolini, A. O.; Pan, Y.; Rahman, K.; MacLennan, D. H.; Emili, A. Proteome Dynamics during C2C12 Myoblast Differentiation. *Mol Cell Proteomics* **2005**, *4* (7), 887–901. <https://doi.org/10.1074/mcp.M400182-MCP200>.
- (38) Casadei, L.; Vallorani, L.; Gioacchini, A. M.; Guescini, M.; Burattini, S.; D’Emilio, A.; Biagiotti, L.; Falcieri, E.; Stocchi, V. Proteomics-Based Investigation in C2C12 Myoblast Differentiation. *Eur J Histochem* **2009**, *53* (4), e31. <https://doi.org/10.4081/ejh.2009.e31>.
- (39) Qhattal, H. S. S.; Liu, X. Characterization of CD44-Mediated Cancer Cell Uptake and Intracellular Distribution of Hyaluronan-Grafted Liposomes. *Mol Pharm* **2011**, *8* (4), 1233–1246. <https://doi.org/10.1021/mp2000428>.

- (40) Rosa, J. M. R. de la; Pingrajai, P.; Pelliccia, M.; Spadea, A.; Lallana, E.; Gennari, A.; Stratford, I. J.; Rocchia, W.; Tirella, A.; Tirelli, N. Binding and Internalization in Receptor-Targeted Carriers: The Complex Role of CD44 in the Uptake of Hyaluronic Acid-Based Nanoparticles (SiRNA Delivery). *Advanced Healthcare Materials* **2019**, *8* (24), 1901182. <https://doi.org/10.1002/adhm.201901182>.
- (41) Chang, J.-S.; Chang, K. L. B.; Hwang, D.-F.; Kong, Z.-L. In Vitro Cytotoxicity of Silica Nanoparticles at High Concentrations Strongly Depends on the Metabolic Activity Type of the Cell Line. *Environ Sci Technol* **2007**, *41* (6), 2064–2068. <https://doi.org/10.1021/es062347t>.
- (42) Mahmoudi, M. Debugging Nano-Bio Interfaces: Systematic Strategies to Accelerate Clinical Translation of Nanotechnologies. *Trends Biotechnol* **2018**, *36* (8), 755–769. <https://doi.org/10.1016/j.tibtech.2018.02.014>.
- (43) Nie, Y.; Zhang, Z.-R.; He, B.; Gu, Z. Investigation of PEG-PLGA-PEG Nanoparticles-Based Multipolyplexes for IL-18 Gene Delivery. *J Biomater Appl* **2012**, *26* (8), 893–916. <https://doi.org/10.1177/0885328210384889>.
- (44) Varkouhi, A. K.; Scholte, M.; Storm, G.; Haisma, H. J. Endosomal Escape Pathways for Delivery of Biologicals. *Journal of Controlled Release* **2011**, *151* (3), 220–228. <https://doi.org/10.1016/j.jconrel.2010.11.004>.
- (45) Gestin, M.; Dowaidar, M.; Langel, Ü. Uptake Mechanism of Cell-Penetrating Peptides. *Adv Exp Med Biol* **2017**, *1030*, 255–264. https://doi.org/10.1007/978-3-319-66095-0_11.
- (46) Lättig-Tünnemann, G.; Prinz, M.; Hoffmann, D.; Behlke, J.; Palm-Apergi, C.; Morano, I.; Herce, H. D.; Cardoso, M. C. Backbone Rigidity and Static Presentation of Guanidinium Groups Increases Cellular Uptake of Arginine-Rich Cell-Penetrating Peptides. *Nature Communications* **2011**, *2* (1), 453. <https://doi.org/10.1038/ncomms1459>.

- (47) Uhl, P.; Grundmann, C.; Sauter, M.; Storck, P.; Tursch, A.; Özbek, S.; Leotta, K.; Roth, R.; Witzigmann, D.; Kulkarni, J. A.; Fidelj, V.; Kleist, C.; Cullis, P. R.; Fricker, G.; Mier, W. Coating of PLA-Nanoparticles with Cyclic, Arginine-Rich Cell Penetrating Peptides Enables Oral Delivery of Liraglutide. *Nanomedicine* **2020**, *24*, 102132. <https://doi.org/10.1016/j.nano.2019.102132>.
- (48) Amack, J. D.; Mahadevan, M. S. The Myotonic Dystrophy Expanded CUG Repeat Tract Is Necessary but Not Sufficient to Disrupt C2C12 Myoblast Differentiation. *Hum Mol Genet* **2001**, *10* (18), 1879–1887. <https://doi.org/10.1093/hmg/10.18.1879>.
- (49) Liang, R.; Dong, W.; Shen, X.; Peng, X.; Aceves, A. G.; Liu, Y. Modeling Myotonic Dystrophy 1 in C2C12 Myoblast Cells. *J Vis Exp* **2016**, No. 113. <https://doi.org/10.3791/54078>.
- (50) Dong, W.; Chen, X.; Wang, M.; Zheng, Z.; Zhang, X.; Xiao, Q.; Peng, X. Mir-206 Partially Rescues Myogenesis Deficiency by Inhibiting CUGBP1 Accumulation in the Cell Models of Myotonic Dystrophy. *Neurol Res* **2019**, *41* (1), 9–18. <https://doi.org/10.1080/01616412.2018.1493963>.
- (51) Meola, G.; Cardani, R. Myotonic Dystrophies: An Update on Clinical Aspects, Genetic, Pathology, and Molecular Pathomechanisms. *Biochim Biophys Acta* **2015**, *1852* (4), 594–606. <https://doi.org/10.1016/j.bbadis.2014.05.019>.
- (52) Wheeler, T. M.; Leger, A. J.; Pandey, S. K.; MacLeod, A. R.; Nakamori, M.; Cheng, S. H.; Wentworth, B. M.; Bennett, C. F.; Thornton, C. A. Targeting Nuclear RNA for in Vivo Correction of Myotonic Dystrophy. *Nature* **2012**, *488* (7409), 111–115. <https://doi.org/10.1038/nature11362>.
- (53) Childs-Disney, J. L.; Stepniak-Konieczna, E.; Tran, T.; Yildirim, I.; Park, H.; Chen, C. Z.; Hoskins, J.; Southall, N.; Marugan, J. J.; Patnaik, S.; Zheng, W.; Austin, C. P.; Schatz, G. C.; Sobczak, K.; Thornton, C. A.; Disney, M. D. Induction and Reversal of Myotonic Dystrophy Type 1 Pre-mRNA Splicing Defects by Small Molecules. *Nat Commun* **2013**, *4*, 2044. <https://doi.org/10.1038/ncomms3044>.

(54) Ketley, A.; Chen, C. Z.; Li, X.; Arya, S.; Robinson, T. E.; Granados-Riveron, J.; Udosen, I.; Morris, G. E.; Holt, I.; Furling, D.; Chaouch, S.; Haworth, B.; Southall, N.; Shinn, P.; Zheng, W.; Austin, C. P.; Hayes, C. J.; Brook, J. D. High-Content Screening Identifies Small Molecules That Remove Nuclear Foci, Affect MBNL Distribution and CELF1 Protein Levels via a PKC-Independent Pathway in Myotonic Dystrophy Cell Lines. *Hum Mol Genet* **2014**, *23* (6), 1551–1562. <https://doi.org/10.1093/hmg/ddt542>.

(55) Giagnacovo, M.; Malatesta, M.; Cardani, R.; Meola, G.; Pellicciari, C. Nuclear Ribonucleoprotein-Containing Foci Increase in Size in Non-Dividing Cells from Patients with Myotonic Dystrophy Type 2. *Histochem Cell Biol* **2012**, *138* (4), 699–707. <https://doi.org/10.1007/s00418-012-0984-6>.

CHAPTER 3

Alcian blue staining: a histochemical technique

**Alcian blue staining to track the intracellular fate of
hyaluronic-acid-based nanoparticles at transmission
electron microscopy**

F. Carton, M. Repellin, G. Lollo, M. Malatesta

European Journal of Histochemistry (2019)

Alcian blue staining to track the intracellular fate of hyaluronic-acid-based nanoparticles at transmission electron microscopy

Flavia Carton,¹ Mathieu Repellin,¹
Giovanna Lollo,² Manuela Malatesta¹

¹Department of Neurosciences,
Biomedicine and Movement Sciences,
Anatomy and Histology Section,
University of Verona, Italy

²Laboratory of Automatic Control,
Chemical and Pharmaceutical
Engineering (LAGEPP), French
National Centre for Scientific Research
(CNRS), UMR 5007, Claude Bernard
University Lyon 1, Villeurbanne, France

Abstract

The main step in the assessment of nanomaterial safety and suitability for biomedical use is the location and the dynamic tracking of nanoparticles (NPs) inside cells or tissues. To precisely investigate the uptake mechanisms and intracellular fate of NPs, transmission electron microscopy is the technique of choice; however, the detection of NPs may sometimes be problematic. In fact, while NPs containing strongly electron dense (*e.g.* metal) components do not require specific detection methods at the ultrastructural level, organic NPs are hardly detectable in the intracellular environment due to their intrinsic moderate electron density. In this study, the critical-electrolyte-concentration Alcian Blue method set up by Schofield *et al.* in 1975 was applied to track hyaluronic-acid-based NPs in muscle cells *in vitro*. This long-established histochemical method proved to be a powerful tool allowing to identify not only whole NPs while entering cells and moving into the cytoplasm, but also their remnants following lysosomal degradation and extrusion.

Introduction

During the last two decades, a massive number of nanoparticles (NPs) have been developed with an increasing interest towards biomedical applications. Innovative nanoparticulate systems have been investigated as *e.g.* drug carriers, hyperthermia-inducing tools, contrast agents, biosensors, sorting systems, scaffold components.¹⁻¹³ As an obvious conse-

quence, extensive *in vitro* and *in vivo* tests have been applied to assess the suitability of the nanosystems for their use in the biological media and their functional efficacy. To assess their toxicological profile, NPs are commonly visualised and tracked inside cells or tissues by conventional or confocal fluorescence microscopy using fluorescent markers.¹⁴ To precisely investigate the uptake mechanisms and intracellular fate of NPs, transmission electron microscopy (TEM) is the technique of choice, although the detection of NPs may sometimes be problematic. NPs containing strongly electron dense components (*e.g.*, iron, silver, gold, silica) do not require specific detection methods,¹⁵⁻¹⁸ while fluorescently-labelled nanoconstructs with intrinsic moderate electron density (*e.g.*, lipid- or polymer-based NPs) can be made easily recognizable by applying techniques of diaminobenzidine (DAB) photo-oxidation.¹⁹⁻²⁰ However, this latter technique is not applicable to all fluorophores since the success of the reaction depends on the capability of the fluorescent agent to generate reactive oxygen species in their excited state; moreover, its application is unfruitful in the presence of fluorescent background or autofluorescent sample components.

Thanks to its high water-binding capacity, biocompatibility and degradability, and non-immunogenicity, hyaluronic acid (HA) is of a great interest in the development of nanoconstructs for a wide variety of biomedical applications, from molecular imaging to targeted drug delivery.²¹⁻²³

In the frame of a study aimed at developing novel biocompatible HA-nanocarriers,¹¹ we observed that these HA-based NPs exhibit a homogeneous and weak electron-density that makes them hardly detectable in the intracellular milieu; unfortunately, the cell types used in our experiments (C2C12 immortalized murine muscle cells) showed a strong intrinsic autofluorescence that prevented to apply DAB photo-oxidation to locate fluorescently-labelled HA-NPs at TEM. We then decided to find an alternative detection method to track the internalization and intracellular traffic of these NPs at the ultrastructural level.

So far, the critical-electrolyte-concentration technique applied to the Alcian Blue (AB) staining is a long-established histochemical method to reveal glycosaminoglycans in tissue slices.²⁴ In 1975, Schofield and coll.²⁵ used this histochemically specific technique to localize and discriminate cartilage mucopolysaccharides at TEM; they also improved the Scott and Dorling's technique demonstrating that the use of low concentrations of AB after fixation resulted in a similar staining pattern as after the original tech-

Correspondence: Manuela Malatesta, Department of Neurosciences, Biomedicine and Movement Sciences, Anatomy and Histology Section, University of Verona, Strada Le Grazie 8, 37134 Verona, Italy. Tel. +30.045.8027569. E-mail: manuela.malatesta@univr.it

Acknowledgements: MR is a PhD student in receipt of a fellowship from the INVITE project of the University of Verona, (PhD Programme in Nanoscience and Advanced Technologies). This project has received funding from the European Union's Horizon 2020 Research and Innovation Programme under the Marie Skłodowska-Curie grant agreement No. 754345.

Contributions: FC and MR contributed equally to this work. All authors contributed to the study conception and design. FC and MR, performed experiments and analysed data; GL, supervised the project and analysed data; MM supervised the project, analysed data and wrote the first draft of the manuscript. All authors read and commented the manuscript, and approved its final version.

Key words: Nanocarriers; hyaluronate; histochemistry; ultrastructure.

Received for publication: 16 November 2019.
Accepted for publication: 11 December 2019.

This work is licensed under a Creative Commons Attribution-NonCommercial 4.0 International License (CC BY-NC 4.0).

©Copyright: the Author(s), 2019
Licensee PAGEPress, Italy
European Journal of Histochemistry 2019; 63:3086
doi:10.4081/ejh.2019.3086

nique (that required the sample fixation and staining be simultaneously performed). In addition, this post-fixation procedure enhanced dye staining by allowing its penetration in the whole sample thickness, whereas in the simultaneous fixation-staining method the reaction was confined to the sample periphery. The staining consisted in electron dense fine granules that did not mask the cellular structural components.

Based on the data present in the literature, we investigated an innovative application of the AB method staining: we originally applied the critical-electrolyte-concentration AB method set up by Schofield *et al.*²⁵ to unequivocally detect HA-based NPs administered to cultured cells which has been never tested before.

Materials and Methods

HA-NPs were prepared by polyelectrolyte complexation, mixing HA (Lifecore

Technical Note

Biomedical, Chaska, MN, USA) and poly-arginine (PArg) (Polypeptide therapeutic solutions, Valencia, Spain) with a molar ratio HA/PArg of 5.77.¹¹ To obtain fluorescent HA-NPs, 10% of the HA was conjugated with fluoresceinamine (Sigma-Aldrich, Saint Louis, MA, USA) as previously described.²⁶ Dynamic light scattering was used to characterize HA-NPs in terms of hydrodynamic diameter, polydispersity index (PDI) and Zeta potential (ζ), using Zetasizer Nano ZS (Malvern Instruments Limited, Malvern, UK).

C2C12 myoblasts (an immortalized murine cell line purchased from ATCC® CRL-1772) were cultured in 75 cm² plastic flasks using Dulbecco's modified Eagle medium, supplemented with 10% (v/v) FBS, 1% (w/v) Glutamine, 0.5% (v/v) Amphotericin B, 100 units/mL of Penicillin-Streptomycin (Gibco, Waltham, MA, USA) and incubated at 37°C with 5% CO₂. Cells were trypsinized in 0.05% EDTA in PBS and seeded onto glass coverslips (12 mm in diameter) in 24-multiwell (6x10³ cells per well). Twenty-four hours after seeding, the cells were treated with 107 µg/mL of either HA-NPs or fluorescent NPs for TEM and bright field/fluorescence microscopy, respectively. During the treatment the percentage of FBS was reduced to 5% (v/v) in order to avoid NPs aggregation. Briefly, cells were administered the HA-NPs for 2 h, then the medium was removed and some samples were immediately fixed (see below) while others were given fresh medium without NPs for further 22 h before being fixed. These experimental conditions were selected based on previous experiments on cultured muscle cells²⁷, since by this procedure the NPs that had not been uptaken by cells were removed from the medium, and it was possible to follow the intracellular fate of the HA-NPs internalised during the 2-h-incubation only. This avoids possible cell overloading for long post-incubation times, and limits the interference of a medium possibly modified by the presence of non-internalised NPs and/or the low FBS concentration (it is worth recalling that C2C12 myoblasts may differentiate into myotubes when FBS concentration is maintained low for long times²⁸). Untreated cell samples were used as control.

For bright field and fluorescence microscopy, control cells and cells treated with fluorescent HA-NPs were fixed with 4% (v/v) paraformaldehyde in PBS, pH 7.4 for 30 min at room temperature. Cells were stained with 1% (w/v) Alcian blue 8GX (Sigma, Saint Louis, MO, USA) in 3% (v/v) acetic acid for 2 h at room temperature, and differentiated in tap water;²⁵ the cells were counterstained with Nuclear fast red (Bio-Optica, Milan, Italy) for 5 min at

room temperature, dehydrated through an ascending series of ethanol, cleared in xylene and finally mounted in Entellan (Merck Millipore). The samples were observed with an Olympus BX51 (Olympus Italia Srl, Milan, Italy) microscope using a 60x objective either under bright field conditions or in fluorescence (100 W mercury lamp) using a 450–480 nm excitation filter, 500 nm dichroic mirror, and 515 nm barrier filter. Images were recorded with an QICAM Fast 1394 digital camera (QImaging, Surrey, BC, Canada) and pro-

cessed using Image-Pro Plus 7.0 software (Media Cybernetics Inc., Rockville, MD, USA).

Fluorescent HA-NPs were also stained in suspension: briefly, 100 µL of AB solution were mixed with an equal volume of NPs solution for 2 h at room temperature. A drop of suspension of these AB-stained HA-NPs was placed onto a glass slide under a coverslip, and observed at the microscope, under the same conditions as above.

For TEM, control cells and cells treated with HA-NPs were fixed with 3% (v/v) glu-

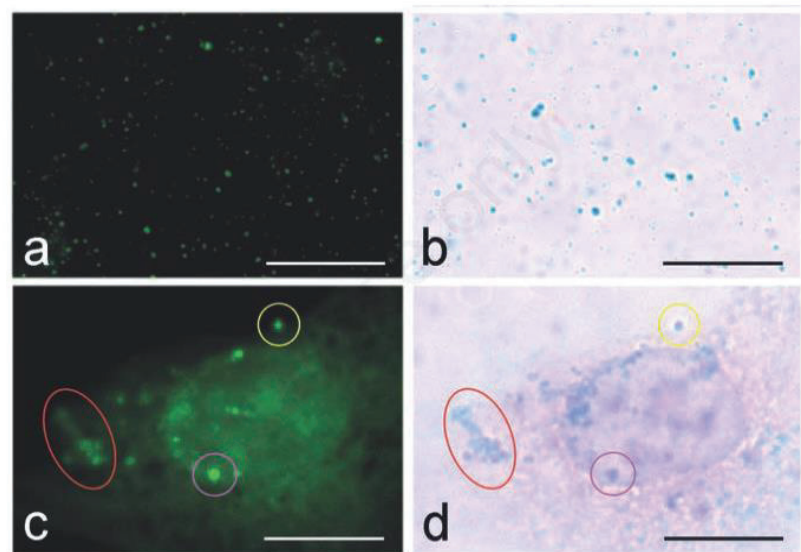


Figure 1. Fluoresceinamine-labelled HA-NPs in suspension as observed at conventional fluorescence microscopy (a) and bright field microscopy after staining with AB (b). c,d) A C2C12 myoblast after 24 h incubation with fluoresceinamine-labelled HA-NPs; the fluorescent signal of NPs (c) mostly overlaps AB staining (d) (encircled areas). Note the high intracellular fluorescence background in (c). Scale bars: 10 µm.

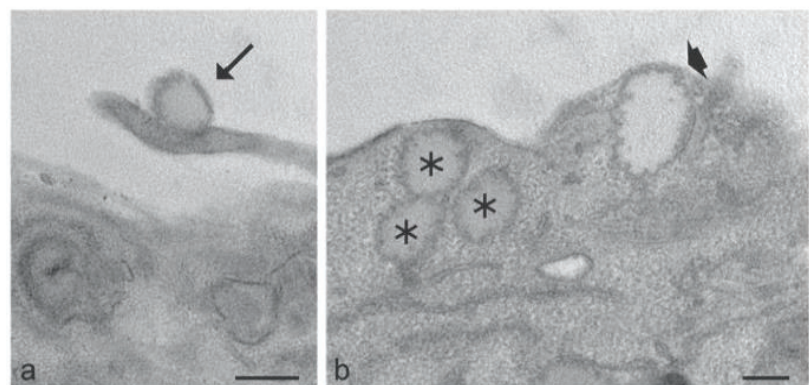


Figure 2. Transmission electron micrographs of C2C12 myoblasts, conventional ultrastructural morphology: a HA-NP (arrow) adheres to the cell surface (a) and residual bodies (asterisks) accumulate in the cytoplasm and sometimes bud from the cell surface (arrowhead) (b). Scale bars: 200 nm.

taraldehyde in PBS pH 7 for 30 min at room temperature, treated with AB as for light microscopy,²⁵ post-fixed with 1% OsO₄ for 1 h at room temperature, dehydrated with acetone and embedded in Epon resin as previously described.²⁹ As a control of staining specificity, some samples were processed as above described but, before AB treatment, the cells were incubated with 1 mg/ml of hyaluronidase (Sigma H3506) in normal saline for 1 h at room temperature. Ultrathin sections were observed without lead staining in a Philips Morgagni transmission electron microscope (FEI Company Italia Srl, Milan, Italy) operating at 80 kV and equipped with a Megaview II camera for digital image acquisition. The images were processed using Image-Pro Plus 7.0 software (Media Cybernetics Inc., Silver Spring, MD, USA).

Results and Discussion

HA-NPs showed a hydrodynamic size of 200 nm, a low PDI <0.1, and negative ζ potential ranging from -24 to -18 mV.

After AB staining in suspension, fluorescent HA-NPs (Figure 1a) appeared as blue dots at bright field microscopy (Figure 1b). Similarly, after NPs internalization in cultured cells, fluorescent HA-NPs appeared as bright green areas or spots (Figure 1c), while they appeared as blue clusters at bright field microscopy (Figure 1d). The overlapping of the blue staining with the green fluorescence signal demonstrated the specificity of the AB reaction for HA-NPs (Figure 1c,d). However, some AB-stained NPs did not match fluorescent NPs: this could be due to combined effect of the cell auto-fluorescence and the release of fluoresceinamine from NPs undergoing enzymatic degradation, which lowers NPs brightness, and the fluorescent signal occurring in the intracellular milieu, which masks NPs fluorescence. As for cell fluorescence, it should be underlined that C2C12 myoblasts show an intrinsic green auto-fluorescence that appeared to be increased after incubation with fluoresceinamine-labelled HA-NPs (*not shown*), thus supporting the hypothesis of the fluoresceinamine spreading following NPs degradation.

At TEM, the AB staining appeared as an irregular granular electron dense product, as Schofield *et al.* observed in cartilage samples.²⁵ In cells treated with HA-NPs, the AB staining was found on roundish structures with a moderate electron density corresponding to the NPs observed in unstained samples (Figure 2a) and to the size evaluated by dynamic light scattering. Stained NPs were observed adhering to the cell surface and inside invaginations of the plasma

membrane (Figure 3 a,b). This evidence of the very early events in the NP uptake process was obtained thanks to the procedure of embedding cells as monolayers²⁹, which allows an optimal preservation of the spatial relationships between NPs and the plasma membrane. The AB staining was observed on intracellular NPs occurring either inside endosomes (Figure 3c) or free in the cytosol (Figure 3d). The occurrence of NPs free in the cytosol likely facilitates the release of fluorescent molecules, thus increasing the intracellular background visible at fluorescence microscopy.

The high concentration of HA in our NPs certainly promoted their intense AB-

positivity at TEM. However, some AB staining was also clearly visible in large roundish structures (300 to 600 nm in diameter) occurring as clusters in the cytoplasm (Figure 3e), according to what observed in unstained samples (Figure 2b). We hypothesize that they represent NP residual bodies. In these residual bodies AB staining was preferentially located at the periphery, suggesting a compartmentalization of HA. To confirm the high sensitivity of AB staining at the ultrastructural level, the presence of HA was still recognizable as AB-positivity even when the residual bodies were found to be extruded from the cell (Figure 3f), probably due to NPs overloading.

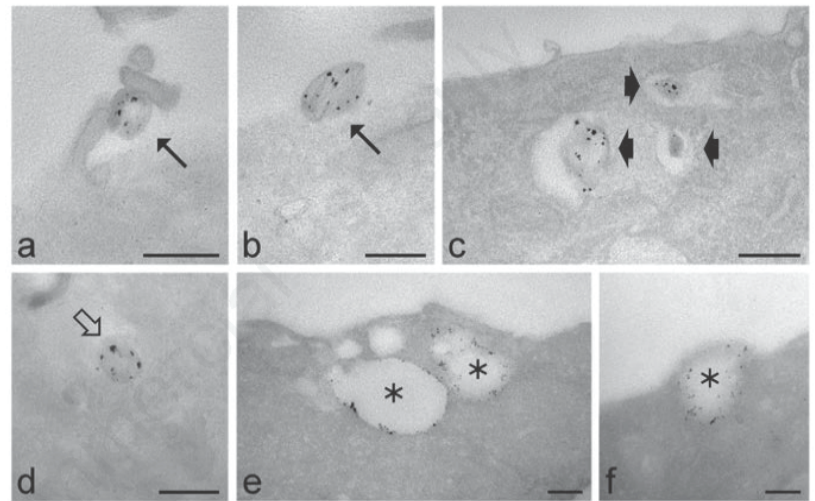


Figure 3. Transmission electron micrographs of C2C12 myoblasts after AB staining. a,b) The electron dense, granular reaction product occurs in HA-NPs (arrows) adhering to the cell surface. c) Three AB-stained HA-NPs are enclosed inside endosomes (arrowheads), just beneath the cell surface. d) A HA-NP free in the cytosol (open arrow) is clearly recognizable in the intracellular milieu. e) Residual bodies containing HA (asterisks) accumulate in the cytoplasm (e) and are extruded from the cell (f). Scale bars: 200 nm.

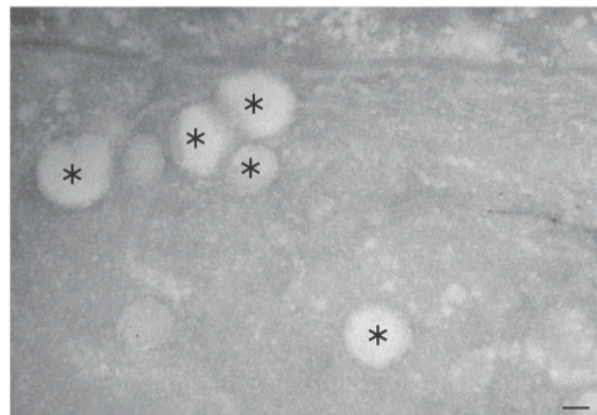


Figure 4. Sample treated with hyaluronidase as AB staining control: note the absence of any specific staining, especially in the residual bodies (asterisks). Scale bar: 200 nm.

No granular electron dense product was ever found in cells incubated with hyaluronidase before AB treatment, thus demonstrating the specificity of the staining procedure for HA at TEM (Figure 4). In addition, no granular reaction was observed in cell organelles of any cell samples or in control cells (not exposed to NPs), consistently with the evidence that intracellular HA is expressed only under particular condition such as inflammation.³⁰

The overall appearance of AB-stained cells was similar as in samples routinely-processed for conventional ultrastructural morphology (Figure 2), although the intrinsic contrast was lower likely due to protein extraction during the staining at acid pH. Nevertheless, it is preferable to avoid the contrast-enhancing staining with lead citrate or uranyl acetate in samples treated with AB because both reagents produce a noisy fine pepper-like precipitate.

In addition to AB staining, other techniques have been developed for HA detection at the ultrastructural level, among which the periodic acid-Schiff method,³¹⁻³³ ruthenium red staining,³⁴ cationized ferritin binding,^{35,36} high iron diamine method,³⁷ gold-conjugated hyaluronidase digestion,^{38,39} labelled HA-binding probes.^{40,41} These techniques often require special fixation procedures, whereas the AB staining is a simple and reliable method for the specific detection of HA in subcellular domains, which may be suitable for both light and electron microscopy under the usual fixation conditions for conventional ultrastructural morphology.

Our results demonstrated that the critical-electrolyte-concentration AB-staining is a powerful tool to thoroughly describe how HA-based NPs do interact with cells in culture, allowing to identify not only whole NPs while entering cells and moving into the cytoplasm, but also their remnants following lysosomal degradation and extrusion. This proves that this long-established staining method may successfully find application in a frontline research domain such as nanotechnology, namely for the ultrastructural study of scarcely electron-dense nanoconstructs that are especially promising drug carriers.

References

- Lim CT, Han J, Guck J, Espinosa H. Micro and nanotechnology for biological and biomedical applications. *Med Biol Eng Comput* 2010;48:941-3. doi: 10.1007/s11517-010-0677-z
- Lollo G, Rivera-Rodríguez GR, Bejaud J, Montier T, Passirani C, Benoit JP, et al. Polyglutamic acid-PEG nanocapsules as long circulating carriers for the delivery of docetaxel. *Eur J Pharm Biopharm* 2014;87:47-54. doi: 10.1016/j.ejpb.2014.02.004
- Bobo D, Robinson KJ, Islam J, Thurecht KJ, Corrie SR. Nanoparticle-based medicines: a review of FDA-approved materials and clinical trials to date. *Pharm Res* 2016;33:2373-87. doi: 10.1007/s11095-016-1958-5
- Fernandes RS, Dos Santos Ferreira D, de Aguiar Ferreira C, Giammarile F, Rubello D, de Barros AL. Development of imaging probes for bone cancer in animal models. A systematic review. *Biomed Pharmacother* 2016;83:1253-64. doi: 10.1016/j.biopha.2016.08.039
- Kaur P, Aliru ML, Chadha AS, Asea A, Krishnan S. Hyperthermia using nanoparticles—Promises and pitfalls. *Int J Hyperthermia* 2016;32:76-88. doi: 10.3109/02656736.2015.1120889
- Sasso MS, Lollo G, Pitorre M, Solito S, Pinton L, Valpione S, et al. Low dose gemcitabine-loaded lipid nanocapsules target monocytic myeloid-derived suppressor cells and potentiate cancer immunotherapy. *Biomaterials* 2016;96:47-62. doi: 10.1016/j.biomaterials.2016.04.010
- Asadi N, Alizadeh E, Salehi R, Khalandi B, Davaran S, Akbarzadeh A. Nanocomposite hydrogels for cartilage tissue engineering: a review. *Artif Cells Nanomed Biotechnol* 2018;46:465-71. doi: 10.1080/21691401.2017.1345924
- Kavoosi F, Modaresi F, Sanaei M, Rezaei Z. Medical and dental applications of nanomedicines. *APMIS* 2018;126:795-803. doi: 10.1111/apm.12890
- Jahangirian H, Lemraski EG, Rafiee-Moghaddam R, Webster TJ. A review of using green chemistry methods for biomaterials in tissue engineering. *Int J Nanomedicine* 2018;13:5953-69. doi: 10.2147/IJN.S163399
- Bamburowicz-Klimkowska M, Poplawska M, Grudzinski IP. Nanocomposites as biomolecules delivery agents in nanomedicine. *J Nanobiotechnology* 2019;17:48. doi: 10.1186/s12951-019-0479-x
- Carton F, Chevalier Y, Nicoletti L, Tarnowska M, Stella B, Arpicco S, et al. Rationally designed hyaluronic acid-based nano-complexes for pentamidine delivery. *Int J Pharm* 2019;568:118526. doi: 10.1016/j.ijpharm.2019.118526
- Suárez PL, García-Cortés M, Fernández-Argüelles MT, Encinar JR, Valledor M, Ferrero FJ, et al. Functionalized phosphorescent nanoparticles in (bio)chemical sensing and imaging - A review. *Anal Chim Acta* 2019;1046:16-31. doi: 10.1016/j.aca.2018.08.018
- Wallyn J, Anton N, Akram S, Vandamme TF. *Biomedical Imaging: Principles, Technologies, Clinical Aspects, Contrast Agents, Limitations and Future Trends in Nanomedicines*. *Pharm Res* 2019;36:78. doi: 10.1007/s11095-019-2608-5
- Boschi F, De Sanctis F. Overview of the optical properties of fluorescent nanoparticles for optical imaging. *Eur J Histochem* 2017;61:2830. doi: 10.4081/ejh.2017.2830
- Poussard S, Decossas M, Le Bihan O, Mornet S, Naudin G, Lambert O. Internalization and fate of silica nanoparticles in C2C12 skeletal muscle cells: evidence of a beneficial effect on myoblast fusion. *Int J Nanomedicine* 2015;10:1479-92. doi: 10.2147/IJN.S74158
- Marinozzi MR, Pandolfi L, Malatesta M, Colombo M, Collico V, Lievens PM, et al. Innovative approach to safely induce controlled lipolysis by superparamagnetic iron oxide nanoparticles-mediated hyperthermic treatment. *Int J Biochem Cell Biol* 2017;93:62-73. doi: 10.1016/j.biocel.2017.10.013
- Pongrac IM, Ahmed LB, Mlinarić H, Jurašin DD, Pavičić I, Marjanović Čermak AM, et al. Surface coating affects uptake of silver nanoparticles in neural stem cells. *J Trace Elem Med Biol* 2018;50:684-92. doi: 10.1016/j.jtemb.2017.12.003
- Steckiewicz KP, Barcinska E, Malankowska A, Zauszkiewicz-Pawlak A, Nowaczyk G, Zaleska-Medynska A, et al. Impact of gold nanoparticles shape on their cytotoxicity against human osteoblast and osteosarcoma in vitro model. Evaluation of the safety of use and anti-cancer potential. *J Mater Sci Mater Med* 2019;30:22. doi: 10.1007/s10856-019-6221-2
- Malatesta M, Giagnacovo M, Costanzo M, Conti B, Genta I, Dorati R, et al. Diaminobenzidine photoconversion is a suitable tool for tracking the intracellular location of fluorescently labelled nanoparticles at transmission electron microscopy. *Eur J Histochem* 2012;56:e20. doi: 10.4081/ejh.2012.20
- Malatesta M, Pellicciari C, Cisterna B, Costanzo M, Galimberti V, Biggiogera M, et al. Tracing nanoparticles and photosensitizing molecules at transmission electron microscopy by diaminobenzidine photo-oxidation. *Micron* 2014;59:44-51. doi: 10.1016/j.micron.2013.12.007
- Morra M. Engineering of biomaterials surfaces by hyaluronan. *Biomacromol*

- lecules 2005;6:1205-23. doi: 10.1021/bm049346i
22. Micale N, Piperno A, Mahfoudh N, Schurigt U, Schultheis M, Mineo PG, et al. A hyaluronic acid–pentamidine bioconjugate as a macrophage mediated drug targeting delivery system for the treatment of leishmaniasis. *RSC Adv* 2015;5:95545-50. doi: 10.1039/C5RA18019H
 23. Dosio F, Arpicco S, Stella B, Fattal E. Hyaluronic acid for anticancer drug and nucleic acid delivery. *Adv Drug Deliv Rev* 2016;97:204-36. doi: 10.1016/j.addr.2015.11.011
 24. Scott JE, Dorling J. Differential staining of acid glycosaminoglycans (mucopolysaccharides) by alcian blue in salt solutions. *Histochemie* 1965;5:221-33. doi: 10.1007/bf00306130
 25. Schofield BH, Williams BR, Doty SB. Alcian Blue staining of cartilage for electron microscopy. Application of the critical electrolyte concentration principle. *Histochem J* 1975;7:139-49. doi: 10.1007/bf01004558
 26. Fudala R, Mummert ME, Gryczynski Z, Rich R, Borejdo J, Gryczynski I. Lifetime-based sensing of the hyaluronidase using fluorescein labeled hyaluronic acid. *J Photochem Photobiol B* 2012;106:69-73. doi: 10.1016/j.jphotobiol.2011.10.005
 27. Guglielmi V, Carton F, Vattemi G, Arpicco S, Stella B, Berlier G, et al. Uptake and intracellular distribution of different types of nanoparticles in primary human myoblasts and myotubes. *Int J Pharm* 2019;560:347-56. doi: 10.1016/j.ijpharm.2019.02.017
 28. Costanzo M, Vurro F, Cisterna B, Boschi F, Marengo A, Montanari E, et al. Uptake and intracellular fate of biocompatible nanocarriers in cycling and noncycling cells. *Nanomedicine (Lond)* 2019;14:301-16. doi: 10.2217/nmm-2018-0148
 29. Costanzo M, Malatesta M. Embedding cell monolayers to investigate nanoparticle-plasmalemma interactions at transmission electron microscopy. *Eur J Histochem* 2019;63:3026. doi: 10.4081/ejh.2019.3026
 30. Hascall VC, Majors AK, De La Motte CA, Evanko SP, Wang A, Drazba JA, et al. Intracellular hyaluronan: a new frontier for inflammation? *Biochim Biophys Acta* 2004;1673:3-12. doi: 10.1016/j.bbagen.2004.02.013
 31. Scott JE, Harbinson RJ. Periodate oxidation of acid polysaccharides inhibition by the electrostatic field of the substrate. *Histochemie* 1968;14:215-20. doi: 10.1007/bf00306317
 32. Scott JE, Harbinson RJ. Periodate oxidation of acid polysaccharides. II. Rates of oxidation of uronic acids in polyuronides and acid mucopolysaccharides. *Histochemie* 1969;19:155-61. doi: 10.1007/bf00281095
 33. Scott JE, Dorling J. Periodate oxidation of acid polysaccharides. 3. A PAS method for chondroitin sulphates and other glycosamino-glycuronans. *Histochemie* 1969;19:295-301. doi: 10.1007/bf00279680
 34. Luft JH. Ruthenium red and violet. I. Chemistry, purification, methods of use for electron microscopy and mechanism of action. *Anat Rec* 1971;171:347-68. doi: 10.1002/ar.1091710302
 35. Eagles PA, Johnson LN, Van Horn C. The distribution of anionic sites on the surface of the chromaffin granule membrane. *J Ultrastruct Res* 1976;55:87-95. doi: 10.1016/s0022-5320(76)80084-6
 36. Wessells NK, Nuttall RP, Wrenn JT, Johnson S. Differential labeling of the cell surface of single ciliary ganglion neurons in vitro. *Proc Natl Acad Sci USA* 1976;73:4100-4. doi: 10.1073/pnas.73.11.4100
 37. Spicer SS, Hardin JH, Setser ME. Ultrastructural visualization of sulphated complex carbohydrates in blood and epithelial cells with the high iron diamine procedure. *Histochem J* 1978;10:435-52. doi: 10.1007/bf01003007
 38. Londoño I, Bendayan M. High-resolution cytochemistry of neuraminic and hexuronic acid-containing macromolecules applying the enzyme-gold approach. *J Histochem Cytochem* 1988;36:1005-14. doi: 10.1177/36.8.3392391
 39. Kan FW. High-resolution localization of hyaluronic acid in the golden hamster oocyte-cumulus complex by use of a hyaluronidase-gold complex. *Anat Rec* 1990;228:370-82. doi: 10.1002/ar.1092280403
 40. Ripellino JA, Bailo M, Margolis RU, Margolis RK. Light and electron microscopic studies on the localization of hyaluronic acid in developing rat cerebellum. *J Cell Biol* 1988;106:845-55. doi: 10.1083/jcb.106.3.845
 41. Egli PS, Graber W. Association of hyaluronan with rat vascular endothelial and smooth muscle cells. *J Histochem Cytochem* 1995;43:689-97. doi: 10.1177/43.7.7608523

**Alcian blue staining to visualize intracellular hyaluronic-
acid-based nanoparticles**

M. Repellin, F. Carton, G. Lollo, M. Malatesta

Histochemistry of Single Molecules: Methods and Protocols, Second Edition

In press (2022)

Because of the copyright rules, only the summary of the manuscript can be reported in this thesis.

Summary

Investigating at transmission electron microscopy the intracellular trafficking of hyaluronic acid-based nanoparticles remains a challenge due to their intrinsic weak electron density. Here we describe a simple protocol to stain hyaluronic acid that allows visualization of hyaluronic acid-based nanoparticles inside cells at both light and electron microscopy. By applying the critical-electrolyte-concentration Alcian blue method, these nanoparticles were observed as blue dots at bright field microscopy or filled with fine electron dense precipitates at transmission electron microscopy.

CHAPTER 4

Lipid-based nanoparticles to modulate protein expression through DNA/RNA tools: a proof-of-concept for treating muscular dystrophies

*M. Repellin, A. Jacquier, C. Martinat, J. Carras, P.Y. Dugas, F. Roussange, S.
Briançon, L. Schaeffer, M. Malatesta, G. Lollo*

In preparation

Lipid-based nanoparticles to modulate protein expression through DNA/RNA tools: a proof-of-concept for treating muscular dystrophies

Authors

Mathieu Repellin^{1,2}, Arnaud Jacquier^{3,4}, Cécile Martinat⁵, Julien Carras^{3,4}, Pierre-Yves Dugas⁶, Florine Roussange⁵, Stéphanie Briançon¹, Laurent Schaeffer^{3,4}, Manuela Malatesta², Giovanna Lollo¹

Affiliations

¹University of Lyon, Université Claude Bernard Lyon 1, CNRS, LAGEPP UMR 5007, 43 bd 11 Novembre 1918, 69622 Villeurbanne, France

²Department of Neurosciences, Biomedicine and Movement Sciences, Anatomy and Histology Section, University of Verona, Strada Le Grazie 8, 37134 Verona, Italy

³Institut NeuroMyogène, University of Lyon 1, CNRS UMR 5310, INSERM U1217, 8 avenue Rockefeller, 69008 Lyon, France

⁴Centre de Biotechnologie Cellulaire, CBC Biotec, CHU de Lyon – Hospices civils de Lyon groupement Est, Bron, France

⁵Université Evry-Paris Saclay, INSERM UMR861, Institut Des Cellules Souches Pour Le Traitement Et L'étude Des Maladies Monogéniques (I-Stem), 2 rue Henri Auguste Desbruères, 91100 Corbeil-Essonnes, France

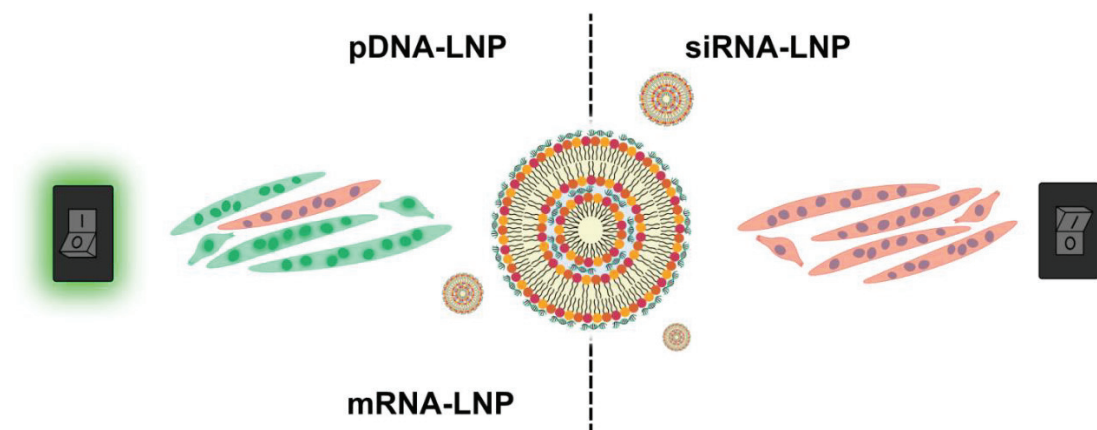
⁶University of Lyon, Université Claude Bernard Lyon 1, CNRS, C2P2 UMR 5265, Villeurbanne, France.

Abstract

Muscular dystrophies (MDs) are genetically inherited degenerative disorders with unmet clinical needs. Despite gene and oligonucleotides-based therapies are providing important technological promises in treating the underlying aetiology of genetic diseases, the requirement of sophisticated delivery carriers is from crucial priority to clinically implement these approaches. Recent achievements carried out

using lipid-based nanoparticles (LNP) for enabling nucleic acids delivery highlighted the suitability and effectiveness of this groundbreaking approach for cancer and vaccines applications. Synthetic systems based on non-viral carriers offers several advantages compared to the current viral vector strategies, overcoming the restricted efficiency associated to viral vectors while avoiding any immunotoxicity. Although the widespread effectiveness of LNP to deliver different DNA or RNA species have been already demonstrated, LNP composition is often modified according to the nucleic acid. In the present investigations, we provided a unique LNP composition to deliver a broad spectrum of nucleic acid as pDNA, mRNA and siRNA for modulating protein expression in muscle cells. Based on our recent patent, nanosystems were optimized to provide the most appropriate complexation of the diverse nucleic acids. *In vitro* studies demonstrated that our LNP efficiently deliver nucleic acids inducing or interfering with eGFP expression, in both C2C12 murine proliferative myoblasts and differentiated myotubes. Interesting transfection efficiency was also demonstrated in a human immortalized muscle cell line. So far, our investigations provide a rational design of LNP platform for delivering small and large nucleic acids payloads that open the range of possibilities to gene therapy strategies for the treatment of MDs.

Keywords: gene therapy, non-viral vectors, nucleic acids, GFP



1. Introduction

Muscular dystrophies (MDs), as the most common Duchenne Muscular Dystrophy (DMD) or Myotonic Dystrophy (DM), are genetically inherited degenerative disorders sharing clinical features of progressive muscle wasting and weakness¹. There are many types of MDs characterized with variable phenotypes and onset ages, correlated to different specific pathophysiology and causing from disability to shortened span life in the most acute forms. The overall combined pooled prevalence of MDs was recently estimated to 16 per 100,000, thus demonstrating the extent of MDs in the current human pathologies². As for most of the genetic diseases, actual conventional treatment approaches are enough to alleviate some symptoms but do not alter genetic mutations at the root cause of the MDs.

Over the last years, the improved understanding of the pathogenesis of MDs allowed the development of innovative nucleic acids-based therapeutic strategies^{3,4}. Success story of such therapeutic strategies for treating neuromuscular disease is substantiated with the recent FDA and commercially approved Zolgensma® for SMA treatment, that proved to deliver a new working gene using AAV-vectors to restore SMN protein levels in motoneurons⁵. Another suitable example is the antisense oligonucleotide splicing modulator Spinraza® to restore protein reading frame of SMN in motoneurons. Thereby, delivery of DNA and RNA species is a promising strategy to modulate protein expression in affected skeletal muscle cells in MDs pathologies.

Although several DNA and RNA strategies open the possibilities to many potential therapeutic approaches, important drawbacks rely on their effective delivery^{6,7}. Because of their natural occurring negative charge and hydrophilic properties, naked oligonucleotides fail to diffuse across cell membranes and are easily and quickly degraded in serum by nucleases, limiting drastically their pharmacokinetic profiles. To overcome these limitations, delivery vectors are crucial to provide long-term effects with a safe and efficient biodistribution profile.

In this context, lipid-based nanoparticles (LNP) have demonstrated their efficiency in nucleic acid delivery, notably with the recent booming success in development of mRNA-vaccines⁸⁻¹⁰. This non-viral delivery approach provides an ideal

alternative to the most commonly used adenovirus or AAV viral vectors associated to limited packaging capacity, unwanted immune system response and potential failure in patients harboring pre-existing antibodies¹¹⁻¹³. Overall, many experimental studies have demonstrated the effective delivery of pDNA, mRNA or siRNA through distinct LNP composition, specially correlated to the cationic or ionizable lipid incorporated into the formulation. Although LNP enabling gene therapy has been widely explored for cancer and more recently for vaccines applications, this field remains poorly investigated for MDs.

The successful treatment of complex MDs will likely require the efficient delivery of different nucleic acid strategies to treat the different affected cells involved. Although many organs or functions as the central nervous system, cardiac or respiratory systems may be involved according to the type of MD and the stage of the disease, skeletal muscle damages represent the main common characteristic clinical features to MDs. To this end, it is essential to treat proliferative myoblasts involved in muscle regeneration but also non-renewing differentiated myotubes forming the basic unit of skeletal muscle. In the present investigation, a unique LNP composition made of lipidic-polymeric hybrid LNP was studied for efficient delivery of different nucleic acids in muscle cells, focusing on pDNA, mRNA and siRNA. The aim was to open perspectives for a broad range of nucleic acid therapeutic strategies for treating MDs. As proof-of-concept to modulate protein expression in muscle cells, nucleic acids were selected to induce or interfere with eGFP expression. To this end, nanosystems were characterized and optimized to obtain appropriate physico-chemical properties while providing the highest nucleic acid complexation efficiency. The most suitable nanosystems were then tested on C2C12 murine skeletal muscle myoblasts and myotubes. Finally, as more representative cell model in the purpose of treating MDs, the efficiency of mRNA-LNP was also demonstrated in human immortalized cell line.

2. Materials and methods

2.1. Materials

pCAGIG was purchased from Addgene (Massachusetts, USA, plasmid #11159). EZ CapTM Cy5 eGFP mRNA was provided by Trilink Biotechnologies (Texas, USA). siRNA interfering with eGFP expression was provided from Eurogentec (Seraing, France). Sodium hyaluronate (HA, weight-average molar mass, $M_w=3.9\times 10^4$ g·mol⁻¹) was obtained from Lifecore Biomedical (Minnesota, USA). HEPES buffer pH 5.5 and Live/dead was purchased from Sigma-Aldrich (Saint-Quentin-Fallavier, France).

2.2. Nanoparticles formulation and characterization

2.2.1. Lipid nanoparticle preparation and complexation with nucleic acids

Lipid-nanoparticles (LNP) were prepared as described in the patent FR2112931. Fluorescent LNP were obtained by adding a Rhodamine-fluorescently labelled lipid to the lipid mixture (2% of the total lipids amount). Different oligonucleotides were complexed LNP: pCAGIG (pDNA) coding for the enhanced green fluorescent protein (eGFP), EZ CapTM Cy5 eGFP mRNA (mRNA-eGFP-cy5) coding for eGFP expression and labelled with cyanine5 and a siRNA interfering with eGFP expression. Complexation was performed by mixing an equal volume of LNP with an adequate quantity of DNA or RNA, to obtain lipoplexes at different nitrogen/phosphate ratio defined as N/P ratio. Lipoplexes were finally coated with HA.

2.2.2. Physico-chemical characterization of complexes

Particle size distribution and surface electrical charge were measured using Malvern Zetasizer[®] Nano ZS (Malvern Instruments S.A, Worcestershire, UK). Hydrodynamic diameter and polydispersity index (PdI) were measured by Dynamic Light Scattering (DLS) using the cumulants method and carried out at 25 °C with an angle of detection of 173°. Zeta potential (ζ) was determined by electrophoresis technique. All samples were diluted in NaCl 1 mM and analyses were performed in triplicate.

LNP morphology was assessed by cryogenic transmission electron microscopy (cryo-TEM). Briefly, 3.5 μL of formulation was added on a LC300-CU LACET grid and plunge-frozen using a Vitrobot (Thermoscientific) to generate vitreous ice. Samples were stored in liquid nitrogen and imaged with a JEM-1400Flash electron microscope operating at 120 kV.

Association efficiency of DNA and RNA was determined using Sybr Green® gel agarose electrophoresis. Samples were diluted in HEPES buffer to a final DNA and RNA amount of 0.2 μg . After addition of RNA gel loading dye, samples were then run on 1 % (w/v) agarose gel for 30 min at 80 V. The DNA and RNA bands were visualized and imaged using the Gel Doc™ EZ imager (Bio-Rad).

2.3. Nanoparticles administration to healthy murine myoblasts and myotubes

2.3.1. Cell culture

C2C12 myoblasts (ATCC® CRL-1772) were cultured under humidified atmosphere with 5 % CO_2 at 37 °C, in 75 cm^2 plastic flasks using Dulbecco's modified Eagle medium (DMEM) GlutaMax (Gibco), supplemented with 10 % (v/v) fetal bovine serum (FBS), 100 units/mL of Penicillin-Streptomycin. To induce differentiation into myotubes, the myogenic induction medium was replaced with myogenic differentiation medium composed of DMEM GlutaMax, supplemented with 1 % (v/v) fetal horse serum (FHS) and 100 units/mL of Penicillin-Streptomycin (Gibco) for 6 days.

For myoblasts and myotubes plating, cells were trypsinized (0.5% trypsin with 0.05 % EDTA in PBS) when sub-confluent, and seeded at 10.000 and 30.000 cells/ cm^2 respectively.

2.3.2. pDNA-, mRNA- and siRNA-nanoparticles transfection efficiency and viability assays

Specific protocols have been set up to optimize in vitro transfection efficiency in myoblasts and myotubes using pDNA, mRNA and siRNA-LNP.

For transfection efficiency study in myoblasts, cells were seeded in flat-bottom 12-well plates. The induction of eGFP was carried out using pDNA and mRNA. For

pDNA treatments, cells were incubated with 5, 7.5 and 10 µg of pDNA associated to LNP at a N/P ratio of 1.5 and 2 during 24 h. Then the medium was removed and replaced with fresh one, while the transfection efficiency was measured after 48 h. For mRNA treatments, myoblasts were treated with 1 and 3 µg of mRNA associated to LNP at a N/P ratio of 1.5 and 2 for 2 h. Then, the medium was removed and replaced with fresh one, while transfection efficiency was assessed after 24 h. To inhibit eGFP expression, cells were treated with 0.5, 1 and 2 µg of siRNA associated to LNP at a N/P ratio of 10 for 2 h. Then, medium was replaced and cells were incubated with 1 µg of mRNA associated to LNP at a N/P ratio of 1.5 for 2 h. The medium was finally replaced with fresh one, while the transfection efficiency was measured after 24 h. Viromer mRNA (Lipocalyx®) and Jet-Prime was used as mRNA and siRNA/pDNA transfection control respectively, according to the manufacturer's instructions. After end-incubation time, cell media were collected and cells were trypsinized with Trypsin-EDTA (0.5 %, Gibco). Cell supernatant media and corresponding detached cells were mixed and stained with a Fixable Live/Dead Violet solution for cell viability assessment. Data were acquired with a BD LSR 2 flow cytometer and eGFP expression and cell viability were analyzed using FlowJo software. Statistical analyses were determined with GraphPad Prism v8.1 software.

For transfection efficiency study in myotubes, cells were cultured onto 4-compartment Labtek culture chamber. For mRNA treatments, myotubes were treated with 0.5 µg of mRNA associated to LNP at a N/P ratio of 1.5. While, in the case of siRNA treatments, cells were treated firstly with 0.25, 0.5 and 1 µg of siRNA associated to LNP at a N/P ratio of 10, followed by 0.5 µg of mRNA associated to LNP at a N/P ratio of 1.5. All treatments were incubated during 2 h, then the medium was removed and replaced with fresh one, while transfection efficiency was assessed after 24 h incubation. Samples were mounted in Fluoromount mounting medium (Invitrogen) and imaged with a Leica DM400 B using a 40X objective. For each sample, the number of eGFP⁺ myotubes were manually counted for 100 fibers.

2.3.3. pDNA-, mRNA- and siRNA-nanoparticles internalization efficiency in myoblasts

For internalization efficiency study, myoblasts were seeded in flat-bottom 12-well plates. The internalization of the nanocarriers was assessed using fluorescent LNP. Myoblasts were then treated with 5 µg of pDNA associated to LNP at a N/P ratio of 1.5, 1 µg of mRNA associated to LNP at a N/P ratio of 1.5 or 1 µg of siRNA associated to LNP at a N/P ratio of 10. Internalization efficiency was assessed after 2, 4, 24 and 48 h of incubation. Samples were incubated with treatments for 2 h, then medium was removed and replaced with fresh one. After each time point, cells were washed, trypsinized with Trypsin-EDTA (0.5 %, Gibco) and stained with a Fixable Live/Dead Violet solution for cell viability assessment. Data were acquired with a BD LSR 2 flow cytometer and data were analyzed using FlowJo software. Statistical analyses were determined with GraphPad Prism v8.1 software.

2.3.4. Uptake and intracellular distribution of LNP in myoblasts and myotubes

For microscopy confocal analysis, myoblasts were seeded onto glass coverslips (12 mm in diameter) in 24-multiwell plate and myotubes were cultured onto 4-compartment Labtek culture chamber. Myoblasts were treated with 1 µg mRNA associated to LNP at a N/P ratio of 1.5 and myotubes were treated with 0.5 µg of mRNA associated to LNP at a N/P ratio of 1.5. Cells were treated for 30 min, 2 and 24 h and then samples were fixed with 4 % (v/v) paraformaldehyde in PBS, for 15 min at room temperature. Cell cytoplasm was stained with Phalloidin-Atto 488 (Sigma) diluted 1:20 in PBS for 1 h at room temperature, while cell nuclei were counterstained with DAPI (stock at 20 mM diluted 1:2000) for 1 h at room temperature. Samples were finally mounted in Fluoromount mounting medium (Invitrogen) and imaging was performed by a Zeiss LSM800 confocal laser scanning microscope (Carl Zeiss AG, Oberkochen, Germany) using a 63X objective.

2.4. Nanoparticles administration to immortalized human skeletal muscle cells

2.4.1. Cell culture

Human immortalized myoblasts cell line (AB1167c4) was obtained from the MyoBank (Insitute of Myology, Paris, France). Myoblasts were cultured under humidified atmosphere with 5 % CO₂ at 37 °C in DMEM GlutaMax (Gibco), supplemented with 20 % (v/v) FBS, 25 µg/mL of fetuin (Sigma-Aldrich), 5 µg/mL of insulin (Gibco), 0.2 µg/mL of dexamethasone (Sigma-Aldrich), 0.5 ng/mL of Fibroblast Growth Factor, 5 ng/mL of Epidermal Growth Factor and 0.1 % (v/v) of gentamicin (Gibco). To induce differentiation into myotubes, the myogenic induction medium was replaced with myogenic differentiation medium composed of DMEM GlutaMax, 1 % of gentamicin and 10 µg/mL of insulin.

For myoblasts and myotubes plating, cells were seeded in 96-well plate precoated with Collagen I (Thermo Fischer Scientific) at a concentration of 30,000 and 100,000 cells/cm² respectively.

2.4.2. mRNA-transfection efficiency and cell confluence

Transfection efficiency study in myoblasts and myotubes was evaluated after treatment with 0.1, 0.25 and 0.5 µg of mRNA associated to LNP at a N/P ratio of 1.5 and 2. Plates were incubated and imaged for 48 h at 37 °C in an Incucyte Zoom time lapse microscopy system (Sartorius). Phase images and green fluorescence images were obtained each 6 hours. Image processing algorithms were applied using Incucyte software to assess the percentage of cells expressing eGFP and the percentage of cell confluence.

3. Results

3.1. Characterization of pDNA, mRNA and siRNA-LNP

3.1.1. LNP preparation and physico-chemical properties

LNP were prepared according to the patent FR2112931. The hydrodynamic diameter was around 30 nm, with a PDI lower than 0.3 (data not shown). The surface

potential of the LNP was positive, with a value of zeta potential (ζ potential) of around +30 mV. Similar results were obtained for fluorescent LNP, demonstrating that the incorporation of PE-Rhodamine into LNP does not affect the physico-chemical properties of LNP.

3.1.2. Nucleic acid complexation to LNP and physico-chemical characterization

Complexation of LNP with nucleic acids were performed varying lipids:nucleic acids ratio, defined as N/P ratio and corresponding to the positive to negative charge ratio. This parameter is one of the most important for the development of carriers for nucleic acids delivery as it influence the charge of complexes, the association efficiency and more importantly the transfection efficiency¹⁴⁻¹⁶. As shown in figure 1, N/P ratio was varied from 1.5 to 4 for higher molecular weight nucleic acids as pDNA and mRNA, and from 2 to 10 for smaller nucleic acids as siRNA. The hydrodynamic diameter of pDNA-LNP, mRNA-LNP and siRNA-LNP at different N/P ratios were relatively similar with a size around 200 nm and a low polydispersity index lower than 0.2. Furthermore, ζ potential of these different complexes were comparable, with a negative value around -20 mV. This negative surface potential of LNP is related to the surface coating of HA acting as a stealth shield covering the cationic charge of uncoated LNP. HA has been proposed as alternative to PEGylation to provide enhanced stability and avoid rapid clearance through the reticulo-endothelial system after administration, while overcoming any potential immune responses triggered from PEG molecules^{17,18}. The physico-chemical characterization of the different complexes obtained with pDNA, mRNA or siRNA demonstrate that the type of nucleic acid and the different N/P ratios tested did not have impact on the size, PdI and ζ potential of the nanosystems.

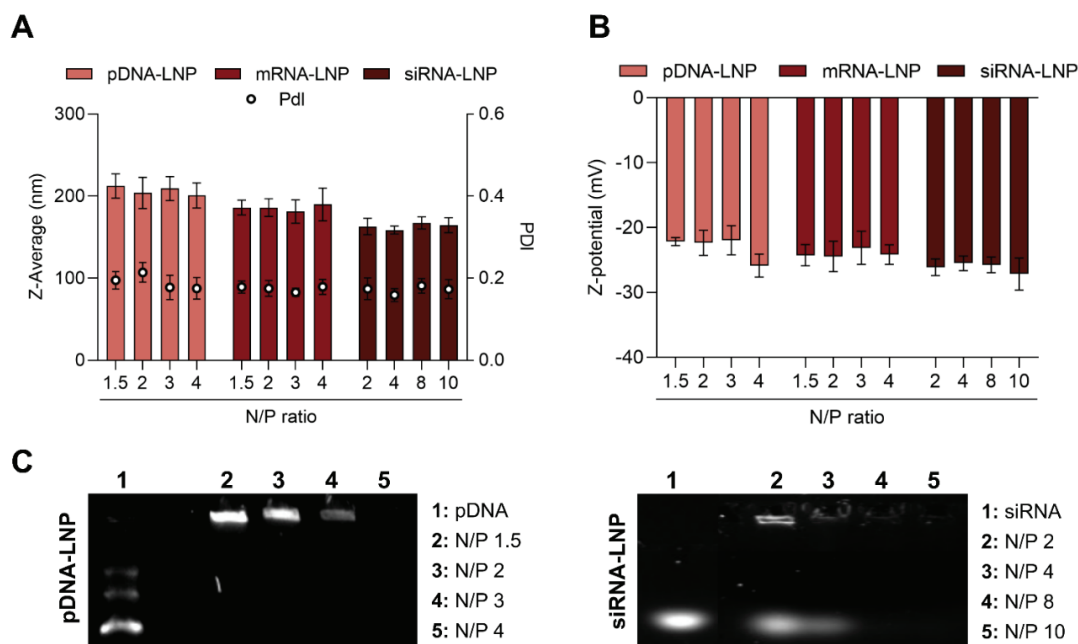


Figure 1: Physico-chemical properties and association efficiency of LNP complexed with pDNA, mRNA or siRNA at different N/P ratio. Physico-chemical characterization of complexes was investigated by DLS to assess the hydrodynamic diameter (A) and ζ potential (B) of each complex. DNA and RNA retardation assays of the different complexes was used to assess the association efficiency of LNP with pDNA and siRNA (C).

3.1.3. Association efficiency of nucleic acid for the different LNP-nucleic acid complexes

Electrophoretic assay was performed to assess the complexation of the nucleic acids with LNP at the different N/P ratios. Figure 1C showed that for pDNA-LNP, pDNA from pDNA-LNP samples was retained compared to pDNA free in solution, demonstrating that pDNA was efficiently complexed with LNP for N/P ratios of 1.5, 2, 3 and 4. This complexation was stronger at higher N/P ratios as demonstrated by the decrease in the band intensities. Similar results were obtained for mRNA-LNP that demonstrated an efficient complexation for N/P ratios of 1.5 to 4 (data not shown). For siRNA-LNP, siRNA was not efficiently complexed with LNP at N/P ratios from 2 to 8 as showed by the presence of RNA bands similar to the one of siRNA free in solution. However, at a N/P ratio of 10, electrophoretic assay show that siRNA was retained, demonstrating the efficient complexation of siRNA to LNP. Heparin displacement assay was conduct on siRNA-LNP at a N/P ratio of 10 (heparin/siRNA (w/w) ratio of 25) in order to release RNA from LNP and confirm that the absence of siRNA band is due to its complexation and not its degradation

(data not shown). Results obtained demonstrated the presence of a siRNA band similar to siRNA free in solution after heparin displacement assay, proving that at a N/P ratio of 10, siRNA is efficiently complexed with LNP and not degraded.

Based on these results regarding the efficiency of the LNP to complex different nucleic acids, we selected for further investigations the N/P ratios 1.5 and 2 for pDNA-LNP and mRNA-LNP and the N/P ratio of 10 for siRNA-LNP.

3.1.4. Morphology of the different LNP-nucleic acid complexes

Morphological study was investigated at Cryo-TEM as it is the most powerful way to observe nanostructures in a frozen-hydrated state representative of their natural state in solution²⁰.

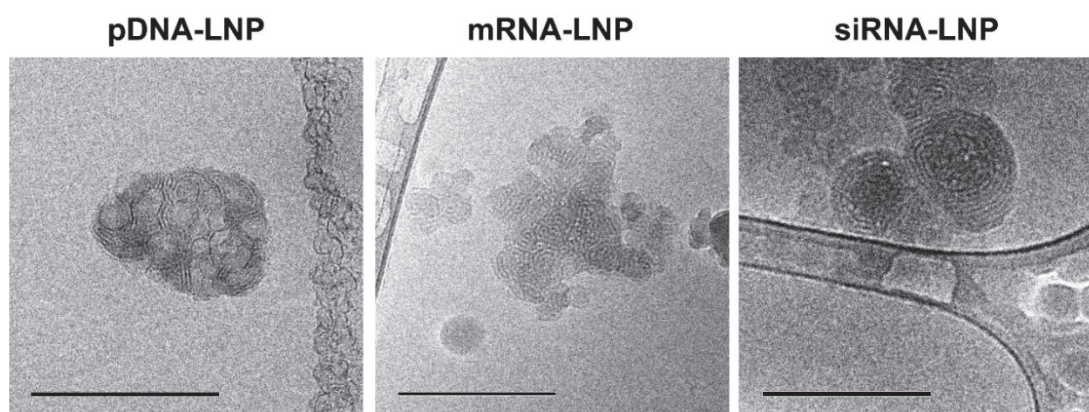


Figure 2: Cryo-TEM images of pDNA-LNP and mRNA-LNP at a N/P ratio of 1.5 and siRNA-LNP at a N/P ratio of 10. Bars: 200 μ m.

As showed by Cryo-TEM images (figure 2), the formation of typical multilamellar particle structures have been obtained for pDNA-LNP, mRNA-LNP and siRNA-LNP. These structures are formed from the rearrangement of the LNP due to the strong electrostatic interactions between cationic lipids and negatively charged nucleic acids. Regarding pDNA-LNP and mRNA-LNP, it seems that complexes are made of several small multilamellar vesicles whereas siRNA-LNP appears as the resultant of isolated larger multilamellar vesicles. This slight difference may be explained by the lower size of siRNA compared to pDNA and mRNA, helping for better reorganization during complexation.

3.2. *In vitro* assays on C2C12 murine muscle myoblasts and myotubes

3.2.1. Internalization efficiency of pDNA-LNP, mRNA-LNP and siRNA-LNP

Investigating the internalization rate and kinetics of LNP is primordial to assess the percentage of cells that internalized LNP over time and to approximatively estimate the delay in DNA incorporation and RNA translation or inhibition. To this end, PE-Rhodamine lipid was incorporated into the composition of the LNP to fluorescently label the particles and the percentage of C2C12 myoblasts with fluorescent LNP was investigated at flow cytometry analyses (figure 3).

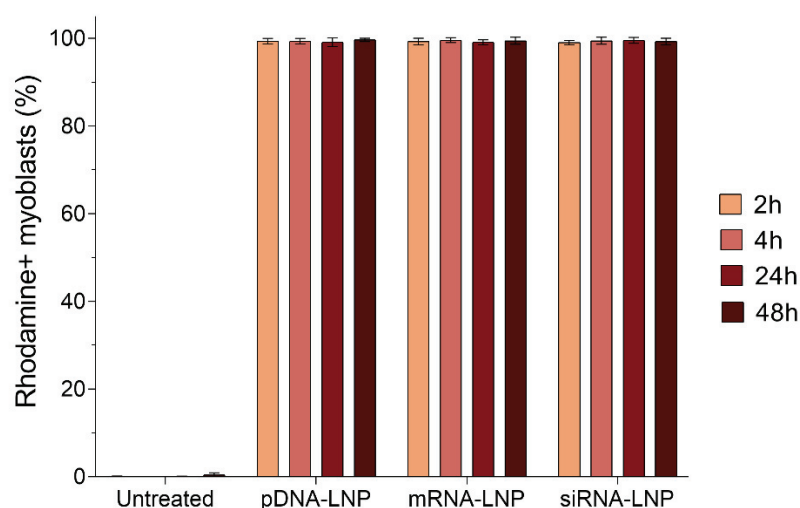


Figure 3: Internalization efficiency of pDNA-LNP and mRNA-LNP at a N/P ratio of 1.5 and siRNA-LNP at a N/P ratio of 10 in C2C12 murine myoblasts after 2, 4, 24 and 48 h treatment.

As showed in figure 3, similar internalization rates were obtained for pDNA-LNP, mRNA-LNP and siRNA-LNP. Flow cytometry analysis showed for all complexes a quick and highly efficient internalization into C2C12 myoblasts, with nearly all the cells positives to the rhodamine signal after only 2 h of incubation. This internalization rate was kept constant up to 48 h, meaning that the different complexes were not totally expelled or degraded from the cells.

3.2.2. Transfection efficiency and cytotoxicity assays of pDNA-LNP and mRNA-LNP

The efficiency of LNP to enter and intracellularly deliver pDNA or mRNA was firstly investigated in myoblasts. To this end, eGFP was used as reporter protein to monitor DNA and RNA transfection efficiency by assessing the percentage of myoblasts expressing eGFP at flow cytometry. As positive control to verified DNA and RNA integrity, commercial transfection agents for pDNA and mRNA transfection were used (Jet-Prime® and Viromer® respectively). Following preliminary assays to investigate the kinetic of transfection of pDNA-LNP and mRNA-LNP and determine the incubation time required to reach the maximum of eGFP expression, the assessment of transfection efficiency was performed after 48 h for pDNA-LNP and 24 h for mRNA-LNP.

Regarding pDNA-LNP, data showed a dose and N/P dependent transfection efficiency profile (figure 4, A). The transfection efficiency of pDNA-LNP at N/P 1.5 was almost two times higher compared to pDNA-LNP at N/P 2 for all concentrations tested. Furthermore, data demonstrated an efficient transfection efficiency of pDNA-LNP comparable to the commercial agent, with up to 60 % of cells expressing eGFP when treated with 10 µg of pDNA associated to LNP. Interestingly, the increase in pDNA treatment (from 5 to 10 µg) only induced a slightly enhancement in the transfection efficiency. The cells treated with pDNA did not show any sign of transfection, with a percentage similar to untreated cells. Regarding the transfection efficiency of mRNA-LNP, the same trend observed with pDNA was obtained (figure 4, B). However, no differences were observed between mRNA-LNP at N/P 1.5 and 2. Also in this case, data showed a highly efficient transfection efficiency comparable to the Viromer® commercial agent, with up to 90 % of myoblasts expressing eGFP when treated with 3 µg of mRNA associated to LNP. As expected, myoblasts treated with only mRNA did not show any sign of transfection.

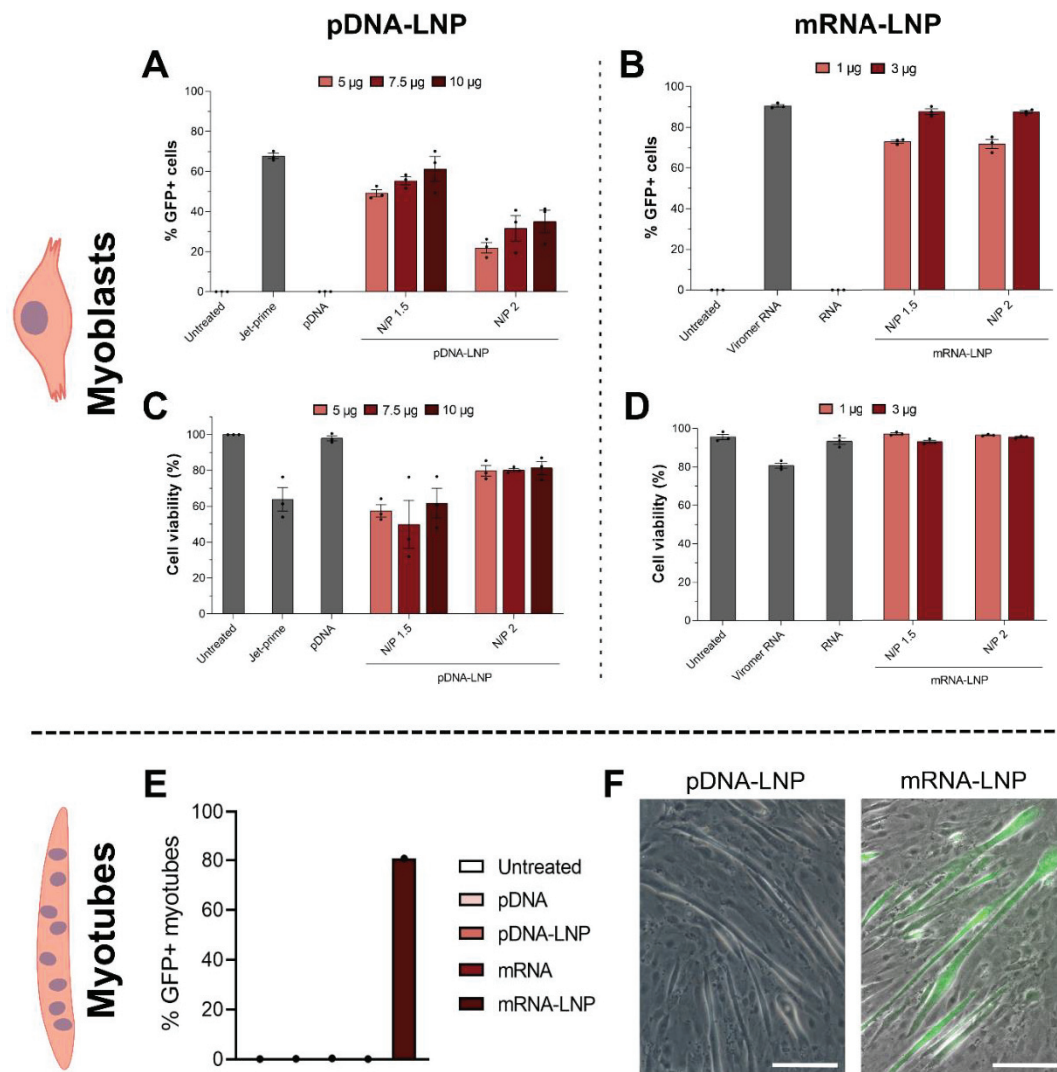


Figure 4: Transfection efficiency and cell viability of pDNA-LNP and mRNA-LNP in C2C12 myoblasts and myotubes. Flow cytometry analyses of C2C12 myoblasts treated with pDNA-LNP (A) and mRNA-LNP (B) to assess the transfection efficiency. Live/dead violet assays of C2C12 myoblasts treated with pDNA-LNP (C) and mRNA-LNP (D) to investigate the cell viability. Transfection efficiency of C2C12 myotubes treated for 48h with 10 μ g of pDNA-LNP and for 24h with 0.5 μ g of mRNA-LNP at a N/P ratio of 1.5 (E). The transfection efficiency was determined at fluorescence microscopy for 100 fibers counted. Conventional fluorescence microscopy images of C2C12 myotubes one day after treatment with pDNA-LNP and mRNA-LNP at N/P ratio of 1.5. Bars: 30 μ m. (F).

To investigate the cytotoxicity induced by the different complexes at the different N/P ratios, a live/dead viability assay was performed. Data showed that cells incubated with pDNA-LNP expressed a decreased in cell viability compared to that of the control, in a similarly trend of the Jet-Prime® commercial agent (figure 4, C). This decrease in cell viability may be correlated to the 24-h incubation time

with pDNA-LNP and shorter incubation-time may enhance the cell viability without altering the transfection efficiency. Regarding myoblasts treated with mRNA-LNP, only a slight decreased in cell viability was observed compared to that of the control with up to 90 % of living cells for all conditions, whereas the Viromer® induced a decreased in cell viability around 80 % (figure 4, D). This higher cell viability compared to pDNA-LNP may be explained by the reduced time of incubation with the mRNA-LNP (2 h).

Based on the results obtained, pDNA-LNP at a N/P ratio of 1.5 that demonstrating a higher transfection efficiency were selected to be proved on myotubes. For mRNA-LNP, although the N/P ratios of 1.5 and 2 demonstrated a similar transfection efficiency, the lower N/P ratio was selected as it corresponds to the formulation with the higher mass concentration of RNA.

The transfection efficiency of pDNA-LNP and mRNA-LNP on myotubes was determined by manual counting of the number of eGFP positive myotubes as these long fibers cannot be analyzed by flow cytometry. Regarding pDNA-LNP, any overt sign of transfection was observed in myotubes, even at the highest dose tested on myoblasts. Moreover, no transfection was also observed for pDNA transfected with the commercial agent, triggering also cell toxicity visualized by the detachment of some myotubes. On the other hand, mRNA-LNP demonstrated a high transfection efficiency on myotubes, with up to 80 % of cells expressing eGFP and without inducing any overt signs of toxicity. This high efficiency was also obtained with only 0.5 µg of mRNA associated to LNP, demonstrating the efficacy of LNP to deliver mRNA. Interestingly, myotubes were found to preferentially express eGFP compared to not-differentiated myoblasts present on the sample.

3.2.3. Intracellular release of mRNA-LNP

The intracellular distribution of LNP and the intracellular release of the nucleic acids in myoblasts and myotubes were investigated at confocal fluorescence microscopy using fluorescent LNP. Confocal fluorescence microscopy analyses demonstrated a rapid and efficient internalization of mRNA-LNP in a time dependent manner both in myoblasts and myotubes. Regarding myoblasts, many particles were found internalized in the cytosol after only 30 min of incubation

(figure 5, A). After 24 h incubation time, LNP were mainly distributed in the perinuclear region without entering the cell nucleus (figure 5, C). Further investigations carried out in immunofluorescence demonstrated that LNP were not accumulated either in the endoplasmic reticulum, nuclear lamins or Golgi apparatus (data not shown). Regarding myotubes, mRNA-LNP were observed mainly localized on the cell membrane after 30 min incubation, indicating an internalization process relatively slower in myotubes than myoblasts (figure 5, E). Confocal fluorescence images demonstrated an efficient internalization of mRNA-LNP after long-incubation time, with many particles found distributed in the cytosol (figure 5, F). Similar distribution pattern in myoblasts and myotubes was also observed for pDNA-LNP and siRNA-LNP using fluorescent LNP (data not shown).

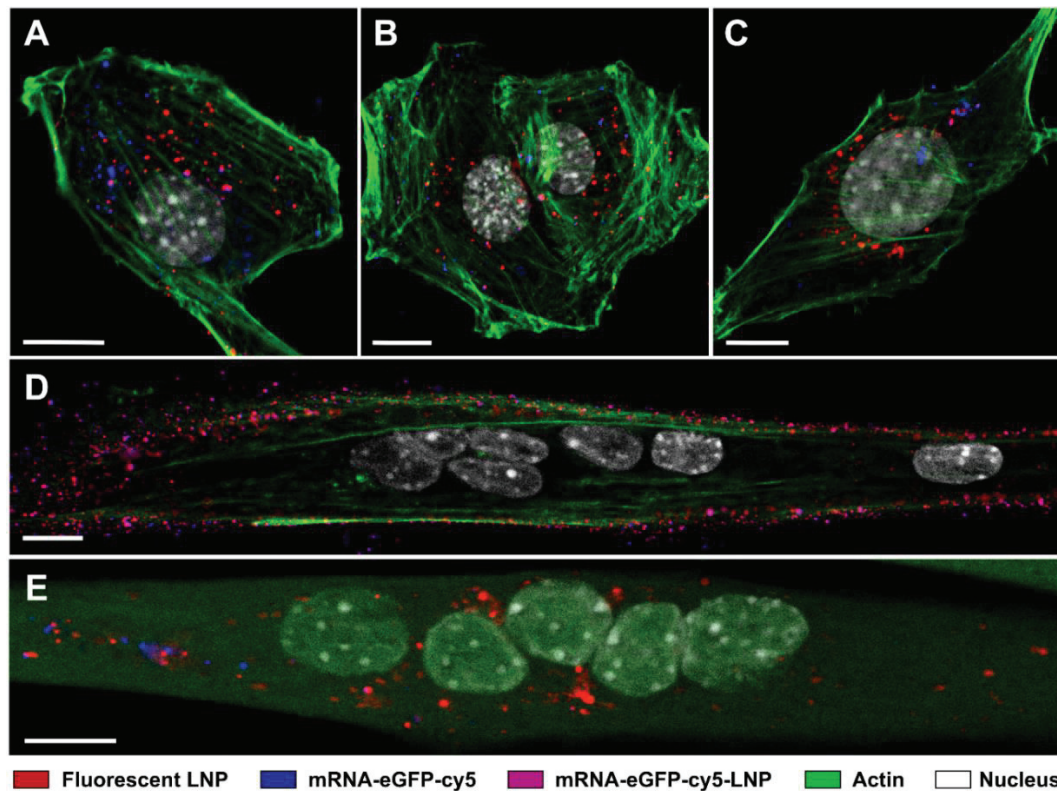


Figure 5: Intracellular distribution of mRNA-LNP and release profile of mRNA in C2C12 myoblasts and myotubes. Confocal fluorescence microscopy analyses of myoblasts (A-C) and myotubes (D-E) treated with 1 μg of mRNA-LNP at a N/P ratio of 1.5 for 30 min (A, D), 2 h (B) and 24 h (C, E). Actin filaments were stained with Phalloidin-Atto-488 and cell nuclei were counterstained with DAPI. Intracellular release of mRNA from LNP was assessed through the colocalization of the LNP and mRNA fluorescent signals. Bars: 10 μm.

To investigate the intracellular release profile of nucleic acids from LNP, mRNA-LNP were selected as mRNA is labelled with cyanine5. To this end, a colocalization

study was performed to infer the overlap of red signal from LNP and blue signal from mRNA, giving rise to a pink signal. Confocal fluorescence images demonstrated in myoblasts a rapid release of mRNA from LNP, with a partial colocalization of mRNA and LNP after 30 min incubation (figure 5, A). After 2 h incubation, almost no colocalization was observed indicating a total release of mRNA from LNP (figure 5, B). Furthermore, the signal of mRNA was nearly absent for cells treated with mRNA-LNP for 24 h, as mRNA has been probably translated in eGFP protein by the cells (figure 5, C). For myotubes, data showed that mRNA and LNP were entirely colocalized during the internalization phase at 30 min incubation time (figure 5, E). After 24 h incubation time, mRNA was totally released from LNP and a decrease in mRNA signal was observed as in myoblasts (figure 5, F).

3.2.4. Transfection efficiency and cytotoxicity assays of siRNA-LNP

The transfection efficiency of siRNA-LNP in myoblasts and myotubes was assessed using an siRNA inhibiting eGFP protein expression. In order to study the efficiency of siRNA-LNP to silence eGFP protein, eGFP expression was induced using mRNA-LNP as it has demonstrated high transfection efficiency in both myoblasts and myotubes. Preliminary assays demonstrated that highest transfection efficiency rates were obtained when cells were firstly treated with siRNA-LNP, followed with mRNA-LNP incubation. Regarding myoblasts, transfection efficiency was investigated using flow cytometry. Data showed a high transfection efficiency of siRNA-LNP in myoblasts with a dose-dependent profile (figure 6, A). Less than 30 % of cells were expressing eGFP for cells treated with 2 μg of siRNA associated to LNP (at a N/P ratio of 10) and 1 μg of mRNA-LNP at a N/P ratio of 1.5, whereas 70 % of cells not treated with siRNA-LNP were expressing eGFP. On the other hand, myoblasts treated with siRNA using Jet-prime® as commercial agent showed to decrease the percentage of cells expressing eGFP only to a value of 50%. Moreover, live/dead assays carried out at flow cytometry demonstrated a totally safe transfection of siRNA using LNP (figure 6, B). Taken together, these results prove an efficiency almost two times higher of LNP than Jet-Prime® to transfect siRNA in myoblasts without inducing cell toxicity.

For myotubes, transfection efficiency of siRNA-LNP was determined by manual counting of the number of GFP positive myotubes as these long fibers cannot be analyzed by flow cytometry. Data showed the same pattern than in myoblasts. Less than 20 % of myotubes were expressing eGFP after treatment with 1 μg of siRNA-LNP at a N/P ratio of 10 and 0.5 μg of mRNA-LNP at a N/P ratio of 1.5, whereas up to 80 % of cells not treated with siRNA-LNP were expressing eGFP (figure 6, C). Hence, these investigations demonstrate to decrease almost by four the percentage of myotubes expressing eGFP without inducing any overt sign of cell toxicity (figure 6, D).

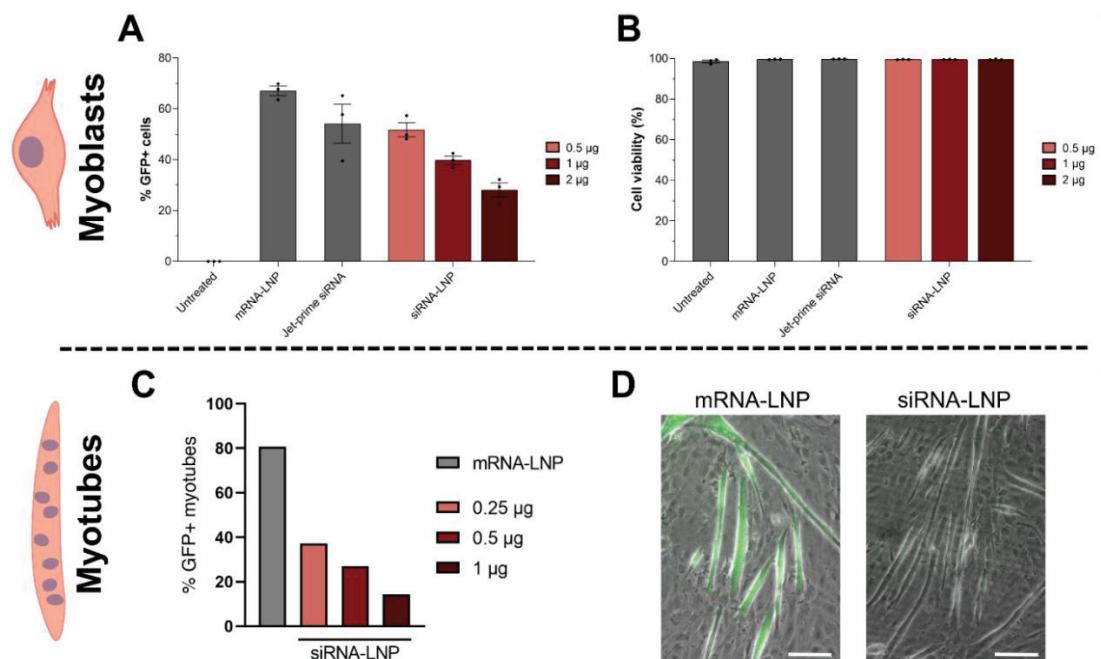


Figure 6: Transfection efficiency and cell viability of siRNA-LNP in C2C12 myoblasts and myotubes. Flow cytometry analyses of C2C12 myoblasts treated with 0.5, 1 and 2 μg of siRNA-LNP at a N/P ratio of 10 before induction of eGFP with 1 μg of mRNA-LNP at a N/P ratio of 1.5 to assess the transfection efficiency (A) and the cell viability (B) 24 h later. Transfection efficiency of C2C12 myotubes treated for 24 h with 0.25, 0.5 and 1 μg of siRNA-LNP at a N/P ratio of 10 before induction of eGFP with 0.5 μg of mRNA-LNP at a N/P ratio of 1.5, determined at fluorescence microscopy for 100 fibers counted. Conventional fluorescence microscopy images of C2C12 myotubes treated with 0.5 μg of mRNA-LNP at a N/P ratio of 1.5 with and without siRNA treatment with 0.25 μg of siRNA-LNP at a N/P ratio of 10. Bars: 20 μm . (D).

3.3. *In vitro* assays on immortalized human skeletal muscle cells

Within the framework of treating muscular dystrophies, human skeletal muscle cells appear as a representative healthy cell model. For this purpose, the efficiency of LNP to deliver mRNA was assessed in immortalized human skeletal myoblasts

using Incucyte time-lapse analyses. After treatment with 0.1, 0.25 and 0.5 μg of mRNA-LNP at a N/P ratio of 1.5 and 2, data showed a high transfection efficiency of mRNA-LNP in a time-dependent manner. The expression of eGFP started after 6 h incubation and the maximum of eGFP positive cells were obtained followed 24 h incubation. These percentage of cells expressing eGFP were relatively constant until 48 h incubation. In comparison to C2C12 murine muscle cells, mRNA-LNP at a N/P ratio of 2 demonstrate a slight lower transfection efficiency than mRNA-LNP at a N/P ratio of 1.5. The highest transfection efficiency was obtained for myoblasts treated with 0.5 μg of mRNA-LNP at a N/P ratio of 1.5, with up to 75 % of cells expressing eGFP. Lipofectamine2000® used as commercial agent to transfect mRNA and thus as positive control, demonstrated a faster transfection efficiency with almost all cells expressing eGFP after 6 h incubation and starting to decrease after 48 h.

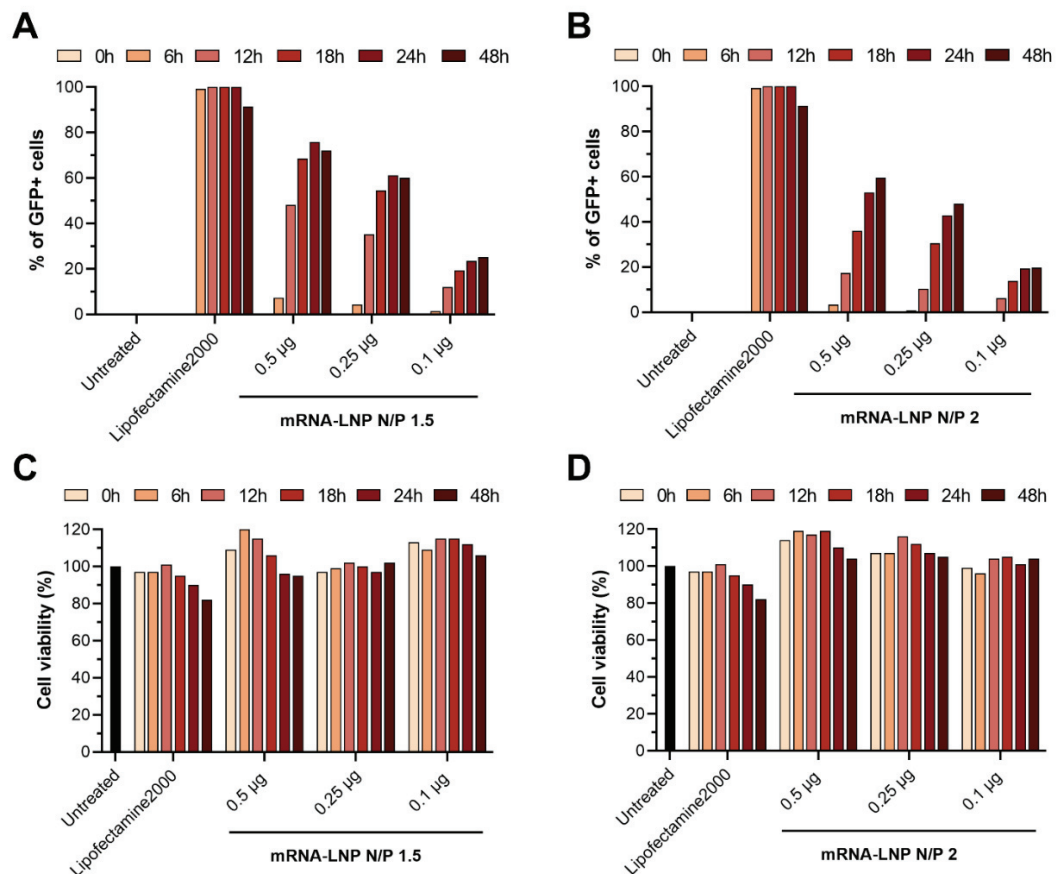


Figure 7: Transfection efficiency and cell viability of mRNA-LNP in immortalized human skeletal muscle myoblasts. Incucyte time-lapse analyses of immortalized human skeletal myoblasts treated with 0.1, 0.25 and 0.5 μg of mRNA-LNP at N/P 1.5 and 2 to assess the transfection efficiency (A-B) and cell viability (C-D).

In the meanwhile, the toxicity of the different complexes was assessed by normalizing the percentage of cell confluence with the one of the untreated controls. Overall, no cell toxicity was demonstrated for all mRNA-LNP complexes and even a slightly higher cell viability was observed compared to the control. Only Lipofectamine2000® presented a decrease in cell viability up to 80 % after 48 h incubation.

4. Discussion

The objective of this present study was to investigate the efficiency of selected LNP to efficiently deliver different DNA and RNA species in proliferative myoblasts and differentiated myotubes. To this end, pDNA, mRNA and siRNA nucleic acid sequences were selected to induce or interfere with eGFP expression.

In this study, DNA and RNA species were complexed to our recently patented LNP formulation. By varying the N/P ratio, high as small molecular weight nucleic acids were efficiently complexed to LNP. Low N/P ratio around 1.5 was sufficient and suitable to complexation of large nucleic acids such as pDNA or mRNA whereas higher N/P ratio around 10 was required to complex small nucleic acid as siRNA. Although no significant differences were observed regarding the morphology of the different systems, they all demonstrated an internal architecture composed of concentric lamellae alternating lipid bilayers and nucleic acid monolayer condensed between them. Such structures have been widely reported for nucleic acids complexed to cationic LNP and proved to be suitable for nucleic acid stability as it promotes better protection from degradation by nucleases^{21–23}.

The ability of our pDNA-LNP, mRNA-LNP and siRNA-LNP to efficiently enter cells were evaluated in C2C12 murine cells, a well-characterized and commonly used skeletal muscle cell line²⁴. Our combined flow cytometry analyses and confocal fluorescence microscopy provided crucial information about the uptake and internalization kinetic of our nanosystems. Firstly, all nanosystems demonstrated a high internalization efficiency in C2C12 myoblasts with nearly all cells containing nanosystems in only 2 h incubation and for up to 48 h. This long intracellular resident time means that nanosystems are not totally expelled from

cells and as suggested in the literature, lipids of LNP have been probably exchanged with the cells once intracellularly released into the cytosol as for extracellular vesicles^{25,26}. Confocal fluorescence analyses demonstrated that nanosystems were rapidly internalized in both myoblasts and myotubes with a cytoplasmic accumulation without entering the cell nucleus. Moreover, intracellular release of mRNA from LNP investigated through a colocalization study showed the intracellular time-dependent release profile of mRNA for both cell types. This high intracellular release of the nucleic acid content is crucial to unveil the therapeutic potential of nucleic acids²⁷.

The transfection efficiency of the different nanosystems were firstly investigated in myoblasts, that are usually easier to transfect than myotubes due to their cellular proliferation rate^{28,29}. As expected, our investigations showed a faster protein expression for mRNA-LNP and siRNA-LNP than pDNA-LNP due to their different intracellular gene transfer processes^{30,31}. The transfection efficiency of pDNA-LNP and mRNA-LNP to induce eGFP expression was comparable to the commercial transfection agent with up to 60 and 90 % of GFP+ cells respectively. To study the inhibition of eGFP protein expression, myoblasts were firstly treated with siRNA-LNP before inducing protein expression using mRNA-LNP. This sequential order of treatment was essential to interfere with eGFP expression immediately when eGFP-coding mRNA was intracellularly released. Our results showed a transfection efficiency two times superior at the commercial transfection agent was obtained. Moreover, our nanosystems did not induce toxicity, except for pDNA-LNP that showed a decrease in cell viability due to the long-time incubation of particles with cells.

More interestingly, the same experiments were also performed on myotubes. This is an essential feature for therapeutic application since skeletal muscles are complex organs made of elongated contractile cells (myofibers) and quiescent resident stem cells (satellite cells)^{32,33}. Despite the high internalization of pDNA-LNP, any overt signs of transfection were visualized in mature myotubes. This phenomenon can be explained through the higher dimension of pDNA compared to the cell pores and through the cell differentiation stage³⁴. As pDNA must reach the cell nucleus to express the protein of interest, pDNA transfection is more challenging into

differentiated cells even if pDNA is correctly delivered intracellularly³⁵. In fact, non-proliferent cells do not process cell division, a crucial step in which cells undergo breakdown and reformation of the nuclear envelope, offering an opportunistic way for pDNA to enter the cell nucleus³⁶. On the contrary, mRNA-LNP and siRNA-LNP demonstrated a high transfection efficiency at even low administered doses, without inducing any over signs of toxicity. These findings are highly promising considering that differentiated myotubes are hard to transfect and that current approach employ the widely controverted electroporation technic^{37–39}. Although other types of carriers as PLGA, mesoporous and liposomes reported a lower uptake capability in myotubes^{40,41}, our LNP showed to efficiently enter myotubes and deliver nucleic acid content. Thereby, our findings hold promise to cure the non-renewing differentiated cells forming the basic unit of skeletal muscles.

Finally, mRNA-LNP were tested in a human immortalized muscle cell lines as more representative healthy cell model in a view of treating muscular dystrophies. Our investigations demonstrated a high transfection efficiency of mRNA-LNP in myoblasts, with up to 80 % of cells expressing eGFP, as in murine muscle myoblasts. Therefore, these encouraging results in human cells proved fruitful to be tested in different established human cell model of MDs expressing the etiology, and the pathophysiological progression^{42–44}.

5. Conclusion

The present investigations demonstrate the suitability of our LNP to deliver pDNA, mRNA and siRNA into both cycling myoblasts and non-cycling myotubes. The high internalization rate and high ability to transfect nucleic acids for inducing or inhibiting eGFP expression, together with the interesting intracellular nucleic acid payload release, demonstrate the efficiency of our LNP as carriers for enabling gene delivery in muscle cells. Thus, exploring the potential of such nanosystems promise to cure not only regenerating muscle cells but also non-renewing affected cells. In summary, the results obtained herein using eGFP protein as reporter gene in healthy murine and human muscle cell lines provide the experimental background for

further studies, to prove the efficacy of our LNP to deliver therapeutic nucleic acid sequences in muscular disease-like cell and animal models. Whereas most currently described LNP aim to deliver one type of nucleic acid, our LNP have been leveraged for more broadly nucleic acid applications and have demonstrated to efficiently bind and deliver different DNA and RNA species into muscle cells. Thereby, this promising approach provides a universal platform technology for delivering small as large nucleic acid payloads and open the range of possibilities to several gene therapy strategies for treating neuromuscular diseases.

Acknowledgments

MR is a PhD student in receipt of a fellowship from the INVITE project of the University of Verona, (PhD Programme in Nanoscience and Advanced Technologies). This project has received funding from the European Union's Horizon 2020 Research and Innovation Programme under the Marie Skłodowska-Curie grant agreement No. 754345. This project has received funding from the RESOLVE project, an initiative funded from the European Union's Horizon 2020 research and innovation programme Euronanomed III.

Confocal microscopy observations were performed at the Centre d'Imagerie Quantitative Lyon-Est (CIQLE) of the University of Lyon.

References

1. Mercuri, E., Bönnemann, C. G. & Muntoni, F. Muscular dystrophies. *The Lancet* **394**, 2025–2038 (2019).
2. Mah, J. K. *et al.* A Systematic Review and Meta-analysis on the Epidemiology of the Muscular Dystrophies. *Canadian Journal of Neurological Sciences* **43**, 163–177 (2016).
3. Andreana, I. *et al.* Nanomedicine for Gene Delivery and Drug Repurposing in the Treatment of Muscular Dystrophies. *Pharmaceutics* **13**, 278 (2021).
4. Aoki, Y. & Wood, M. J. A. Emerging Oligonucleotide Therapeutics for Rare Neuromuscular Diseases. *J Neuromuscul Dis* **8**, 869–884.
5. Commissioner, O. of the. FDA approves innovative gene therapy to treat pediatric patients with spinal muscular atrophy, a rare disease and leading genetic cause of infant mortality. *FDA* <https://www.fda.gov/news-events/press->

announcements/fda-approves-innovative-gene-therapy-treat-pediatric-patients-spinal-muscular-atrophy-rare-disease (2020).

6. Garber, K. Worth the RISC? *Nature Biotechnology* **35**, 198–202 (2017).
7. Degors, I. M. S., Wang, C., Rehman, Z. U. & Zuhorn, I. S. Carriers Break Barriers in Drug Delivery: Endocytosis and Endosomal Escape of Gene Delivery Vectors. *Acc. Chem. Res.* **52**, 1750–1760 (2019).
8. Kulkarni, J. A. *et al.* The current landscape of nucleic acid therapeutics. *Nat. Nanotechnol.* **16**, 630–643 (2021).
9. Sahin, U. *et al.* COVID-19 vaccine BNT162b1 elicits human antibody and TH1 T cell responses. *Nature* **586**, 594–599 (2020).
10. Baden, L. R. *et al.* Efficacy and Safety of the mRNA-1273 SARS-CoV-2 Vaccine. *N Engl J Med* NEJMoa2035389 (2020) doi:10.1056/NEJMoa2035389.
11. Verdera, H. C., Kuranda, K. & Mingozzi, F. AAV Vector Immunogenicity in Humans: A Long Journey to Successful Gene Transfer. *Mol Ther* **28**, 723–746 (2020).
12. Fitzpatrick, Z. *et al.* Influence of Pre-existing Anti-capsid Neutralizing and Binding Antibodies on AAV Vector Transduction. *Mol Ther Methods Clin Dev* **9**, 119–129 (2018).
13. Bisset, D. R. *et al.* Therapeutic impact of systemic AAV-mediated RNA interference in a mouse model of myotonic dystrophy. *Hum. Mol. Genet.* **24**, 4971–4983 (2015).
14. Kulkarni, J. A. *et al.* Fusion-dependent formation of lipid nanoparticles containing macromolecular payloads. *Nanoscale* **11**, 9023–9031 (2019).
15. Gary, D. J., Min, J. B., Kim, Y., Park, K. & Won, Y.-Y. The Effect of N/P Ratio on the In Vitro and In Vivo Interaction Properties of PEGylated Poly(2-(dimethylamino)ethyl methacrylate)-Based siRNA Complexes. *Macromol Biosci* **13**, 1059–1071 (2013).
16. Zhang, H. *et al.* Together is Better: mRNA Co-Encapsulation in Lipoplexes is Required to Obtain Ratiometric Co-Delivery and Protein Expression on the Single Cell Level. *Advanced Science* **9**, 2102072 (2022).
17. Giménez-Marqués, M. *et al.* GraftFast Surface Engineering to Improve MOF Nanoparticles Furtiveness. *Small* **14**, e1801900 (2018).

18. Bano, F., Carril, M., Di Gianvincenzo, P. & Richter, R. P. Interaction of Hyaluronan with Cationic Nanoparticles. *Langmuir* **31**, 8411–8420 (2015).
19. Vader, P., van der Aa, L. J., Engbersen, J. F. J., Storm, G. & Schiffelers, R. M. Physicochemical and Biological Evaluation of siRNA Polyplexes Based on PEGylated Poly(amido amine)s. *Pharm Res* **29**, 352–361 (2012).
20. Stewart, P. L. Cryo-electron microscopy and cryo-electron tomography of nanoparticles. *Wiley Interdiscip Rev Nanomed Nanobiotechnol* **9**, (2017).
21. Kulkarni, J. A., Cullis, P. R. & van der Meel, R. Lipid Nanoparticles Enabling Gene Therapies: From Concepts to Clinical Utility. *Nucleic Acid Ther* **28**, 146–157 (2018).
22. Majzoub, R. N., Ewert, K. K. & Safinya, C. R. Cationic liposome–nucleic acid nanoparticle assemblies with applications in gene delivery and gene silencing. *Philosophical Transactions of the Royal Society A: Mathematical, Physical and Engineering Sciences* **374**, 20150129 (2016).
23. Kulkarni, J. A. *et al.* On the Formation and Morphology of Lipid Nanoparticles Containing Ionizable Cationic Lipids and siRNA. *ACS Nano* **12**, 4787–4795 (2018).
24. McMahon, D. K. *et al.* C2C12 cells: biophysical, biochemical, and immunocytochemical properties. *Am J Physiol* **266**, C1795-1802 (1994).
25. Zinger, A. *et al.* Bioinspired Extracellular Vesicles: Lessons Learned From Nature for Biomedicine and Bioengineering. *Nanomaterials (Basel)* **10**, E2172 (2020).
26. Costanzo, M. *et al.* Formulative Study and Intracellular Fate Evaluation of Ethosomes and Transethosomes for Vitamin D3 Delivery. *Int J Mol Sci* **22**, 5341 (2021).
27. Paramasivam, P. *et al.* Endosomal escape of delivered mRNA from endosomal recycling tubules visualized at the nanoscale. 2020.12.18.423541 (2021) doi:10.1101/2020.12.18.423541.
28. Mortimer, I. *et al.* Cationic lipid-mediated transfection of cells in culture requires mitotic activity. *Gene Ther* **6**, 403–411 (1999).
29. Neuhaus, B. *et al.* Nanoparticles as transfection agents: a comprehensive study with ten different cell lines. *RSC Adv.* **6**, 18102–18112 (2016).

30. Gupta, A., Andresen, J. L., Manan, R. S. & Langer, R. Nucleic acid delivery for therapeutic applications. *Advanced Drug Delivery Reviews* **178**, 113834 (2021).
31. Ibraheem, D., Elaissari, A. & Fessi, H. Gene therapy and DNA delivery systems. *International Journal of Pharmaceutics* **459**, 70–83 (2014).
32. Yin, H., Price, F. & Rudnicki, M. A. Satellite cells and the muscle stem cell niche. *Physiol Rev* **93**, 23–67 (2013).
33. Frontera, W. R. & Ochala, J. Skeletal muscle: a brief review of structure and function. *Calcif Tissue Int* **96**, 183–195 (2015).
34. Watanabe, A. *et al.* Effect of particle size on their accumulation in an inflammatory lesion in a dextran sulfate sodium (DSS)-induced colitis model. *Int J Pharm* **509**, 118–122 (2016).
35. Munkonge, F. M. *et al.* Identification and functional characterization of cytoplasmic determinants of plasmid DNA nuclear import. *J Biol Chem* **284**, 26978–26987 (2009).
36. Ellenberg, J. *Dynamics of Nuclear Envelope Proteins During the Cell Cycle in Mammalian Cells*. *Madame Curie Bioscience Database [Internet]* (Landes Bioscience, 2013).
37. Acsadi, G. *et al.* A differential efficiency of adenovirus-mediated in vivo gene transfer into skeletal muscle cells of different maturity. *Human Molecular Genetics* **3**, 579–584 (1994).
38. Trollet, C., Scherman, D. & Bigey, P. Delivery of DNA into muscle for treating systemic diseases: advantages and challenges. *Methods Mol Biol* **423**, 199–214 (2008).
39. Lee, J. E., Bennett, C. F. & Cooper, T. A. RNase H-mediated degradation of toxic RNA in myotonic dystrophy type 1. *Proc Natl Acad Sci U S A* **109**, 4221–4226 (2012).
40. Costanzo, M. *et al.* Uptake and intracellular fate of biocompatible nanocarriers in cycling and noncycling cells. *Nanomedicine (Lond)* **14**, 301–316 (2019).
41. Guglielmi, V. *et al.* Uptake and intracellular distribution of different types of nanoparticles in primary human myoblasts and myotubes. *Int J Pharm* **560**, 347–356 (2019).

42. Arandel, L. *et al.* Immortalized human myotonic dystrophy muscle cell lines to assess therapeutic compounds. *Dis Model Mech* **10**, 487–497 (2017).
43. Abujarour, R. *et al.* Myogenic Differentiation of Muscular Dystrophy-Specific Induced Pluripotent Stem Cells for Use in Drug Discovery. *Stem Cells Translational Medicine* **3**, 149–160 (2014).
44. Mondragon-Gonzalez, R. & Perlingeiro, R. C. R. Recapitulating muscle disease phenotypes with myotonic dystrophy 1 induced pluripotent stem cells: a tool for disease modeling and drug discovery. *Dis Model Mech* **11**, dmm034728 (2018).

CHAPTER 5

Antisense oligonucleotide delivery using lipid nanoparticles to reverse the splicing defects in DM1

Preliminary data

1. Aim of the work

The last part of this PhD thesis was dedicated to the association of a therapeutic nucleic acid sequence for treating DM1 with the previously developed LNP. To this end, an RNase H-active ASO described in the literature has been selected³⁹. This sequence has been generated to specifically bind the toxic CUG-repeats of the mutant DMPK RNA and induce their cleavage through RNase-H enzyme degradation. Therapeutic efficacy assays carried out *in vitro* in a DM1 cell model demonstrated the efficiency of this gapmer (using Lipofectamine2000 as commercial transfection agent) to disrupt up to 80 % of ribonuclear foci. However, these promising *in vitro* results were compromised by a limited *in vivo* therapeutic efficiency when administered by intramuscular injection using electroporation. Furthermore, some signs of toxicity were evidenced on muscle histological analyses. Possible reasons related to these *in vivo* limitations include low efficiency and toxic effects of the electroporation delivery strategy that may be not clinically conceivable. For this purpose, LNP appears as a suitable strategy to overcome these issues. Thus, ASO association to LNP was firstly optimized and nanosystems were characterized in terms of physico-chemical properties. Then, intracellular distribution and release of ASO from LNP were investigated in healthy C2C12 myoblasts and myotubes. Finally, the *in vivo* biodistribution of the LNP and ASO in healthy mice was investigated using an innovative association of complementary radiolabeling and fluorescent imaging techniques. Therefore, radiolabeled LNP were monitored and quantified using NanoSPECT/CTTM and gamma counter analysis whereas ASO was monitored using fluorescent imaging *in vivo* system. Overall, the objective of this work was to provide a suitable nanosystem to be tested *in vitro* and *in vivo* in DM1 cell and animal models.

2. Material and methods

2.1. Lipid-nanoparticles preparation

Materials and methods related to the formulation of LNP and fluorescent-LNP were identical to the ones described in the chapter 4. To radiolabel particles, DTPA-LNP were prepared to complex ¹¹¹In. To this end, 0.5% mol/mol of PE-DTPA was added to the lipid solution prior microfluidic mixing.

2.2. ASO complexation to LNP

The present ASO sequence has been manufactured as described by Lee et al³⁹: AGCAGCAGCAGCAG. This ASO sequence was made of phosphorothioate nucleotides and the 3' cap ending nucleotides were made of 2'-Methoxyethyl nucleotides. Furthermore, to obtain a fluorescently labelled ASO sequence, a cyanine 5 were added on the 5'-terminaison. Complexation was performed by mixing an equal volume of LNP with an adequate quantity of ASO, to obtain lipoplexes at N/P ratios of 2, 4, 8 and 10. Lipoplexes were finally coated with HA.

2.3. Physico-chemical characterization of ASO-LNP

Nanosystems were characterized as previously described in chapter 4.

2.4. Intracellular distribution and intracellular release of ASO from LNP

C2C12 murine myoblasts and myotubes were cultured as previously described in chapter 4. The intracellular distribution and release of ASO from LNP were investigated at fluorescent microscopy confocal imaging using fluorescently-labelled LNP. For microscopy confocal analysis, myoblasts were seeded onto 12 mm-glass coverslips in 24-multiwell plates at the density of 10,000 cells/well whereas to obtain myotubes, myoblasts were seeded onto 4-compartements Labtek culture chamber at the density of 40,000 cells/well and induced for differentiation for 6 days. Myoblasts were treated with 1 µg of ASO associated to LNP at a N/P ratio of 10 for 30 min, 2 and 24 h and myotubes for 2 h and 48 h. For long-incubation time points, cells were incubated with treatments for 2 h and were then given fresh medium. After each time point, cells were fixed with 4 % (v/v) paraformaldehyde in PBS, for 15 min at room temperature. Cell cytoplasm was stained with Phalloidin-Atto 488 (Sigma) diluted 1:20 in PBS for 1 h at room temperature, while cell nuclei were counterstained with DAPI (stock at 20 mM diluted 1:2000) for 1 h at room temperature. Samples were finally mounted in Fluoromount mouting medium (Invitrogen) and imaging was performed by a Zeiss LSM800 confocal laser scanning microscope (Carl Zeiss AG, Oberkochen, Germany) using a 63X objective.

2.5. *In vivo* biodistribution of ASO-fluorescently labelled associated to radiolabeled LNP

All animal experiments were approved by the local animal ethics of University Claude Bernard Lyon 1 and mice were bred according to French and European regulations (authorization number 30771). Experiments were conducted on C57BL/6J female at 8-10 weeks of age obtained from Charles River® (Saint-Germain-Nuelles, France).

Surface radiolabeling of liposomes was carried out by incubation 4.17 μmol (500 μL) of liposomes with 85.8 MBq (100 μL) of ^{111}In at 60 °C for 30 minutes. This led to an amount of radioactivity of 20.58 GBq/mmol. Radiolabeling efficiency was assessed by instant thin layer chromatography on silica-gel strips (iTLC-SG, Biodex Medical Systems, Shirley, USA) using HEPES 100 mM pH 5.5 as mobile phase and determined radiochemical purity was over 97 %. Lipoplexes were prepared at a N/P ratio of 10. Briefly, 1.25 μmol (150 μL) of radiolabeled liposomes (0.63 μmol of DOTAP) were incubated at room temperature with 0.2 nmol of ASO, (equivalent to 0.244 μmol of phosphate), for 30 minutes. Then, a solution of HA was added to complexes.

Formulations were intravenously (i.v.) injected to mice under anesthesia with 3% of isoflurane. Mice received an injection of around 4 MBq ^{111}In chelated to DTPA LNP. Mice were randomly divided in three groups: 30 min, 2, 6 and 24 h. At each time points, mice were firstly imaged at NanoSPECT/CT™ *in vivo* animal imager (Bioscan Inc., Washington D.C, USA) and at fluorescent imaging *in vivo* system composed of light-tight chamber with a back-thinned CCD-cooled camera ORCAIIBT-512G (Deutschland GmbH, Herrsching am Ammersee, Germany). Then, at each time points, mice were sacrificed by cervical dislocation and tissues and organs were harvested for *ex vivo* fluorescent imaging and gamma quantification. *Ex vivo* images were analyzed using the Wasabi software 1.5 (Hamamatsu Photonics Deutschland GmbH, Herrsching am Ammersee, Germany) and *ex vivo* quantification of organ radioactivity was carried out with a Wizard 3” gamma counter (Perkin Elmer, Waltham USA).

3. Results

3.1. Physico-chemical characterization of ASO-LNP

As performed for pDNA-LNP, mRNA-LNP and siRNA-LNP, the complexation of ASO with LNP was performed varying the N/P ratio. As shown in Figure 8, the hydrodynamic

diameter of ASO-LNP at N/P ratios from 2 to 10 were relatively similar with a size around 160 nm, a polydispersity index lower than 0.2 and a negative ζ potential around -30 mV.

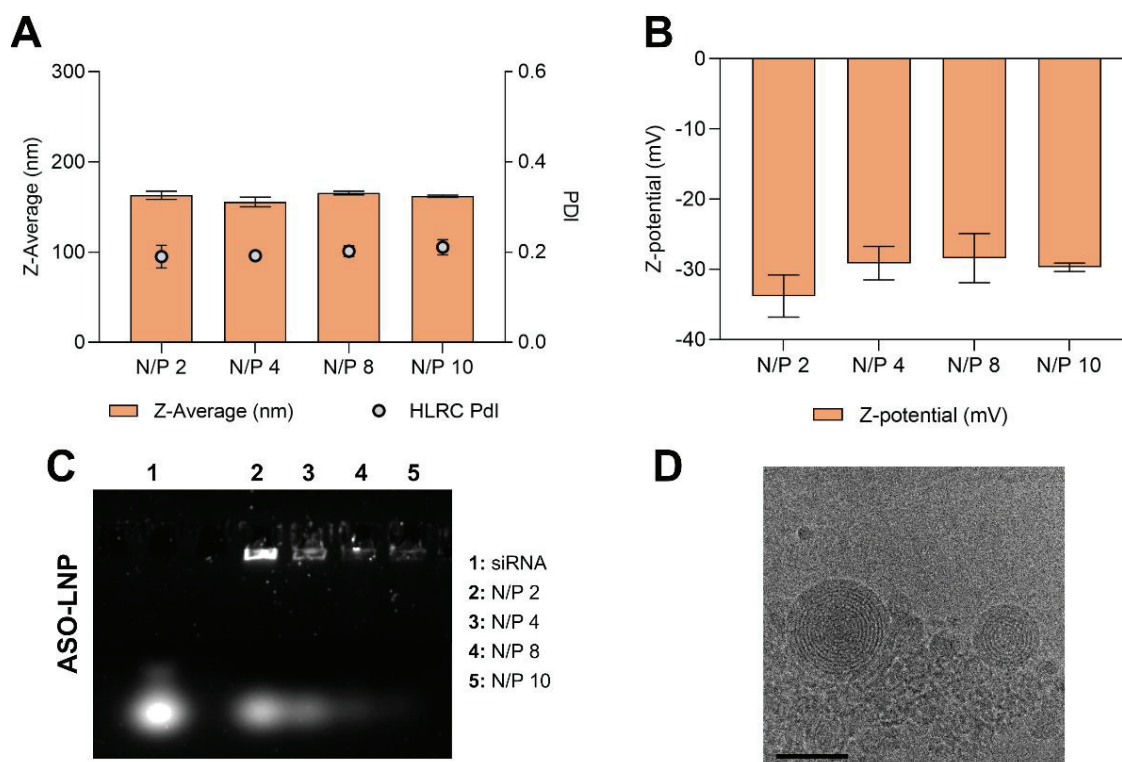


Figure 8: Physico-chemical properties and association efficiency of ASO complexed with LNP at different N/P ratio. Physico-chemical characterization of complexes was investigated by DLS to assess the hydrodynamic diameter (A) and ζ potential (B) of each complex. DNA retardation assay of the different complexes was used to assess the association efficiency of ASO with LNP (C). Cryo-TEM images of ASO-LNO at a N/P ratio of 10. Bars: 100 μ m.

Electrophoretic assays were performed to assess the complexation of ASO with LNP at these different N/P ratios. Figure 6C showed that ASO was not efficiently complexed with LNP at N/P ratios from 2 to 8, as showed by the presence of ASO band similar to the one of ASO free in solution, but demonstrated an efficient complexation of ASO with LNP at a N/P ratio of 10. The morphology of ASO-LNP at a N/P ratio of 10 was investigated at Cryo-TEM. Figure 6D showed an identical internal architecture than siRNA-LNP, with the formation of multilamellar vesicles composed of concentric lamellae alternating lipid bilayers and nucleic acid monolayer.

Based on the results obtained, ASO-LNP at a N/P ratio of 10 was selected for further investigations.

3.2. Intracellular distribution and intracellular release of ASO from LNP

The intracellular distribution of LNP and the intracellular release of fluorescent ASO in myoblasts and myotubes were investigated at confocal fluorescence microscopy using fluorescent LNP (see Figure 9).

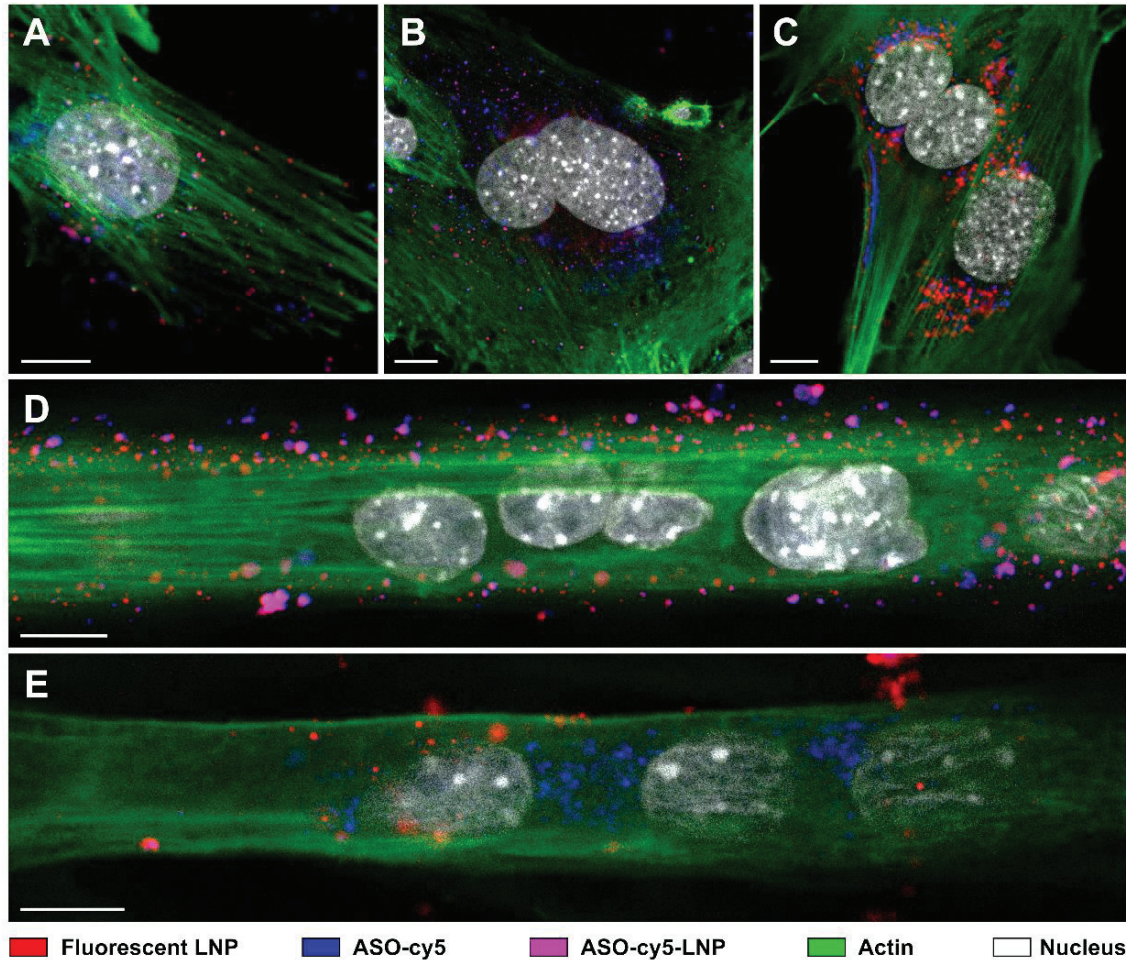


Figure 9: Intracellular distribution of ASO-LNP and release profile of ASO in C2C12 myoblasts and myotubes. Confocal fluorescence microscopy analyses of myoblasts (A-C) and myotubes (D-E) treated with 1 μg of ASO-LNP at a N/P ratio of 10 for 30 min (A, D), 2 h (B) and 24 h (C, E). Actin filaments were stained with Phalloidin-Atto-488 and cell nuclei were counterstained with DAPI. Intracellular release of ASO from LNP was assessed through the colocalization of the LNP and ASO fluorescent signals. Bars: 10 μm .

Confocal images demonstrated a rapid and efficient internalization of ASO-LNP in both myoblasts and myotubes. Regarding myoblasts, many ASO-LNP were found to be internalized in the cytosol after only 30 min of incubation and ASO was found entirely associated to LNP. After 2 and 24h, particles were found accumulated in higher amount and distributed in the perinuclear region without entering the nucleus. Moreover, ASO was highly released in the cytoplasm after already 2 h incubation time. Regarding

myotubes, a high internalization efficiency with a similar trend was also observed. After 30 min incubation, ASO was found entering myotubes together with LNP whereas after 24 h incubation ASO was totally released in the cytoplasm. Despite this nucleic acid cannot provide easily visual control of transfection as for GFP expression, the intracellular distribution and release profile of ASO-LNP hold promises to efficiently delivered ASO in both myoblasts and myotubes.

3.3. *In vivo* biodistribution of ASO-LNP

To determine the organ selectivity of our ASO-LNP after i.v. administration, a biodistribution study was performed using innovative association of complementary radiolabeling and fluorescent imaging techniques. Radiolabeled LNP were monitored and quantified using NanoSPECT/CT™ and gamma counter analysis whereas ASO was monitored using fluorescent imaging *in vivo* system. Mice were injected with fluorescent-labelled ASO and ¹¹¹In-labelled LNP at a N/P ratio of 10 with a dose corresponding to about 6 MBq and 2.5 µg of ASO. Imaging and quantification were performed at 30 min, 2, 6 and 24 h after administration.

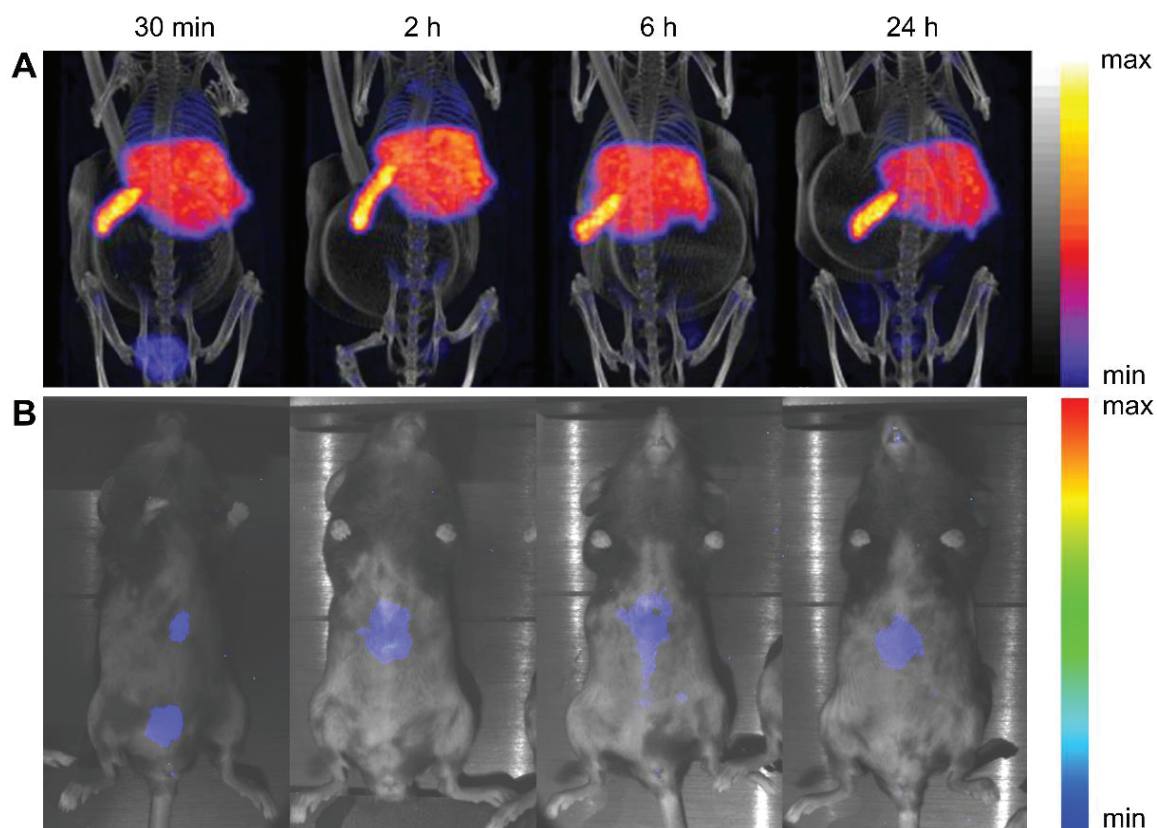


Figure 10: MicroSPECT/CT (A) and fluorescent (B) *in vivo* imaging of C57BL/6J mice injected with ASO associated to ¹¹¹In-LNP at a N/P ratio of 10 after 30 min, 2, 6 and 24 h.

Regarding *in vivo* imaging, clear images were obtained for all time points, with a visual mostly particle accumulation in the spleen and the liver (Figure 10). At 30 min, ASO-LNP were also found in lower amount in the bladder, resulting from natural urinary excretion. Also, MicroSPECT/CT imaging showed the slight presence of LNP in the lungs after 30 min and 2 h, that was eliminated over-time.

To determine the organ selectivity of our ASO-LNP, radiolabeled quantification and fluorescence semi-quantitative analysis were investigated for each animal organ (Figure 11). The amount of radioactivity of ^{111}In -LNP was quantified with a gamma counter and normalized and presented as a percentage of injected dose per gram of tissue (%/ID/g), while the intensity of ASO was semi-quantified and normalized and presented as a percentage of intensity per surface area.

Gamma counting and fluorescence intensity analyses demonstrated slight difference in the biodistribution profile of ASO and LNP. Quantitative biodistribution of ^{111}In -LNP demonstrated a majority splenic accumulation with around 65 % of the ID/g and liver accumulation of about 20 % of the ID/g. These distributions were constant under 24 h. ASO-LNP were also slightly distributed in the lungs with around 15 % of the ID/g at 6 h, that was decreased to 6 % after 24 h, meaning that particles were not accumulated in the lungs. The different muscles collected (heart, diaphragm, tibialis, gastrocnemius, soleus and extensor digitorum longus (EDL) did not show particles distributed among them. Fluorescence semi-quantitative imaging demonstrated a high percentage of ASO taken up by the reticuloendothelial system with a similar intensity signal per surface area in the liver and spleen. Interestingly, fluorescence biodistribution showed a similar profile in the mice kidneys, that was not observed for ^{111}In -LNP. The distribution in liver, spleen and kidneys were constant under 24 h. Finally, ASO was also distributed in the lungs within 30 min and were progressively eliminated at 24 h.

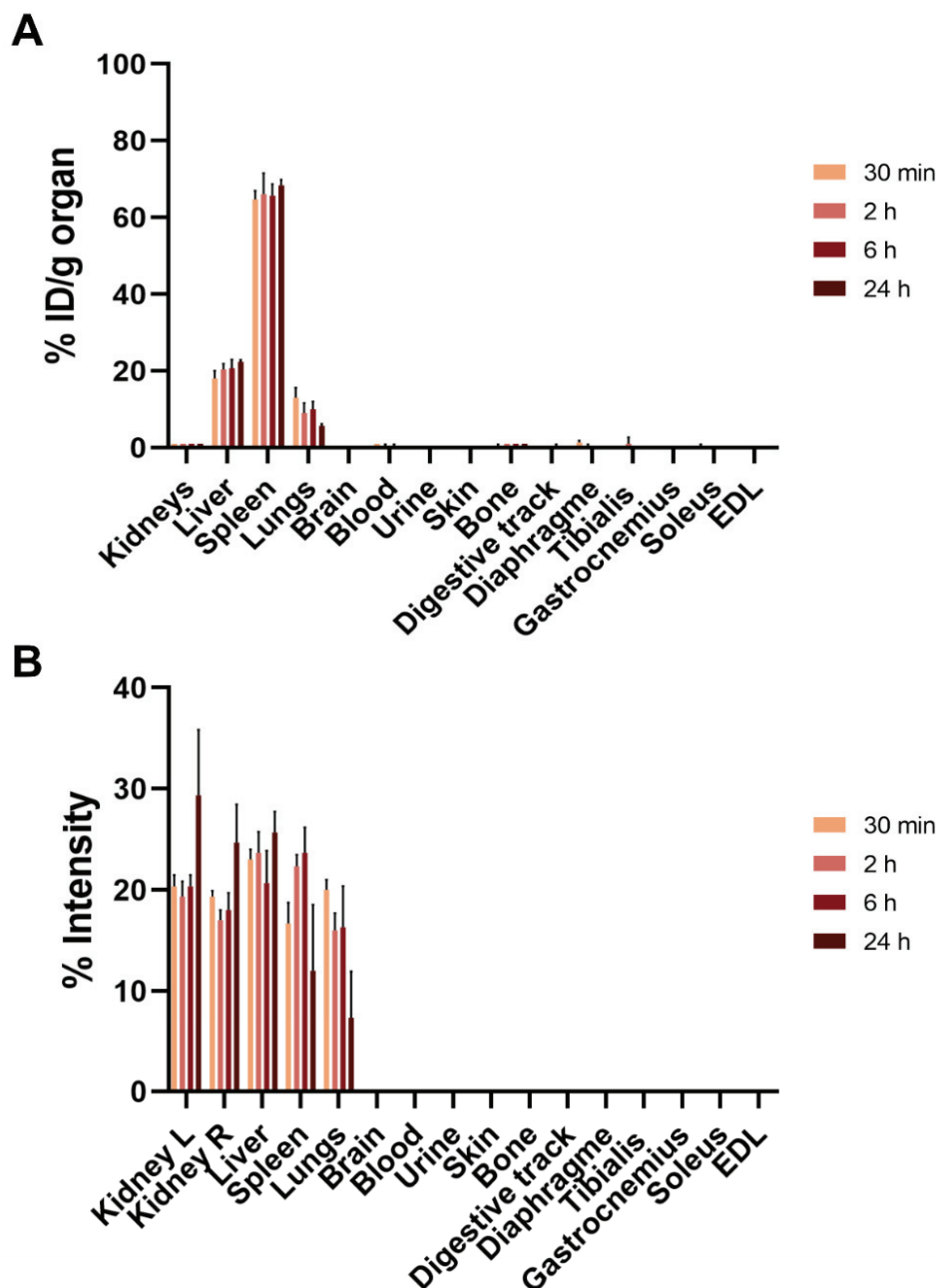


Figure 11: Quantitative biodistribution of ¹¹¹In-LNP (A) and semi-quantitative biodistribution of ASO (B) at 30 min, 2, 6 and 24 h after i.v. injection in C57B/6J mice expressed as percentage of injected dose per gram of tissue and percentage of intensity per surface area respectively (n=3 mice per group).

4. Discussion

The objective of this work was to efficiently associate a therapeutic ASO sequence to our LNP in order to provide an oligonucleotide-based therapy for treating DM1.

Physico-chemical characterization of ASO associated to LNP at different N/P ratios demonstrated that ASO was efficiently complexed only at a N/P ratio of 10. This

observation is in line with the N/P ratio required to complex siRNA (see chapter 4), demonstrating that a higher amount of cationic charge is needed for the complexation of small nucleic acids. Hydrodynamic diameter, zeta potential and morphology were similar to the properties of siRNA-LNP as they have almost a similar size of nucleic acid sequence (14 and 20 bases respectively).

The intracellular distribution and release of ASO from LNP investigated at confocal microscopy showed a time-dependent internalization and release profile in murine myoblasts and myotubes. Our investigations demonstrated that nanosystems were rapidly internalized in both myoblasts and myotubes with a cytoplasmic accumulation without entering the cell nucleus. Moreover, ASO was efficiently released over time in the intracellular milieu, holding promise to unveil the therapeutic potential of this nucleic acid¹⁷⁵.

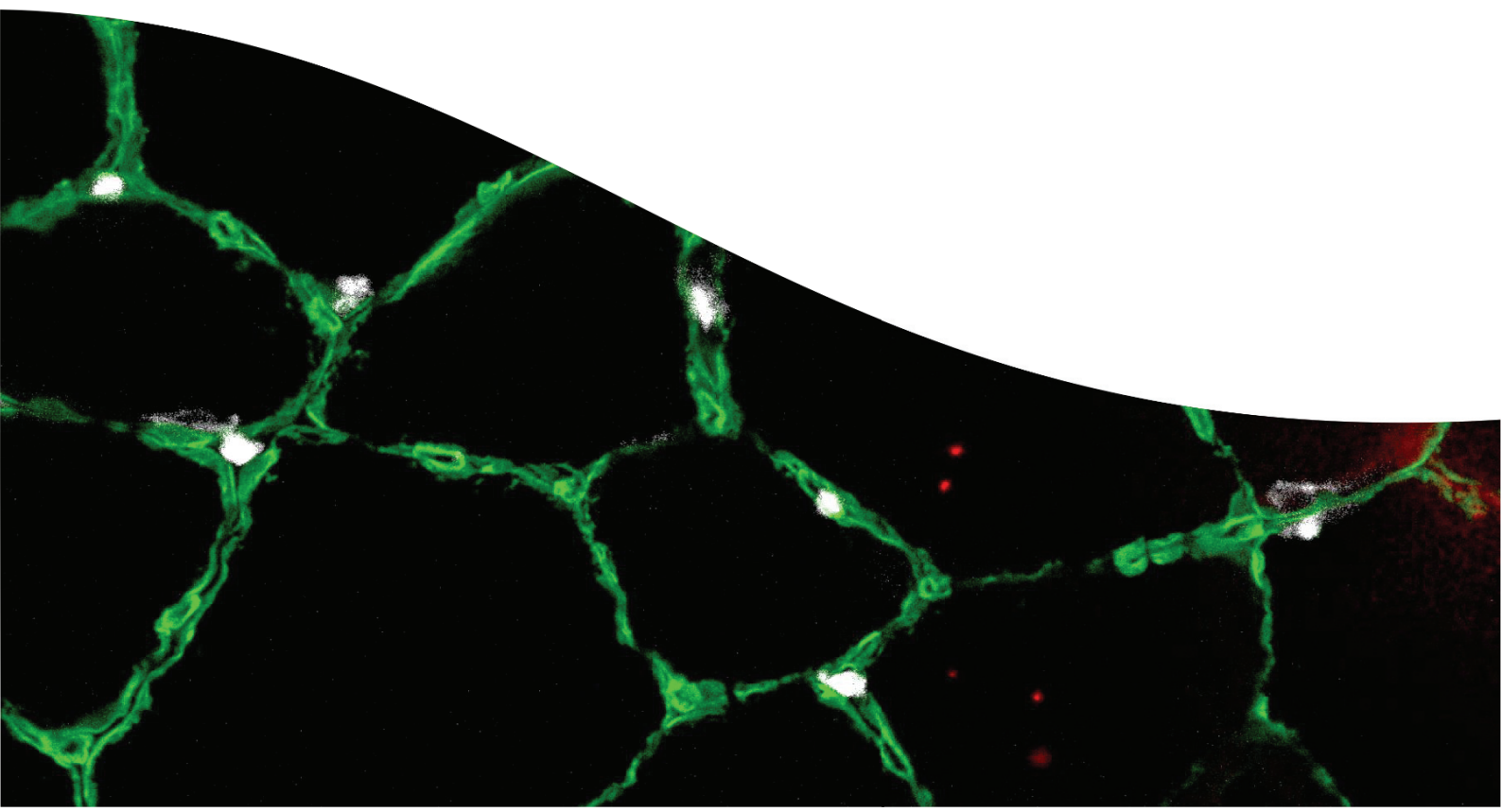
Finally, biodistribution studies were performed to investigate the organ selectivity of ASO-LNP an innovative association of complementary radiolabeling and fluorescent imaging techniques to assess the distribution of LNP and ASO, respectively, after i.v. administration. Globally, a high percentage of LNP and ASO were taken up by the reticuloendothelial system. This organ selectivity has been mainly proved to be dictated by the surface charge and the chemical composition of LNP^{176–178}. In fact, Kranz et al. showed how negatively charged lipoplexes were mainly accumulated in the spleen¹⁷⁷. Thus, our findings of specific accumulation of the negatively charged ASO-LNP in the spleen is in line with other scientific works. Interestingly, fluorescence signal of ASO were observed distributed in the kidneys whereas no ¹¹¹In-LNP were quantified in these organs. Owing to the dimensions of LNP and ASO, it is highly possible that a part of ASO was released from LNP after i.v. administration and cleared from the blood circulation by urinary excretion. Indeed, preferential accumulation of ASO in the kidneys has been mainly reported^{179,180}.

Main limitation in this study relies on the poor distribution of ASO-LNP in muscle tissue. This marginal distribution profile may be related to two essential parameters. Firstly, healthy animals do not express the same phenotypes of disease-like models such as inflammation, fibrosis, altered physiological barriers or other features that can lead to an opportunistic internalization way. Another main parameter that should be investigated to obtain a higher distribution in muscles is the administration route. Different

administration route has been employed for *in vivo* LNP injection and has demonstrated different organ selectivity¹⁸¹⁻¹⁸³. Regarding muscular pathology applications, intramuscular (i.m.) injections remains the most studied administration route^{42,181,184,185}. However, this administration route remains more as a local treatment, and may injure a muscle that is already atrophied and have difficulty to regenerate.

Overall, although i.v. injection did not demonstrate a high distribution of ASO-LNP in muscles, we can suppose that repeated safe administration may enhance the distribution in muscles while providing long-term effects. In fact, compared to viral vectors, LNP have low *in vivo* immunogenicity that allows repeated administration¹⁸⁴. Further *in vivo* biodistribution studies of ASO-LNP should be performed in DM1 mice model using different administration routes to determine the most suitable conditions for ASO delivery in muscles and pave the way to therapeutic applications.

CONCLUDING REMARKS



CONCLUDING REMARKS

The overall goal of this interdisciplinary research project was aimed to provide novel drug and gene delivery platforms using nanomedicine for treating skeletal muscle disorders in DM1. Despite the recent breakthrough of nanomedicine to treat different diseases, poor attention has been paid to muscular dystrophies and in particular to DM1. Nowadays, a crucial lack of effective therapy is clearly identified and nanomedicine is a suitable solution to the administration of experimental molecules that face *in vivo* marginal benefits due to limitation of toxicity and/or distribution. To this end, this research project has been focused on two different main axes: encapsulation of PTM in a context of drug repurposing and development of gene and oligonucleotide delivery nanosystems.

To achieve in these different approaches, a step-by-step methodology has been adopted. After screening in the literature of the therapeutic compounds to incorporate in nanocarriers, the resultant nanosystems have been optimized in terms of physico-chemical properties to provide suitable NPs. Then, main investigations have been carried out *in vitro* in cultured skeletal muscle cell lines. These *in vitro* studies are essential to assess the toxicity, internalization pathway, intracellular distribution and fate, release of the payload content and therapeutic efficacy. Our investigations have been performed on muscle cells at diverse differentiation stage: myoblasts and myotubes. Myoblasts are actively cycling cells acting in regenerating muscle whereas myotubes are terminally differentiated cells that form the basic unit of the skeletal muscle tissue¹⁸⁶. Thus, the *in vitro* assessments were crucial to establish the therapeutic strategy that may be employed to treat either the stem cell population or the differentiated muscle fibers. Finally, the most promising nanosystems have been investigated for *ex vivo* or *in vivo* biodistribution in healthy models for the further perspectives to be tested for therapeutic efficacy in mice model of DM1.

The first milestone of this research project was devoted to the repurposing of PTM, an FDA-approved antiparasitic drug that demonstrated therapeutic efficacy *in vitro* to reverse some splicing features of DM1^{27,72}. Although PTM was not clinically investigated due to substantial toxicity at the potentially effective doses, nanomedicine appears as suitable to increase PTM internalization and reduce the required doses. The aim of this work was to deliver PTM to skeletal muscle cells using nanosystems essentially made of HA. This natural polysaccharide was selected for its natural origin as important component of the extracellular matrix, thus ensuring to be non-immunogenic, highly biocompatible and biodegradable^{125,187,188}. HA has been widely explored in nanomedicine, especially because the specific binding of HA for CD44 receptors prove fruitful for anticancer targeting^{189,190}. Owing to the expression of CD44 receptors also in myoblasts and myotubes as crucial modulator of early myogenesis¹²⁹, CD44 receptors represents an effective strategy for increasing accumulation of HA-PArg NPs and the associated drug at the pathological site.

Previous work has demonstrated the suitability of HA to associate PTM¹³⁷. The present investigations highlighted the effectiveness of HA-NPs to deliver PTM in C2C12 murine myoblasts and myotubes. The cytotoxicity study was an important requirement to demonstrate the biocompatibility of these nanosystems and also to determine the most suitable concentration of HA-PArg NPs for the further studies. HA-PArg NPs were not toxic on myoblasts and myotubes and once loaded with PTM, nanosystems were less tolerated. This slightly lower biocompatibility was related to the toxicity of PTM that showed a similar cytotoxicity profile. Microscopical analysis demonstrated the high internalization efficiency of HA-PArg NPs in myoblasts and myotubes, highlighting the key role of CD44 receptors in the uptake of the nanocarriers. Furthermore, our investigations provide unequivocal evidence that HA is sensitive to the intravacuolar acidification arising from the gradual maturation of endosomes and promote the endosomal-escape process of the NPs. In fact, our observations lead to the conclusions that buffering effect is responsible for HA protonation, decreasing the interaction of HA with PArg that thereby promote fusion with the endosomal membrane. Although buffering effect for cationic nanocarriers has been widely demonstrated, this work

is one of the first to evidence buffering effect on negative polymeric NPs. In the purpose to have informations regarding the biodistribution of HA-PArg NPs in complex biological matrix, a fluid dynamic system to maintain *ex vivo* soleus muscle was used¹⁹¹. This system was ideal to use organs and tissues explanted from untreated animals that were destined to be discarded, matching properly with the principles of the 3Rs. Such biological investigations are crucial since skeletal muscle is a complex organ made of myofibers and satellite cells joined together by vascularized connective tissues. HA-PArg NPs were found to diffuse in the whole muscle in a few hours but were mainly entrapped in the connective tissue. However, at long incubation times, NPs were efficiently internalized in the myofibers whereas the extracellular NPs were removed by macrophages. Finally, we set-up a novel DM1 cell model to demonstrated the therapeutic efficacy of PTM-Loaded NPs. This cellular model represented an ideal alternative to cell from DM1 patients that are rare and difficult to maintain *in vitro* due to their pathological phenotype. HA-PArg NPs demonstrated a high therapeutic efficiency, halving the number of nuclear foci with a safety concentration of only 10 μ M of PTM loaded into HA-PArg NPs, whereas PTM as-in showed a lower efficiency. It is likely that the therapeutic advantage of PTM-loaded NPs relies on their high uptake into myoblasts and sustained release of PTM in the cytosol. In conclusion, all these encouraging results taken together highlighted the potency of our PTM-loaded NPs nanosystems as efficient and biocompatible nanocarrier for delivering PTM into skeletal muscle and mitigate DM1 pathology.

Motivated by the promises of a gene-therapy-based strategy to promote targeted, efficient and long-term treatments for genetic disease, the second approach adopted in this project was focused on the development of nucleic acid delivery using LNP. As different nucleic acid-based strategy may be employed to modify DMPK gene expression, disrupt DNA CTG or RNA CUG expansion repeats, our investigations aimed to study the effectiveness of our LNP to deliver different types and molecular weight nucleic acids as pDNA, mRNA and siRNA. Indeed, delivery of different types of nucleic acids enable to adopt different therapeutic strategies. Although the widespread effectiveness of LNP to deliver different DNA or RNA species have been already demonstrated, distinct LNP

compositions are often used according to the nucleic acid to be delivered. As proof-of-concept, our investigations firstly focused on acid nucleic sequences to modulate protein expression in skeletal muscle cells by inducing or interfering with eGFP expression.

The results obtained demonstrated the suitability of our LNP to associate each type of nucleic acid. Changing only the N/P ratio enables to efficiently complex large as small nucleic acids. Interestingly, incorporation of DNA or RNA did not modify the physico-chemical properties of the nanosystems. Although an efficient complexation is an important parameter, it does not mean that the system will transfect efficiently nucleic acids into cells. In fact, some cationic polymers or polypeptides as polyethyleneimine or poly-L-lysine have been widely used for gene delivery but despite their highly efficient ability to associate nucleic acids, complex biological barriers at the cellular level (cellular entry, escape from the lysosomal pathway, intracellular trafficking and release) restrict their transgene expression efficacy¹⁹².

The recent booming success of mRNA-vaccines highlighted the potency of LNP to transfect RNA into cells. The present investigations are in line with the promises of this delivery approach. Our LNP showed to efficiently deliver pDNA, mRNA and siRNA through a unique composition of the vector. Regarding pDNA and mRNA, similar transfection efficiency to commercial transfection agent were obtained in myoblasts: this is promising for clinical translation as the commercial transfection agents are unsuitable for *in vivo* administration. Regarding myotubes, only mRNA-LNP demonstrated to be efficient, as pDNA did not succeed to enter cell nucleus in differentiated cells that do not undergo cell division, even if pDNA is correctly released into the cytoplasm. For silencing GFP expression using siRNA, our investigations demonstrated a high transfection efficiency on both myoblasts and myotubes, even more efficient than the commercial transfection agent.

Taken together, these promising results demonstrate the effectiveness of our LNP composition to deliver different types of nucleic acids and highlight specially the potential of our mRNA-LNP and siRNA-LNP to treat myoblasts and myotubes. Thus, the potential of such nanosystems promises to cure not only regenerating muscle cells but also non-renewing affected cells. Although no therapeutic strategy

is focused on mRNA for treating DM1, such systems appear as very promising and may be suitable for other muscular dystrophies with protein expression deficiency as for DMD. On the contrary, siRNA-based therapeutic strategies are studied to inhibit DMPK gene expression and the downstream toxic CUG-containing RNA.

Motivated by the effectiveness of our LNP to deliver nucleic acids to control GFP expression, we further investigated the association of a therapeutic nucleic acid sequence in the purpose to treat the DM1 pathological mechanism.

To this end, an RNase H-active ASO sequence described in the literature to induce cleavage of the CUG-repeats RNA has been selected. This sequence was suitable to be repurposed for nanomedicine application as the authors demonstrated marginal *in vivo* benefits correlated to the electroporation delivery strategy. The complexation of this ASO sequence with our LNP was highly efficient at an N/P ratio of 10 as for siRNA. The necessity of a high N/P ratio to complex an ASO is consistent with siRNA association as their molecular weight are nearly similar. Our preliminary *in vitro* results highlighted the ability of our vector to intracellularly release ASO in healthy murine myoblasts and myotubes. Once intracellularly released from LNP, some ASO were also interestingly found to locate into the nucleus, whereas LNP were only distributed into the cytosol. This observation holds promise to cleave CUG-repeats from DMPK RNA that is retained into the nucleus and thereby decreased the number of pathological nuclear foci in DM1 *in vitro* models.

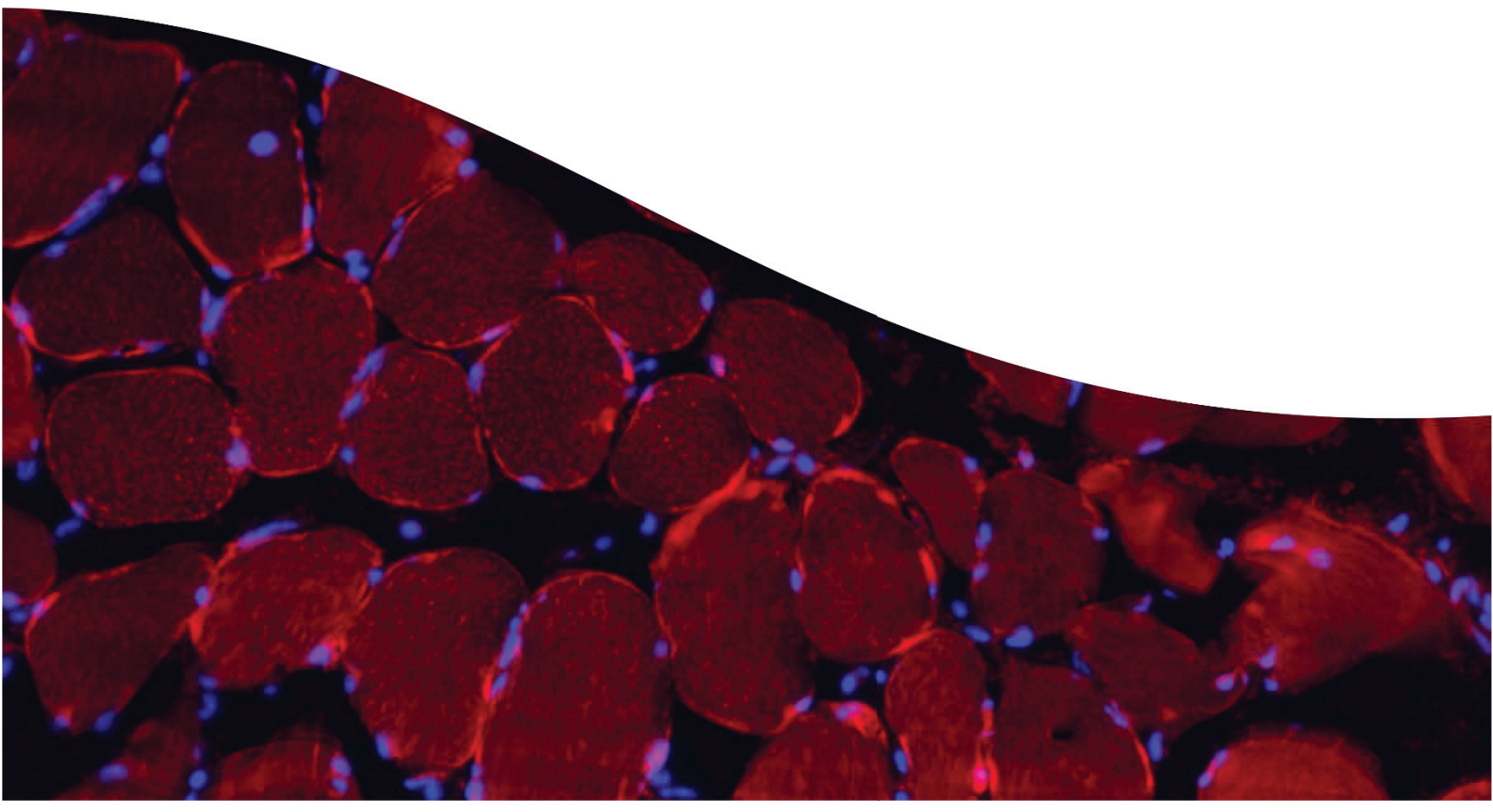
The preliminary *in vivo* results have been obtained on healthy animals to investigate the biodistribution of LNP and release of ASO through i.v. injection. *In vivo* results demonstrated a high distribution of LNP into the liver and the spleen as typically described for LNP. The combined radiolabeling and fluorescent imaging techniques demonstrated that after administration, a part of ASO were probably dissociated and eliminated by the kidneys whereas the other part followed the same distribution pattern than LNP. Despite the lack of distribution of nanosystems in investigated muscles, two main critical points must be taken in mind to discuss about the efficiency of these nanosystems. Firstly, different administration routes as i.m. injection may be considered to investigate the biodistribution of a nanosystem for skeletal delivery. Secondly, investigation of

biodistribution in DM1 mice model, which presents altered barriers and thereby opportunistic internalization ways, may change the biodistribution profile of the nanosystems.

Future perspectives on this research project will be focused on the therapeutic assays of ASO-LNP. A scientific collaboration with laboratories expert in DM1 cell and animal models has been established and will allow to investigate the *in vitro* and *in vivo* therapeutic efficiency and biodistribution in suitable models.

This collaborative work will be crucial to provide the necessary complementary expertise from different research fields, while fostering a creative environment to find solutions for the possible drawbacks and helping to reach the expected goals. The promising results obtained in this research work and the current research perspectives allow foreseeing that, in near future, a therapeutic for DM1 will hopefully be available.

REFERENCES



REFERENCES

1. Thornton, C. A. Myotonic Dystrophy. *Neurologic Clinics* **32**, 705–719 (2014).
2. Johnson, N. E. *et al.* Population-Based Prevalence of Myotonic Dystrophy Type 1 Using Genetic Analysis of Statewide Blood Screening Program. *Neurology* **96**, e1045–e1053 (2021).
3. De Antonio, M. *et al.* Unravelling the myotonic dystrophy type 1 clinical spectrum: A systematic registry-based study with implications for disease classification. *Rev Neurol (Paris)* **172**, 572–580 (2016).
4. Bird, T. D. Myotonic Dystrophy Type 1. in *GeneReviews*® (eds. Adam, M. P. *et al.*) (University of Washington, Seattle, 1993).
5. Turner, C. & Hilton-Jones, D. The myotonic dystrophies: diagnosis and management. *Journal of Neurology, Neurosurgery & Psychiatry* **81**, 358–367 (2010).
6. Taneja, K. L., McCurrach, M., Schalling, M., Housman, D. & Singer, R. H. Foci of trinucleotide repeat transcripts in nuclei of myotonic dystrophy cells and tissues. *J Cell Biol* **128**, 995–1002 (1995).
7. Pettersson, O. J., Aagaard, L., Jensen, T. G. & Damgaard, C. K. Molecular mechanisms in DM1 — a focus on foci. *Nucleic Acids Research* **43**, 2433–2441 (2015).
8. Mahadevan, M. *et al.* Myotonic dystrophy mutation: an unstable CTG repeat in the 3' untranslated region of the gene. *Science* **255**, 1253–1255 (1992).
9. Meola, G. & Cardani, R. Myotonic dystrophies: An update on clinical aspects, genetic, pathology, and molecular pathomechanisms. *Biochim Biophys Acta* **1852**, 594–606 (2015).
10. Tomé, S. & Gourdon, G. DM1 Phenotype Variability and Triplet Repeat Instability: Challenges in the Development of New Therapies. *Int J Mol Sci* **21**, E457 (2020).

11. Davis, B. M., McCurrach, M. E., Taneja, K. L., Singer, R. H. & Housman, D. E. Expansion of a CUG trinucleotide repeat in the 3' untranslated region of myotonic dystrophy protein kinase transcripts results in nuclear retention of transcripts. *Proc Natl Acad Sci U S A* **94**, 7388–7393 (1997).
12. Malatesta, M., Cardani, R., Pellicciari, C. & Meola, G. RNA Transcription and Maturation in Skeletal Muscle Cells are Similarly Impaired in Myotonic Dystrophy and Sarcopenia: The Ultrastructural Evidence. *Front Aging Neurosci* **6**, 196 (2014).
13. Timchenko, L. T. *et al.* Identification of a (CUG)_n triplet repeat RNA-binding protein and its expression in myotonic dystrophy. *Nucleic Acids Res* **24**, 4407–4414 (1996).
14. Miller, J. W. *et al.* Recruitment of human muscleblind proteins to (CUG)_n expansions associated with myotonic dystrophy. *EMBO J.* **19**, 4439–4448 (2000).
15. Paul, S. *et al.* Interaction of muscleblind, CUG-BP1 and hnRNP H proteins in DM1-associated aberrant IR splicing. *The EMBO Journal* **25**, 4271–4283 (2006).
16. Nakamori, M. *et al.* Splicing biomarkers of disease severity in myotonic dystrophy. *Ann Neurol* **74**, 862–872 (2013).
17. Perdoni, F. *et al.* RNA/MBNL1-containing foci in myoblast nuclei from patients affected by myotonic dystrophy type 2: an immunocytochemical study. *Eur J Histochem* **53**, e18 (2009).
18. Holt, I. *et al.* Muscleblind-Like Proteins: Similarities and Differences in Normal and Myotonic Dystrophy Muscle. *The American Journal of Pathology* **174**, 216–227 (2009).
19. Teplova, M. & Patel, D. J. Structural insights into RNA recognition by the alternative-splicing regulator muscleblind-like MBNL1. *Nat Struct Mol Biol* **15**, 1343–1351 (2008).
20. Kanadia, R. N. *et al.* A Muscleblind Knockout Model for Myotonic Dystrophy. *Science* **302**, 1978–1980 (2003).

21. Timchenko, L. T., Timchenko, N. A., Caskey, C. T. & Roberts, R. Novel proteins with binding specificity for DNA CTG repeats and RNA CUG repeats: implications for myotonic dystrophy. *Hum Mol Genet* **5**, 115–121 (1996).
22. Huichalaf, C. *et al.* Expansion of CUG RNA repeats causes stress and inhibition of translation in myotonic dystrophy 1 (DM1) cells. *The FASEB Journal* **24**, 3706–3719 (2010).
23. Thornton, C. A., Wang, E. & Carrell, E. M. Myotonic dystrophy: approach to therapy. *Current Opinion in Genetics & Development* **44**, 135–140 (2017).
24. López-Morató, M., Brook, J. D. & Wojciechowska, M. Small Molecules Which Improve Pathogenesis of Myotonic Dystrophy Type 1. *Front Neurol* **9**, 349 (2018).
25. Konieczny, P. *et al.* Myotonic dystrophy: candidate small molecule therapeutics. *Drug Discov. Today* **22**, 1740–1748 (2017).
26. Reddy, K., Jenquin, J. R., Cleary, J. D. & Berglund, J. A. Mitigating RNA Toxicity in Myotonic Dystrophy using Small Molecules. *IJMS* **20**, 4017 (2019).
27. Warf, M. B., Nakamori, M., Matthys, C. M., Thornton, C. A. & Berglund, J. A. Pentamidine reverses the splicing defects associated with myotonic dystrophy. *Proc Natl Acad Sci U S A* **106**, 18551–18556 (2009).
28. Siboni, R. B. *et al.* Biological Efficacy and Toxicity of Diamidines in Myotonic Dystrophy Type 1 Models. *J. Med. Chem.* **58**, 5770–5780 (2015).
29. Jenquin, J. R. *et al.* Furamidine Rescues Myotonic Dystrophy Type I Associated Mis-Splicing through Multiple Mechanisms. *ACS Chem Biol* **13**, 2708–2718 (2018).
30. Jenquin, J. R., Yang, H., Huigens, R. W., Nakamori, M. & Berglund, J. A. Combination Treatment of Erythromycin and Furamidine Provides Additive and Synergistic Rescue of Mis-Splicing in Myotonic Dystrophy Type 1 Models. *ACS Pharmacol Transl Sci* **2**, 247–263 (2019).

31. Pascual-Gilabert, M., López-Castel, A. & Artero, R. Myotonic dystrophy type 1 drug development: A pipeline toward the market. *Drug Discov Today* **26**, 1765–1772 (2021).
32. Wheeler, T. M. *et al.* Reversal of RNA Dominance by Displacement of Protein Sequestered on Triplet Repeat RNA. *Science* **325**, 336–339 (2009).
33. Evers, M. M., Toonen, L. J. A. & van Roon-Mom, W. M. C. Antisense oligonucleotides in therapy for neurodegenerative disorders. *Advanced Drug Delivery Reviews* **87**, 90–103 (2015).
34. Klein, A. F. *et al.* Peptide-conjugated oligonucleotides evoke long-lasting myotonic dystrophy correction in patient-derived cells and mice. *J Clin Invest* **129**, 4739–4744 (2019).
35. Foff, E. P. & Mahadevan, M. S. Therapeutics development in myotonic dystrophy type 1. *Muscle Nerve* **44**, 160–169 (2011).
36. Overby, S. J., Cerro-Herreros, E., Llamusi, B. & Artero, R. RNA-mediated therapies in myotonic dystrophy. *Drug Discovery Today* **23**, 2013–2022 (2018).
37. Bennett, C. F. & Swayze, E. E. RNA Targeting Therapeutics: Molecular Mechanisms of Antisense Oligonucleotides as a Therapeutic Platform. *Annu. Rev. Pharmacol. Toxicol.* **50**, 259–293 (2010).
38. Wheeler, T. M. *et al.* Targeting nuclear RNA for in vivo correction of myotonic dystrophy. *Nature* **488**, 111–115 (2012).
39. Lee, J. E., Bennett, C. F. & Cooper, T. A. RNase H-mediated degradation of toxic RNA in myotonic dystrophy type 1. *Proc Natl Acad Sci U S A* **109**, 4221–4226 (2012).
40. Jauvin, D. *et al.* Targeting DMPK with Antisense Oligonucleotide Improves Muscle Strength in Myotonic Dystrophy Type 1 Mice. *Mol Ther Nucleic Acids* **7**, 465–474 (2017).
41. Batra, R. *et al.* Elimination of Toxic Microsatellite Repeat Expansion RNA by RNA-Targeting Cas9. *Cell* **170**, 899–912.e10 (2017).

42. Batra, R. *et al.* The sustained expression of Cas9 targeting toxic RNAs reverses disease phenotypes in mouse models of myotonic dystrophy type 1. *Nat Biomed Eng* **5**, 157–168 (2021).
43. Klein, A. F., Dastidar, S., Furling, D. & Chuah, M. K. Therapeutic Approaches for Dominant Muscle Diseases: Highlight on Myotonic Dystrophy. *Curr Gene Ther* **15**, 329–337 (2015).
44. Coonrod, L. A. *et al.* Reducing Levels of Toxic RNA with Small Molecules. *ACS Chem. Biol.* **8**, 2528–2537 (2013).
45. Nelson, C. E., Robinson-Hamm, J. N. & Gersbach, C. A. Genome engineering: a new approach to gene therapy for neuromuscular disorders. *Nat Rev Neurol* **13**, 647–661 (2017).
46. Raaijmakers, R. H. L., Ripken, L., Ausems, C. R. M. & Wansink, D. G. CRISPR/Cas Applications in Myotonic Dystrophy: Expanding Opportunities. *IJMS* **20**, 3689 (2019).
47. Marsh, S., Hanson, B., Wood, M. J. A., Varela, M. A. & Roberts, T. C. Application of CRISPR-Cas9-Mediated Genome Editing for the Treatment of Myotonic Dystrophy Type 1. *Mol Ther* **28**, 2527–2539 (2020).
48. Furling, D. Cas9 targeting of toxic foci of RNA repeats. *Nat Biomed Eng* **5**, 130–131 (2021).
49. Provenzano, C. *et al.* CRISPR/Cas9-Mediated Deletion of CTG Expansions Recovers Normal Phenotype in Myogenic Cells Derived from Myotonic Dystrophy 1 Patients. *Mol Ther Nucleic Acids* **9**, 337–348 (2017).
50. Dastidar, S. *et al.* Efficient CRISPR/Cas9-mediated editing of trinucleotide repeat expansion in myotonic dystrophy patient-derived iPS and myogenic cells. *Nucleic Acids Res* **46**, 8275–8298 (2018).
51. Lo Scudato, M. *et al.* Genome Editing of Expanded CTG Repeats within the Human DMPK Gene Reduces Nuclear RNA Foci in the Muscle of DM1 Mice. *Molecular Therapy* **27**, 1372–1388 (2019).

52. Dastidar, S. *et al.* Comprehensive transcriptome-wide analysis of spliceopathy correction of myotonic dystrophy using CRISPR-Cas9 in iPSCs-derived cardiomyocytes. *Mol Ther* S1525-0016(21)00398-1 (2021) doi:10.1016/j.ymthe.2021.08.004.
53. Wang, Y. *et al.* Therapeutic Genome Editing for Myotonic Dystrophy Type 1 Using CRISPR/Cas9. *Mol Ther* **26**, 2617–2630 (2018).
54. Pinto, B. S. *et al.* Impeding Transcription of Expanded Microsatellite Repeats by Deactivated Cas9. *Mol Cell* **68**, 479-490.e5 (2017).
55. Mousele, C. *et al.* Long-term Safety and Efficacy of Mexiletine in Myotonic Dystrophy Types 1 and 2. *Neurol Clin Pract* **11**, e682–e685 (2021).
56. Bassez, G. *et al.* Improved mobility with metformin in patients with myotonic dystrophy type 1: a randomized controlled trial. *Brain* **141**, 2855–2865 (2018).
57. AMO Pharma Limited. *A Randomized, Double-Blind Study to Evaluate the Efficacy and Safety of Tideglusib Versus Placebo for the Treatment of Children and Adolescents With Congenital Myotonic Dystrophy (REACH CDM)*. <https://clinicaltrials.gov/ct2/show/NCT03692312> (2021).
58. ICTRP Search Portal. <https://trialsearch.who.int/Trial2.aspx?TrialID=JPRN-jRCT2051190069>.
59. Harmony Biosciences, LLC. *A Randomized, Double-Blind, Placebo-Controlled Study to Evaluate the Safety and Efficacy of Pitolisant on Excessive Daytime Sleepiness and Other Non-Muscular Symptoms in Patients With Myotonic Dystrophy Type 1, Followed by an Open-Label Extension*. <https://clinicaltrials.gov/ct2/show/NCT04886518> (2021).
60. Expansion Therapeutics, Inc. *Double-Blind, Placebo-Controlled, Dose-Range-Finding, Crossover Trial of Single Day Administration of ERX-963 in Adults With Myotonic Dystrophy Type 1*. <https://clinicaltrials.gov/ct2/show/NCT03959189> (2021).
61. Avidity Biosciences, Inc. *A Randomized, Double-Blind, Placebo-Controlled, Phase 1/2 Study to Evaluate the Safety, Tolerability, Pharmacokinetics*

and Pharmacodynamics of Single and Multiple-Doses of AOC 1001 Administered Intravenously to Adult Myotonic Dystrophy Type 1 (DMI) Patients. <https://clinicaltrials.gov/ct2/show/NCT05027269> (2021).

62. Angelbello, A. J. *et al.* Precise small-molecule cleavage of an r(CUG) repeat expansion in a myotonic dystrophy mouse model. *PNAS* **116**, 7799–7804 (2019).

63. Ramon-Duaso, C. *et al.* Protective effects of mirtazapine in mice lacking the Mbnl2 gene in forebrain glutamatergic neurons: Relevance for myotonic dystrophy 1. *Neuropharmacology* **170**, 108030 (2020).

64. Bargiela, A. *et al.* Increased Muscleblind levels by chloroquine treatment improve myotonic dystrophy type 1 phenotypes in in vitro and in vivo models. *PNAS* **116**, 25203–25213 (2019).

65. Cerro-Herreros, E. *et al.* Therapeutic Potential of AntagomiR-23b for Treating Myotonic Dystrophy. *Mol Ther Nucleic Acids* **21**, 837–849 (2020).

66. Stedman, W. AT466 - Myotonic Dystrophy Type 1. *Astellas Gene Therapies* <https://www.astellasgenetherapies.com/myotonic-dystrophy-type-1>.

67. Pipeline: precision genetic medicines for rare and common diseases. *NeuBase Therapeutics, Inc.* <https://www.neubasetherapeutics.com/pipeline/>.

68. Zhang, W. *et al.* Treatment of Type 1 Myotonic Dystrophy by Engineering Site-specific RNA Endonucleases that Target (CUG)_n Repeats. *Mol Ther* **22**, 312–320 (2014).

69. Matsumoto, J. *et al.* The Dimeric Form of 1,3-Diaminoisoquinoline Derivative Rescued the Mis-splicing of Atp2a1 and Clcn1 Genes in Myotonic Dystrophy Type 1 Mouse Model. *Chemistry* **26**, 14305–14309 (2020).

70. MDA Clinical & Scientific Conference 2022. *MDA Clinical & Scientific Conference 2022* <https://mdaconference.org/node/1279>.

71. Pushpakom, S. *et al.* Drug repurposing: progress, challenges and recommendations. *Nature Reviews Drug Discovery* **18**, 41–58 (2019).

72. Pohlig, G. *et al.* Efficacy and Safety of Pafuramidine versus Pentamidine Maleate for Treatment of First Stage Sleeping Sickness in a Randomized,

Comparator-Controlled, International Phase 3 Clinical Trial. *PLoS Negl Trop Dis* **10**, e0004363 (2016).

73. Garber, K. Worth the RISC? *Nature Biotechnology* **35**, 198–202 (2017).

74. Degors, I. M. S., Wang, C., Rehman, Z. U. & Zuhorn, I. S. Carriers Break Barriers in Drug Delivery: Endocytosis and Endosomal Escape of Gene Delivery Vectors. *Acc. Chem. Res.* **52**, 1750–1760 (2019).

75. González-Barriga, A. *et al.* Cell membrane integrity in myotonic dystrophy type 1: implications for therapy. *PLoS One* **10**, e0121556 (2015).

76. Mendell, J. R. *et al.* Current Clinical Applications of In Vivo Gene Therapy with AAVs. *Mol Ther* **29**, 464–488 (2021).

77. Wang, D., Tai, P. W. L. & Gao, G. Adeno-associated virus vector as a platform for gene therapy delivery. *Nat Rev Drug Discov* **18**, 358–378 (2019).

78. Bisset, D. R. *et al.* Therapeutic impact of systemic AAV-mediated RNA interference in a mouse model of myotonic dystrophy. *Hum. Mol. Genet.* **24**, 4971–4983 (2015).

79. Verdera, H. C., Kuranda, K. & Mingozi, F. AAV Vector Immunogenicity in Humans: A Long Journey to Successful Gene Transfer. *Mol Ther* **28**, 723–746 (2020).

80. Fitzpatrick, Z. *et al.* Influence of Pre-existing Anti-capsid Neutralizing and Binding Antibodies on AAV Vector Transduction. *Mol Ther Methods Clin Dev* **9**, 119–129 (2018).

81. Zischewski, J., Fischer, R. & Bortesi, L. Detection of on-target and off-target mutations generated by CRISPR/Cas9 and other sequence-specific nucleases. *Biotechnol Adv* **35**, 95–104 (2017).

82. Ikeda, M. *et al.* Unexpected Mutations by CRISPR-Cas9 CTG Repeat Excision in Myotonic Dystrophy and Use of CRISPR Interference as an Alternative Approach. *Mol Ther Methods Clin Dev* **18**, 131–144 (2020).

83. Naeem, M., Majeed, S., Hoque, M. Z. & Ahmad, I. Latest Developed Strategies to Minimize the Off-Target Effects in CRISPR-Cas-Mediated Genome Editing. *Cells* **9**, E1608 (2020).
84. Luther, D. C., Lee, Y. W., Nagaraj, H., Scaletti, F. & Rotello, V. M. Delivery approaches for CRISPR/Cas9 therapeutics in vivo: advances and challenges. *Expert Opin Drug Deliv* **15**, 905–913 (2018).
85. Song, X. *et al.* Delivery of CRISPR/Cas systems for cancer gene therapy and immunotherapy. *Adv Drug Deliv Rev* **168**, 158–180 (2021).
86. Wang, D., Zhang, F. & Gao, G. CRISPR-Based Therapeutic Genome Editing: Strategies and In Vivo Delivery by AAV Vectors. *Cell* **181**, 136–150 (2020).
87. Kim, B. Y. S., Rutka, J. T. & Chan, W. C. W. Nanomedicine. *N Engl J Med* **363**, 2434–2443 (2010).
88. Shi, J., Votruba, A. R., Farokhzad, O. C. & Langer, R. Nanotechnology in Drug Delivery and Tissue Engineering: From Discovery to Applications. *Nano Lett.* **10**, 3223–3230 (2010).
89. Key, J. & Leary, J. F. Nanoparticles for multimodal in vivo imaging in nanomedicine. *Int J Nanomedicine* **9**, 711–726 (2014).
90. Baetke, S. C., Lammers, T. & Kiessling, F. Applications of nanoparticles for diagnosis and therapy of cancer. *Br J Radiol* **88**, 20150207 (2015).
91. van der Meel, R. *et al.* Smart cancer nanomedicine. *Nature Nanotechnology* **14**, 1007–1017 (2019).
92. Acharya, G., Mitra, A. K. & Cholkar, K. Chapter 10 - Nanosystems for Diagnostic Imaging, Biodetectors, and Biosensors. in *Emerging Nanotechnologies for Diagnostics, Drug Delivery and Medical Devices* (eds. Mitra, A. K., Cholkar, K. & Mandal, A.) 217–248 (Elsevier, 2017). doi:10.1016/B978-0-323-42978-8.00010-3.
93. Tenzer, S. *et al.* Rapid formation of plasma protein corona critically affects nanoparticle pathophysiology. *Nature Nanotechnology* **8**, 772–781 (2013).

94. Blanco, E., Shen, H. & Ferrari, M. Principles of nanoparticle design for overcoming biological barriers to drug delivery. *Nat Biotechnol* **33**, 941–951 (2015).
95. Sung, Y. K. & Kim, S. W. Recent advances in polymeric drug delivery systems. *Biomaterials Research* **24**, 12 (2020).
96. Ickenstein, L. M. & Garidel, P. Lipid-based nanoparticle formulations for small molecules and RNA drugs. *Expert Opinion on Drug Delivery* **16**, 1205–1226 (2019).
97. Wang, Y. *et al.* Mesoporous silica nanoparticles in drug delivery and biomedical applications. *Nanomedicine* **11**, 313–327 (2015).
98. Daraee, H. *et al.* Application of gold nanoparticles in biomedical and drug delivery. *Artificial Cells, Nanomedicine, and Biotechnology* **44**, 410–422 (2016).
99. Dufès, C., Uchegbu, I. F. & Schätzlein, A. G. Dendrimers in gene delivery. *Advanced Drug Delivery Reviews* **57**, 2177–2202 (2005).
100. Gabizon, A. *et al.* Clinical studies of liposome-encapsulated doxorubicin. *Acta Oncol* **33**, 779–786 (1994).
101. DOXIL approved by FDA. *AIDS Patient Care* **9**, 306 (1995).
102. Anselmo, A. C. & Mitragotri, S. Nanoparticles in the clinic: An update post COVID-19 vaccines. *Bioengineering & Translational Medicine* **6**, e10246 (2021).
103. Sahin, U. *et al.* COVID-19 vaccine BNT162b1 elicits human antibody and TH1 T cell responses. *Nature* **586**, 594–599 (2020).
104. Baden, L. R. *et al.* Efficacy and Safety of the mRNA-1273 SARS-CoV-2 Vaccine. *N Engl J Med* NEJMoa2035389 (2020) doi:10.1056/NEJMoa2035389.
105. Naahidi, S. *et al.* Biocompatibility of engineered nanoparticles for drug delivery. *Journal of Controlled Release* **166**, 182–194 (2013).
106. Mitchell, M. J. *et al.* Engineering precision nanoparticles for drug delivery. *Nat Rev Drug Discov* **20**, 101–124 (2021).
107. Wolfram, J. *et al.* Safety of nanoparticles in medicine. *Curr Drug Targets* **16**, 1671–1681 (2015).

108. Pasut, G. & Veronese, F. M. State of the art in PEGylation: the great versatility achieved after forty years of research. *J Control Release* **161**, 461–472 (2012).
109. Harris, J. M. & Chess, R. B. Effect of pegylation on pharmaceuticals. *Nat Rev Drug Discov* **2**, 214–221 (2003).
110. Pietersz, G. A., Wang, X., Yap, M. L., Lim, B. & Peter, K. Therapeutic targeting in nanomedicine: the future lies in recombinant antibodies. *Nanomedicine (Lond)* **12**, 1873–1889 (2017).
111. Clemons, T. D. *et al.* Distinction Between Active and Passive Targeting of Nanoparticles Dictate Their Overall Therapeutic Efficacy. *Langmuir* **34**, 15343–15349 (2018).
112. Bennet, D. & Kim, S. *Polymer Nanoparticles for Smart Drug Delivery. Application of Nanotechnology in Drug Delivery* (IntechOpen, 2014). doi:10.5772/58422.
113. Martínez Rivas, C. J. *et al.* Nanoprecipitation process: From encapsulation to drug delivery. *Int J Pharm* **532**, 66–81 (2017).
114. Fan, W., Yan, W., Xu, Z. & Ni, H. Formation mechanism of monodisperse, low molecular weight chitosan nanoparticles by ionic gelation technique. *Colloids Surf B Biointerfaces* **90**, 21–27 (2012).
115. Lombardo, S. M., Günday Türeli, N., Koch, M., Schneider, M. & Türeli, A. E. Reliable release testing for nanoparticles with the NanoDis System, an innovative sample and separate technique. *Int J Pharm* **609**, 121215 (2021).
116. Desgouilles, S. *et al.* The Design of Nanoparticles Obtained by Solvent Evaporation: A Comprehensive Study. *Langmuir* **19**, 9504–9510 (2003).
117. Fessi, H., Puisieux, F., Devissaguet, J. Ph., Ammoury, N. & Benita, S. Nanocapsule formation by interfacial polymer deposition following solvent displacement. *International Journal of Pharmaceutics* **55**, R1–R4 (1989).

118. Ding, S., Anton, N., Vandamme, T. F. & Serra, C. A. Microfluidic nanoprecipitation systems for preparing pure drug or polymeric drug loaded nanoparticles: an overview. *Expert Opin Drug Deliv* **13**, 1447–1460 (2016).
119. Karnik, R. *et al.* Microfluidic platform for controlled synthesis of polymeric nanoparticles. *Nano Lett* **8**, 2906–2912 (2008).
120. Zielińska, A. *et al.* Polymeric Nanoparticles: Production, Characterization, Toxicology and Ecotoxicology. *Molecules* **25**, E3731 (2020).
121. Yoo, J.-W., Irvine, D. J., Discher, D. E. & Mitragotri, S. Bio-inspired, bioengineered and biomimetic drug delivery carriers. *Nat Rev Drug Discov* **10**, 521–535 (2011).
122. Sreekumar, S., Goycoolea, F. M., Moerschbacher, B. M. & Rivera-Rodriguez, G. R. Parameters influencing the size of chitosan-TPP nano- and microparticles. *Sci Rep* **8**, 4695 (2018).
123. De Jong, W. H. & Borm, P. J. A. Drug delivery and nanoparticles: applications and hazards. *Int J Nanomedicine* **3**, 133–149 (2008).
124. Severino, P. *et al.* Alginate Nanoparticles for Drug Delivery and Targeting. *Curr Pharm Des* **25**, 1312–1334 (2019).
125. Morra, M. Engineering of Biomaterials Surfaces by Hyaluronan. *Biomacromolecules* **6**, 1205–1223 (2005).
126. Cheng, C. J., Tietjen, G. T., Saucier-Sawyer, J. K. & Saltzman, W. M. A holistic approach to targeting disease with polymeric nanoparticles. *Nat Rev Drug Discov* **14**, 239–247 (2015).
127. Mattheolabakis, G., Milane, L., Singh, A. & Amiji, M. M. Hyaluronic acid targeting of CD44 for cancer therapy: from receptor biology to nanomedicine. *J Drug Target* **23**, 605–618 (2015).
128. Chen, C., Zhao, S., Karnad, A. & Freeman, J. W. The biology and role of CD44 in cancer progression: therapeutic implications. *J Hematol Oncol* **11**, 64 (2018).

129. Mylona, E., Jones, K. A., Mills, S. T. & Pavlath, G. K. CD44 regulates myoblast migration and differentiation. *J Cell Physiol* **209**, 314–321 (2006).
130. Battistini, F. D., Olivera, M. E. & Manzo, R. H. Equilibrium and release properties of hyaluronic acid-drug complexes. *Eur J Pharm Sci* **49**, 588–594 (2013).
131. Choi, K. Y. *et al.* Self-assembled hyaluronic acid nanoparticles for active tumor targeting. *Biomaterials* **31**, 106–114 (2010).
132. Milletti, F. Cell-penetrating peptides: classes, origin, and current landscape. *Drug Discov Today* **17**, 850–860 (2012).
133. Lättig-Tünnemann, G. *et al.* Backbone rigidity and static presentation of guanidinium groups increases cellular uptake of arginine-rich cell-penetrating peptides. *Nature Communications* **2**, 453 (2011).
134. Stewart, K. M., Horton, K. L. & Kelley, S. O. Cell-penetrating peptides as delivery vehicles for biology and medicine. *Org Biomol Chem* **6**, 2242–2255 (2008).
135. Oyarzun-Ampuero, F. A., Goycoolea, F. M., Torres, D. & Alonso, M. J. A new drug nanocarrier consisting of polyarginine and hyaluronic acid. *Eur J Pharm Biopharm* **79**, 54–57 (2011).
136. Matha, K. *et al.* Bioinspired hyaluronic acid and polyarginine nanoparticles for DACHPt delivery. *Eur J Pharm Biopharm* **150**, 1–13 (2020).
137. Carton, F. *et al.* Rationally designed hyaluronic acid-based nano-complexes for pentamidine delivery. *Int J Pharm* **568**, 118526 (2019).
138. Lollo, G., Benoit, J.-P. & Brachet-Botineau, M. Drug delivery system for platinum-based drugs. (2020).
139. Weyhers, H., Ehlers, S., Hahn, H., Souto, E. B. & Müller, R. H. Solid lipid nanoparticles (SLN)--effects of lipid composition on in vitro degradation and in vivo toxicity. *Pharmazie* **61**, 539–544 (2006).

140. Müller, R. H., Mäder, K. & Gohla, S. Solid lipid nanoparticles (SLN) for controlled drug delivery - a review of the state of the art. *Eur J Pharm Biopharm* **50**, 161–177 (2000).
141. Müller, R. H., Radtke, M. & Wissing, S. A. Nanostructured lipid matrices for improved microencapsulation of drugs. *Int J Pharm* **242**, 121–128 (2002).
142. Shirodkar, R. K., Kumar, L., Mutalik, S. & Lewis, S. Solid Lipid Nanoparticles and Nanostructured Lipid Carriers: Emerging Lipid Based Drug Delivery Systems. *Pharm Chem J* **53**, 440–453 (2019).
143. Teixeira, M. C., Carbone, C. & Souto, E. B. Beyond liposomes: Recent advances on lipid based nanostructures for poorly soluble/poorly permeable drug delivery. *Prog Lipid Res* **68**, 1–11 (2017).
144. Forssen, E. A. & Ross, M. E. Daunoxome® Treatment of Solid Tumors: Preclinical and Clinical Investigations. *Journal of Liposome Research* **4**, 481–512 (1994).
145. Madden, T. D., Janoff, A. S. & Cullis, P. R. Incorporation of amphotericin B into large unilamellar vesicles composed of phosphatidylcholine and phosphatidylglycerol. *Chem Phys Lipids* **52**, 189–198 (1990).
146. Bulbake, U., Doppalapudi, S., Kommineni, N. & Khan, W. Liposomal Formulations in Clinical Use: An Updated Review. *Pharmaceutics* **9**, 12 (2017).
147. Johnson, S. M., Bangham, A. D., Hill, M. W. & Korn, E. D. Single bilayer liposomes. *Biochimica et Biophysica Acta (BBA) - Biomembranes* **233**, 820–826 (1971).
148. Allen, T. M. & Cullis, P. R. Liposomal drug delivery systems: from concept to clinical applications. *Adv Drug Deliv Rev* **65**, 36–48 (2013).
149. Chaudhary, N., Weissman, D. & Whitehead, K. A. mRNA vaccines for infectious diseases: principles, delivery and clinical translation. *Nat Rev Drug Discov* **20**, 817–838 (2021).
150. Kim, J., Eygeris, Y., Gupta, M. & Sahay, G. Self-assembled mRNA vaccines. *Adv Drug Deliv Rev* **170**, 83–112 (2021).

151. Kulkarni, J. A., Cullis, P. R. & van der Meel, R. Lipid Nanoparticles Enabling Gene Therapies: From Concepts to Clinical Utility. *Nucleic Acid Ther* **28**, 146–157 (2018).
152. Kulkarni, J. A. *et al.* The current landscape of nucleic acid therapeutics. *Nat. Nanotechnol.* **16**, 630–643 (2021).
153. Cullis, P. R. & Hope, M. J. Lipid Nanoparticle Systems for Enabling Gene Therapies. *Molecular Therapy* **25**, 1467–1475 (2017).
154. Akinc, A. *et al.* The Onpattro story and the clinical translation of nanomedicines containing nucleic acid-based drugs. *Nature Nanotechnology* **14**, 1084–1087 (2019).
155. Hou, X., Zaks, T., Langer, R. & Dong, Y. Lipid nanoparticles for mRNA delivery. *Nat Rev Mater* (2021) doi:10.1038/s41578-021-00358-0.
156. Zhao, Y. & Huang, L. Chapter Two - Lipid Nanoparticles for Gene Delivery. in *Advances in Genetics* (eds. Huang, L., Liu, D. & Wagner, E.) vol. 88 13–36 (Academic Press, 2014).
157. Malone, R. W., Felgner, P. L. & Verma, I. M. Cationic liposome-mediated RNA transfection. *Proc Natl Acad Sci U S A* **86**, 6077–6081 (1989).
158. Semple, S. C. *et al.* Rational design of cationic lipids for siRNA delivery. *Nat Biotechnol* **28**, 172–176 (2010).
159. Kulkarni, J. A., Witzigmann, D., Leung, J., Tam, Y. Y. C. & Cullis, P. R. On the role of helper lipids in lipid nanoparticle formulations of siRNA. *Nanoscale* **11**, 21733–21739 (2019).
160. Cheng, X. & Lee, R. J. The role of helper lipids in lipid nanoparticles (LNPs) designed for oligonucleotide delivery. *Advanced Drug Delivery Reviews* **99**, 129–137 (2016).
161. Han, X. *et al.* An ionizable lipid toolbox for RNA delivery. *Nat Commun* **12**, 7233 (2021).
162. Schlich, M. *et al.* Cytosolic delivery of nucleic acids: The case of ionizable lipid nanoparticles. *Bioeng Transl Med* e10213 (2021) doi:10.1002/btm2.10213.

163. Kauffman, K. J. *et al.* Optimization of Lipid Nanoparticle Formulations for mRNA Delivery in Vivo with Fractional Factorial and Definitive Screening Designs. *Nano Lett.* **15**, 7300–7306 (2015).
164. Ryals, R. C. *et al.* The effects of PEGylation on LNP based mRNA delivery to the eye. *PLoS One* **15**, e0241006 (2020).
165. Knop, K., Hoogenboom, R., Fischer, D. & Schubert, U. S. Poly(ethylene glycol) in drug delivery: pros and cons as well as potential alternatives. *Angew Chem Int Ed Engl* **49**, 6288–6308 (2010).
166. Wagner, A. *et al.* GMP Production of Liposomes—A New Industrial Approach. *Journal of Liposome Research* **16**, 311–319 (2006).
167. Leung, A. K. K., Tam, Y. Y. C., Chen, S., Hafez, I. M. & Cullis, P. R. Microfluidic Mixing: A General Method for Encapsulating Macromolecules in Lipid Nanoparticle Systems. *J Phys Chem B* **119**, 8698–8706 (2015).
168. Viger-Gravel, J. *et al.* Structure of Lipid Nanoparticles Containing siRNA or mRNA by Dynamic Nuclear Polarization-Enhanced NMR Spectroscopy. *J Phys Chem B* **122**, 2073–2081 (2018).
169. Koynova, R. & Tenchov, B. Recent Progress in Liposome Production, Relevance to Drug Delivery and Nanomedicine. *Recent Patents on Nanotechnology* **9**, 86–93 (2015).
170. Weisman, S., Hirsch-Lerner, D., Barenholz, Y. & Talmon, Y. Nanostructure of cationic lipid-oligonucleotide complexes. *Biophys J* **87**, 609–614 (2004).
171. Evers, M. J. W. *et al.* State-of-the-Art Design and Rapid-Mixing Production Techniques of Lipid Nanoparticles for Nucleic Acid Delivery. *Small Methods* **2**, 1700375 (2018).
172. Leung, A. K. K. *et al.* Lipid Nanoparticles Containing siRNA Synthesized by Microfluidic Mixing Exhibit an Electron-Dense Nanostructured Core. *J Phys Chem C Nanomater Interfaces* **116**, 18440–18450 (2012).

173. Maurer, N. *et al.* Spontaneous entrapment of polynucleotides upon electrostatic interaction with ethanol-destabilized cationic liposomes. *Biophys J* **80**, 2310–2326 (2001).
174. Kulkarni, J. A. *et al.* On the Formation and Morphology of Lipid Nanoparticles Containing Ionizable Cationic Lipids and siRNA. *ACS Nano* **12**, 4787–4795 (2018).
175. Paramasivam, P. *et al.* Endosomal escape of delivered mRNA from endosomal recycling tubules visualized at the nanoscale. 2020.12.18.423541 (2021) doi:10.1101/2020.12.18.423541.
176. Levchenko, T. S., Rammohan, R., Lukyanov, A. N., Whiteman, K. R. & Torchilin, V. P. Liposome clearance in mice: the effect of a separate and combined presence of surface charge and polymer coating. *Int J Pharm* **240**, 95–102 (2002).
177. Kranz, L. M. *et al.* Systemic RNA delivery to dendritic cells exploits antiviral defence for cancer immunotherapy. *Nature* **534**, 396–401 (2016).
178. Cheng, Q. *et al.* Selective organ targeting (SORT) nanoparticles for tissue-specific mRNA delivery and CRISPR–Cas gene editing. *Nature Nanotechnology* **15**, 313–320 (2020).
179. Carome, M. A. *et al.* Distribution of the cellular uptake of phosphorothioate oligodeoxynucleotides in the rat kidney in vivo. *Nephron* **75**, 82–87 (1997).
180. Peng, B. *et al.* Tissue distribution and physiologically based pharmacokinetics of antisense phosphorothioate oligonucleotide ISIS 1082 in rat. *Antisense Nucleic Acid Drug Dev* **11**, 15–27 (2001).
181. Wei, T., Cheng, Q., Min, Y.-L., Olson, E. N. & Siegwart, D. J. Systemic nanoparticle delivery of CRISPR–Cas9 ribonucleoproteins for effective tissue specific genome editing. *Nature Communications* **11**, 3232 (2020).
182. Carrasco, M. J. *et al.* Ionization and structural properties of mRNA lipid nanoparticles influence expression in intramuscular and intravascular administration. *Commun Biol* **4**, 956 (2021).

183. Pardi, N. *et al.* Expression kinetics of nucleoside-modified mRNA delivered in lipid nanoparticles to mice by various routes. *J Control Release* **217**, 345–351 (2015).
184. Kenjo, E. *et al.* Low immunogenicity of LNP allows repeated administrations of CRISPR-Cas9 mRNA into skeletal muscle in mice. *Nat Commun* **12**, 7101 (2021).
185. Lee, K. *et al.* Nanoparticle delivery of Cas9 ribonucleoprotein and donor DNA in vivo induces homology-directed DNA repair. *Nat Biomed Eng* **1**, 889–901 (2017).
186. Kislinger, T. *et al.* Proteome dynamics during C2C12 myoblast differentiation. *Mol Cell Proteomics* **4**, 887–901 (2005).
187. Becker, L. C. *et al.* Final report of the safety assessment of hyaluronic acid, potassium hyaluronate, and sodium hyaluronate. *Int J Toxicol* **28**, 5–67 (2009).
188. Kogan, G., Soltés, L., Stern, R. & Gemeiner, P. Hyaluronic acid: a natural biopolymer with a broad range of biomedical and industrial applications. *Biotechnol Lett* **29**, 17–25 (2007).
189. Ganesh, S., Iyer, A. K., Morrissey, D. V. & Amiji, M. M. Hyaluronic acid based self-assembling nanosystems for CD44 target mediated siRNA delivery to solid tumors. *Biomaterials* **34**, 3489–3502 (2013).
190. Ganesh, S., Iyer, A. K., Gattacceca, F., Morrissey, D. V. & Amiji, M. M. In vivo biodistribution of siRNA and cisplatin administered using CD44-targeted hyaluronic acid nanoparticles. *J Control Release* **172**, 699–706 (2013).
191. Carton, F., Calderan, L. & Malatesta, M. Incubation under fluid dynamic conditions markedly improves the structural preservation in vitro of explanted skeletal muscles. *Eur J Histochem* **61**, 2862 (2017).
192. Barua, S. *et al.* Discovery of Cationic Polymers for Non-viral Gene Delivery using Combinatorial Approaches. *Comb Chem High Throughput Screen* **14**, 908–924 (2011).

APPENDIX

VALORIZATION

The diverse works carried out during this PhD thesis has been valorized in different ways, through the publication of scientific articles, the filing of a patent and oral or poster presentation at scientific congresses.

Looking through the literature of the topic of this thesis, it appears clearly that no scientific review was presenting the advantage of nanomedicine for muscular dystrophies treatment and not even describing the few different nanosystems studied until now. To this end, we published a scientific review in *Pharmaceutics* journal on the different nanosystems described in preclinical studies for the most common neuromuscular dystrophies: DMD and DM1. Another review was published on *Microscopie* journal to highlight the electron microscopy techniques that may be employed to characterize nanoparticles in biological environment.

Regarding the different results obtained, one experimental work has been submitted to the journal of *Nanomedicine: nanotechnology, biology and medicine* and is currently under review, and a second one is in preparation. A histological staining technique has been published through two diverse ways: as a technical note in the European Journal of Histochemistry and as protocol in the book chapter *Histochemistry of Single Molecules: Methods and Protocols, Second Edition*.

Looking at the promising results obtained with LNP to deliver nucleic acids in muscle cells, one patent has been filed (FR 2112931).

Finally, the different results obtained during this PhD has been presented in international scientific congresses:

- Unified congress of the society GEI SIBSC-SII, Italy (poster communication)
- 14th Multinational Congress on Microscopy 2019, Italy (oral communication)
- CRS BeneLux & France Early Career Scientist Meeting 2021, on-line (short communication talk – Best pitch presentation award)
- CRS 2021 Virtual Annual Meeting, on-line (oral communication)
- Multinational Congress on Microscopy 2021, on-line (oral communication)
- SFNano 2021, France (oral communication)
- CRS Local Chapters Meeting 2022, Germany (short communication talk)
- ESCDD 2022, Netherlands (poster presentation)